Can plantar pressure predict foot motion?

Can Plantar Pressure Predict Foot Motion?

Friso Hagman

Printed by Universiteitsdrukkerij, Technische Universiteit Eindhoven
Cover design: Elke Eelbode

CIP-DATA LIBRARY TECHNISCHE UNIVERSITEIT EINDHOVEN

Hagman, Friso

Can Plantar Pressure Predict Foot Motion? / by Friso Hagman.
Eindhoven : Technische Universiteit Eindhoven, 2005.
Proefschrift. - ISBN 90-386-0694-X
NUR 919
Subject headings: biomechanics / pressure measurement / joint motions / data analysis
2000 Mathematics Subject Classification: 92B05, 70B10

Can Plantar Pressure Predict Foot Motion?

PROEFSCHRIFT

ter verkrijging van de graad van doctor aan de
Technische Universiteit Eindhoven, op gezag van de
Rector Magnificus, prof.dr.ir. C.J. van Duijn, voor een
commissie aangewezen door het College voor
Promoties in het openbaar te verdedigen
op woensdag 9 november 2005 om 16.00 uur

door

Friso Hagman

geboren te Heino

Dit proefschrift is goedgekeurd door de promotoren:

prof.dr.ir. C.J. van Duijn
en
prof.dr. B. van Gheluwe

Copromotor:
dr.ir. S.J.L. van Eijndhoven

Acknowledgements

Almost seven years ago, I had to make a crucial decision. I had just finished the technical mathematics program of Technische Universiteit Eindhoven (TU/e) with a specialisation in coding theory and cryptology. At that time, I realised that working in this specialism meant turning away from one of the great loves of my life: sports, at least in any professional context. To join my love for sports and my love for mathematics, I became (and still am) very interested in biomechanics. The enrolment in the program Wiskunde voor de Industrie (WvdI) brought about the rolling of sphere in the right direction. This sphere has not yet stopped rolling.

I was fortunate to be accepted for the WvdI program by dr.ir. Stef van Eijdhoven and dr.ir. Fons van de Ven. Stef, as coordinator (later director) of the program, you gave me the freedom to specialise myself in biomechanics. During the last stages of my final project, you arranged the continuation of my final project as a Ph.D project at TU/e. During my Ph.D project, you have spend many hours reading all words in this thesis at least once, discussing ideas, and offering your remarkable insight. I am very grateful for the role you have played during these first years of my working life; you will make a writer out of me! Fons, thank you for sharing with me some of the modelling ideas that have found their way into this thesis. I am also very grateful for your support and never fading optimism.

Besides TU/e, Vrije Universiteit Brussel participated in this Ph.D project. During the last four years, my workplace was at the biomechanics laboratory, where I was supervised by prof.dr. Bart van Gheluwe. As part of the WvdI program, I visited the laboratory for the first time during a three months project. Then, Bart introduced me to the many avenues of biomechanics, but especially to foot biomechanics. Bart also acquainted me with RSscan International, where I performed my final project. Bart, thank you very much for introducing me to biomechanics, for co-financing this

Ph.D project, for the discussions always filled with the right amount of passionate arguments, for the pleasant (working) environment, and for the possibility to continue in the profession I desire.

I would like to express my gratitude to prof.dr. Dirk de Clercq, and prof.dr. Peter Aerts for their comments and suggestions during many meetings we had over the last four years. During these meetings, the Ph.D students and staff of the biomechanics laboratories of Ghent and Antwerp were also present. To Anneleen, Tine, Jos, Pierre, Sophie, Veerle, Kris, Ann, and Evie: thank you for the pleasant times we had at these meetings, but also in both cities and at conferences. I would like to express my gratitude to prof.dr.ir. Hans van Duijn and dr. Mark Lake for their comments and suggestions on the final version of this thesis.

For the research described in this thesis, a pressure plate system played a very important role. The system we used is manufactured by RSscan International. Since my stay at RSscan for my final project (WvdI), I have received a tremendous amount of support from the complete staff. Thank you: Jempi, Wim, Bart J., Bart L., Mireille, Katrien, Bjorn, Tim, and Jan.

The research in this thesis would not have been possible without the 126 individuals who dedicated their time, and feet, to participate in this study. Thank you all!

From the Technische Universiteit Eindhoven, I would like to thank the members of the applied analysis group, presently named CASA. In particular, I would like to thank Dave Bekers for discussing many things, most of them absolutely not related to this thesis.

From the Vrije Universiteit Brussel, I would like to thank the members of BIOM and BETR. In particular, I would like to thank Freddy, Peter D., Elke, Nathalie, William, Peter C., Martine, Kerstine, Lode, Rita, Marijn, Guy, Evert, René, Kristine, Steve, Kristof, Wouter, and all sports instructors. For designing the cover and restyling most of the illustrations found in this thesis, I would sincerely like to thank Elke Eelbode.

Finally, I would like to thank my immediate family. My parents, Anita and Jaap, I thank you for your support, understanding, and your believe that I would finish my education. Last, but first in my heart, I would like to thank my wife Nadine for her love and support, but above all for her patience with a husband that lately spend a lot of time behind computers and who was not always in the best of moods.

Friso Hagman, Zonhoven, 26 September 2005

Contents

Chapter 1

Introduction

The use of two legs to move about is a quality of humans. After an extensive period of evolution, walking and running are the most natural forms of human locomotion. Other forms of human locomotion do exist: some are developmental in nature such as crawling in case of very young children, others are situational such as stair climbing and hurdling. In this thesis, we focus primarily on gait, that is walking, with an occasional side step to running.

Though natural, these two forms of locomotion are by no means infallible. Deficiencies to the locomotion system make up an important part of the injuries sustained in our present day society. Besides injuries, the locomotion system is susceptive to deceases. Both injuries and deceases change our gait pattern from its natural, "normal state", to a sometimes painful, or ineffective gait.

Since the problems accompanying gait disorders have a great impact on both the individual (for example restraint mobility) and society (for example loss of working hours), the professional community involved in gait analysis is numerous. This area of study draws the attention of both the medical and the scientific world. These communities are constantly trying to better understand the underlying processes of gait. The knowledge acquired is used to medically treat gait disorders, and to scientifically indicate intrinsic factors that may lead to the development of future individual gait problems.

To analyse gait, a variety of measurement devices are used. An important measuring device is the video-based or cinematographical-based motion analysis system. Such a system analyses the kinematic part of locomotion, i.e., the determination of

positions of human body segments during gait. Classically, a force plate system is used together with a motion analysis system in order to assess the dynamical characteristics of locomotion. More specifically, the force plate measures the resultant forces of the foot during foot unroll.

A more recently used measuring device in gait analysis is the pressure plate system. This system measures the distribution of pressure perpendicular to the plate in a two-dimensional grid underneath the foot during foot unroll. It allows insight into the local loading of the foot during the foot-to-ground contact phase. In the remainder of this thesis, we will refer to this phase as the stance phase.

The topic of this thesis is the analysis of foot mechanics. In gait analysis, historically the foot has taken up an import role, see Section 1.1. However, only in the last decennia thorough analyses of the foot as a three-dimensional segment have been possible because of the improvement of measurement devices such as the pressure plate. In this thesis, we will combine measurements from all three previously described measurement devices. A four-segment foot model will be measured using a motion analysis system. These measurements will be *synchronised* with the measurements from the force platform and the plantar pressure plate, see Figure 1.1 for an overview of the measurement set-up. With all these measurements, we will introduce a description of new characteristics of foot mechanics. Furthermore, we will present a model of foot motion based on the introduced characteristics. The main feature of this foot model is that it uses pressure plate data only to simulate foot kinematics. Therefore, the functionality of the pressure plate system is extended to the simulation of foot kinematics. At present, foot kinematics are analysed with motion analysis systems only. This thesis gives impulse to using a pressure plate accompanied with the proposed model as an alternative to analyse foot kinematics.

This chapter consists of four sections. In Section 1.1, we describe an overview of developments reported in foot mechanics literature. However, the research specifically related to plantar pressure measurement systems is summarised in Section 1.2 and a more extensive overview is presented in Appendix A. In Section 1.3, the main objectives and the chosen strategies are described. The conclusions of our research in relationship to these main objectives are described in Chapter 6. This introductory chapter ends with Section 1.4, in which we present the thesis organisation.

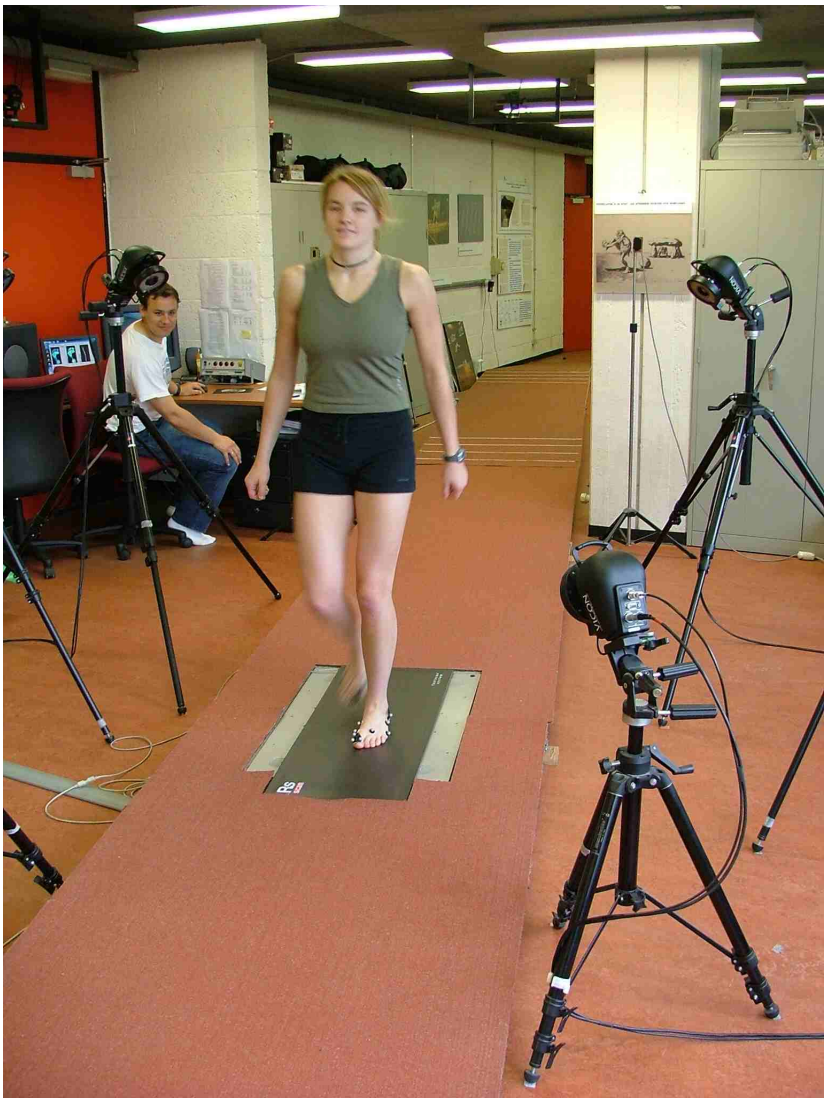

Figure 1.1 An overview of the measurement set-up.

1.1 Overview of Foot Mechanics

Anatomy

Anatomy has probably been the first science that looked at the foot and started the

discussion about its structure and function. The building blocks of the human body are the bones. All other structures that are involved in the mechanics of locomotion are linked to bones. For all humans, it goes without saying that arms and legs are different, but numerically the upper leg has one bone and so does the upper arm, the lower arm has two bones and so does the lower leg. Even foot and hands do not differ that much, 26 bones in a foot against 27 bones in a hand. Taking a closer look, we are able to see that both hand and foot have five digits and that the thumb and big toe both have digits containing two bones while all other digits have three bones, see Figure 1.2. In every day live, it is evident that we use our feet and hands differently. Evolution might have transformed our feet from a more hand-shaped and hand-functional segment to what it is today. From a simple wiggling of the feet and hands, we are able to observe that feet are much less flexible than hands are. Still, 26 bones are standard in a foot with even a lot more articulations. Although feet do not wiggle like hands do, something must be holding them together. The first structure that limits the amount of movement in a foot and takes care of its stability are the ligaments. In Figure 1.3, we depicted some of the ligaments between foot bones. The size and structure of these ligaments are very different from one place to the next. This ligamentous tissue can not be actively used for movement generation since it does not have the contractile elements as in muscles. The muscles of the foot, see Figure 1.4, are active connections between foot bones, so-called intrinsic foot muscles, or between a bone in the foot and a bone in the upper or lower leg, called eccentric foot muscles. The muscles together with bone geometry and ligaments define the range of motion of two adjacent bones with respect to one another.

Besides bones, ligaments, and muscles (and there tendons), the fat pads on the plantar side of the foot, which are situated between the skin and the above structures, play an important role in the function of the foot. Mostly, the fat pads help in dissipating impact energy over the plantar side of the foot. Thus, they have been proven to be effective in damping the impact force during initial heel-ground contact.

The impact energy dissipation role of the fat pads could only be validated in the last century because adequate measurement devices were not yet available. In earlier days, scientist based there conclusions purely on anatomy and a sharp mind. A lot of conclusions from these early days were proven to be valid by experimental research. A number of observations about foot structure and function were, however, disproved. One of these observations concerns the three different arches of the foot. In anatomy

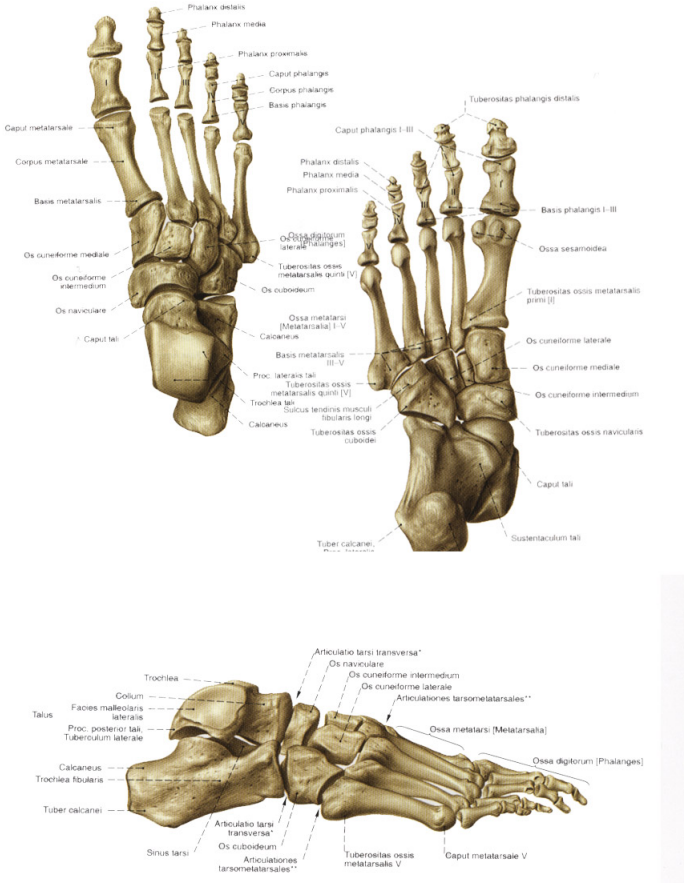

Figure 1.2 The bones of the foot. In the upper left part of the image the dorsal side of the foot is depicted, in the upper right part the plantar side of the foot is depicted, and in the lower part the lateral side is depicted. Illustrations taken from the Sobotta Atlas of Human Anatomy.

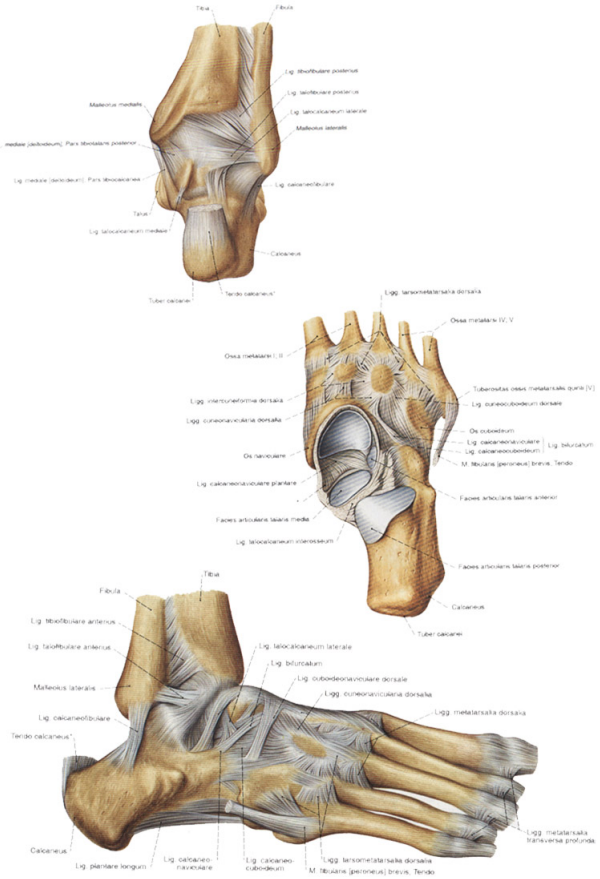

Figure 1.3 Some ligaments in the foot. In the upper image the foot is depicted proximally in the frontal plane, in the middle image a dorsal view of the foot is depicted, and in the lower image the foot is depicted laterally. Illustrations taken from the Sobotta Atlas of Human Anatomy.

books, for example Kapandji [104, 1986], it is stated that the foot basically makes contact with the ground through three bony contact sites: the calcaneus, the head of the first metatarsal, and the head of the fifth metatarsal. The latter two were supposed to form the medial-lateral foot arch. It might be that the observation of

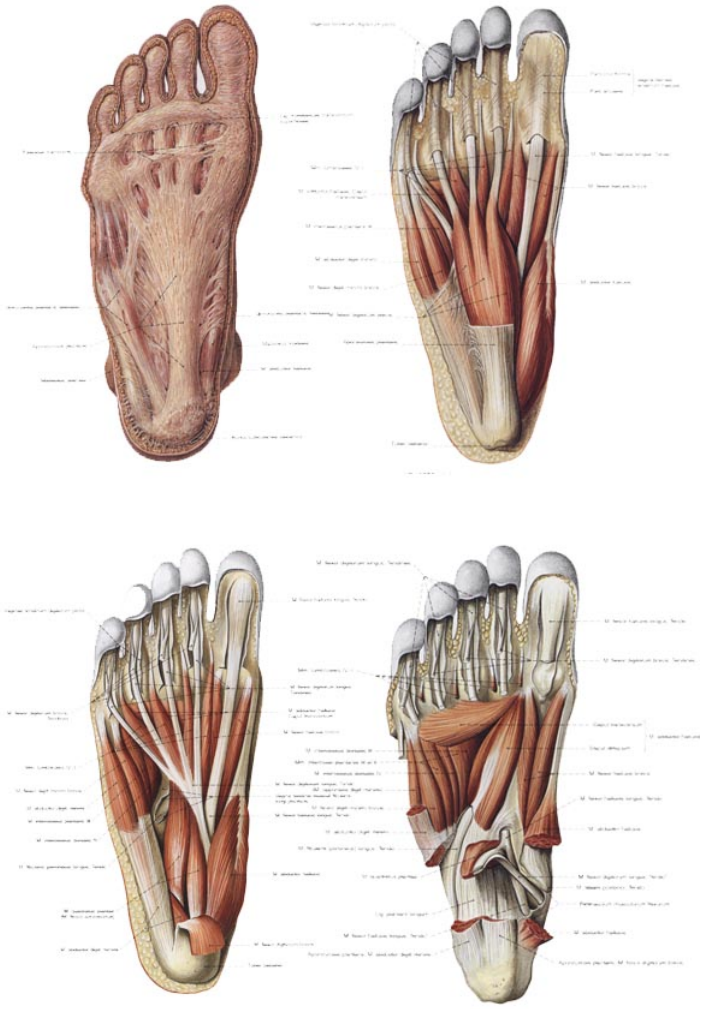

Figure 1.4 Four muscle layers on the plantar side of the foot. From the upper left corner to the lower right corner, layers of musculair tissue are presented from the outer layers to the inner layers. Illustrations taken from the Sobotta Atlas of Human Anatomy.

a medial-lateral arch was made while the feet were non weight-bearing. With the introduction of plantar pressure measurement systems, it was possible to check this observation. Researchers ([87], [77] and [48]) showed that during walking and running there was no such thing as a medial-lateral foot arch because of significant high pressures underneath the central forefoot. De Cock et al. [48, 2005] showed that in most individuals not the first and fifth metatarsal head but the second and third metatarsal head beard the larger amount of pressure. So, the introduction of pressure plate systems and force plate systems were instrumental in studying the interaction between foot (with or without shoe) and ground. Both devices were introduced in the last century (Elftmann 1939, in Nigg and Herzog [154, 1994]) and they arose at the same time as the use of photogrammetry to study motion. However, the limited capabilities of the electronics used at that time did not allow for detailed studies of the movement of feet and its segments.

Foot Motion

In the last decennia, motion analysis systems based on video methods have increasingly improved their performance. In the beginning of this period, motion analysis was two-dimensional and focussed on whole-body motion. The motion of the foot that could be described in this whole-body motion was the dorsal/plantar flexion of the foot around the ankle joint (Winter [213, 1991]). Therefore, the foot was assumed to be one rigid body defined by a line through the length axis of the foot. Some authors shifted attention away from the whole body and to the lower leg. A lot of two-dimensional studies (in [152] and [202]) focussed on so-called rearfoot motion, which is the motion of the rear part of the foot (calcaneus and talus) and the lower leg (tibia and fibula)in the frontal plane, see Figure 1.5. In this sense, the pronation/supination and calcaneal inversion/eversion motions were quantified, see Figure 1.6. This motion was observed in a variety of conditions, for example barefoot, shod, overground, on a treadmill, and during different velocities. Also, from epidemiology studies (in McClay [131, 2000]), this motion pattern could be related to certain sustained injuries, hence its importance. A final remark about the two-dimensional foot motion modelling comes from the studies performed by Stacoff ([190], [191]), who was probably the first to introduce a multi-segment foot model. His model consisted of a rearfoot (calcaneus), and a forefoot (head of metatarsal one and five). In the frontal plane, he studied the torsion between the two segments. From his findings, one is able to extract

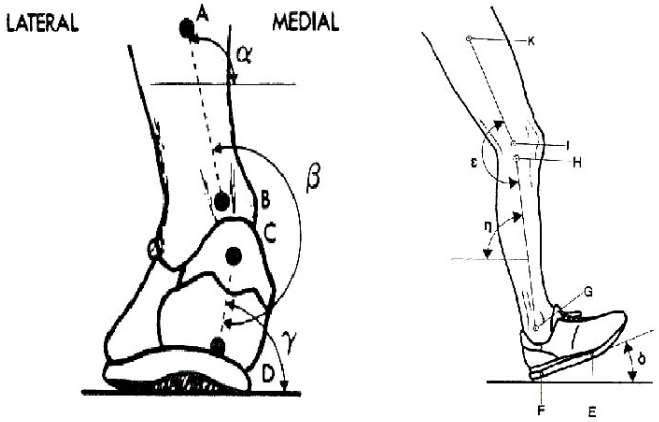

Figure 1.5 A sagittal and frontal marker set up to register motion. Illustration from *Biomechanics of running shoes* by B.M Nigg with permission

torsion curves that have a steep increase at the end of the stance phase, see Figure 1.7. This is probably not real torsion motion. One of the problems with two-dimensional motion analysis are the parallax errors. Using only one camera, the plane of the camera should be parallel to the plane of motion that one wants to study. In case of foot motion, this is not feasible since a foot unroll is not constrained to one camera plane. The frontal plane of the foot undergoes a motion of about 90° with respect to the transverse ground plane. This problem is inherent to the two-dimensional approach, which was the standard at that time. With the further development of motion analysis systems, it became possible to measure motion in its true three-dimensional nature. One of the first to describe rearfoot motion in three dimensions were Soutas-Little et al., [188, 1986] using a Euler or Cardan representation of motion. They compared the supination/pronation, or, inversion/eversion motion of the foot with respect to the two-dimensional and three-dimensional approach. New research appeared exploring foot motion in different conditions, such as barefoot, shod, standing , walking, running, but also on methodology of measurements, such as the relationship between the measurements of external kinematics to the motion of the underlying bone ([153], [8], [169], [54], [13], [132], [170], [171], [192], [124], [127], [126]). Although methodology issues still remain, we think that there is now a beter understanding of their influence on outcome measures. The performance of motion analysis systems kept increasing

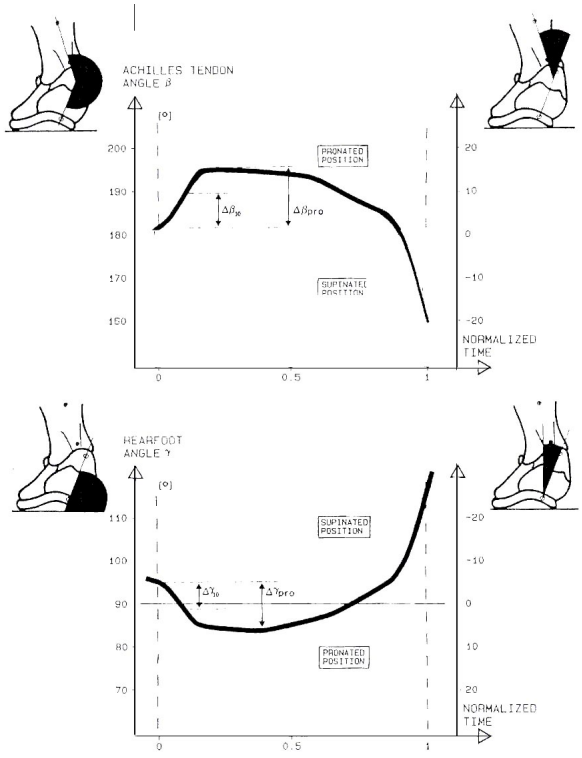

Figure 1.6 Quantification of rearfoot motion. Illustration from *Biomechanics of running shoes* by B.M Nigg with permission

such that better resolution and higher measurement frequencies were obtained with relatively less expensive systems. These performance enhancements led to the introduction of multiple-segment foot-models being measured three dimensionally ([5], [26],[98], [97], [42], [115], [38], [150], [166], and [79]). Also, in the present study, we will employ the use of three-dimensional foot models. Since no standardisation in multiple foot models is yet available, we introduce a multiple foot motion model based on research performed by Carson et al. [26, 2001] and Hunt et al. [98, 2001] and [97, 2004]. To conclude this part on foot motion, we formulate some ideas about the the future. We start with research presently undertaken by Nester et al. [149, 2003], using cadaver feet and a simulation device. This device simulates the stance phase of locomotion by

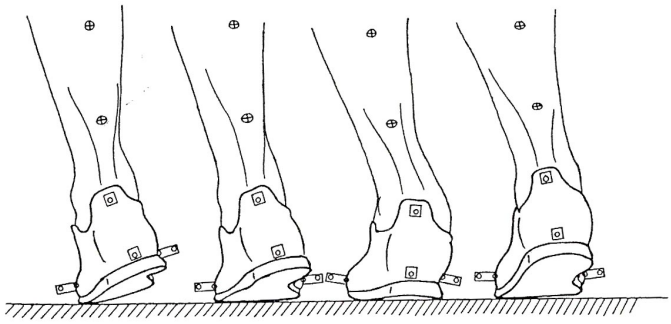

Figure 1.7 Stacoffs rearfoot motion model. Illustration from Stacoff [191] with permission.

applying force to the bone structure of the cadaver feet, representing the influence of the body on the foot, and by activating a selected number of muscles. To almost all bones in the cadaver feet, four markers are attached rigidly and directly. With this set-up, the researchers were able to describe motion between most foot bones during simulated gait. Naturally, healthy individuals can not be subjected to measurements where bone pins are used. Therefore, we believe that in the near future motion analysis on healthy individuals will be directed towards both a standarisation of multiple foot models and incorporation of these motion models into a multiple-segment model for the whole body.

Foot Models

Besides foot motion, there exist models of the foot, or parts of it, that are not related to measurement of motion directly. The interaction of the plantar surface of the foot, the fat pad, with the ground has been studied ([72], [75], [137], [118]). For this kind of modelling, the researchers use previous and present research regarding the mechanical properties of these fat pads. The heel fat pad is a topic that has been thoroughly looked at from a material point of view ([200], [2], [36], [108], [141]). Both the stress-strain relationship and the deformation during different activities have been reported in literature. Another type of modelling started from anthropometrical measurements together with motion and force data in order to construct a geometrical model of the foot ([183], [143], [144], [38], [6], [7], [101], [182]). These models were used to calculate

internal loading of bones, and moments around joints . The use of a geometrical model to simulate motion is found in the work of Anderson and Pandy [4, 2001]. Their model consists of a two-segment geometrical foot model, but with the plantar interaction with the ground described by a separate viscoelastic model. We were unable to find other multiple-segment geometrical models of the foot, or parts of it. In the present study, we will introduce geometrical models of parts of the foot that simulate motion.

After the description of foot kinematics (foot motion models) was introduced, research was oriented into a few directions. First, the description of foot kinematics in a variety of conditions was described. Second, the impact of structural and functional foot characteristics on motion and loading of the foot was described. From the description of kinematics of the foot, we come to the description of pressure underneath the foot. The plantar pressure loading characteristics were measured with plantar pressure measurement devices and they are the topic of the next section. We have described the research in the area of plantar pressure measurement in a different section since the use of a pressure plate system is crucial for the simulation of motion from our models. Specifically, our models use the pressure distribution as only input to simulate foot motion.

1.2 Pressure Plate Related Research

Historical Pressure Research

All papers on plantar pressure research we were able to find, were written within a period of 33 years. The first publication was by Hutton and Drabble on "an apparatus to give the distribution of vertical load under the foot" in 1972. Consulting the literature list of this publication and other publications, the first paper on pressure plates is credited to Elftman in a publication dating back to 1934

However, measuring pressure with a pressure plate was not the first quantitative measurement of pressure on the plantar side of the foot. The French scientist Etienne Jules Marey (1838-1904) was responsible for the first measurement of pressure underneath the foot. He invented shoes with air chamber combined with a pneumatic recording device, see Figure 1.8. This being only one of his many inventions and research projects, he is recognised as the person who brought biomechanics out of the observational era and into an era of quantification ([28] and [154]). Besides studies using the plantar pressure plate, we will discuss studies using an insole pressure mea-

surement system also.

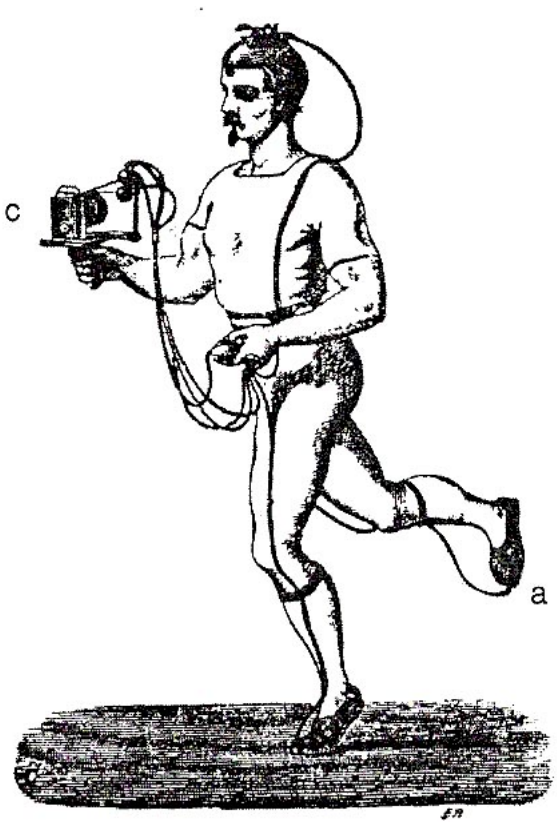

Figure 1.8 Marey's pressure measurement device. Illustration from *Biomechanics of the musculoskeletal system* from B.M Nigg and W. Herzog with permission.

The remainder of this section is divided in two parts. The first part describes the trends in research from the literature from the first article of Hutton and Drabble to the research in present days. The second part describes plantar pressure research closely related to our research project.

General Trends in Plantar Foot Pressure Research

The early publications about pressure measurement research is characterised by many papers reporting on new devices ([99], [85],[1], [50], [29], [18], and [102], [69], [9], [162], [86], [30], [207]. [96]). In general, the articles describe the technical evolution of pressure distribution measurement from visual techniques to systems that are able to determine pressure distribution numerically. Lord [119, 1981] describes in a review article most of these early pressure measurement devices, covering the developments from Elftmann in 1934 until 1981. Lords publication differentiaties three measurement technologies, namely direct print, visualisation techniques, and force plate or load cell systems.

The direct print technique is based on an imprint of the foot on a certain material (for example inkt on paper, or indentations on aluminum foil). The imprint is not dynamical and illustrates the pressure distribution during the complete stance phase as one distribution. Most of the imprint techniques are used to asses foot structure and peak pressure, where the peak pressure is only known qualitatively. One development by Grieve (cf. Lord, [119]) made it possible to quantify the compound pressure distribution.

The visualisation techniques are different from the direct print technique in the sense that they are able to visualise the *dynamic* pressure distribution. Most of the visualisation techniques use photography or video systems to record instantaneous pressure distribution. Some of these techniques were quantified such that numerical values of the pressure distribution could be recorded. The visualisation of the pressure distribution was instant, but the data processing time to obtain numerical pressure distributions was rather long. Cavanagh et al. [29, 1980] called the work involved unacceptably laborious.

The force plate or load cell systems are different from the other two techniques primarily because the technique is not visual or optical in nature. These techniques all use load cells to register pressure. Some systems combine a force plate with a switch box such that the instantaneous contact area is known (Draganich et al. [50, 1980]), other systems use smaller loading cells combined in a rectangular grid structure such that the contact surface is discretised. Although visualisation of the foot is not possible or, because of the size of sensors, not very accurate, numerical data are almost immediately available for analysis.

Many more reviews describing plantar pressure measurement technology followed:

Hughes et al. [95, 1987], Roy [180, 1988], Alexander et al. [3, 1990], Schaff, [185, 1993], and Cobb and Claremont [37, 1995]. The review of Alexander et al. [3, 1990] addresses the evolution of plantar pressure measurement techniques and clinical findings. They discuss more than six techniques to measure pressure. The pressure plates based on measured pressure within a transducer matrix are discussed starting from a plate no larger than 25cm by 17cm to the development of a commercial pressure plate (EMED SF system, Novel company) of size 27.4cm by 48.8cm with 2 sensors per cm^2, measuring at 70Hz. In the section on clinical applications a number of topics are discussed. Besides the diabetic foot and the rheumatoid foot other foot disorders and their effect on plantar pressure are described. The section on foot disorders is similar to Lord's review (Lord [119, 1981]) with the benefit of discussing nine extra years of research. Besides the above mentioned topics, the authors describe normal walking, running, and the effects of shoe wear and immoblisation devices. The section on normal walking mentions the "normal" path of the CoP including the moments of acceleration and deceleration. It also mentions the time points of peak pressures and impulses (=pressure-time integrals) underneath different areas as a percentage of contact time. Some implications are mentioned with respect to aging: collapse of the longitudinal arch. In the section on pressure measurement in shoes, the use of shear transducers by Pollard et al. (in Alexander, [3, 1990]) was discussed. Both shear components are maximally underneath the metatarsal heads and are less present in the hallux. The heel pad is subjected to a small amount of medial shear force.

In these reviews, we notice a shift from methodology of pressure measurement technology to its use in clinical and research environments, see the review of clinical findings by Lord et al. [122, 1986]. This was largely credited to the introduction of micro computers and commercial available systems ([122], [215], [3]).

Shifting the focus from methodology to application, it is necessary to obtain physical quantities from pressure data. A logical first step is to divide the plantar pressure distribution into areas of interest for the purpose of research. Usual areas of interest are

1. Rearfoot
2. Midfoot
3. Forefoot.

4. Medial and lateral rearfoot
5. Medial and lateral midfoot
6. Medial, central and lateral forefoot.
7. Five metatarsals (or their heads)
8. Hallux
9. Lesser toes as one area
10. Lesser toes as four separate areas

Examples of division of the complete area in subareas, also called masks, are given in Figure 1.9 and Figure 1.10. In the first figure, we illustrate masks of plantar pressure distribution data using a pressure plate. The second and third picture depict two masks of the complete pressure distribution with different complexity. In most studies were pressure plate measurements were involved these types of masks were used. Mostly, automated software was used to place the mask. In most cases, it is possible to correct the automatic placement manually. The third picture of Figure 1.9 shows a different kind of masking. In contrast to the complete masking in the other two cases, this mask is local. Such a local mask is useful for local loading characteristics of structures of interest. In comparison, a complete mask will also contain these foot structures of interest, but since larger areas are taken into account the pressure underneath these structures is mostly underestimated. In Figure 1.10, the two top pictures illustrate examples of insole masks. These masks are easer to construct since the outline of the foot is predetermined by the insole. The last picture in Figure 1.10 illustrates again a pressure plate mask. Although, this picture depicts a toddlers plantar pressure ([78]), we will use this picture in the discussion of related physical quantities.

We did not find studies that researched the effects of pressure variables quantities with respect to subarea definitions. Most papers did not reveal the determination criteria on which the proposed mask was based.

Having defined a mask for the plantar pressure distribution, the next step is to introduce pressure related quantities using data from the subareas defined by the mask. Given a mask, the most obvious quantity is pressure in time underneath each part of foot determined by the mask, see Figure 1.11. In the literature, we found the following extensive list of variables:

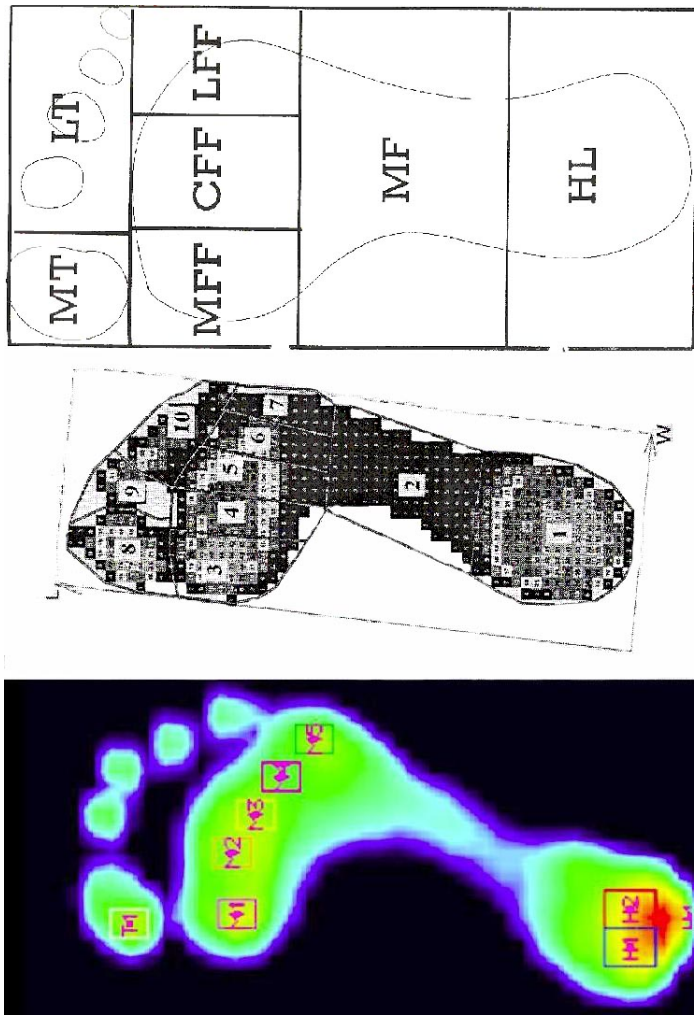

Figure 1.9 Masks used with pressure plates. Illustrations from Kernozek and LaMott [109], Hayafune et al. [84], and De Cock et al [48], all with permission.

1. For the trivial mask (complete foot) the following quantities:

   (a) *CoP path and its location.*
   The Centre of Pressure (CoP) path and a foot axis are illustrated in the

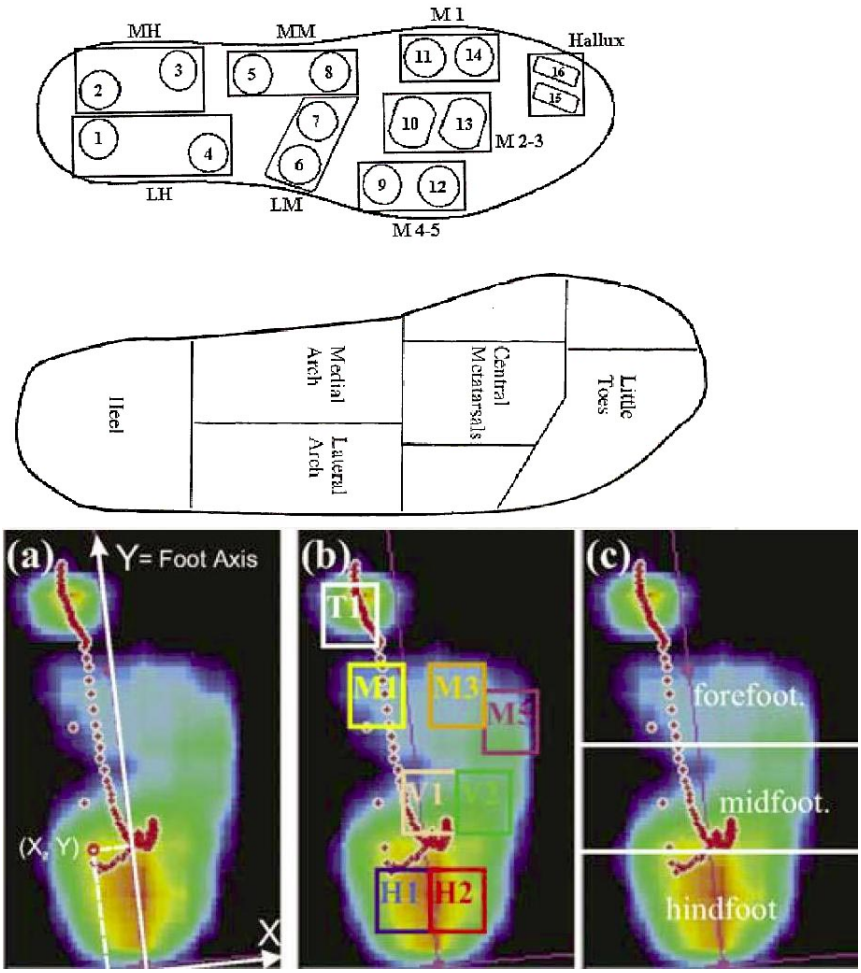

Figure 1.10 Masks used with pressure insoles and masks used for toddlers. Illustrations from Burnfield et al. [23] and Hallemans et al. [78], all with permission

last picture of Figure 1.10. Location of the CoP path is mostly expressed with respect to this axis and the one perpendicular to it. Distance to the foot-axis, maximum distance to a foot-axis, range of distance around the foot-axis, anterior-posterior distance changes at certain time instances or

in certain time interval are used as variables.

(b) *CoP velocity.*
The same variables as for the CoP path and its location are used.

(c) *Integrated CoP with respect to a foot axis.*

2. For any mask, the following quantities:

(a) *Duration of the stance phase and contact times of the areas of interest.*

(b) *Size of the contact area at a certain time point and maximum size.*

(c) *Local peak and mean pressures underneath areas of interest.*

(d) *Local peak and mean forces underneath areas of interest.*

(e) *Time until local peak pressures are attained.*

(f) *Time until local peak forces are attained.*

(g) *Maximum loading rate of areas of interest.*

(h) *Time to maximum loading rate of areas of interest.*

(i) *Pressure-time integrals in areas of interest.*

(j) *Force-time integrals in areas of interest.*

(k) *Ratios.*
One local pressure divided by another (or the sum of some local pressures divided by the some of others), or relative pressure-time integrals by dividing a pressure-time integral by the sum of all pressure-time integrals, etc.

(l) *Differences.*
In this more recently used quantity, pressure values from certain locations are subtracted from other pressure values at other locations.

One further distinction can be made between variables that use absolute values and variables that are normalised.

In Appendix A, we describe some studies using pressure distribution. The topics are very diverse and therefore, we classified the articles described in this appendix using the following topics: high heels, methodology, insoles, running, diabetic feet, infants and young children, therapeutic shoes, miscellany, databases, structure and function, hemiparetic patients, and the foot as a sensory organ. Besides the diversity

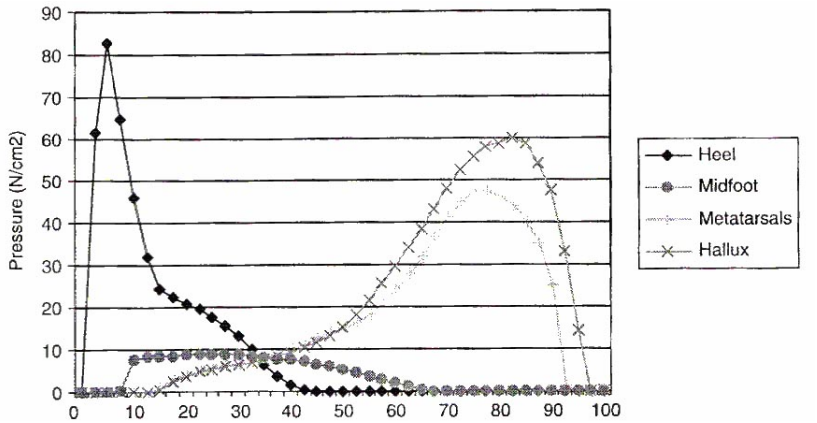

Figure 1.11 Example of pressure-time curves in subareas of the plantar pressure distribution from Hallemans et al. [77] with permission.

of the topics, miscellany is in itself even more diverse. The studies ranging from leg length discrepancies (D'Amico et al. [45, 1985]) via patients after rotationplasty (Hillmann et al. [88, 2000]) to the comparison between two different military boots (Arndt et al. [11, 2003]) show the diversity of research using pressure measurements.
In contrast to the abundance of studies that employed plantar pressure distribution data as a research tool, very few are relevant to our particular research project. The ones that were relevant, are discussed in the next section.

Plantar Pressure Research related to our Research

The literature on plantar pressure research does not contain many reference to dynamical mechanical models that use plantar pressure plate measurements as only input. The closest to mathematical modelling using data from a pressure plate system was the publication of Hansen et al. [81, 2004]. Instead of a pressure plate, they used a force plate and used resultants CoP paths as input data to their model. The CoP path can be obtained from a pressure plate system also. The CoP data was simultaneously recorded together with Motion Analysis System (MAS) data of the foot, the lower leg, and the upper leg in the sagittal plane. The authors refer to the work of Perry [163, 1992], who described the function of the ankle-foot complex as a three-rocker system. First, the heel rocker is active during the stance phase until the forefoot fully contacts

the ground. Second, the ankle rocker is active from forefoot contact until heel lift and third, the forefoot rocker is activated from heel lift until foot-ground contact is lost, see Figure 1.12. The authors in this study describe the CoP path in the sagittal plane of the foot, which is called the roll-over pattern. These patterns are given for the time period starting at heel impact and ending at contra-lateral heel impact. Within the foot reference frame, circular fits were calculated for these CoP paths normalised to individuals length. The authors propose to use these roll-over patterns in the design of prosthetic foot and lower limbs. Regarding our research, the roll-over pattern could be of interest in modelling the heel, see Figure 1.13. The pattern itself indicates the geometrical structure needed in the model. This study is two-dimensional and therefore the geometrical structure relates mainly to the dorsal flexion/plantar flexion of the heel and not to the other two planes of motion including the frontal plane with the important calcaneal inversion/eversion motion. Hansen et al. used the CoP path of the complete pressure distribution underneath the foot. In case of the heel, it is more appropriate to use a local CoP path for the heel rocker, calculated on an area containing only the heel, or to limit the time interval from heel impact till forefoot contact.

In a study by Jacobs [101, 2001], a static model of the first and second ray was combined with pressure plate measurements and anthropometrical data to determine forefoot forces involved in obtaining sagittal plane equilibrium. The time point in the push off phase is the moment at which the second force peak in the vertical ground reaction data appeared. Pressure data from a previous study by Jacobs and co-workers (Hayafune N., Hayafune Y., and Jacobs [84]) was used as external force input to the model. The internal musculair and bony forces were calculated with these external forces and with the anthropometrical measurements obtained from eight fresh, cadaver, unpaired feet of unknown origin. Although this study is important and continues on the ground breaking research of Stokes et al. [194, 1979], we will not be able to use its result since we are interested in a dynamical model.

As Jacobs, Gefen et al. [67] studied internal muscular and bony forces and stresses using pressure plate data. In contrast to Jacobs, they recorded simultaneously plantar pressure data and motion data using digital radiographic fluoroscopy. Both data sets were used in calculating the previously mentioned forces and stresses in the foot with a finite element solver. Gefen's model is three-dimensional in nature with material properties of both skeletal and soft tissue components. This study is of interest for our

Figure 1.12 The three rockers of the foot. The first row depicts the heel rocker, the second row depicts the ankle rocker, and the third row depicts the forefoot rocker.

research because both motion and pressure were measured simultaneously. However, the paper of Gefen et al. does not reveal any details on how measurement devices were integrated. The authors did not indicate the precision of determining the position of the pressure measurement system with respect to the motion analysis system. Also,

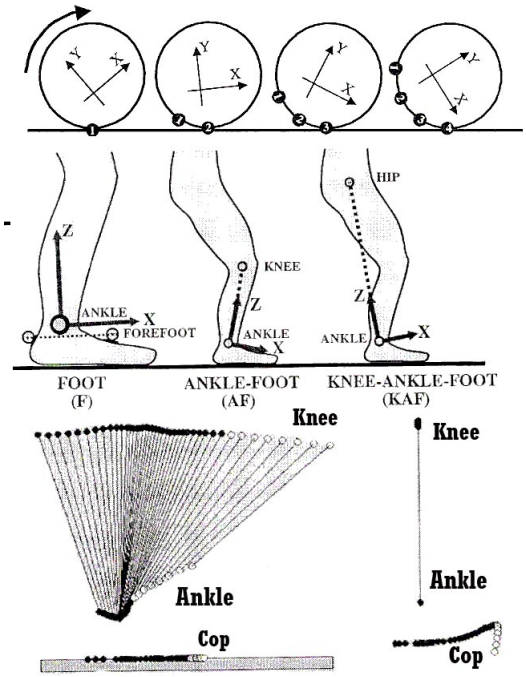

Figure 1.13 Ideas of roll-over shapes. The first row depicts the idea of the roll-over shapes and the connection with the CoP path in the global reference frame and the CoP path with respect to a local moving reference frame. The second row depicts the local reference frames of foot, ankle-foot, and knee-ankle-foot. The third row depicts an example of the lateral knee and ankle marker in the sagittal plane together with the CoP path in the global reference frame. Also in the third row, the CoP path is depicted in the local reference frame of the knee-ankle-foot system. Illustrations from Hansen et al. [81, 2004] with permission.

timing effects such as synchronisation of both devices are not discussed. The use of Gefen's foot model in our research is not possible due to the geometrical complexity they put into the model and the use of digital fluoroscopy as input.

In the methodological orientated paper of Giacomozzi et al. [70, 2000], plantar pressure, force and body-segment kinematics were measured in an integrated measurement set-up. They used a five-segment model containing the shank and four foot segments. All data was measured with a measurement frequency of 100Hz. The pres-

sure plate, 0.4m by 0.6m; sensor size 5mm by 5mm, was rigidly connected to a Kistler force platform of the same dimensions, which was used also to dynamically calibrate the pressure plate. According to the abstract of this article, the authors validated both spacial alignment and time synchronisation. Spacial alignment effects between the three measurement devices were studied using a point loading test. This test involved a volunteer performing an inverse pendular movement with a 1.5m metallic rod that had a sharp tip acting on the centre of a circular steel plate with a diameter of 34.5mm. A cluster of four markers was fixed about half way on the metal rod. Five trials were performed for each of the five selected locations on the combined platforms. The displacements of all three measurement devices for a given location were studied as a measure of accuracy. We think that this did not prove the accuracy of the devices, but rather their repeatability. Another spatial alignment test was the X-ray superimposition in which the pressure plate was superimposed on an X-ray film cassette. The authors concluded that from a qualitative point of view, there is good agreement between pressure distribution and anatomy, meaning highest pressures correspond quite well to relevant foot joints. Besides validation of spacial alignment, the authors also proposed a subdivision of the plantar surface on the basis of the motion trajectories of the markers with a criterion based on the z-components of these markers. This is the first article we came across that describes simultaneous registration of force, plantar pressure, and motion with different measurement devices and different registration devices. The registration devices are the computers that are integrated to form one functional integrated unit for the sake of measurement. Hence, the internal clocks of these devices should be synchronised such that the on-set of measurement is the same for all devices. Moreover, all internal clocks should have equal accuracy. Although mentioned in their abstract, we were not able to trace results of any type of synchronisation validation in their paper. Finally, Giacomozzi et al. briefly addressed the correctness of the force signal when a pressure plate functions as medium between force platform and foot. They only reported a decrease in frequency response of 5.5% .

However, the question remains if the force signal being measured in such a set-up is accurate enough. This particular problem was addressed in more detail by Cornwall et al. [40, 1995]. Overall, the authors concluded that both the vertical ground reaction force and the plantar pressures can be reliably measured with a combined plate system. Besides this topic, Cornwall et al. simulated anterior-posterior shear at the time point

of maximum plantar pressure using the combination of peak vertical force, time to peak pressure, and stance duration ($R = 0.77$). Therefore, both studies, Giacomozzi et al. and Cornwall et al., addressed a number of methodological issues regarding the integration of force, pressure, and motion in one measurement. An extra in the latter study was the simulation of foot characteristics, namely anterior-posterior shear force, from pressure plate measurements.

In a follow up study by Stebbins et al. [193, in press], the integrated measurement set-up of Giacomozzi et al. was used to introduce an automated division of the plantar pressure distribution into five sub-areas. The division method was found to be reliable for feet of healthy children. Following up the study by Cornwall et al. Cordero et al. [59, in press], addressed the temporal simulation of ground reaction forces using pressure distributions from insole measurements. Thus Cordero et al. were able to simulate ground reaction forces and its application points. Their method is applicable to inverse dynamics analysis without any constraints on foot placement.

The studies by Giacomozzi et al. and Stebbins at al. are the only ones we found in which force, pressure, and motion were measured simultaneously. MacWilliams et al. [128, 2003] did measure all this three quantities but not in an integrated fashion. Pressure and motion were measured simultaneously, and force and motion were measured simultaneously. A force signal was matched to the trials containing pressure and motion such that the stance phase in the force signal was closest to the average stance phase of the five pressure plate trials. Using interpolation, the force signal was adapted such that it could be used in combination with all pressure plate trails. The pressure distribution data was measured with an Emed system running at 50Hz and was subdivided into six areas. The medial and lateral shear forces and free moments from the force plate trial were distributed over these six areas in proportion to the normal force in each area at each time frame. A lower-leg model with nine foot segments was developed in the BodyBuilder software of Vicon where local forces and free moments were combined with kinematic data. The goal of MacWilliams study was to provide normative data for foot joint angles, moments, and powers during gait of adolescents (age between 7 and 16 years). The overall conclusion of this study was that single link models of the foot significantly overestimate ankle joint power during gait. The results of this study should be interpreted with some caution. It is a serious shortcoming that not all measurements were integrated. Moreover the distribution

of the shear forces and free moments over the six areas was directly based on the proportion of percent normal force in these areas. In a study by Perry et al. [164, 2002], sensors measuring both plantar pressure and shear forces of diabetic individuals were used. These sensors were part of a plate measuring with a frequency of 37Hz. One of Perry's conclusions was that peak shear and peak pressure did not occur at the same time point. We conclude that the coupling between shear force components and vertical force components is not as suggested by MacWilliams et. al, therewith influencing all kinetic results of their study.

In 2004, Imhauser et al. [100] combined pressure and motion measurement in an in-vitro study. They studied the effect of posterior tendon dysfunction on the plantar pressure characteristics and on the kinematics of arch and rearfoot. From the methodological section of this paper, it remains unclear how the measurement devices interacted in measuring both pressure underneath the foot and three-dimensional motion of parts of the foot. The established link between the magnitude of muscular/tendon loading and the position of the CoP is noteworthy. Imhauser et al. found a highly dependent relationship between these two parameter. They concluded that the posterior tibialus tendon is a strong invertor of the subtalar joint when ligaments preventing a flat foot deformity are intact.

In a study by Chang et al. [32, 2004], motion and force were measured simultaneously. They also measured pressure, but the paper does not reveal if this was measured in an integrated manner. With motion and pressure measured in this study, a relationship between a foot axis determined on the basis of motion data and one determined on the basis of pressure data was found. Although the specific procedure of determining the foot axis using motion data was not disclosed and determination of the foot axis in the pressure data was performed manually, a significant correlation of $r = .92$, $P < 0.001$ was found.

In a study by Cornwall et al. [43, 2003], the CoP path was quantified in two ways by the lateral-medial area index and by the lateral-medial force index, with adequate between-trial-reliability. For this quantification study, an experiment was set up including 105 individuals that underwent the measurements. From these 105 individuals, 30 individuals returned for a second experiment where rearfoot kinematics (foot with respect to shank) were measured. The quantities related to the second experiment were the eversion angle at heel impact, the range of eversion, and the maximum value of eversion angle. In this experiment, pressure and motion were not

measured simultaneously, but the data-sets per individual were combined to see if relationships between the CoP quantities and the rearfoot kinematic quantities exist. Cornwall et. al. concluded that such a relationship did not exist, stating "... the idea that the CoP pattern is representative of rearfoot motion is too simplistic. ..." . The latter is in contradiction with a direct relationship between CoP and rearfoot motion presented in this thesis.

Although Rosenbaum et al. [179, 1994] measured motion and pressure simultaneously while the individuals walked at three velocities, they did not look into possible relationships between both sets of data. Only an indirect relationship was found between medialisation of the loading pattern underneath the foot, and a more pronounced pronation motion indicated by increased eversion of the rearfoot. Rosenbaum et al. emphasised the need for controlling and monitoring walking speed when comparing foot loading characteristics of different groups of subjects.

The specific and general literature suggests a lot of work was done in the field of foot modelling and pressure measurement. The combination of the two fields has not yet been investigated to its full potential. Yet, the combination of measurement devices in an integrated set-up to measure human locomotion has till now not drawn the attention of a large number of researchers. To be able to study foot modelling based only on pressure measurements an integrated measurement set-up of force, pressure and motion is a first necessity. The way we dealt with the problems accompanying research in this field, and what the specific objectives were of our project are formulated in the next section.

1.3 Objectives and Strategies

The main objective of the our research project is the design of a mechanical model to simulate and characterise foot motion based solely on input of plantar pressure distribution measurements.

Especially in clinical settings, acquisition of information on foot motion by using a pressure plate measurement system is extremely useful. Advantages are both in cost and use. The direct method of measuring motion is using a Motion Analysis Systems (MAS). Such MAS system is much more expensive than a pressure plate system, and its use demands more technical abilities and is more time consuming than a pressure

plate system. Apart from the highly educated technical operators, time is required in setting-up the system, measurement registration, and data processing. All this could be avoided if a pressure plate system would yield the same information as MAS. However, pressure plate systems do not measure motion directly. Thus, extending the possibilities of a pressure plate system such that characteristics of foot motion can be determined would be a great step forward in clinical gait analysis. It would enforce the use of pressure plated in clinical settings.

In our research, we choose the following strategy : We designed a large scale experiment involving 126 individuals. The experiments resulted in a database containing integrated force, pressure and motion data.

The experiment was designed to meet the following objectives:

1. *Description of heel motion from pressure plate measurements validated by MAS measurements.*

2. *Description of forefoot motion from pressure plate measurements validated by MAS measurements.*

3. *Description of the motion of the first metatarsophalangeal joint from pressure plate measurements validated by MAS measurements.*

4. *Description of the connection between rearfoot and forefoot.*

Objective one and two have been accomplished and objective three has been accomplished partly. Objective four could not be achieved within this project.

In accomplishing the first objective, we determined the motion of a general rigid body rolling over a rigid plate by making use of the differentially geometry concept of curvature tensors linked to the contact path between body and ground. For the contact path, we used an adapted CoP path. The CoP path was calculated from the plantar pressure distribution for any given trial by determining that area within the distribution that only contained the heel. Subsequently, we determine the CoP of the pressure distribution of the heel at every instance of time. An adaptation of CoP paths should be calculated because soft tissue structures around the calcaneus are not of uniform thickness. We discovered that this adaptation was not an individual

characteristic. As a rigid body, we used a sphere. From the data, we determined the optimal radius of the sphere to by 7cm for the whole population. Hence, the radius of the sphere was also not an individual characteristic. For validation, we compared motion of the sphere using pressure data with the exact motion of the heel as found from measurements with a motion analysis system. For the description of the motion, we choose an angular representation decomposing the motion into plantar flexion/dorsi flexion, calcaneal inverion/eversion, and abduction/abbduction. The rearfoot model describes up to 75% of the motion patterns, accurately, for the period starting at heel contact and ending at forefoot contact. We conclude that the rolling motion of a rigid sphere with a 7cm radius over a rigid plate is an acceptabel model for the motion of the heel.

For reaching the second objective, we determined the motion of the metatarsal heads. Using MAS, we measured motion of metatarsal heads while they were in contact with the ground. This motion was so small that it was not significant for the pressure measurements, it was in the order of the dimension of a pressure sensor. In 97.7% of the trials, the position of the metatarsal heads during motion was contained in a 90% covering circle with a diameter less than two times the length of a pressure sensor diagonal. We conclude that metatarsal motion can not be observed by a pressure plate with the presently used resolution.

We determined the metatarsal curve from the position of the metatarsal heads in the pressure data. The position of this curve was validated by MAS using markers attached to metatarsal heads one and five, and one marker attached between metatarsal heads two and three. This metatarsal curve determined a contact curve. Thus, we proposed a mechanical model for the forefoot that consists of a bend cylinder with an contact curve equal to the metatarsal curve. The size of the radius of this cylinder was determined by the rolling motion of this cylinder describes the rotation of the foot about the metatarsal heads and the rolling motion was contained within the two lengths of a pressure sensor diameter.

As for the third objective, the research is in a preliminary stage. We know already that there is a strong correlation between certain pressure variables and certain motion variables, all related to timing aspects.

1.4 Thesis Organisation

As any thesis in the field of biomechanics, also this thesis starts with a description of methodology, which can be found in Chapter 2. Our measurement methodology is not an integrated one in the sense that in the laboratory set-up pressure, and force and motion were measured simultaneously. One of the sections of Chapter 2 describes general data processing, and in particular considers the following topics: coupling of devices, data accuracy, and construction of local reference frames.

In the Chapters 3, 4, and 5, for convenience of the reader, we summarise aspects of measurement set-up and conclusions from Chapter 2. Thus, these chapters become self-sustained.

Chapter 3 contains a mechanical model of heel motion. The model is based on the fundamental law of kinematics; pressure distribution underneath the heel area is the only input to simulate heel motion. The model is validated with motion analysis data.

In Chapter 4, we introduce the metatarsal curve, which connects the metatarsal heads. The position of this curve is determined from pressure distribution data. Validation is performed with motion analysis data. The concept of a metatarsal curve suggests a mechanical model, an inverse arch, for the forefoot. We describe this model and its motion characteristics at the end of this chapter.

Chapter 5 contains a statistical analysis. We investigate the relationships between motion related variables of the first metatarsophalangeal joint and pressure related variables. These pressure variables are related to a division of the foot into elven subareas.

The focus of our study is on the existence of relationships between pressure data and motion data. Overall conclusions of our study are presented in Chapter 6. With this we conclude the main body of the thesis.

The thesis is accompanied by four appendices, which contain lots of side information. In the first appendix, we present details about plantar pressure literature. The other three appendices contain additional information of Chapter 2, 3, and 4, respec-

tively. Besides results, these appendices contain detailed descriptions of the database structure enabling any researcher in the field to access this database. Thus, we include a detailed explanation how the measurements were registered and processed, and we discuss the database structure, the data structure of database entries, and the Matlab applications that were designed for processing the data.

Computational Details

All computations were performed in the Matlab 6.5 environment on a Dell Inspiron 4150, Intel Pentium 4 processor 1.8GHz with 512Mb of RAM, running the Windows 2000 professional operating system.

Chapter 2

Methodology

In the first section of this chapter on methodology, we describe in detail the experiments. In the second section, general data processing is described. In the section on experiments, the topics are experimental design, measurement statistics, measurement devices, measurement protocol, and measurement data description. In the section on general data processing, we reveal how the data were integrated into one database. For this, we needed to establish a coupling between the two main sources of data, namely, the pressure distribution data and the kinematic data. To characterise the data limitations, we discuss the quality of the measured data. Subsequently, this quality was enhanced by filtering and interpolation. The section also contains the division of the stance duration in foot phases, and selections of local reference frames and orientations.

The overall goal of this chapter is two-fold: (1) discussion of all necessary steps to be taken before the data can be analysed, and (2) construction of a data set that is publicly accessible.

2.1 Experiments

2.1.1 Experimental design and statistics

Finding foot motion characteristics and constructing models based on these characteristics require a variety of locomotion conditions (here: normal walking, fast walking and running) to be measured. This variety makes it possible to formulate motion characteristics that are specific for a certain condition, and enables showing limitations of

a certain characteristic with respect to different locomotion conditions. Furthermore, generalisation of foot motion characteristics across conditions can be validated with this approach.

We employed three distinct session types to measure a variety of locomotion conditions. The first type consisted of a walking condition in which the individual performed 20 trials; ten with the left foot in contact with the ground, and ten with the right foot. The velocity of walking was self-chosen and was assumed to be an individual's "normal" walking pattern. Normal walking is simply called walking in the remainder of this chapter.

The second type consisted of a walking and running condition in which the individual performed 20 trials in total: ten walking trials at a self-chosen velocity, and ten running trials set at a velocity of 12km/h (an average of 12.0km/h with a standard deviation of 0.5km/h). In both conditions, the ten trials were split up into five trials for the left foot and five trials for right. The order of conditions was always first walking and then running.

The third type consisted of a walking condition, a fast walking condition, and a running condition. During this session, fifteen trials were measured, left foot only. The trials were split into three times five trials representing, walking, fast walking, and running, performed in this order. Again, walking velocity was self chosen and running was set at a velocity of 12km/h (an average of 12.1km/h with a standard deviation of 0.4km/h). The fast walking velocity was calculated from the walking condition. It was taken to be 25 percent faster than the mean velocity during walking within a average bandwidth of 0.4km/h. We measured the left foot only in order to limit the duration of the measurement sessions to be about equal to the duration of the other two. Consequently, in planning the measurements a priori knowledge of the measurement session was not necessary since all sessions had equal time slots.

Equal measurement time duration enabled at random assignment of individuals to different types of measurement sessions. In our experiments, we measured 126 individuals in total, according to a fixed measurement protocol, see Section 1.2.4. They were equally divided over the three measurement sessions: 44 individuals performed the first session type (walking), 40 individuals performed the second (walking and running), and 42 performed the third (walking, fast walking and running). In total, data of 2310 trials were registered. From these trials, only 47 failed to meet the criteria

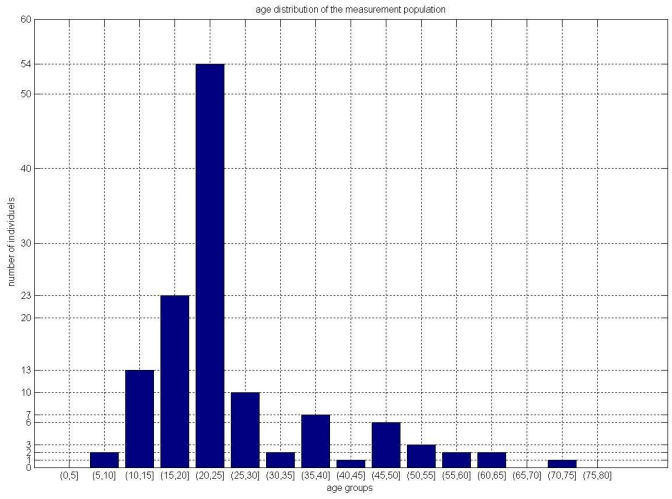

Figure 2.1 An overview of the age distribution within the measured population

of acceptance due to a number of errors (see Appendix B.3 for a detailed list of the errors). This led to a trial drop out of about 2.0%.

Out of the 126 individuals 78 were male and 48 were female, which led to a division of 61.9% male and 38.1% female. The age distribution is presented in Figure 2.1.

Students from the Vrije Universiteit Brussel, in the age groups (15,20] and (20,25], constituted the larger part of the population.

The performed measurements were non-invasive in nature and therefore complied with university guidelines. All individuals gave their consent prior to the start of their measurement session.

2.1.2 Measurement Devices

The devices used in this research project were a motion analysis system, a plantar pressure plate system, a force plate, and a velocity measurement system. In this subsection, the details of these devices are given.

The Motion Analysis System (MAS) was a 612 system from Vicon. This system consisted of the following parts: a central computer/processing unit, M1 cameras, a

sixteen bit 64 channel analogue box, an L-frame, a calibration wand, and software applications. The central processing unit connected the computer of the experimenter to the Vicon system. The connection was made through Ethernet cards and a cross link cable. From the central processing unit all cameras were attached in groups of three with a maximum of four groups and therefore of twelve cameras. The unit contained also different types of connecters to interact with measurement devices that are not connected to the analogue box. The interaction was primarily used to share time points such as start and end points of measurement.

In the present set-up, six cameras were used. The measurement frequency of these cameras can be set to 60Hz, 120Hz, and 250Hz. In this study, we used the maximum frequency of 250Hz for the following reasons: First, feet undergo a rapid change in motion pattern from full swing to zero velocity for those parts in contact with the ground. To measure this interaction accurately, a high measurement frequency is helpful. Secondly, the measurement frequency of the cameras is half of the maximum frequency of the pressure plate running at a frequency of 500Hz. Foot motion characteristics will be based on relationships between plantar pressures data and kinematic data. Therefore, the higher the frequency, the more data are available for stance duration. The decision to take a high measurement frequency costed a drop in camera resolution, from 1024 by 986 at 60Hz to 663 by 547 at 250Hz. To counter this problem, the cameras were placed as close as possible to the measurement object, see Figure 2.2

The analogue box, in the present set-up, was used to register the data from the force plate (eight channels). With the Vicon software application Workstation, theedimensional data were measured, processed, and exported to an ASCII format.

The plantar pressure plate system was a 1m by 0.4m pressure plate from RSscan, see Figure 2.3. It contained 8192 pressure sensors of size 3.5mm by 3.5mm that were arranged in a rectangular grid. Except for the sensors at the edges, all centres of the sensors were spaced equally in the length and width direction of the plate. The spacing in the length direction was 7.62mm and in the width direction 5.08mm. The maximum measurement frequency of 500Hz with a maximum measurement time of two seconds was set. The sensors measured the pressure perpendicular to the plate by differences in current resistance. This relationship is nonlinear and the loading and unloading curves are not the same and change with sensor material aging. The non-linearity of this relationship resulted in slightly lower precision in determining lower pressures

Figure 2.2 The camera set-up around the coupled plate system

values.

The pressure plate was attached to a data box called the 3D-box. During a measurement, this box registered and, subsequently, sent the data to the connected computer. Besides a data buffer, the 3D-box was used to register force plate data using its eight bit analogue to digital converter running at the same frequency as the plate. Finally, the 3D-box contains three connectors and one FM antenna to interact with other measurement devices. This interaction was focussed on synchronisation of the starting time point of measurement with the Vicon systeem.

Footscan software version 6.42 was used to register the data and to export the data to an ASCII format. Another important usage of the application was continuous calibration of the total vertical force registered by the pressure plate at every measurement time point by using the total vertical force of the force plate at that time point.

The force plate system is a 0.9m by 0.6m three-dimensional force measurement system from Kistler containing four piezo crystals, see Figure 2.3. The crystals were

Figure 2.3 The coupled plate system. A one meter pressure plate is attached to a 90cm force plate. The L-frame in the left lower hand side is used to unify the local reference frames of the force plate and the motion analysis system.

arranged symmetrically around the centre of the plate at the four corner points. The measurement data of the force plate were divided into eight analogue force channels: four for the z-direction, two for the y-direction, and two for the x-direction. All eight analogue channels were individually connected to a charge amplifier. The signal from the eight charge amplifiers was split into two identical signals. One set ran through summing amplifiers preserving three analogue channels as output: the total force in the x-, y-, and z-direction. These channels were connected to the 3D-box of the Footscan systeem that registers the data using an eight bit A/D converter at a frequency of 500Hz. The other set of eight channels was connected to the analogue box of the Vicon system that registered the data using a sixteen bit A/D converter at a frequency of 1250Hz.

The average velocity measurement system contains two pairs of infrared photo cells. The two pairs were placed as two gates perpendicular to the runway, connected to an electronic timing box. The box registered the time that a subject spent between the two gates. Since the distance between the gates was set to 3m46, we were able to calculate the average locomotion velocity of the subject in this interval. The height of the cells was adjusted to the individual's height such that the shoulder or the head of the individual intersected with the infrared rays. We choose for head or neck because no other body segments intersect the rays during locomotion.

2.1.3 Integrated Measurement Set-up

The runway was the central part of our measurement set-up. All other devices were either integrated, such as the force plate and pressure plate, or strategically placed around it. All measurement activities, in this case, walking, fast walking and running, were performed on the runway. It is 19m00 in length, 1m10 in width, and 0m11 elevated from the laboratory floor. It is made out of a wooden body with a top-layer of sport tapestry taped to it.

The runway itself was divided into three areas: the preparation area (10m90), the recording area (1m36) and the deceleration area (6m74). The preparation area was used to accelerate to a stable motion pattern. Subsequently, this stable pattern was measured in the recording area that contains all measurement devices. After the measurement was registered the individuals decelerate in the third area such that they were able to change direction and return to the preparation area.

Integration of force plate and pressure plate was established by removing part of the runway such that the force plate fitted in this part without being in contact with the runway. The borders between runway and force plate were in the order of a few millimetres. Subsequently, the pressure plate was attached to the force plate such that it fitted on one side and hing 0.1 metre over on the other side. However, it was not in contact with the floor, being at a distance of about 2mm above the wooden part of the runway. The top layer of both pressure plate and runway were at the same level constituting an integrated system on which individuals perform their trials.

The cameras were positioned around the combined plate system such that their angular spacing was almost homogeneous, see Figure 2.2. All cameras were focussed on a measurement volume with the combined plate system in the middle. In practice, the volume contained the combined plate system and a height of about 40cm above the plates. The chosen measurement volume was about 90cm by 60cm by 40cm.

The average velocity measurement system was placed in the recording area such that one gate was positioned before the pressure and force plate, and the other was placed behind the plates.

The motion analysis system and the pressure plate system were synchronised through a coax cable between the J2-connector of the Vicon processing unit and the trigger-in-connector of the Footscan 3D-box. At the moment the Vicon system started measuring, it connected both wires in the coax-cable such that the voltage dropped to zero instantaneously. The 3D box used this time point of instant voltage drop to start the pressure plate measurements. Only, the average velocity measurement device was not connected in any way to one of the other devices.

2.1.4 Measurement Protocol and Measurement Data Description

Before measurement started, each individual was given an explanation of the study, first on the objective, thereafter, more detailed on the measurement set-up and measurement protocol. The latter was envisaged in order to give an individual a clear understanding about the nature of the measurements in which they were involved. During these explanations, the individual was informed about the number of trials and about the specific session type that would be undertaken, see Section 2.1.1.

The explanation was given during marker placement. Preceding this step, the individuals were asked to remove socks and shoes and free the lower limb of any cloth. In some cases, this meant changing into shorts (in case running was involved) in others it meant pulling the trousers up to around the knee (in case only walking was involved). To be able to attach the markers to the feet in a precise and repeatable manner, the individual was asked to stand on top of a table. In this case, we could attach the markers in a controlled environment at eye level.

To one foot, twelve markers were attached. Selection of the marker positions was related to the following anatomical structures:

1. four markers on the calcaneus,
2. three markers on the hallux,
3. one marker on the base of metatarsal one,
4. one marker on the base of metatarsal five
5. one marker on the head of metatarsal one,
6. one marker on the head of metatarsal five,
7. one marker between the heads of metatarsal two and three.

The three markers that were used to track the motion of the hallux were attached to a rigid marker plate. In turn, this marker plate was fixed to the skin of the hallux. The same is true for the four markers on the calcaneus. Two sizes of marker plates were available for both the calcaneus and the hallux. They were derived from the feet of a man with size 44 and a woman with size 38, both European size.

Figure 2.4 illustrates markers and marker plates attached to an individual foot. The marker plates for the hallux could be used for all individuals measured. This in contrast to the heel marker plates, which did not fit all individuals because of the smaller size of their heels, predominantly in younger and female individuals. In this case, four markers were attached to the heel in the following configuration: two markers were placed on the most bony part of the heel (medial and lateral), one was placed on the intersection of the Achilles tendon and the calcaneus, and one was placed a few (more than four) centimetres above the intersection but still on the Achilles tendon. The previous set-up resembled the marker set-up of a heel marker plate and its

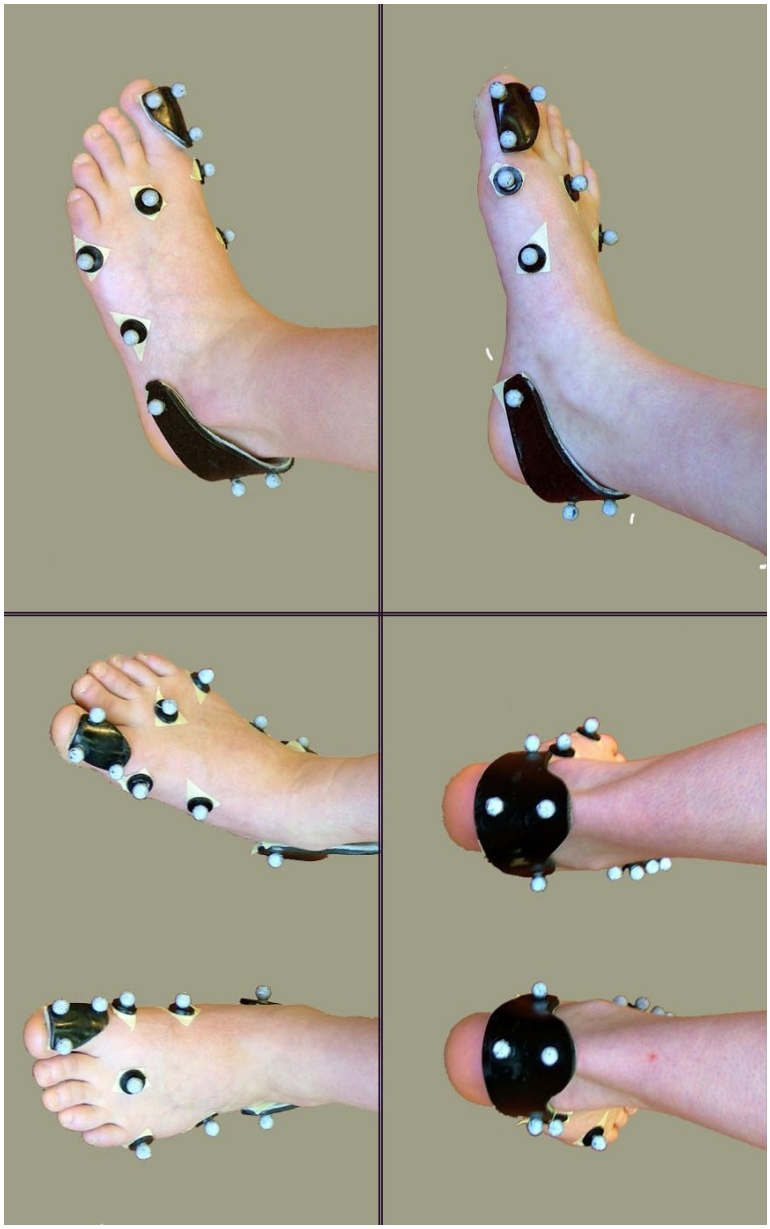

Figure 2.4 An overview from four sides of marker placement.

attachment to the heel. The hallux marker plates were attached such that the length direction (proximal-distal direction) of the hallux coincided with the medial proximal and medial distal marker of this plate.

After the markers had been attached, the individual was taken for a static measurement trial. During this static trial only the position of the markers were registered in order to be able to establish the local segment reference frames with respect to this static position. A static trial was taken with the individual in a relax stance with the knees extended and feet slightly in exo-rotation.

A familiarisation process was the next, and final, task before measurement registration started. In this process, the individuals were trained to place one foot on the coupled plate system with their eyes fixated at a selected point on the wall at the end of the runway.

Placement of the foot on the coupled plate system was important since all measurement devices were set-up such that this specific area was optimally covered. Foot placement in the middle of a plate does not sound like a natural thing to do during walking down a runway at a self-chosen velocity. The natural walking pattern of an individual is altered into a kind of targeting pattern when the foot must be placed on a pre-determined position. To avoid this targeting kind of behaviour, four numbered lines were used as starting positions for the walking and fast walking condition, and four other lines for the running condition. All lines consisted of white sticky tape and were placed perpendicular to the direction of progression. The distance from line one, the one closest to the plate systems, to the middle of the force plate was 4m45 in case of the (fast) walking condition, and 8m69 in case of the running condition, see Figure 2.5. Mutual distance between the lines was 0m25.

While the individuals performed their practice trials, we checked the position of their feet with respect to the ideal position in the middle of the force plate. The numbered lines were used to adjust the position of the individual's foot on the plate. After several practice trials, the individuals felt adjusted to the testing environment and testing condition. This process was repeated for all different conditions within one measurement session. Figure 2.6 illustrates a walking trial.

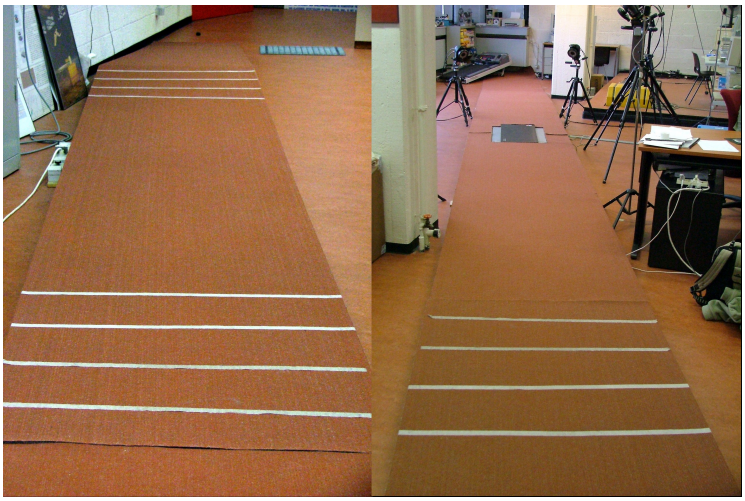

Figure 2.5 The runway: on the left hand side the first half and on the right hand side the second half.

After this familiarisation process, the measurements of the dynamic trials started. During the dynamic trials, we operated two computers connected to the motion analysis system and the pressure plate system such that both registered the trial. After a trial, the force plate was reset and the time duration between the two gates of infra red photo cells was written down on the personal information sheet of the individual.

Besides the time durations, the personal information sheet contained the individual's name, measurement date, weight (measured in the biomechanics laboratory), shoe size (European), age, and gender. Also, it contained two anthropological measures: maximum flexion in the first metatarsophalangeal joint and the width of the calcaneus. Maximum flexion was measured in accordance with the directions given by Root et al. [177, 1971]. Calcaneus width was measured with a sliding calliper at the smallest width in the saggital plane and midway in the posterior-anterior direction of the calcaneus.

A more extensive and visual description of the preliminary and dynamic measurement steps can be found in Appendix B.

After the measurement session ended, data of the session was stored at the work-

Figure 2.6 An example of a walking trial

station of the Vicon system and at the workstation of the Footscan system. Before actual data processing could take place, pre-processing steps were undertaken. In the Vicon system, the markers were labelled such that the relationship between marker and anatomical position was established. In the next step, marker paths and force plate data were exported to an ASCII file for analyses. From the way the vicon database was set up, all trials exported from the Vicon system had a basic file structure with the extension 'csv'.

For the Footscan system, pre-processing entailed exporting plantar pressure data and force plate data, into files with an ASCII file format. The data were exported into four files per trial containing the total pressure distribution during the stance phase, the pressure distribution aggregated over the stance phase, the force plate data during the stance phase, and the force plate data during the complete measurement time of a trial. The extensions of these trials are 'dyn', 'max', 'Fs', and 'Fv, respectively. The extensions are presided by a basic file structure expanded with the symbol 'L' or 'R' just prior to the trial number in case of a left or right trial.

We present an example of a complete exported data set for individual Joe Black, trial 10, left foot:

Vicon system	**Footscan system**
'Joe Black 10.csv'	'Joe Black L10.dyn'
	'Joe Black L10.max'
	'Joe Black L10.Fs'
	'Joe Black L10.Fv'

For the detailed structure of these files, we refer to Appendix B

The measurement data of an individual that was used for further analysis contained all export files of all trials in a single directory named after the individual. The personal information sheet of an individual was converted to useable digital form in Matlab. For every individual, there are fifteen fields:

LastName:	'Black'	
FirstName:	'Joe'	
Age:	30	in years
ShoeSize:	44.5	in European size
Weight:	103	in kg
MTPH:	[76 84]	in degrees
Calc:	[51 49]	in mm
Aver_Times:	[1x20 double]	in ms
Org_ReTest:	1	
HeelCup:	1	
Failed:	[ ]	
Remarks:	[ ]	
M_Data	[25 3 2004]	
Session:	'wandelen lopen'	
Gender	'M'	

The Matlab environment is used to further integrate all trials of one measurement session into one matlab m file. The structure of such an m file is identical for all individuals. Coupling the measurement database with the personal information database helps in accessing all information of one individual. The exact details of this database such as the definition of the entries of the fifteen fields (MTPH means first metatarsophalangeal joint) are found in Appendix B.5. A copy of the database is freely available for every researcher working in the field of foot mechanics.

2.2 General Data Processing

2.2.1 Kinematic and Pressure Measurement Data Coupling

Synchronisation

In the present set-up, three measurement devices were connected. The force plate was connected to both the Footscan system and the Vicon system. In turn, both systems were connected through a so-called synchronisation cable; from Vicons' J2 connector to the trigger in/synch in coax port of the Footscan system.

The time synchronisation of pressure data with force data, and motion data with force data was performed in the respective systems. Both systems register this com-

bination of data (either force and pressure, or force and kinematics) with their own internal clock as time reference. To be able to synchronise the two systems at the start of measurement, a signal (TTL) was send from the Vicon system to the Footscan system. However, we were not sure about the delay on this channel, and about the accuracy and stability of both internal clocks.

To asses synchronisation of the systems through the J2-coax cable, we used the vertical force registered in both systems. The force plate supplied analogue signals to both systems, continuously. In turn, the systems used their individual A/D converters to store the information in digital form. In case of the Vicon system, the force data was converted at a measurement frequency of 1250Hz with a sixteen bit converter. The force data was obtained from eight channels, two channels for the x-component of the force, two channels for the y-component, and four channels for the z-component. The channels of the z-component of the force have an accuracy of about 0.15N per bit (16bit over a range of 10.000N is 10.000N/16bit$\approx$ 0.15N per bit). This means that the bit noise of the vertical component of the force was about 0.60N. The Footscan system converted the force data at a measurement frequency of 500Hz with an 8-bit converter. In contrast with the Vicon system, the force data in the Footscan system was obtained from one channel per force component. The footscan system was set to a maximum vertical force component of 3000N, which resulted in an accuracy of 11.70N per bit. In Figure 2.7, we have depicted vertical force curves from an arbitrary trial as registered by both systems.

To compare two force signals from one arbitrary trial, we introduce a measure for signal correlation (SC). Let $\mathbf{x}$ and $\mathbf{y}$ represent two signals with $\mathbf{x}$ and $\mathbf{y}$ in $\mathbb{R}^n$ and signal length n. We take the natural measure for signal correlation:

$$SC(\mathbf{x},\mathbf{y}) := \frac{(\mathbf{x},\mathbf{y})}{\|\mathbf{x}\|\,\|\mathbf{y}\|} = \cos\angle(\mathbf{x},\mathbf{y}). \tag{2.1}$$

The meaningfulness of this measure follows from the following orthogonal decomposition:

$$\frac{\mathbf{y}}{\|\mathbf{y}\|} = \frac{(\mathbf{x},\mathbf{y})}{\|\mathbf{x}\|\,\|\mathbf{y}\|}\frac{\mathbf{x}}{\|\mathbf{x}\|} + \left(\frac{\mathbf{y}}{\|\mathbf{y}\|} - \frac{(\mathbf{x},\mathbf{y})}{\|\mathbf{x}\|\,\|\mathbf{y}\|}\frac{\mathbf{x}}{\|\mathbf{x}\|}\right) \tag{2.2}$$

According to the Cauchy-Schwartz inequality

$$\forall_{\mathbf{x},\mathbf{y}\in\mathbb{R}^n} \quad -1 \leq SC \leq 1. \tag{2.3}$$

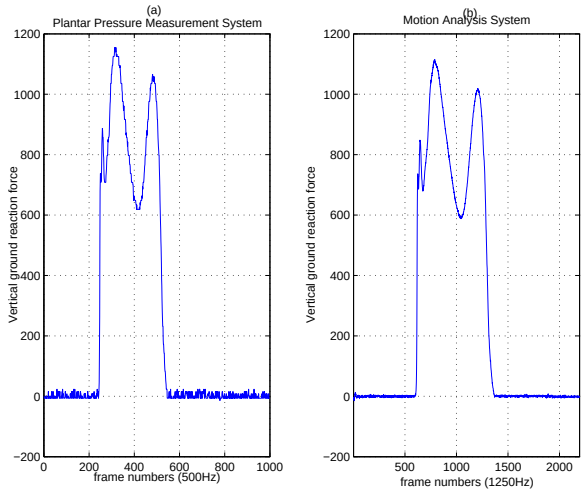

Figure 2.7 An example of vertical ground reaction force of an arbitrary trial registered by (a) the pressure plate system, and (b) the motion analysis system

The closer SC is to 1, the better the signals $\mathbf{x}$ and $\mathbf{y}$ are correlated. It is not hard to see that SC is one only if $\exists_{\lambda>0}\ \mathbf{y} = \lambda\,\mathbf{x}$, which means a perfect correlation.

The above measure is integrated in a Matlab application, see Appendix B.4.2, to calculate signal correlations between the force signals for all trials in our population. We studied the effects of a delay in starting time and accuracy of the internal clocks. We down sized the force plate signal from 1250Hz to 250Hz in case of the Vicon system, and from 500Hz to 250Hz in case of the Footscan system. We performed time shifts on the MAS force signal and adjusted for length. The time shifts were performed in an interval from 80ms before to 80ms after the starting time point of measurement as determined by MAS. The size of this interval, 160ms, was chosen such that it is about one fourth of an average stance phase. Therefore, we believed the size of this interval to be large enough to detect any trends in signal correlation. A typical SC time shift curve is depicted in Figure 2.8.

The results of this synchronisation test were: (1) in all trials the highest SC value was encountered at the zero time shift level, and (2) the average SC was .9992 with a standard deviation of .0029. Before we draw conclusions from these results, we con-

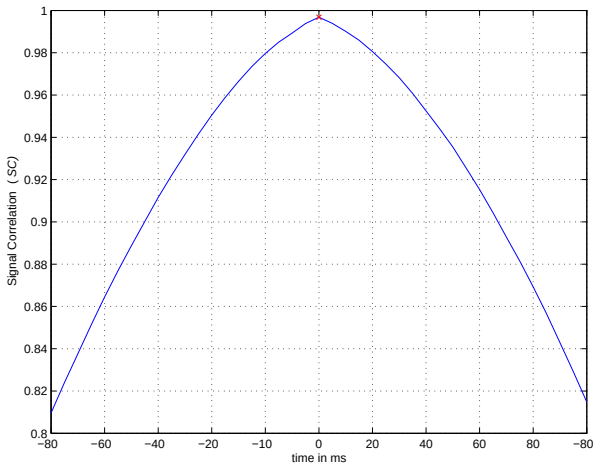

Figure 2.8 An example of a typical SC curve is depicted for two vectors where one vector undergoes time shifts in the interval [-80ms,80ms]. The signal correlation is highest in the case of no time shifts with a value of .997.

sider an another test that analysed differences of begin and end time points of the stance phase between the two force signals .

The beginning and end of the stance phase in terms of a vertical ground reaction signal are traditionally calculated by applying a threshold scheme. The logical assumption is that there is an occurrence of contact between foot and force plate if the force plate registers a value beyond a certain force level. The vertical ground reaction force has a steep ascent, see Figure 2.7, such that the true signal changes more rapidly and with a higher amplitude than the noise does. This determination of the beginning of the stance phase can be achieved by applying a threshold scheme. Also, the end of the stance phase was determined with a threshold scheme. Although, the descent of the vertical force signal is usually less steep than the ascent. Therefore, the noise level does play a role here. We designed a threshold scheme using thresholds from 30N up to 200N with 1 N increments.

Begin and end time points were calculated for these 171 thresholds, for both vertical force signals, and for all 2263 trials. Subsequently, we calculated the differences between the begin points and the differences between the end points for all thresh-

olds. In Figure 2.9, we have depicted the results of these calculations. We see that the results are different, indeed, for the begin time point and the end time point. The mean curve of the begin time points has a lowest value of -1.02ms and a highest value of 0.66ms (see Figure 2.9 (b)). For almost all thresholds, the difference in begin time point is within a bandwidth of 4ms. In the present measurement set-up, the measurement frequencies were 250Hz, 500Hz and 1250Hz. This means a measurement every 4ms, 2ms and 0.8ms, respectively. We compared the signals with a frequency of 500Hz (PPPS) and 1250Hz (MAS force signal). We conclude that the 4ms difference in begin time point is within the accuracy of the slowest measurement device. For the differences in end points, the order is about double the order of the begin points; about 2 frames in the slowest measurement device. There is also a difference in trend; the curve of the begin points stays always close to zero, while the end points curve tends to zero.

From the two synchronisation tests, we conclude:

1. Both force signals have the same begin time point,
2. The end time point of both force signals is the same up to 2 frames in the slowest measurement device,
3. The signals have a high correlation; average .9992 with a standard deviation of .0029,
4. Signal correlation is at its maximum at zero timing shift between the signals, and this holds for all trials.

From conclusion three, it follows that the registered force signals are the same. By a combination of conclusions one, two, and four, we observe that no delays and no inaccuracies in internal clocks of both systems are found. Therefore, the overall conclusion is that the synchronisation procedure between MAS and PPPS is well performed. A counter remark to this conclusion is the sensitivity of these tests. Using techniques within matlab, we removed data at the beginning of force signals for PPPS data such that a delay effect was introduced. Also, we used a cubic spline to lengthen and shorten the stance phase. With these constructed signals, we found that the signal correlation test detects delay effects of 2ms (one frame at 500Hz) and detects frequency changes from 500Hz to 498Hz and from 500Hz to 502HZ. The signal correlation test is,

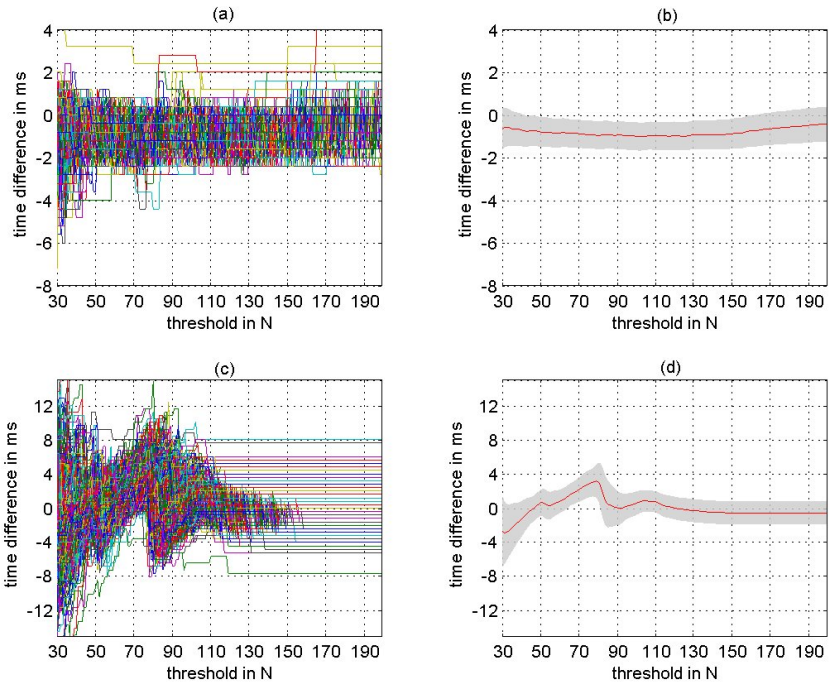

Figure 2.9 The differences in start time point of all trials (2263) between MAS force signals and PPPS force signals is depicted in (a) and (b). In (a) all trials are depicted and in (b) the average difference and one standard deviation curve are depicted. The difference in end time point are depicted in (c) and (d). In (c) all trials are depicted and in (d) the average and one standaard deviation are depicted

therefore, a sensitive test, which strengthens the above conclusions. A more extensive description of this sensitivity analysis is found in Appendix B.6.

Spacial Alignment

Besides synchronisation, we have to align measurement devices in space to be able to relate spacial information from one device to the other. In practice, this means that we have to know the relationships between the different local reference frames of three measurement devices, MAS, PPPS, and the force plate.

The relationship between the Local Reference Frame (LRF) of MAS and the LRF of the force plate are generally known by using a frame with markers. Also in our set-up such a frame, the L-frame, was used. Every measurement day began with placing the frame on top of the force plate in a prescribed manner (prescribed in the MAS manual), see Figure 2.3. A static calibration trial was performed within MAS that, in turn, led to the determination of the local reference frame of the force plate with respect to the LRF of MAS.

Since the pressure plate was taped to the force plate, the relationship between the LRF of the pressure plate and the LRF of the force plate remained the same during all measurement sessions. If the placement of the L-frame was performed in a repeatable and accurate way over all measurement days, then we needed to establish the relationship between the LRF's of MAS and PPPs only once. To check, if the placement of the L-frame was repeatable and accurate, we measured the coordinates of the four markers in 20 trials. We repeatedly placed the L-frame, registered the marker coordinates and removed the L-frame. Because of the construction of the L-frame, differences in placement could only arise from translation in the x- and y-direction and rotation about the z-axis of the global reference frame. For all trials, we calculated the translations and rotations and subsequently compared these values between trials.

The worst difference between trials in rotation was 0.70 degrees. This seems to be negligible, but recalling that the pressure plate is 90cm by 40cm, placed in the centre of the force plate, the error becomes worse when a foot is placed further away from the origin of the LRF. For example when a foot is placed in the middle of the force

plate, the rotation error (RE) for the sensor in the middle of the foot is

$$\begin{aligned} RE &= \begin{bmatrix} 350mm \\ 450mm \end{bmatrix} - \begin{bmatrix} \cos(0.70°) & -\sin(0.70°) \\ \sin(0.70°) & \cos(0.70°) \end{bmatrix} \begin{bmatrix} 350mm \\ 450mm \end{bmatrix} \\ &= \begin{bmatrix} 5.5mm \\ -4.2mm \end{bmatrix}. \end{aligned} \tag{2.4}$$

The first component of RE is the distance change in x-direction, the second element is the distance change in y-direction of this sensor.

The sensor in the top right corner of the pressure plate is susceptive to the largest rotation error. If the foot is placed in an area containing this sensor, the RE equals:

$$\begin{aligned} RE &= \begin{bmatrix} 550mm \\ 900mm \end{bmatrix} - \begin{bmatrix} \cos(0.70°) & -\sin(0.70°) \\ \sin(0.70°) & \cos(0.70°) \end{bmatrix} \begin{bmatrix} 550mm \\ 900mm \end{bmatrix} \\ &= \begin{bmatrix} 11.0mm \\ -6.7mm \end{bmatrix}. \end{aligned} \tag{2.5}$$

Next, the translation error of the origin of the L-frame was determined by the closest marker point to the origin. The worst case behaviour within 20 trials was

$$\begin{aligned} \Delta\text{x} &= 2.9mm \\ \Delta\text{y} &= 2.0mm \end{aligned} \tag{2.6}$$

Combining (2.4), (2.5), and (2.6), we find for the overal spatial errors:

$$\begin{aligned} & & \text{middle} & & \text{top right corner} \\ \Delta\text{x} &= & 8.4mm & & 13.9mm \\ \Delta\text{y} &= & 6.2mm & & 8.7mm \end{aligned} \tag{2.7}$$

The spacial error of the middle of the plate for the y-direction is within the measurement accuracy of the sensor length of the pressure plate (7.62mm). The error in the y-direction for the top right corner is almost within measurement accuracy. Regrettable, the errors in x-direction for both middle and the top right corner are significantly greater than the existing measurement accuracy (5.08mm). The top right corner has a spatial error in the x-direction of almost three times measurement accuracy.

We conclude that the errors are too great that one measurement does not suffices to determine the relationship between the LRFs of MAS and PPPS.

This problem had to be solved. An alignment measurement session before measurement started was introduced. The alignment session was performed on fourteen of the

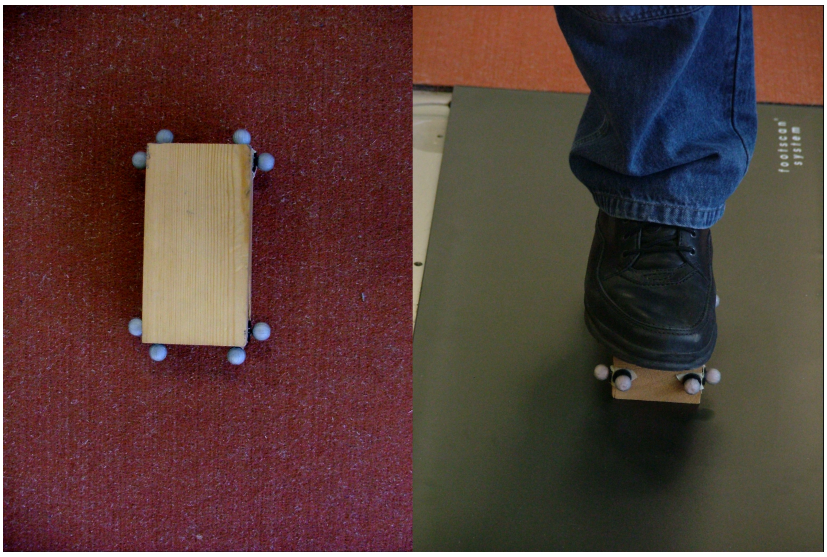

Figure 2.10 On the left hand side, a top view of the wooden block with the eight markers attached to it. On the right hand side, an example of an alignment trial

sixteen days of measurement. On March 23, 2004, we did not perform the alignment session, and on March 19, 2004, we decided to use the alignment information from the day before. An alignment session consisted of a minimum of five measurements trials with a wooden block placed at different positions on the plate, see Figure 2.10. This wooden block had two markers at every corner point on both connecting sides. The surface of the wooden block in contact with the pressure plate is 150.6mm in length and 79.0mm in width. During the measurements trials both the pressure imprint and the coordinates of the markers attached to the block are registered. A staff member balanced on top of the block during measurement registration to have a clear pressure imprint. With the use of the markers, the middle of the block was calculated during every trial within the LRF of MAS. The pressure measurement of every trial was also used to determine the middle of the block within the LRF of PPPS. The block placed completely in the second half of the pressure plate, had a different origin to express the data, than the block placed in the first half. Since the block was placed by hand, small rotations were introduced. To diminish the effect of these rotations on determining the relationship between the two LRFs, we chose the middle of the block as the point

used for comparison.

Using the middle points of the wooden block in the two LRFs in the different trials solved the problem of finding a relationship between the different LRFs. The relationship between the LRF of PPPS and MAS was expressed by a rotation about the z-axis and a translation in the x- and y-direction of the LRF of MAS. First, we looked at the rotation part. From the L-frame replacing test, we knew that the angle of rotation is in the order of one degree. Therefore, we chose a grid of minus three to plus three degrees with a step size of .1 degrees. For every grid point, we recalculated the centres of the wooden block from MAS data. Subsequently, the differences in x-direction and y-direction for every trial between MAS and PPPS were calculated. Ideally, the differences in the two directions would be the same for all trials. In practice, this was not the case. Therefore, we singled out the worst differences in x-direction, Δx_{worst} and y-direction, Δy_{worst}. For the y-direction we split up the data in a first half and second half part. The following measure was used to determine the variance of the difference:

$$Alignment\ Variance = \sqrt{\Delta x_{worst}^2 + \Delta y_{worst}^2}. \tag{2.8}$$

Calculating of (2.8) over the complete grid gave us an impression of the rotation that resulted in the smallest alignment error, called *Alginment Variance*, for a given measurement day. The assumption was that the grid is fine enough to visualise the minimum error. This assumption was verified by taking different step sizes. We found no differences in the measure for step sizes up to 0.01 degrees.

An example of the measure *Alignment Variance* for the chosen grid, March 30, 2004, is depicted in Figure 2.11. The depicted curve shows a global minimum at .8 degrees. The presence of a global minimum in the *Alignment Variance* curve is a feature we have encountered every measurement day. Table 2.1 contains the translation and rotation information for all measurement days. Also, the worst difference in x- and y-direction is given in this table. From Table 2.1, we conclude that most measurement days have worst case errors closely to, or below, pressure plate measurement accuracy. Greater errors are found on the 20^{th} of March, on the 3^{th} of April, and on the 5^{th} of May. Measurements of these days were not used for that type of research where alignment between PPPS and MAS is needed. Also, the 23^{th} of March is not taken into account because there was lack of alignment information. In total, 36 individuals are excluded from alignment studies, retaining 90 individuals. The table is included in the database such that an automated Matlab application is able to relate the spacial

Table 2.1 Accuracy of alignment. Column one contains the measurement data. Columns two, three and four contain the translation in x-direction, the translation in y-direction of the first half of the plate, and the translation in the y-direction of the second half of the plate. Column five contains the rotation about the z-axis. Columns six and seven contain the worst case difference in x- and y-direction from the wooden block alignement test

Date	Δx	$\Delta y_{1^{st}}$	$\Delta y_{2^{th}}$	rotation	Δx_{worst}	Δy_{worst}
March 18	151.0mm	36.8mm	524.5mm	-0.4°	3.4mm	5.1mm
March 20	141.4mm	45.3mm	538.2mm	1.5°	7.3mm	4.6mm
March 24	148.7mm	39.1mm	527.9mm	0.1°	3.3mm	5.2mm
March 25	151.4mm	36.8mm	526.8mm	0.1°	4.9mm	1.5mm
March 26	146.6mm	40.0mm	531.9mm	0.4°	3.6mm	5.9mm
March 30	145.4mm	41.2mm	534.7mm	0.8°	3.1mm	2.6mm
April 1	147.4mm	39.8mm	530.9mm	0.4°	1.7mm	3.5mm
April 3	139.6mm	42.0mm	535.2mm	1.4°	9.4mm	5.5mm
May 1	145.4mm	40.9mm	531.3mm	0.5°	4.3mm	3.2mm
May 5	145.3mm	39.5mm	530.7mm	0.6°	6.8mm	2.8mm
May 6	146.4mm	41.0mm	532.0mm	0.6°	3.5mm	6.5mm
May 7	158.0mm	33.7mm	521.3mm	-0.9°	3.8mm	4.2mm
May 8	142.9mm	39.9mm	529.5mm	0.7°	5.3mm	3.3mm
May 13	146.0mm	38.6mm	529.9mm	0.4°	5.4mm	5.5mm

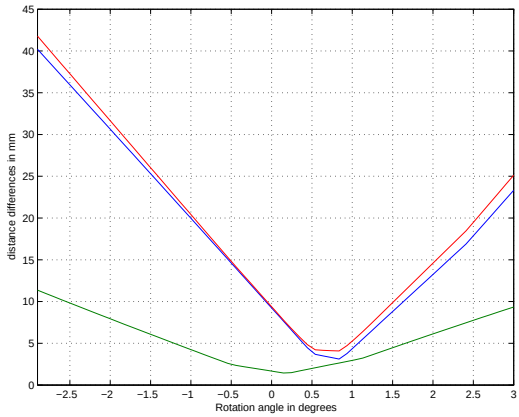

Figure 2.11 Determination of alignment. The blue curve represents the worst case difference in x-direction, the green curve represents the worst case difference in y-direction, and the red curve represents the measure *Alignement Variance*. A minimum for *Alignement Variance* is present at an angle of 0.8 degrees and has a value of 4.1mm

information of the two measurement devices to each other.

2.2.2 Data Accuracy

In the present set-up, we collected data from four devices and performed two types of anthropological measurement. Studying data from these sources, we found that it was important to know their accuracy. The accuracy of these data should be taken into account in sections on results, conclusions and discussions.

In this subsection, we discuss the limitations to the data-set. The emphasis is mainly on the kinematic data.

The first part of the data-set contains the anthropological measures. All anthropological measures were performed by one researcher such that there was no inter-tester variability. From Van Gheluwe et al. [201, 2002], it followed that inter-tester variability yields a higher error than intra-tester variability. So, one tester measures repeatedly and accurately, but measurements of different testers are not easily comparable.

The second part of the data-set contains the average locomotion velocity registered by the infrared gates and the electronic timing device. The electronic timing device measured time accurate up to a millisecond. The distance between the infrared gates was measured as 3m46.

A time measurement in ms, t, is converted into its mean velocity, v, by the following calculation

$$v = \frac{3.46}{t} 1000 \text{ m/s}. \tag{2.9}$$

This equation reveals that measurement errors in the distance between the gates are time dependent and decrease if the measurement time increases. Furthermore, it follows that measurement errors in timing are also time dependent and decrease with measurement time.

We assumed that we determined the length between the gates within a measurement accuracy of 2cm and the measured time with an accuracy of 2ms. The maximum velocity difference due to measurement inaccuracy is

$$VMA = \pm 0.01 \text{m/s}, \tag{2.10}$$

where VMA means Velocity Measurement Accuracy and where for t all values stored in the database were used. Therefore, VMA is the average measurement accuracy of all trials with a standard deviation of 0.007 m/s.

The third part of the data-set contains the force plate data. In the previous subsection, we described the consequence of an A/D convertor on the accuracy of the force signal. According to Kistler (from their manufactures manual), the error made during force plate measurement and amplifying the force signals is within three percent of the signal value at every measurement time point.

The fourth part of the data-set contains the pressure distribution data. Timing issues such as internal clock consistency and accuracy were already checked in comparison to MAS. A few issues remained: (1) accuracy and consistency of the pressure sensors, (2) accurate determination of the stance phase.

The pressure sensors themselves were continually calibrated during a measurement trial, see Section 2.1.2. However, this calibration is not done on an individual sensor, but on the sensors as a whole. We had no information about the sensor to sensor accuracy. The main question was wether all sensors measure pressure in the same

way, or wether sensors behave differently according to location. The manufacturer performs tests to establish a uniform measuring sensor array. However, in the tests we performed with the wooden block (see the previous subsection), we registered a diversity of non-uniform pressure distributions. Manufacturer tests would predict a uniform pressure distribution. Some explanations why we did not measure uniform pressure distributions are:

1. The wooden block did not have a completely flat surface;
2. The pressure plate is not completely flat;
3. The polymer on top of the plate did not have a uniform thickness;
4. The PPPS is not capable to register quasi-static pressure distributions accurately;
5. Sensors do not measure pressure data uniformly.

At the moment, we are not able to asses this aspect of the accuracy of pressure data.

As for the accuracy of determining the stance phase, the Footscan software application version 6.3.42. uses an algorithm to isolate the stance phase. A user has acces only to the stance phase as determined by this algorithm. An alternative is offered by the force plate signal that is exported from the measurement screen (see Appendix B) and can be assessed during the complete measurement time. Because an 8bit A/D convertor and a measurement frequency of 500Hz was used by the 3D-box, it is likely that the algorithm does not produce an accurate enough stance phase. Therefore, we compared the isolation of the stance phase by the Footscan software with the golden standard using the force plate data registered by MAS with a sixteen bit A/D convertor. To isolate the stance phase from MAS force plate data the following algorithm was used:

1. From the signal noise, the mean and three-times standard deviation were calculated.
2. The signal was corrected such that the average of the noise equaled zero.
3. Values above 100N were found. The first value in the signal above 100N and the last value above 100N were used as initial points.

4. From both initial points, the algorithm calculated backwards in time to the first time point that was underneath three standard deviations, and the algorithm calculated forward in time to the first time point that was underneath three standard deviations The points prior to these events were taken to be the start and end time point of the stance phase.

Figure 2.12 illustrates the difference in both begin and end time points of the third session type (walking/fast walking/running). All individuals for which all trials could be retained were used in this analysis. This entails a comparison of 170 trials for all three conditions. From this figure, we conclude:

1. Only little differences are found between the measurement conditions. The footscan algorithm is accurate in determining the stance phase;

2. The begin time point is determined accurately taking into account that the lowest measurement frequency is 250HZ;

3. The begin time point is determined more accurately than the end time point.

The above results indicate that the three different measurement conditions do not necessitate a different time handling of the data. Also, a time interval that starts at the beginning of contact has no significant loss of data due to the algorithm employed by the PPPS software application. A time interval that contains the end of foot contact may lead to loss of pressure data due to the employed algorithm. However, the impact of this data loss on results is dependent on the studied phenomena and therefore should be assessed for every situation separately.

The fifth part of the data-set contains the kinematic data from MAS. We studied the quality of this data set by performing two dynamic tests. Both tests involved checking the position of markers with respect to each other knowing that the markers were attached to a rigid structure and therefore should be at fixed distances of each other.

The first test was performed at the beginning of a measurement day (the same days as the spacial alignment tests were performed) and consisted out of six trials with a hand-like object, see Figure 2.13. With this object, the global foot motion during foot-to-ground contact was simulated, both three times for a right foot and three times for a left foot. The hand-like object had thirteen markers attached to it.

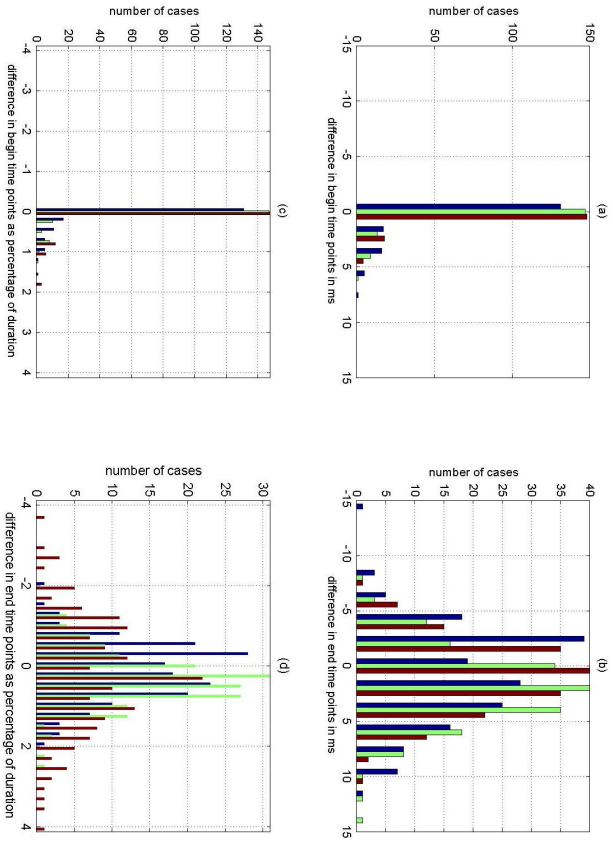

Figure 2.12 Differences in begin and end time points. The left-hand side, (a) and (c), depicts the difference in begin time point. The right hand side, (b) and (d), depicts the differences in end time point. The upper half uses a millisecond scale as value for these differences and the lower half uses percentage of stance duration as value for these differences. The conditions are expressed such that walking is depicted by the color blue, fast walking by the color green, and running by red

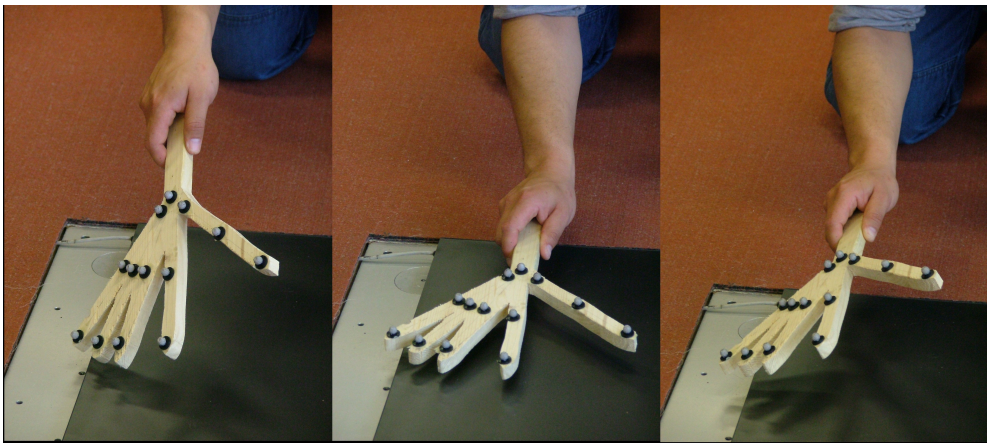

Figure 2.13 The hand-like object during a simulation of a right foot unroll.

Thus 78 combinations of two markers and therefore 78 distances should remain equal during measurement time. To investigate the extent to which MAS considered a rigid structure as being rigid, all simulation data were combined to one simulation of about 37 seconds. In Figure 2.14, we have depicted distance differences of the 90 percent confidence interval of pairs of markers. Since the marker distance data was not normally distributed, tested with the Lilliefors test at a significance level of 5%, a 90 percent confidence interval was used instead of an interval based on standard deviations. In the remainder of this study, we use the relationship, as depicted in Figure 2.14, to help distinguish between the motion of markers and possible measurement inaccuracies in motion patterns. For example, in studying the distance between the first and fifth metatarsal head marker, we neglect trends in distance changes during a chosen time interval, because they were smaller than the 90% range interval for marker pairs of that specific length.

Errors that occur in determining marker positions by MAS reflect on the calculation of segmental orientation in space. To study these errors, we again use the hand-like object. Angles were calculated from two vectors constructed from markers on the object. The top marker (at the root of the hand) was always included in the calculations. First, we looked at angles in the smallest possible triangle of this object. This triangle has the following 90% confidence intervals for the range of its three angles: 1.9 degrees,

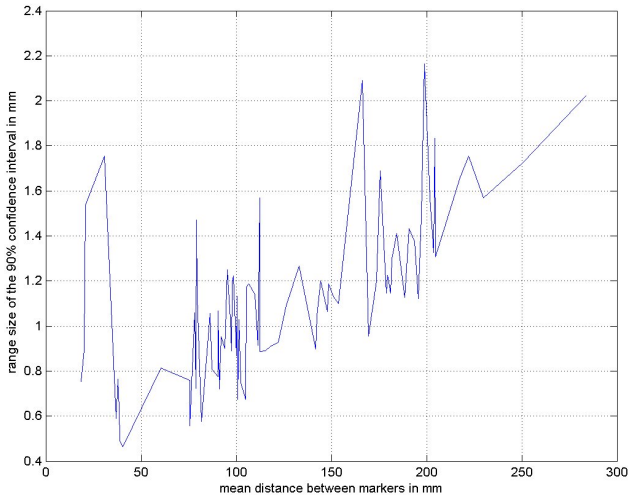

Figure 2.14 the relationship between distance between two 'fixed' markers and the 90% confidence interval describing distance changes

2.2 degrees, and 1.2 degrees. The respective average angles were 54.8 degrees, 91.3 degrees, and 33.9 degrees.

Since these angles were calculated using the cosine rule, characteristics of cosine influence angle calculations. This means that error calculations are stable in the neigbourhoud of 90 degrees and unstable in the neigbourhoud of zero degrees.

The characteristics of cosine do not explain the previously mentioned error ranges. The angle closest to 90 degrees has the largest error range. Another mechanism must be present. We put forward the following hypothesis: based on the discrete grid used by every camera to determine marker position, and given two vectors, the smaller the length of the shortest vector, the greater the error range becomes.

To test this hypotheses, we calculated the 90% confidence interval for the angle range in three cases. Calculations for the first case are already carried out, namely the case where the top marker and the two closest markers are taken. They have a mean angle of 91.3 degrees with a 90% confidence interval of 2.2 degrees. We follow the paths from the top marker to the two closest markers down the hand-like object such that we arrive at markers that are on the same 'finger'. The second case considers the top

marker and two markers on the 'midhand' and the third case considers the top marker and two markers at the distal digits. These cases resulted in an average angle of 89.8 degrees with 90% confidence interval for the error range of .3 degrees and .2 degrees respectively. In the three cases, the length of the vectors are 20.4mm and 31.2mm, 100.3mm and 109.8mm, and 201.7mm and 225.9mm, respectively. Although, we did not prove the hypothesis, we regard the findings as a trustworthy explanation of the phenomenon. In turn, this information will be used in the calculation of orientation as described in Section 2.2.5.

In studying the errors in segmental orientation, we looked also at the measurements themselves. In the marker set-up, we always used the hallux marker plates. These plates have a rigid structure with three markers attached to it. In the second test, we used these three markers and calculated again the 90% confidence interval of the angle determined by the two longest vectors, which have a length of 23.7mm and 33.8mm. From the data, we obtained an average angle of 43.6 degrees. Moreover, with the experimental measurement data, we were able to distinguish errors for all three locomotion velocities, and for left or right feet. Figure 2.15 shows the different error ranges. We used data from the walking, fast walking and running sessions, to distinguish between errors due to different locomotion velocities, and we used data from the walking sessions to distinguish between left and right.

In Figure 2.15, we did not depict four trials that showed an error range greater than 2 degrees (the greatest is a 3 degree range).

These calculated 90% confidence intervals left us to conclude that with increasing velocity the error becomes greater although not spectacular. In 96.4%, 95.7% and 80% of the cases the error range is less than 1.2° for the walking, the fast walking and the running condition respectively. So, even for the running condition a 1.2° range, as found in the first test, is still accurate for 80% of the cases. Corresponding percentages for the left and right walking trials were 92.2% and 96.9%. This emphasises that left and right feet were measured with the same accuracy.

The conclusion from the test with the hand-like object and from the hallux experimental data is that the kinematic data were obtained with high accuracy, and that we are able to distinguish stable motion characteristics from the measurement data.

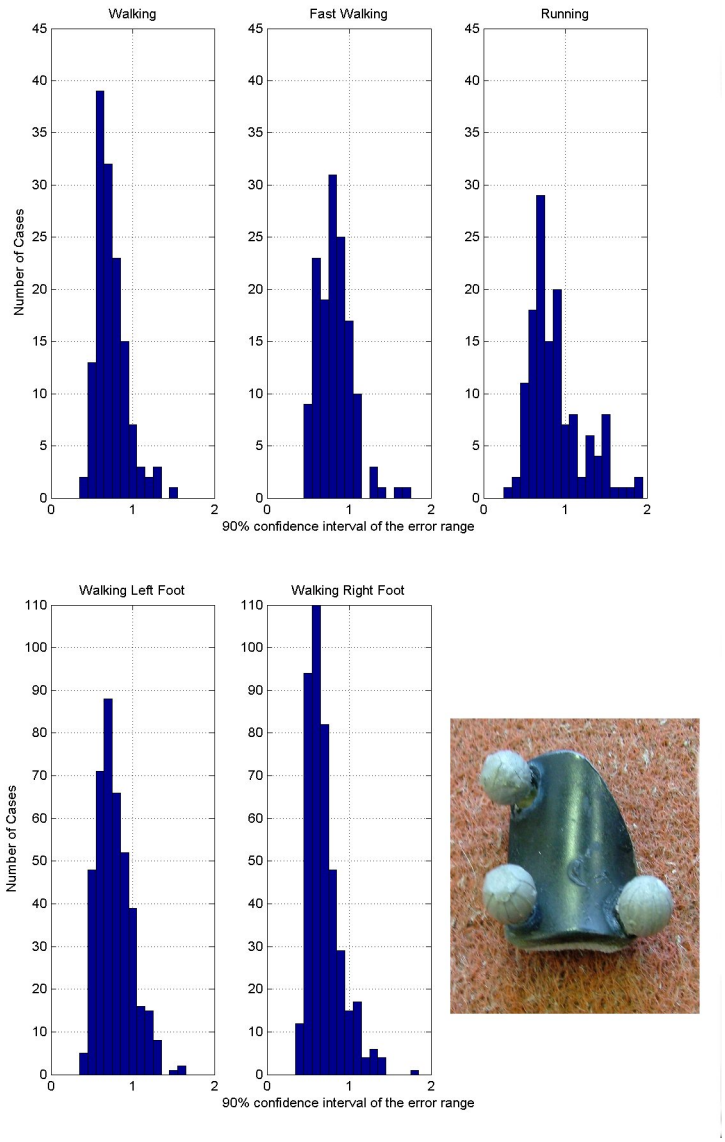

Figure 2.15 The distribution of the 90% confidence intervals of the error range. In the upper half of the figure, we depict trials from all three locomotion conditions. In the lower half of this figure, we depict the trials from the walking session split up into trials of the left and the right foot.

2.2.3 Filtering and Interpolation

In a study by Giakas and Baltzopoulos [71, 1997], different filtering an interpolation routines were studied for displacements, velocities, and acceleration of biomechanical walking data. They discussed the performance of six methods and concluded that there were three methods most appropriate for the given biomechanical walking data: the power spectrum assessment method [46], the generalised cross validation spline method [216], and the least squares cubic splines method [187].

In our study, the least squares cubic splines method was chosen for two reasons: (1) there is no difference in performance compared to the other two methods, and (2) this method is available in the Matlab environment.

2.2.4 Description of Foot Phases

Since the foot performs different functions during contact, the stance phase of both walking and running should be partitioned into four smaller phases. At the start of the stance phase, the foot acts as a shock absorber, then it is a stable almost non moving object and finally the foot acts as a propulsion device propelling the body into the direction of progression. In literature, all kinds of partitions of the stance phase are described ([163] and [210]). Most of the descriptions are based on a specific locomotion mode such as walking and running, or for a specific patient population such as cerebral palsy. The time points of the events determining start and end of these different phases are generally determined on the bases of kinematic information, not in the least using kinematic information of the contra lateral limb. As commended on by De Cock et al. [48, 2005], it is impossible to use kinematic information of the contra lateral limb to determine foot phases in running since a double support phase is not present. To be able to compare our three locomotion modes in our study, walking, fast walking, and running, we propose to use the same criteria for all these locomotion modes to partition the stance phase.

Instead of using kinematic information for the definition of events, we employed the use of plantar pressure distribution only. First, we must return to the central research questions stating: "find foot motion characteristics that can be measured by using a pressure plate system only". The definition of foot events and foot phases *are* foot motion characteristics. Thus, the use of these events and phases adds a new dimension to the study of plantar pressure foot motion characteristics. Second,

all events are described in terms of foot structures that are contacting or leaving the ground. A pressure plate gives the opportunity to measure foot structures in a specific and most direct way. All combined, it is logical to use plantar pressure distribution data to define key events of the stance phase.

We took the same foot events as in De Cock et al. [48]. In turn, they based their choice of events on the work of Winter [213] and Blanc et al. [20] Although, we use the same events as proposed by De Cock and her co-workers, we determined these foot events in a completely different way. De Cock et al. used a semi-automated method that placed eight sub-areas over seven anatomical structures (the medial and lateral heel, the metatarsal heads and the hallux) in the peak pressure footprint. The on-set and off-set times of these sub-areas (heel areas: 22.9mm by 15.2mm; metatarsal and hallux: 15.2mm by 10.2mm) were used to determine the events. Five events are used:

1. **First Foot Contact (FFC):** the first time point at which contact between foot and ground is established;
2. **First Metatarsal Contact (FMC):** the first time point at which contact between a metatarsal head and the ground is established;
3. **Fore Foot Flat (FFF):** the first time point at which contact between *all* metatarsal heads and the ground is established;
4. **Heel Off (HO):** the first time point at which the heel is no longer in contact with the ground;
5. **Last Foot Contact (LFC):** the last time point at which the foot is still in contact with the ground.

Illustrations of these events are presented in Figure 2.16.

We determine these key events differently.

For the first and the fifth event, we used the three times standard deviation criteria on the force plate signal as prescribed in Section 2.2.2. Results of De Cock and her co-workers and our results were both based on the same type of pressure plate. It was shown that FFC is the same for their method and ours. The time point of LFC can be different between the methods, as is already explained in Section 2.2.2.

For determining the HO event, we consider the foot as divided in a rearfoot area(heel area), midfoot area, and forefoot area. The HO is defined to be the time point at which there is no more pressure in the heel area.

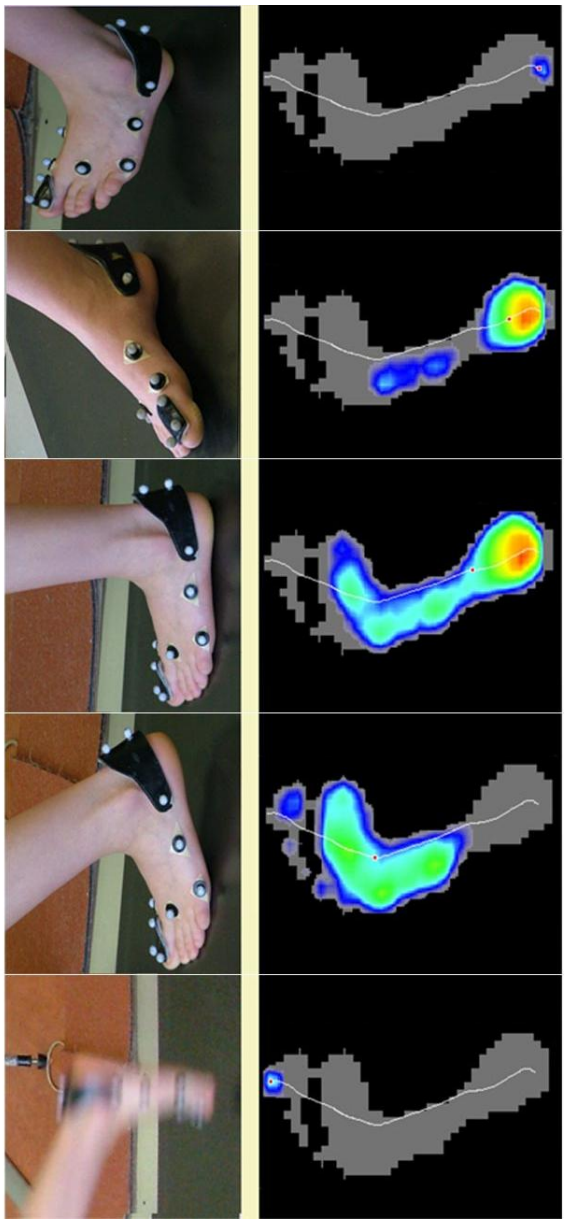

Figure 2.16 From top to bottom the events First Foot Contact, First Metatarsal Contact, Fore Foot Flat, Heel Off, and Last Foot Contact are depicted cinematographically and by the plantar pressure distribution

For determining FMC and FFF, we need to know the positions of the metatarsal heads. In Section 2.2.6, the division of the pressure distribution into elven areas is discussed. The forefoot area was divided into five areas all containing one metatarsal. Pressure-time curves can be obtained from the five metatarsal areas. The onset and offset time points of pressure curves in these areas are directly used to determine FMC and FFF.

With the use of these five events described above, the foot phases are determined for a heel-to-toe foot unroll. In case of walking and fast walking, this type of unroll was performed by all individuals, in contrast to running. In Cavanagh and Lafortune [29, 1980], it was already observed that during running some individuals first contact the ground with their forefoot, a combination of forefoot and midfoot, or with the foot as a whole. In case of initial contact with forefoot or combined forefoot and midfoot, there are discrepancies in heel contact. Some individuals still show a heel contact phase where others show no such phase. In our data-set, all these foot motion patterns are present during running. In this thesis, we used only the running trials with a heel-to-toe motion pattern.

Conclusively, in this thesis we require the following phases of foot contact:

1. **Initial Contact Phase (ICP):** from FFC till FMC;
2. **Forefoot Contact Phase (FFCP):** from FMC till FFF;
3. **Foot Flat Phase (FFP):** from FFF till HO;
4. **Forefoot Push Off Phase (FFPOP):** from HO till LFC.

2.2.5 Local Reference Frames and Orientation

With our choice of marker set-up, four segments are defined: the rearfoot, the lateral midfoot, the medial midfoot, and the hallux. From the markers within every segment, a local reference frame is constructed. The static trial was used to determine the initial orientation of the LRFs of these segments.

The reason not to directly use marker positions to determine initial orientation is the inherent inaccuracy in placing markers at most anatomical landmarks. In case of the metatarsal head markers, it is our experience that the anatomical structures are well defined and small in size and therefore marker placement should be accurate.

However, in case of the markers attached to the heel (directly or with a marker plate) these landmarks are also well defined but not small in size. The later makes accurate repeatable placement very hard.

For the four segments, we now describe the local reference frame, initial orientation, and the calculation of orientation.

The rearfoot segment

Four markers are attached to the heel (two proximally, one lateral, and one medial). A number of possibilities exists for the definition of a local reference frame for the rearfoot segment. For instance, every combination of three markers can be used to define a plane. This plane is expressed by two vectors of the six vectors that can be constructed from these markers. The outer product of the chosen two vectors would give the third orthogonal vector. Together, these three vectors define a local reference frame.

Therefore, we are able to chose from four planes with twelve combinations of vector pairs to describe the plane. In total, 48 local reference frames are possible with the scheme proposed above. The errors in a construction of a local reference frame in this manner are discussed in Section 2.2.2. From this section, it follows that all mirrored local reference frames have the same error. Therefore, our choice is limited to twelve possible reference frames. Furthermore, the conclusions of this section point out that only one choice is optimal: the local reference frames that is constructed from the two largest vectors is susceptive to the smallest errors in orientation. We choose this local reference frame for the rearfoot.

To express the orientation of the rearfoot segment, a relationship between anatomical meaningful axes and the LRF of the segment must be known. Previously, we discussed the use of markers placed at anatomical landmarks to achieve such a relationship. However, we used arguments with respect to minimizing errors in determining the LRF. A consequence is the loss of any relationship between the rearfoot LRF and the anatomical axes of the rearfoot. An initial orientation is introduced to overcome this problem. From the marker data during the static trial, a vector is defined: from the middle between the lateral and medial heel marker to the marker between the second and third metatarsal head. This vector is projected on the $z = 0$ plane of the global reference frame and taken to be the proximal-distal axis of the segment. In the $z = 0$ plane, a vector is constructed perpendicular to the proximal-distal axis

with a positive x-component in the global reference frame. This vector is the medial-lateral axis. In conclusion, the initial orientation consists of the proximal-distal axis (or length axis of the foot), the medial-lateral axis, and the z-axis of the global reference frame. Naturally, the relationship with the LRF of the rearfoot is the rotation matrix between the initial orientation and the rearfoot LRF calculated with marker data from the static trial. The expression of the orientation is always in the initial orientation of a segment.

Besides the above initial orientation for the rearfoot, we constructed a second initial orientation. This new reference frame is almost similar to the previous one. Only the definition of the medial-lateral axis is extended with a z-component. The difference between the z-components of the lateral and the medial calcaneus marker in the static trial are used to define the z-component of medial-lateral axis. The third axis directly follows from the outer product between the medial-lateral axis and the proximal-distal axis. Since this axis has a positive medial-lateral x-component, the difference for a right rearfoot segment is defined as the z-component of the lateral calcaneal marker with the z-component of the medial calcaneal marker subtracted from it. In case of a left rearfoot segment the order of the markers is reversed.

For the rearfoot segment, three angles in the Cardan representation are used to express the orientation of the rearfoot with respect to the laboratory reference frame. The angles are related to calcaneal inversion/eversion (CIE), calcaneal plantar flexion/dorsiflexion (CPD), and calcaneal abduction/adduction (CAA). It follows from the Cardan representation of orientation that six rotation sequences are possible. We have to choose one that is the most relevant. From an anatomical and historical perspective, the common motion description of the calcaneus is chosen: first CAA, second CPD, and third CIE. In the 2D studies of rearfoot orientation ([152]), only the CIE angle is expressed. Within these studies the researchers always look at projections of heel markers on a frontal plane. In this frontal plane the angle between the projected markers and a LRF of the plane is determined to express calcaneal inversion/eversion. With the present sequence choice, we also calculate the calcaneal inversion/eversion in such a frontal plane. Even beter, the frontal plane used coincides with the frontal plane of the foot due to definition of the length axis in the initial orientation. This is beter than in the case of the 2D studies since they mostly used a frontal plane perpendicular to the direction of progression. We are aware of at least one 3D study that uses the same angle definition to express CIE, namely Van Gheluwe et al. [204, 1995], but

through a different calculation method. Other 3D studies are hard to find since most of the 3D studies that have kinematic foot data, express the orientation of the foot with respect to the shank ([5], [26],[98], [97], [42], [115], [38], [150], [166], and [79]). A second argument for the use of this rotation sequence is that CAA from MAS data is the same as the abduction/adduction angle used to express foot position in plantar pressure measurement systems. The two remarks above enable the comparison of our orientation data with previously performed research using a pressure plate system only.

The metatarsal segments

Two metatarsal segments are constructed using the five markers attached to the metatarsal structures. The first segment is called the Medial MidFoot (MMF) segment and it uses the two markers attached to the first metatarsal head and the marker attached between the heads of metatarsal two and three to track its motion during a dynamic trial. The second segment is called the Lateral MidFoot (LMF) and used the two markers attached to the fifth metatarsal head and the marker attached between the heads of metatarsal two and three to track its motion during a dynamic trial. The construction of these tracking frames was again according to the directions that followed from Section 2.2.2.

The initial orientation for these two segments is defined in a similar fashion. The proximal-distal axis of both midfoot segments is defined by the two pairs of markers that are on a metatarsal (metatarsal one and five). The medial-lateral axis is again defined such that the x-component is positive. Also, this axis has a zero z-component and is perpendicular to the proximal-distal axis. With these restrictions, the medial-lateral axis is uniquely determined. The third axis follows directly from the outer product between the medial-lateral axis and the proximal-distal axis.

For these metatarsal segments, the three angles of the Joint Coordinate System (JCS, Grood and Suntay [74, 1983], and Cole et al. [39, 1993]) are used to express the orientation of the these segments with respect to second initial orientation of the calcaneus (CAL2).

The hallux segment

The hallux segment is constructed with the tree markers attached to the hallux marker plates to track its motion during a dynamic trial. The construction of this tracking frame is in accordance with directions from Section 2.2.2.

The initial orientation for this segment (Hal) is defined by the proximal and the distal hallux marker. Analogue to the midfoot segments, the proximal-distal axis is defined by these markers and the medial-lateral axis by calculating the vector that has a positive x-component, a zero z-component, and is perpendicular to the proximal-distal axis. The third axis follows again by calculating the outer product between the previous axes.

The orientations of the hallux segment is expressed as three angles of the Joint Coordinate System (Grood and Suntay [74, 1983], and Cole et al. [39, 1993]) with respect to MMF.

2.2.6 Pressure Distribution Division and Derived Physical Quantities

In Section 1.2, we discussed the masking of plantar pressure distributions and the physical quantities derived from the plantar pressure measurement. In this subsection, we discuss the specific mask used in this research project and the physical quantities derived with this mask.

In Section 1.2, we noted the lack of information about methodology used to define masks. In literature, both automated masking and manual masking strategies are employed. Today, most pressure measurement systems allow a combination of both strategies using the automated masking as a starting point for a manual follow up.

There are a few exceptions in this lack of foot division methodology. In a paper by Canavagh and Rodgers [27, 1987], they described the anterior-posterior division of the foot according to a fix ratio of $\frac{1}{3} - \frac{1}{3} - \frac{1}{3}$ from the heel to the highest point in the forefoot neglecting the toes. Another example is the paper of Speksnijder et al. [189, 2005], in which they mention a anterior-posterior and medial-lateral division of the foot according to certain ratio's, see Figure 2.17.A. Finally, in a paper by Burns, [24]; 2004, a posterior-anterior division was made based of anatomical measurements. Burns measured foot skeletons and divided the foot into a rearfoot area of 31%, a midfoot area of 19%, and a forefoot area (containing metatarsal heads and toes) of 50% relative to foot length, see Figure 2.17.B.

In our mask we define a medial and lateral rearfoot area containing the heel only, a medial and lateral midfoot area, five metatarsal areas, a hallux area, and a lesser

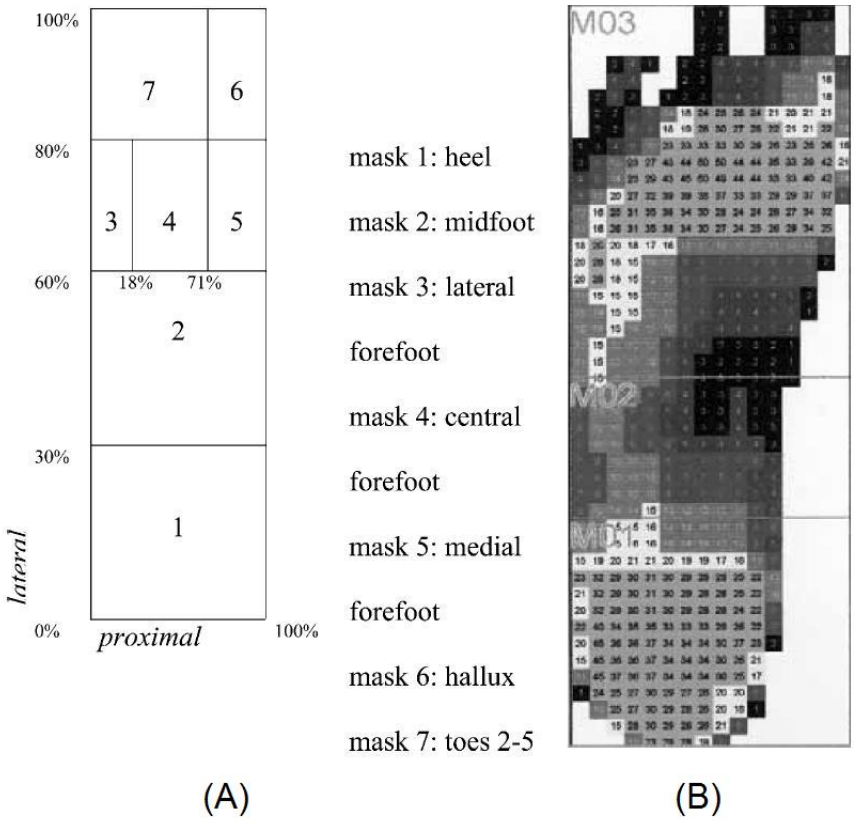

Figure 2.17 Examples of foot masks methodology. In (A), the mask as defined by Speksnijder et al. [189]. In (B), the mask as defined by Burns [24]. Both illustrations are depicted with permission.

toe area, see Figure 2.18.

First, we use the posterior-anterior ratio division as constructed by Burns. From private correspondence with Burns, we found out that the pressure data used for his division was the maximum pressure distribution. He mentioned that foot length was calculated using only the anterior-posterior direction of his pressure system, an insole system. Using an insole system the length of the foot is not subjected to the abduction/adduction position of the foot with respect to the line of progression. In our case, we used a pressure plate system such that foot length is subjective to foot position on the plate. Nevertheless, we used vertical lines in the local coordinate system of the pressure plate systeem to define rearfoot, midfoot, and forefoot. The rational is that the influence of the sensor area defined by vertical lines with respect to lines perpendicular to the foot axis are limited. If we assume that such a vertical line is determined with an accuracy of two length sensors, the foot position influence is maximal with the person having the largest feet width. In our population this width was about 11cm. Thus the abduction/abduction angle of the foot with respect to the line of progression should be over 8° in absolute terms. Although, values above 8° are present in our population, the influence hardly goes beyond a few sensors that are present in the edge of each area. We will return to this topic when we discuss medial-lateral division of the foot area.

Another problem of using a pressure plate instead of an insole system is the rolling motion of the heel at the start of foot-to-ground contact and the rolling of the hallux at the end of contact. Both phenomena enlarge the pressure distribution pattern. If the maximum value of every sensor over contact time is taken to form the maximum pressure image and the division is constructed based on this enlarged foot imprint then the length of the foot can be overestimated with as much as five length sensors, or 3.8cm. We did correct for this problem by taken the dynamic pressure distribution instead of the maximum pressure image and using a time interval where the pressure distribution contains a large number of active sensors. More details are found in the Matlab application **Foot_Area_Division_v4**, which is described in the Appendix B.4.2.

Second, we calculated a foot axis based on three different methods using the maximum pressure image. The first method was a geometric inertial axis method applied the whole foot, the second was a geometric inertial axis method applied to the rearfoot

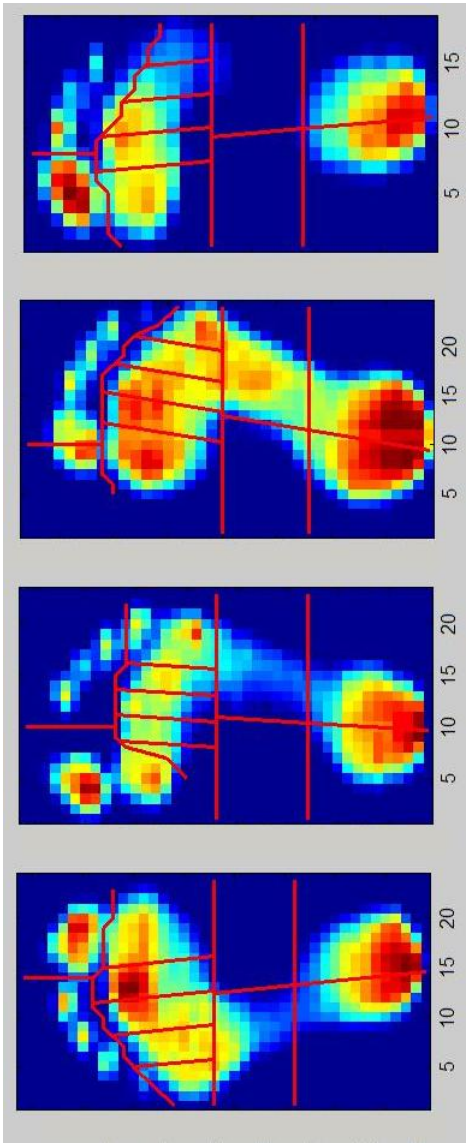

Figure 2.18 Foot mask used in our research. In these four images, we depict from bottom to top an example of a trial that was automatically and correctly masked, an example of a trial where a left foot was assumed while it was a right foot, an example of a trial where the hallux area was chosen incorrectly, and an example of a trial where the toe area was chosen incorrectly.

and the forefoot separately, and the third was a CoP method applied to the rearfoot and the forefoot. The orientation of axes from all methods were compared to the axis defined by the line through the middle of the lateral and medial heel marker and the marker between metatarsal heads two and three. We choose this foot axis based on the fact that most individuals show a central push of sequence of the metatarsal heads, see De Cock et al. [48, 2005]. Thus leaving the ground with metatarsal heads two and three. The axis from MAS data is taken to be the golden standaard because this axis comes from a direct measurement. The results of these comparisons are found in Appendix B.7. We used the direction of the foot axis to define the medial-lateral division of the rearfoot area and the medial-lateral division of the midfoot area. We also used this direction in defining the direction of the anterior-posterior lines used in dividing the forefoot into five metatarsal areas.

Third, we divided the forefoot in a toe area and a metatarsal area. Two distinct edge detecting algorithms were developed to accomplish this task. The first algorithm scans the foot in the length direction starting from the toes. It provides an initial condition for the second algorithm that predominantly scans in the medial-lateral direction of the foot. Another initial condition for the second algorithm is the knowledge wether the pressure measurement originates from a left or right foot. A simple criterion was developed to verify this: the number of active sensors in the y-direction of the forefoot area were counted and divided in to two groups. The two groups were constructed such that the forefoot area was divided into two equal parts with respect to the width of the foot. The criterion was that the group with most active sensors in the y-direction contained the hallux and therefore it was known if it was a left or right foot. An obvious assumption is the presence of a hallux and the less obvious assumption is an asymmetry in forefoot anatomy.

Fourth, the toe area is further divided into an area containing the hallux and an area containing the remaining toes. The algorithm responsible for this division primarily uses a medial-lateral scanning technique after summing the values along the y-direction of the local pressure measurement reference system.

Fifth, the metatarsal area was divided into five areas that should contain the five metatarsal heads. As mentioned before the anterior-posterior lines in this area have the same direction as the foot-axis. The areas were constructed based on ratios with respect to the width of the foot expressed along an axis perpendicular to the foot axis. The following ration scale was used: [.35 .1533 .1533 .1533 .19], where the first entry

Table 2.2 Errors in dividing the foot into subareas. The errors related to the determination of toe areas, hallux areas, and if feet were left or right are expressed in this table.

Condition	Toe area	Hallux area	Left or Right Foot
Walking	3.2%	0.5%	0.4%
Running	3.7%	0.0%	0.1%
Combined	3.3%	0.5%	0.5%

refers to the first metatarsal area and so on. Two researchers both experienced in manually dividing plantar pressure distribution data studied the effects of this ratio division in the walking session group and concluded that the division was very close to their manual division.

As further validation, the errors made by the different algorithms were verified for the complete population of 126 individuals. We looked for errors in determining the toe area within the forefoot area, in determining the hallux area, and in determining if feet were right or left. The fast walking trials were counted as walking trials. The overall results of this analysis is found in Table 2.2. The overall result indicates a succes rate of 95.7% in dividing feet according to the chosen mask.

In combination with these division algorithms, we implemented two applications able to extract information from the different subareas. The first application was implemented to extract the CoP path from any given pressure distribution. The second application focusses more on local physical quantities. It extracts from a given area at every time point the total pressure, total force, number of active sensors, the location of the highest pressure sensor, and the value of the highest pressure sensor. Using these quantities, we are able to calculate all the physical quantities discussed in Section 1.2.

2.3 Summary of Methodology

In this chapter, we introduced the methodology used for our study. In this final section, we summarise the main topics. Our integrated set-up consists out of a force platform, a pressure plate, a motion analysis system, and a mean velocity measurement device.

Besides the latter, all measurement devices are coupled. The following steps were taken to assure accuracy and quality of data:

- *Synchronisation of force, pressure and motion data.*
  In both MAS and PPPS, force platform data was registered. This data was used to establish accuracy of synchronisation. A signal correlation measure was introduced. The sensitivity of this measure was studied and it was concluded to be sufficiently sensitive to detect delay and frequency differences between both force signals. With this measure, we established that the synchronisation was within measurement accuracy.

- *Alignment of pressure and motion data.*
  The local reference frames of these two systems were aligned using a wooden block. The block was placed on top of the pressure plate at a number of locations. The centre of the block was determined in both systems. Using all centres, the rotation and translation needed to go from one local reference frame to the other was calculated. This process was repeated at the beginning of all measurement days.

- *Accuracy of motion data.*
  We determined the accuracy of motion data using a control object containing a multitude of markers. The distance between markers and the angle between them were assessed. The outcome will be used for the interpretation of results.

- *Accuracy of pressure data.*
  The accuracy of pressure data could not be assessed with respect to individual sensor values, because the appropriate devices to perform this analysis were not available.

- *Filtering and interpolation.*
  In our study, we use the least square cubic splines method.

- *Foot phases and events.*
  In our study, we use the same definition of phases and events as suggested by de Cock et al., [48, 2005]. However, we determined the phases and events in a slightly different way. In the study by de Cock et al, A local mask was used while we use a complete mask of the foot divided into eleven subareas.

Chapter 3

Rearfoot Motion

Simulated Heel Motion from Pressure Plate Measurements

3.1 Introduction

In the seventies and eighties of the last century, extensive studies on the lower extremity have been carried out based on measurements of two-dimensional nature obtained from high-speed cinematography (McClay et al.[131]). From these studies, it has been concluded that excessive subtalar pronation is linked to running-related injuries, and that the eversion of the calcaneus is a reliable predictor of the amount of pronation (Nigg [152], Van Gheluwe et al. [202]). Nowadays, the analysis of the rearfoot is performed using a three-dimensional approach. However, improving the approach from two-dimensional to three-dimensional did not alter the conclusion that excessive subtalar pronation is linked to running-related injuries (Lundberg [125]). In this chapter, instead of analysing the motion of the rearfoot by means of cinematography, a pressure plate system is used. In the case of cinematography, there is a direct link between the temporal measurements and the motion of the calcaneus. In the case of a pressure measurement system, there is no such link since not the motion itself is measured but the temporal pressure distribution resulting from the motion. Therefore, additionally, a mechanical model is needed that links these pressure distribution measurements to calcaneal motion. Furthermore, the motion of the calcaneus can be described only

when heel and plate are in contact with each other. This is a limitation of the use of a pressure measurement system, but luckily the motion of interest, excessive subtalar pronation, takes place during heel-ground contact. The mechanical model mentioned above, uses the pressure distribution as input to the model. The pressure distribution, at each measurement time point, is used to compute the temporal path of the centre of pressure (CoP). This temporal path is the basis of our mechanical model, since we describe the motion mechanically as the rolling of the rigid calcaneus over a rigid plate, where the CoP at each instance is the contact point. Thus, while the input to the model is the temporal pressure distribution, the output of the model is the motion of the calcaneus in the three cardinal planes with respect to a fixed reference frame.

Because of the used input, a mathematical tool has been developed that relates input to desired output. The approach taken to link plantar pressure distribution to rearfoot kinematics differs from all other approaches so far. Models found in literature either calculate foot kinematics on the basis of cinematography (([153], [8], [169], [54], [13], [132], [170], [171], [192], [124], [127], [126])), or describe foot kinematics (and kinetics) on a purely theoretical basis ([183], [143], [144], [38], [6], [7], [101], [182]). There seems to be no literature available that uses pressure plate measurements as direct input to a kinematical model.

Therefore, the purpose of this study is to simulate three-dimensional rearfoot kinematics during heel contact solely from pressure plate measurements. The benefits of simulating rearfoot kinematics with the use of a pressure plate system are a reduction in both measurement cost and measurement time, because no cinematographical data recording is required. These benefits are best viewed within the clinical practice, where there is a need for information about both rearfoot kinematics and pressure loading. However, time is often so restricted that a full gait analysis cannot be performed. Therefore, time and cost saving measurements provide a possible solution.

3.2 Model

3.2.1 Description of the Model

The mechanical model finds it basis in the following ideas: (1) it uses the measurements from a pressure measurement system as input, (2) it contains mathematical equations describing contact between heel and plate, and (3) it produces the temporal orientation of the heel in terms of Cardan angles, see Figure 3.1.

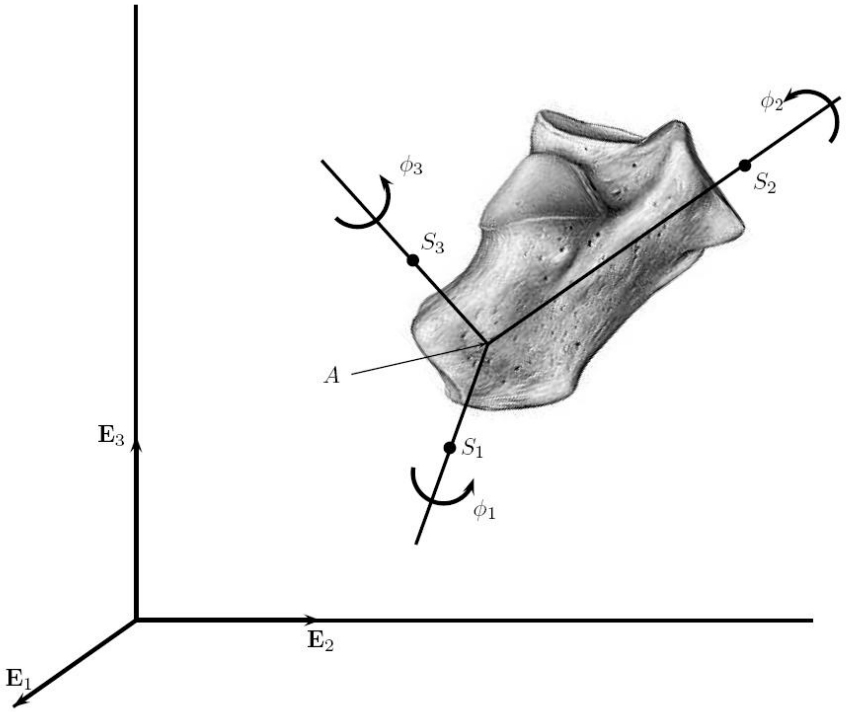

Figure 3.1 The calcaneus reference frame with respect to the plate reference frame $O\mathbf{E}_1\mathbf{E}_2\mathbf{E}_3$. The angles ϕ_1, ϕ_2 and ϕ_3 are the Cardan angles, and the points S_1, S_2, S_3 and A span the calcaneus reference frame.

In the first step, the heel in contact with the plate is considered a four-layer system: the calcaneus on top, the soft tissues between calcaneus and plate and the elastic layer of the plate in between, and the rigid layer of the plate at the bottom, see Figure 3.2 (a). Top and bottom layer are rigid, while intermediate layers are elastic. The elastic layers transfer the forces exhibited by the calcaneus on the pressure plate into a temporal pressure distribution over a finite contact area. At each measurement time point, this pressure distribution is used to compute the temporal path of the centre of pressure (CoP).

In the second step, the two intermediate layers are considered as one layer on top

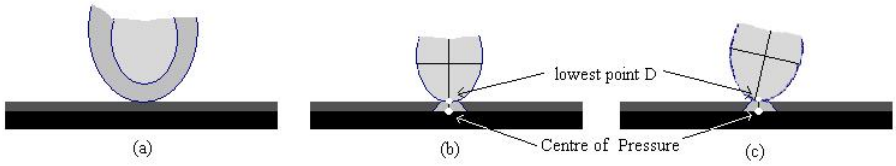

Figure 3.2 (a) the four-layer system, where the calcaneus is depicted in light grey and the rigid layer of the plate is depicted in black. In (b) and (c), a graphical interpretation of step two is given, where (b) and (c) are taken as different subsequent time steps. The distance between point D and the Centre of Pressure is equal in both (b) and (c). The light grey area within the elastic layer shows the influence of this layer on the measured pressure distribution.

of the plate, see Figure 3.2 (b). This makes sense because the elastic properties of the plate layer do not influence the pressure distribution measurement to the same extent as the soft tissue layer does. In the third step, the influences of the elastic layer besides from the obtained pressure distribution are neglected, thus obtaining a rigid contact system. Assuming local concavity of the calcaneal surface, there exists a point on the plate having minimum distance to the calcaneal surface, see Figure 3.2 (c). This point is supposed to coincide with the computed CoP. Moreover, changes in this minimum distance are assumed to be small in comparison to the global motion of the calcaneus. Therefore, this distance is taken constant during heel contact.

The final problem is to calculate the orientation of a rigid body rolling over a rigid plate when the contact points on the plate are known at discrete time points, see Figure 3.3. An implicit assumption for describing the motion as rolling motion is no spin motion between heel and plate. In this section, we will discuss a rolling rigid body with an arbitrary geometry, and thereafter the specific case of a spherical geometry.

Assumptions

In the model description part, a few assumptions are made to translate the rolling motion of the heel over a pressure plate into the rolling rigid-body problem. Here, we discuss the assumptions explicitly.

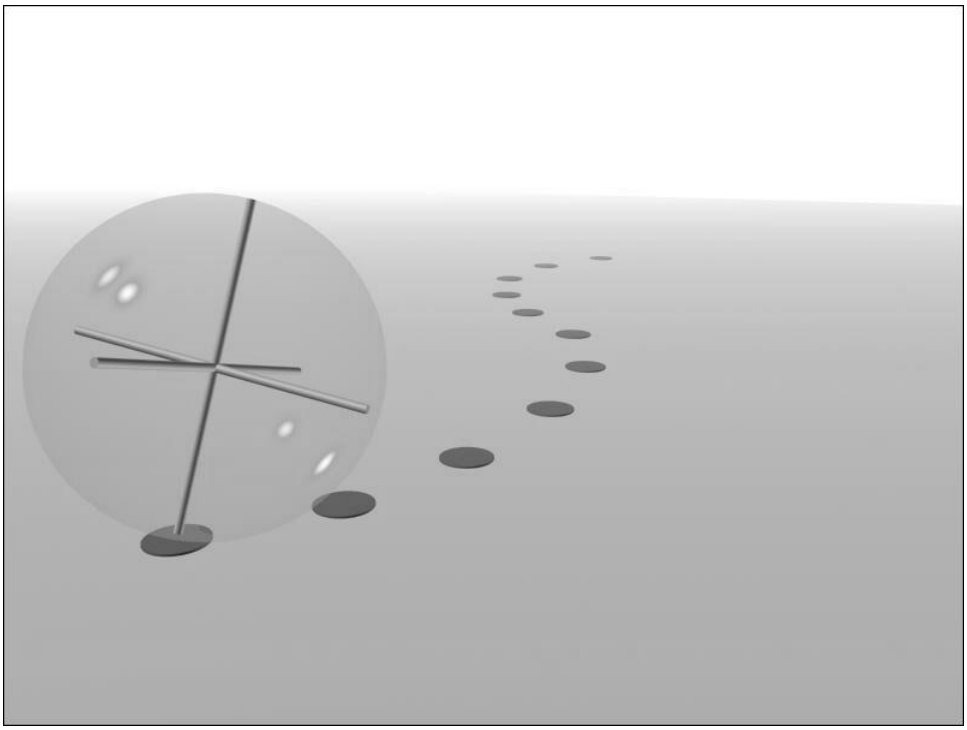

Figure 3.3 A rigid sphere with a local coordinate system rolling over a rigid plate, created by J. Gaublomme.

1. *The calcaneus is assumed to be rigid.*
   This is a fair assumption because the calcaneus shows very little elastic deformity. However, for young children, this assumption might not be valid since the calcaneus is not completely ossified. At this age, it consists for the greater part of more flexible cartilage tissue. In the population measured to validate the mechanical model, no such young children (Hennig et al. [87], 1991) were present.

2. *The soft tissues that surround the calcaneus and that are in contact with the plate are assumed homogeneous, isotropic and of uniform thickness*
   This assumption is necessary for the second modelling step where the soft tissue clamped around the calcaneus was considered as a flat layer on top of the

plate. However, it is not evident that this assumption holds. A violation against this assumption has direct consequences for the relationship between CoP and the lowest point on the calcaneal surface. In Figure 3.2 (c), the influence of a non-isotropic heel fat pad with non-uniform thickness would shift the CoP path medially if the heel fat pad is less elastic at the lateral and medial border of the heel than it is in between these borders.

3. *The calcaneal surface is locally convex.*
   With the term locally, we refer to that part of the surface of the calcaneus that consists of the set of lowest points on the calcaneal surface during heel contact. Anatomy learns us that the plantar side of the calcaneus has a medial and lateral tuberculum. This would contradict the existence of a locally convex surface. However, we have found no report in the literature that there may exist a double hump in the pressure distribution of the heel. The heel contact area is certainly large enough to contain both tuberculi. Therefore, we believe that two factors cause the absence of a double hump. First, assumption 2 is only partly valid such that the soft tissue around the tuberculi and the tuberculi themselves form one functional unit, a functional heel bone. Second, the CoP-path of the heel area shows little movement in the medio-lateral direction such that the CoP is located predominately in the neigbourhood of only one of the tuberculi. The first factor is difficult to validate, but it is the reason why we will speak about heel motion instead of calcaneal motion. An illustration of the second factor is found in Figure 3.4.

4. *The temporal CoP path coincides with the path described by the projection onto the plate of the lowest point of the calcaneus during motion.*
   This assumption is a direct consequence from the previous two assumptions. Since some questions are raised with respect to these assumptions, we will propose a correction to the CoP path such that the projection of the lowest point of the functional heel bone (see previous assumption) coincides with the corrected CoP path. This proposition is found in Section 3.3.

5. *The calcaneus performs no spin with respect to the axis normal to the plate.*
   Although this motion might occur, it would, for a finite contact area, be accompanied by slip, which is not very likely to occur. Moreover, a plantar pressure

plate system is not able to detect it. Therefore, this assumption is necessary to define a well-posed problem. In other words, the number of degrees of freedom of what is measured must equal the number of what is simulated. On one hand, the contact path on a plate is calculated on the basis of pressure distribution measurements constituting two degrees of freedom. On the other hand, the functional heel bone is a rigid body that generally has six degrees of freedom. In the rolling rigid problem, the rigid object is constantly connected to a plate, which reduces the degrees of freedom to three. Since there is no spin motion, rotations about an axis perpendicular to the plate are not possible, meaning that the number of degrees of freedom is reduced to two.

6. *The distance of the lowest point of the calcaneus to the pressure plate is small with respect to the overall motion of the calcaneus during heel contact.*
A few studies discuss the deformation of the heel pad during walking (Gefen et al. [66], 2001) and running (De Clercq et al. [36], 1994). These authors found maximum deformations of 3.8-4.8mm in walking and 8.7-9.2mm in running. Using our database of measurements, we were able to match a subject in weight and age to the ones used in the study by Gefen et al. ([66], 2001). This individual has a typical range of motion of 19-20mm for the z-components of the heel markers. Therefore, the deformation is about 25% of the total range of motion. Naturally, this is not small with respect to the motion of these z-components. The range of motion of the y-components are typically around 30mm and the range of motion of the x-components is around 5mm. Therefore, the change in distance of the lowest point is not small with respect to the overall motion of the calcaneus. The influence of the change in lowest point comes, besides from its absolute motion, from the time frame in which it is present. In running, the heel fat pad deforms rapidly. In about 12-15ms, it reaches its maximum and is almost stable thereafter. In walking, deformations reach their maximum more slowly, after about 25% of stance duration, and are not stable thereafter.

This does not directly lead to a violation of assumption 4, but might have an influence on the geometry of the rolling rigid body.

3.2.2 Input - Model - Output

Essential in the model is the use of pressure plate measurements of the heel as input. The model transfers these measurements to heel motion expressed in Cardan angles. To be able to calculate these angles, a fixed laboratory reference frame and a local heel reference frame are selected. Definition of the laboratory frame and construction of the local heel reference frame are discussed in Section 2.2.5. In the next part of this section on Model Equations, the local reference frame is determined from the kinematical equation (3.4), which is a recurrence equation in time. It relates the motion of the heel, calculated from a contact path that follows from a pressure distribution, to time series, $\mathbf{T}(t_k)$, of local reference frames. On the other hand the local heel reference frame time series is expressed by using the chosen Cardan sequence of Section 2.2.5, cf. Wittenburg [214, 1977, pp19-25].

$$\mathbf{T}(t_k) = \begin{bmatrix} c_2\,c_3 + s_2\,s_1\,s_3 & -c_2\,s_3 + s_2\,s_1\,c_3 & s_2\,c_1 \\ c_1\,s_3 & c_1\,c_3 & -s_1 \\ -s_2\,c_3 + c_2\,s_1\,s_3 & s_2\,s_3 + c_2\,s_1\,c_3 & c_2\,c_1 \end{bmatrix}, \tag{3.1}$$

where $c_i = \cos(\phi_i(t_k))$, $s_i = \sin(\phi_i(t_k))$, and $i = 1, 2, 3$. In this expression, ϕ_1 is the abduction/adduction angle, ϕ_2 is the plantar flexion/dorsal flexion angle, and ϕ_3 is the calcaneal inversion/eversion angle. Combining both the found expression of $\mathbf{T}(t_k)$ with (3.1) enables us to calculate the chosen Cardan angles. This calculation can be performed in different ways, but it is made unique by restricting the angles to the range [-180°,180°]. We use the following equations under the constraint that $cos(\phi_1(t_k)) > 0$:

$$\begin{aligned} \phi_1(t_k) &= \arcsin(-T_{2,3}), \\ \phi_2(t_k) &= \arccos\left(\frac{T_{3,3}}{\cos(\phi_1(t_k))}\right) = \arcsin\left(\frac{T_{1,3}}{\cos(\phi_1(t_k))}\right), \\ \phi_3(t_k) &= \arccos\left(\frac{T_{2,3}}{\cos(\phi_1(t_k))}\right) = \arcsin\left(\frac{T_{2,1}}{\cos(\phi_1(t_k))}\right), \end{aligned} \tag{3.2}$$

where T_{ij} refers to the i^{th} row and j^{th} column of the transformation matrix. For the calculation of the angles, we adapted a Matlab code made available by Reinschmidt (International Society of Biomechanics web pages), see Appendix C.2.

3.2.3 Model Equations

In this section, we will describe the motion of the heel, more specifically, the motion of the contact point of the heel with the plate. This contact point C traverses in time a path on the plate surface. Since we assume that C coincides with the centre of pressure CoP, this path of C is equal to the CoP-path we are looking for. We will describe this motion in a *backward* direction, meaning that we follow the CoP-path from a known final position backward to its initial position. In modelling this motion, we make the fundamental assumption that the surface of the calcaneus can locally, i.e. in the direct vicinity of the contact point, be approximated by the surface of a sphere. Thus, we want to model the motion of the calcaneus as the motion of a rolling sphere over a plane as depicted in Figure 3.3.

To this end, we introduce a local orthonormal reference frame $\{A\mathbf{e_1}\mathbf{e_2}\mathbf{e_3}\}$ attached to the calcaneus, see Figure 3.1, or Figure 3.3. To describe the motion of this local reference frame with respect to the fixed laboratory frame $\{O\mathbf{E_1}\mathbf{E_2}\mathbf{E_3}\}$, the positions of four points A, S_1, S_2, S_3 (A the origin, and S_1, S_2, S_3 points on the three local axes, see Figure 3.1) must be known at every measurement time point. The fundamental law of kinematics can be used to calculate the positions of these four points at all times t. This law states that the velocity of each material point $\mathcal{P}$ of a rigid body $\mathcal{B}$ described by its position vector $\mathbf{x}_P \equiv \mathbf{x}(t)$ with respect to O, satisfies

$$\mathbf{v}(t) = \mathbf{v}_A(t) + \boldsymbol{\omega}(t) \times \mathbf{y}(t) \ , \qquad \left(\mathbf{v}(t) = \tfrac{\mathrm{d}\mathbf{x}}{\mathrm{d}t}\right) \ , \tag{3.3}$$

where $\mathbf{v}_A$ denotes the velocity of the specific point $\mathcal{A} \in \mathcal{B}$, $\boldsymbol{\omega}$ denotes the angular velocity of the rigid body $\mathcal{B}$, and $\mathbf{y} = \mathbf{x} - \mathbf{x}_A$, the position vector of $\mathcal{P}$ with respect to $\mathcal{A}$. A backward discretisation in time of the equation: $\mathbf{v} = \frac{\mathrm{d}\mathbf{x}}{\mathrm{d}t}$ yields

$$\mathbf{x}(t_{k-1}) = \mathbf{x}(t_k) - \Delta t \mathbf{v}(t_k) \ , \tag{3.4}$$

where Δt is the measurement time step, and $t_k = k\Delta t$. Equation (3.3) applied at time t_k gives

$$\mathbf{v}(t_k) = \mathbf{v}_A(t_k) + (\boldsymbol{\omega}(t_k) \times [\mathbf{x}(t_k) - \mathbf{x}_A(t_k)]) \ . \tag{3.5}$$

At this point, we assume that at time $t = t_{k+1}$, and later, the whole motion of $\mathcal{B}$ is known, and that for every $\mathcal{P} \in \mathcal{B}$ its position $\mathbf{x}(t_k)$ at time t_k is determined from (3.4) with $k \to k+1$. So, in order that we can use (3.5) in (3.4) to determine the position of $\mathcal{P}$ at time t_{k-1}, we still need to determine the unknowns $\mathbf{v}_A(t_k)$ and $\boldsymbol{\omega}(t_k)$. For this,

we first take for $\mathcal{P}$ the momentary (at $t = t_k$) contact point $\mathcal{C} \in \mathcal{B}$, which, being the *material* momentary contact point of the calcaneus with the plate, has zero velocity (pure rolling, no slip). Then, (4.8) yields

$$\mathbf{v}_A(t_k) = -(\boldsymbol{\omega}(t_k) \times [\mathbf{x}_C(t_k) - \mathbf{x}_A(t_k)]) \ . \tag{3.6}$$

Here, and only at time t_k, $\mathbf{x}_C(t_k)$ is also the position of the point C, the contact point but now considered as a point of the plate. The contact point C traverses with a certain, non-zero, velocity a path, the contact path, on the plate. Note that $\mathcal{C}$ and C coincide at $t = t_k$ but not at $t > t_k$ or $t < t_k$.

With (3.6), a relation between $\mathbf{v}_A(t_k)$ and $\boldsymbol{\omega}(t_k)$ has been established. What remains to be done is the calculation of the angular velocity $\boldsymbol{\omega}(t_k)$ at time t_k. This calculation is performed with the use of differential geometry and results in the following statement:

Let a rigid body $\mathcal{B}$ be rolling over a rigid plate such that the point of contact between the rigid body and the plate forms a smooth path in time: $\mathbf{x}_C(t)$. Let at time t_k the point C have a velocity $\mathbf{v}_C(t_k)$ along this path, such that $\mathbf{v}_C(t_k) = (\mathbf{x}_C(t_k) - \mathbf{x}_C(t_{k-1}))/\Delta t$ (recall that here C is a point on the plate). Then, the angular velocity of the rigid body $\mathcal{B}$ at time t_k is given by

$$\boldsymbol{\omega}(t_k) = \mathcal{S}|_C \left(\mathbf{v}_C(t_k) \times \mathbf{n}|_C\right) \ , \tag{3.7}$$

where $\mathcal{S}|_C$ is the curvature tensor at point $\mathcal{C}$ of the surface of $\mathcal{B}$, and $\mathbf{n}|_C$ is the outward normal in $\mathcal{C}$ on that surface.

A mathematical proof of this theorem can be found in Hagman, [59] 2001.

With the use of (3.5)-(3.7), the right-hand side of the recurrence relation (3.4) is known completely, and we can now determine the new position at time t_{k-1} of every point $\mathcal{P} \in \mathcal{B}$, so also for the material points $\mathcal{A}$,$\mathcal{S}_1$,$\mathcal{S}_2$,$\mathcal{S}_3$. Therefore, having determined, at arbitrary time t, the position vectors $\vec{AS}_i = \mathbf{y}_{S_i}(t) = s_i \mathbf{e}_i(t)$, $i = 1, 2, 3$, directed along the axes of the local reference frame, the orientation of this frame, rigidly attached to the calcaneus, is known at every measurement time point t_k. Here, s_i is the fixed, constant, length $|\mathbf{y}_{S_i}|$ of $\vec{AS}_i$, the distance from $\mathcal{S}_i$ to $\mathcal{A}$. The associated unit

vectors $\mathbf{e}_i$, with $\mathbf{e}_i = \mathbf{y}_{S_i}/s_i$ for $i = 1, 2, 3$, are used to calculate the transformation matrix $\mathbf{T}$ from its definition:

$$\mathbf{T}(t_k) = [\mathbf{e}_1; \mathbf{e}_2; \mathbf{e}_3] = \left[\frac{\mathbf{y}_{S_1}(t_k)}{s_1}; \frac{\mathbf{y}_{S_2}(t_k)}{s_2}; \frac{\mathbf{y}_{S_3}(t_k)}{s_3}\right] . \tag{3.8}$$

The matrix $\mathbf{T}$ is the representation of the transformation, or rotation, tensor $\mathcal{T}$ with respect to the laboratory frame $\{O\mathbf{E_1}\mathbf{E_2}\mathbf{E_3}\}$, which describes the transformation, rotation, from $\mathbf{E_i}$ to $\mathbf{e_i}$ according to

$$\mathbf{e}_i(t) = \mathcal{T}(t)\mathbf{E}_i . \tag{3.9}$$

The looked-for Cardan angles follow then by using the results of (3.8) in (3.1).

Still one problem remains; the geometry of the rolling object, the calcaneus, should be determined. Assuming that in the neighbourhood of the contact point, and at time t_k, this geometry is a sphere with radius R (in general $R = R(t_k)$), one can determine in a straightforward manner the Cardan angles in the way as described above. In doing this, it is used that now the curvature tensor $\mathcal{S}$ always equals the identity tensor multiplied by R^{-1}. Moreover, the normal vector is $\mathbf{n} = -\mathbf{E}_3$. In the remainder of this chapter, we shall always assume that, locally, the surface of the calcaneus coincides with the surface of a sphere.

Let $\mathcal{A}$, being in the centre of the sphere, at time t_k have the position vector

$$\mathbf{x}_A(t_k) = x_A(t_k)\mathbf{E}_1 + y_A(t_k)\mathbf{E}_2 + R\mathbf{E}_3 , \tag{3.10}$$

then

$$\mathbf{x}_C(t_k) = x_C(t_k)\mathbf{E}_1 + y_C(t_k)\mathbf{E}_2 = x_A(t_k)\mathbf{E}_1 + y_A(t_k)\mathbf{E}_2 , \tag{3.11}$$

and

$$\mathbf{y}_C(t_k) = -R\mathbf{E}_3 . \tag{3.12}$$

Moreover, we have

$$\mathbf{v}_C(t_k) = \mathbf{v}_A(t_k) = \frac{1}{\Delta t}[(x_A(t_k) - x_A(t_{k-1}))\mathbf{E}_1 + (y_A(t_k) - y_A(t_{k-1}))\mathbf{E}_2] , \tag{3.13}$$

by which (3.7) results in

$$\begin{aligned} \omega(t_k) &= -\frac{1}{R}(\mathbf{v}_C(t_k) \times \mathbf{E}_3) \\ &= \frac{1}{R\Delta t}[(-y_A(t_k) + y_A(t_{k-1}))\mathbf{E}_1 + (x_A(t_k) - x_A(t_{k-1}))\mathbf{E}_2] . \end{aligned} \tag{3.14}$$

The above deduction relates the contact path ($\mathbf{x}_C(t)$) to the motion of a rolling sphere ($\mathbf{x}_A(t)$,$\boldsymbol{\omega}(t)$). A reciprocal relationship can be derived also. Starting from (3.4) and using successively (3.5), and (3.10)-(3.15), we derive, for arbitrary $\mathcal{P} \in \mathcal{B}$,

$$\begin{aligned}
\mathbf{x}(t_{k-1}) - \mathbf{x}(t_k) &= \Delta t \mathbf{v}(\mathbf{t_k}) = -\Delta t(\mathbf{v_A}(\mathbf{t_k}) + (\boldsymbol{\omega}(t_k) \times \mathbf{y}(t_k))) \\
&= \Delta t(\boldsymbol{\omega}(t_k) \times \mathbf{y_C}(t_k)) - \Delta t(\boldsymbol{\omega}(t_k) \times \mathbf{y}(t_k)) \\
&= \Delta t((\mathbf{v_C}(\mathbf{t_k}) \times \mathbf{E}_3) \times \mathbf{E}_3) + \frac{\Delta t}{R}((\mathbf{v_C}(\mathbf{t_k}) \times \mathbf{E}_3) \times \mathbf{y}(t_k)) \\
&= -\Delta t \mathbf{v_C}(\mathbf{t_k}) + \frac{\Delta t}{R}((\mathbf{v_C}(\mathbf{t_k}), \mathbf{y}(t_k))\mathbf{E}_3 - (\mathbf{y}(t_k), \mathbf{E}_3)\mathbf{v_C}(\mathbf{t_k})) \\
&= -\Delta t \left[1 + \frac{1}{R}(\mathbf{y}(t_k), \mathbf{E}_3)\right] \mathbf{v_C}(\mathbf{t_k}) + \frac{\Delta t}{R}(\mathbf{v_C}(\mathbf{t_k}), \mathbf{y}(t_k))\mathbf{E}_3 \\
&= \left[1 + \frac{1}{R}(\mathbf{y}(t_k), \mathbf{E}_3)\right] (\mathbf{x}_C(t_{k-1}) - \mathbf{x}_C(t_k)) + \\
&\quad + \frac{\Delta t}{R}(\mathbf{v_C}(\mathbf{t_k}), \mathbf{y}(t_k))\mathbf{E}_3 \ , \qquad (3.15)
\end{aligned}$$

which can be rewritten as

$$\frac{1}{R}(\mathbf{y}(t_k), \mathbf{E}_3)(\mathbf{x}_C(t_{k-1}) - \mathbf{x}_C(t_k)) = \frac{\Delta t}{R}(\mathbf{v_C}(\mathbf{t_k}), \mathbf{y}(t_k))\mathbf{E}_3 - (\mathbf{y}(t_{k-1}) - \mathbf{y}(t_k)) \ . \qquad (3.16)$$

Let, compare with (3.9),

$$\mathbf{y}(t) = \mathcal{T}(t)\mathbf{Y} \ , \qquad (3.17)$$

where $\mathbf{Y}$ is the position of $\mathcal{P}$ when $\mathbf{e}_i$ coincides with $\mathbf{E}_i$ (the reference state), then (3.16) transforms into

$$\mathbf{x}_C(t_{k-1}) = \mathbf{x}_C(t_k) - \Delta t \frac{(\mathbf{v_C}(\mathbf{t_k}), \mathbf{y}(t_k))}{(\mathbf{y}(t_k), \mathbf{E}_3)}\mathbf{E}_3 + R\frac{(\mathcal{T}(t_{k-1}) - \mathcal{T}(t_k))\mathbf{Y}}{(\mathcal{T}(t_k)\mathbf{Y}, \mathbf{E}_3)} \ . \qquad (3.18)$$

Taking the inner product of this equation with $\mathbf{E}_\alpha$, where $\alpha = 1, 2$, we arrive at

$$(\mathbf{x}_C(t_{k-1}), \mathbf{E}_\alpha) = (\mathbf{x}_C(t_k), \mathbf{E}_\alpha) + R\frac{((\mathcal{T}(t_{k-1}) - \mathcal{T}(t_k))\mathbf{Y}, \mathbf{E}_\alpha)}{(\mathcal{T}(t_k)\mathbf{Y}, \mathbf{E}_3)} \ . \qquad (3.19)$$

We note that this equation holds for arbitrary $\mathcal{P}$, so also when $\mathcal{P}$ is one of the points $\mathcal{S}_i$ on the axis $\mathbf{E}_i$, $i = 1, 2, 3$. In the latter case, $\mathbf{Y} = s_i\mathbf{E}_i$, and then (3.19) turns into

$$(\mathbf{x}_C(t_{k-1}), \mathbf{E}_\alpha) = (\mathbf{x}_C(t_k), \mathbf{E}_\alpha) + R\frac{(T_{\alpha i}(t_{k-1}) - T_{\alpha i}(t_k))}{T_{3\alpha}(t_k)} \ , \qquad (3.20)$$

with $\alpha \in (1, 2)$ and $i \in (1, 2, 3)$.

3.3 Methods

To validate the output of the mechanical model, Cardan angles originating from the model should be compared with the golden standard, i.e. Cardan angles originating from MAS measurements. The sets of Cardan angles in this study are obtained from measurements, starting from initial foot contact and ending at toe off. For the comparison between Cardan angles of the heel from PPPS and MAS, the time interval is restricted from first foot contact to heel off. Naturally, it is not possible to ascertain model curves after heel off since after this time point the heel is no longer registered by PPPS. The two temporal events, first foot contact and heel off, were determined using the force platform and pressure plate, respectively. The definitions of these temporal events, and others, are discussed in detail in Section 2.2.4. The outline of the foot is known from the pressure measurements. On the basis of these outlines, the foot is divided into different areas among them a heel area, see Section 2.2.6 . The pressure distribution of this heel area is used as the input to the mechanical model.

Measurement Methodology

The measurements were conducted using a 612 Vicon system with six M-cameras running at 250Hz. Furthermore, a 1.0m by 0.4m pressure plate system constructed by RSscan International was used to measure the plantar food pressures at a frequency of 500Hz (8192 sensors, 8bits, maximum value of 127N/sensor). Also, a 0.9m by 0.6m force plate running at 1250Hz, constructed by Kistler, was used to dynamically calibrate the pressure plate. Finally, a 3D data box constructed by RSscan International was used to synchronise all measurement devices.

Four markers were attached to the heel to track its motion. Predominately, we used heel marker plates to which the four markers were attached. This was a problem for small and narrow heels. In such a case, we attached isolated markers to the heel such that they resembled the outline of the marker plates.

From the registered pressure distributions, the heel area was isolated and the areas' pressure distribution was taken as input for the mechanical model.

Three measurement conditions were employed that all contained walking trials. Walking trials of an individual were selected if at least three trials could be used for analysis. In 83 out of a total of 125 individuals that participated in this study, their left and right foot were measured at least 5 times and at most 10 times per foot. For the remaining 42 individuals, 5 trials for the left foot were measured. The individuals had

an average age of 25.7 years with a standard deviation of ± 11.9 years ([10y,72y]) and an average weight of 68.9kg with a standard deviation of ± 14.9kg ([32kg,116.5kg]). The population consists of 48 women and 77 man. The number of individuals not able to wear marker plates was 22.

All other details about measurement methodology are found in Chapter 2.

Model Sensitivity and Parameter Correction

Pressure distribution of the heel area is an input parameter to the mechanical model. From this heel area, CoP paths are calculated. After this, the function of input parameter is taken up by the CoP path. It is evident that changes in the heel area result in different CoP paths. Therefore, model sensitivity is in part a consequence of the sensitivity of the CoP path to changes in heel area.

Another input of the mechanical model is the radius of the sphere. For all trials of all individuals, we calculated the optimal radius such that the range of motion of the plantar/dorsal flexion angle of the model and MAS curves were equal. Sensitivity of the Cardan angles to changes in the radii of spheres was then calculated with respect to group average.

After an optimal radius was found, we looked at possible corrections to the CoP path as suggested in the assumption part of this chapter. We choose a linear correction with maximal influence at first foot contact and no influence at the end of the chosen time interval. We calculated the optimal correction for all trials and studied the sensitivity of this parameter with respect to the average of all corrections of all individuals' trials. The magnitude of the correction was determined using the reciprocal relationship between contact path and heel motion, see (3.20). The local heel reference frames together with the optimal radius were used to construct a contact path from MAS measurements. At first, the end point of this contact path was (0,0), because it is not possible to generate valid coordinates within the pressure plate system on the basis of a local reference frame from MAS. To be able to compare this contact path with the CoP path from the pressure plate, a translation was performed such that the final coordinates of the contact path were the same as the final coordinates of the CoP path. The magnitude of correction was chosen to be the difference in x-component between the first coordinates of both paths, see Figure 3.4. The correction was applied in a linearly decreasing way from the starting point to the end point. This method is called the begin-end point method. A second correction method, the regression

method, employed the technique of linear regression to find the coefficients, a_1 and a_2 of the equation $y = a_1\, x + a_2$, where y is a vector containing the differences between the x-components of the CoP path and the contact path, and x is a vector of length N such that $x(k) = 1 - (k-1)/(N-1)$, $k = 1, \ldots, N$. So, the correction is still lineair, but differs from the first method by using the complete CoP and contact path instead of only their begin and end points. In Figure 3.4, an example is given of a CoP path, a contact path, and consequences of applying both correction methods.

In the previous three paragraphs, we discussed testing model sensitivity with re-

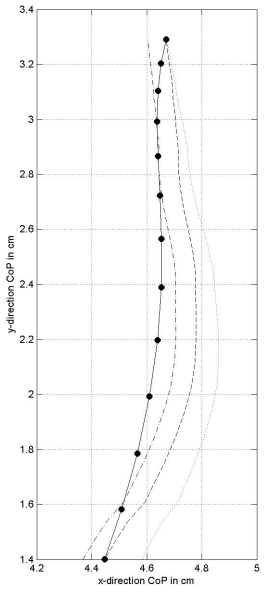

Figure 3.4 An example of a contact path and a CoP path of one trial during the initial contact phase. The solid line is the contact path calculated from MAS measurements. The dotted line is the CoP path calculated from PPPS measurements. The dashed line is the corrected CoP path after the begin-end point method was applied. The dashed-dotted line is the corrected CoP path after the regression method was applied.

spect to the input parameters CoP path and radius. Also, parameter correction was

discussed in the form of corrections to the CoP path on the basis of a contact path calculated from MAS measurements. The results of the latter two, radius sensitivity and CoP corrections, are implicitly dependent on the time interval chosen. The time intervals, we have selected range from as short as initial contact phase to as long as heel contact phase. In total, we introduce eight additional time intervals. All time intervals start at first foot contact while their end time points are determined by the time points that divide the interval from first metatarsal contact till heel lift in nine equal buckets. The selection of these ten intervals helps in assessing model sensitivity, parameter corrections, and model validation in the time domain.

Validation Method

Cardan angles from MAS and PPPS were both calculated from raw data in the Matlab environment. Specific details of these calculations are found in Appendix C.2. To be able to compare the Cardan angles from both systems, we need to define an initial condition for the heel reference frame calculated with the model. Two approaches were employed to solve the initial condition problem:

1. *The time point of first metatarsal contact is taken to have zero orientation.*
   This means that the average angle curves calculated from MAS and PPPS data have in both cases a zero standard deviation at first metatarsal contact. This approach removes partly the natural variation of these angles between gait trials, which might be a disadvantage. On the other side, the angles were calculated from the model and PPPS data without using any information of MAS data. A consequence of this approach is depicted in Figure 3.5.

2. *The initial orientation is determined calculating a least square correction based on the distances between the curves obtained from MAS and PPPS on a trial-to-trial basis and applying this correction to the model curves.*
   This approach does really need information of MAS to determine initial positions, see Figure 3.6. On the other hand, it upholds the natural variation of gait.

For validation of our approach, we used the calculated inversion/eversion curves on the basis of the measurements of both systems. The curves are considered the same if:

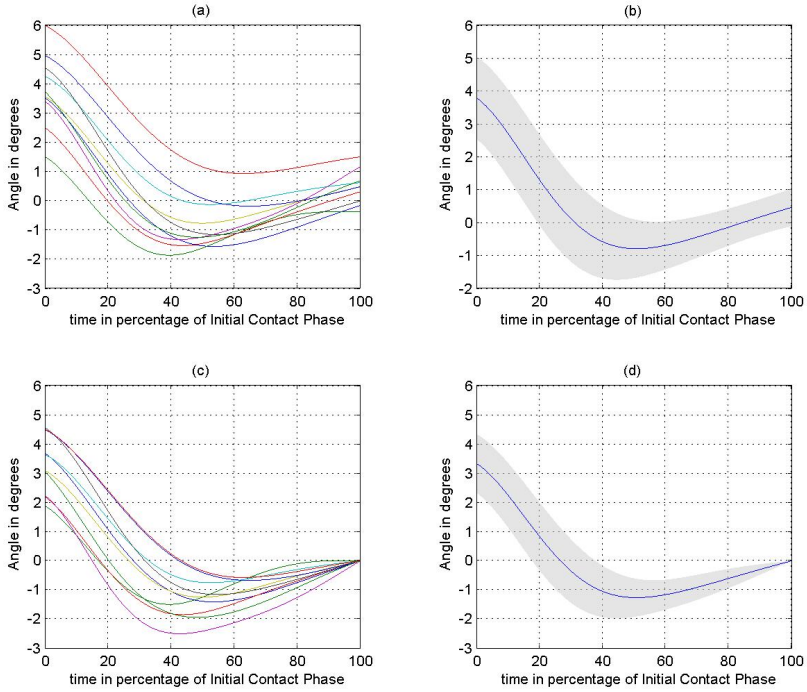

Figure 3.5 In all graphs, the time period is expressed in percentage of initial contact phase, from first foot contact to first metatarsal contact. Graph(a) contains all inversion/eversion curves of all trials of one individual measurement with MAS, while graph (b) contains the average curve with a standard deviation band. The same holds for graphs (c) and (d) with the exception that now at the moment of first metatarsal contact the angle is taken to have a zero degree value. This means that all trial curves have been supplied with an individual trial value to ascertain the sought-after effect.

the average model curve is within 1.5° of the average MAS curve, or within one standard deviation of the average MAS curve during 90% of the selected time interval.

The 90% of interval length was chosen allowing the possibility that a single frame, or

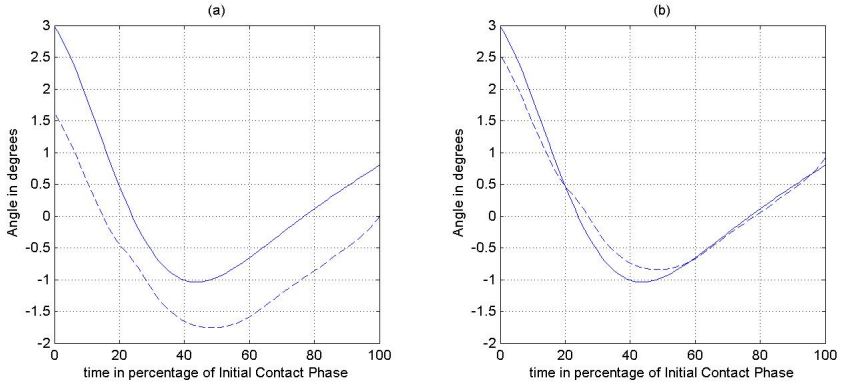

Figure 3.6 In graph (a), inversion/eversion curves are depicted (inversion is positive) calculated from MAS data (solid lines) and calculated from PPPS data (dashed lines). The example concerns an arbitrary trial of an individual from first foot contact till first metatarsal contact, the initial contact phase. In graph (b), the same two curves are depicted but with a least square correction of 0.93 degrees added to the model curve.

perhaps two frames, are not in the one-standard deviation band. The choice for the absolute angle difference value of 1.5° is based on the variations in length between the different heel markers and the accuracy of kinematic data as discussed in Section 2.2.2. The average lengths of vectors that are used for determining the local heel reference frame are both about 8cm. Based on the previously mentioned section on kinematic data accuracy, the angle values are calculated with an accuracy between 2.2° and 0.3°, and slightly closer to 0.3° than to 2.2° based on the lengths of the vectors. However, from the same section, we see that the variation in vector lengths is about 3 times larger than when the markers are rigidly connected. From the previous considerations, we come to the believe that 1.5° as absolute angle difference resembles the measurement accuracy in the case of heel orientation angles.

3.4 Results

Optimal Radius and Radius Sensitivity of the Sphere

The data from 43 individuals that performed the walking condition were used to

study stability and optimality of the radius parameter in the mechanical model. In the mechanical model, heel motion is regarded as the rolling of a sphere with an individual-related optimal radius. For the selected ten time intervals the optimal radii were calculated. In Figure 3.7, we show both the group averages for the ten time intervals as well as two extreme examples. The group averages for left trials, (a), and right trials, (b), appear to be similar. The examples, (c) and (d), show that the group average is constructed from a variety of individual possibilities.

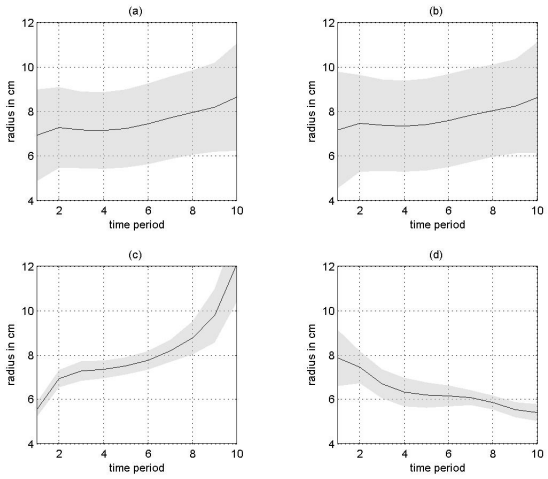

Figure 3.7 In all graphs, the numbers on the x-axis are related to the ten time periods defined in the part on Model Sensitivity and Parameter Correction in Section 3.4. In graph (a) and (b), the average and standard deviation of radii of left and right feet are depicted. In graph (c) and (d), two examples are depicted from two individuals left trials. In this case, the standard deviation is calculated with respect to the different trials within an individuals measurement session.

In initial contact phase, the maximum difference between average inversion/eversion curves was obtained from curves calculated with optimal radii and from curves with the fixed average radius of 7cm. The latter radius is the average radius of all trials, left and right combined, and of all individuals. In Figure 3.8, we depict the results of the maximum differences in a histogram. For convenience, we also present the histogram of the optimal radii for the initial contact phase. From Figure 3.8, we notice that 71.0%

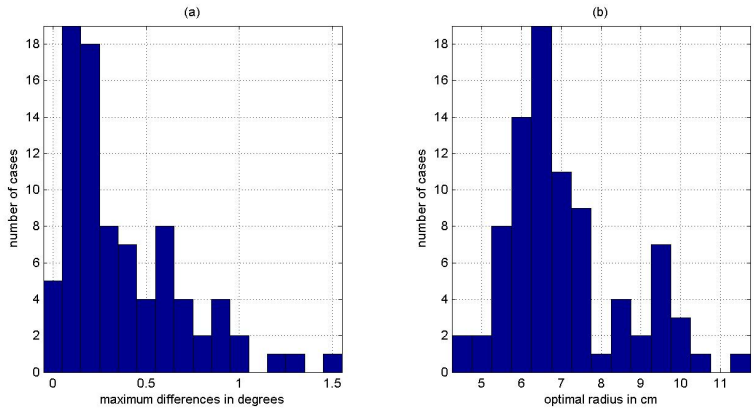

Figure 3.8 In graph (a), the maximum difference is depicted as a distribution between the inversion/eversion curve constructed from optimal radii and using the average radii. In graph (b), the distribution of the optimal radii in case of the initial contact phase is depicted.

of all individuals' sessions have less than half a degree of maximum inversion/eversion angle difference. In Figure 3.9, two representative examples are given. One was taken from the 71.0% set and the other one from the remaining set.

In an effort to verify existence of a relationship between individuals' optimal radii and the calculated maximum differences found, the list of individuals with a maximum difference between MAS and PPPS inversion/eversion curves larger than 0.95° was compared to the list of individuals with optimal radii larger than 9.7cm. The idea was that large differences between average radii and optimal radii were related to large maximum angle differences. However, we could only find one individual present in both lists. The others present in the maximum difference list have optimal radii smaller than 5.9cm. The expected relationship could, therefore, not be justified.

The overal result of this analysis is that the radius of the sphere in the mechanical model is not a critical parameter when average radii are compared to optimal radii. Therefore, the average radii could be used in the mechanical model instead of the optimal radii. This brings us one step closer to our objective, because optimal radii were calculated using MAS data, and our objective was to use only plantar pressure data to obtain heel motion.

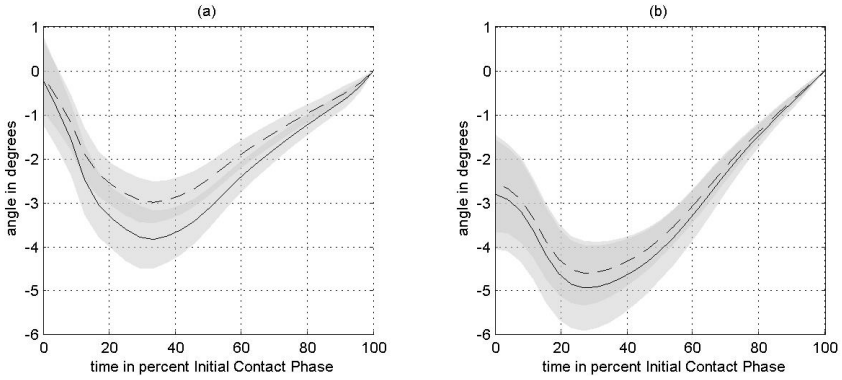

Figure 3.9 Two examples of average inversion/eversion curves with a one standard deviation band. The solid lines are related to curves constructed from optimal radii and the dashed lines are related to curves constructed from the average radius of 7.0cm. The standard deviation band is depicted in transparant grey. In case the standard deviation band of both average and optimal overlay the same area the intensity of the grey level is enhanced. In graph (a), an example is depicted from the set, representing 29% of total, in which the optimal and average curves have a maximum difference larger than half a degree (here 0.80° to be precise). In graph (b), an example is depicted where this difference is smaller than half a degree (here 0.34° to be precise)). It is noted that both examples have a chosen initial orientation for the inversion/eversion curves of zero degrees at the end of the initial contact phase.

Sensitivity and Correction of the Centre of Pressure Paths

The sensitivity of the CoP path is completely determined by what we define as heel area. Although, several definitions of the heel areas in plantar pressure distributions are known in literature (see Section 1.2), corresponding implementations using the present dynamic plantar pressure measurement is not straightforward. In Section 2.2.6, we introduce our division of the pressure distribution of the foot. In essence, the heel area is defined by a line perpendicular to the length direction of the pressure plate, and expressed as a number of sensors in this length direction. So, for example, if the heel area has been defined by a sensor number in the y-direction, the heel area consists of all sensors with a y-direction sensor number less than or equal to this number, see Figure 3.10.

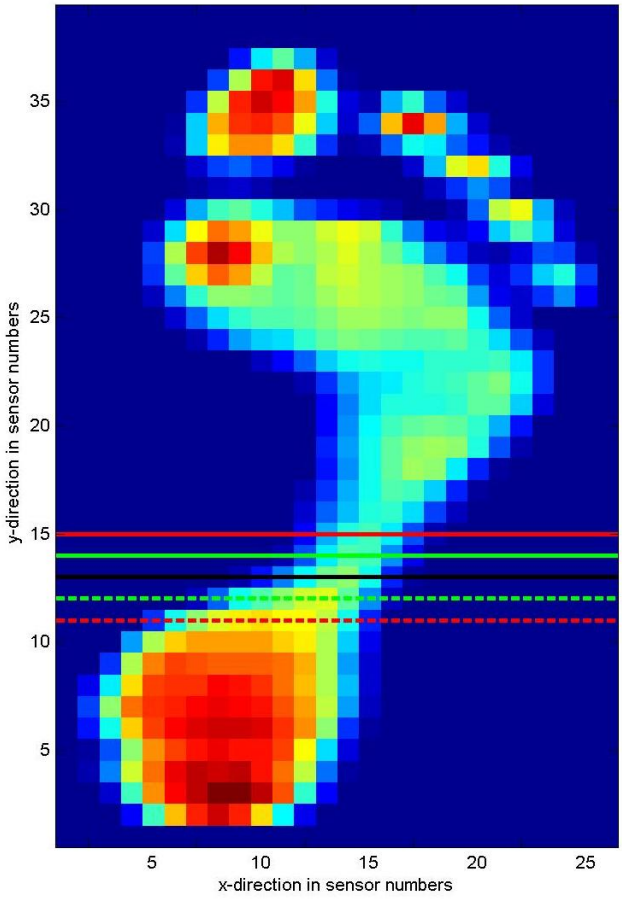

Figure 3.10 In this graph, an example is given of maximum plantar pressure distribution with a determination of the heel area. The area algorithm defines the heel area to be all sensors beneath and including the line though sensors with a y-sensor number of thirteen, the black line. One y-sensor length below this black line is depicted by the dashed green line and one y-sensor length above this black line is depicted by the solid green line. Two y-sensor length below this black line is depicted by the dashed red line and two y-sensor length above this black line is depicted by the solid red line.

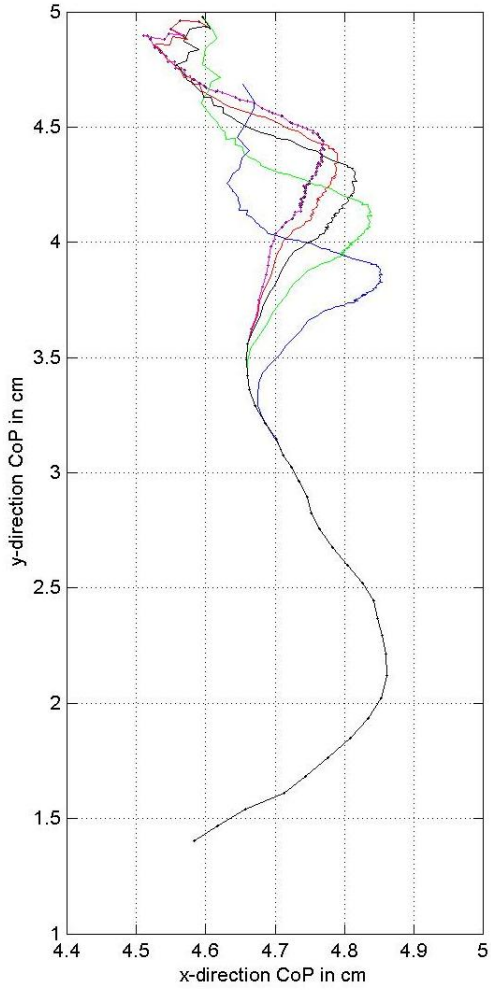

Figure 3.11 In this graph, five CoP paths are depicted. The black curve is the CoP path constructed using the heel area as defined in the Appendix 2.2.6. The blue line is the CoP path constructed using two y-sensor lines less to determine the heel area. The green line is the CoP path constructed using one line less. The red line is the CoP path constructed using one line more. The circle marker line is the CoP path constructed using two lines more.

To study the effect of our choice of heel areas, we consider four other horizontal lines, one or two sensors above or below the chosen one, see Figure 3.10. The largest length difference is between the two above and two below lines and has a length of 3.1cm. To compare CoP paths, both the deviation in distance and in time were looked at. In Figure 3.11, we depict the CoP paths for these five heel areas of one individual. Initially, the CoP paths were the same, but they start to deviate from a certain time point on. All individuals show this pattern. In studying how sensitive the CoP path is for the choice of heel area, the consequences of the deviations of the CoP paths on the inversion/eversion angles calculated from the mechanical model are given in Table 3.2. Angle differences were calculated on a trial bases. From the five inversion/eversion curves, related to the five heel areas, four angle difference curves were calculated. The angle difference functions are calculated by subtracting the values for the inversion/eversion angle of the chosen heel area from the other four angle curves. Per trial, the average and maximum angle difference were calculated together with the time point of maximum difference. Per individual, all trial values of average difference, maximum difference and time to maximum were averaged. The histograms of the average angle differences are depicted in Figure 3.12, together with two examples of angle difference curves for two selected trials of one individual. Furthermore, the time points where the different CoP paths start to deviate were calculated, see Table 3.1. This concludes the part on sensitivity.

For the correction of CoP paths, the reciprocal equations (3.20) were used to calculate contact paths from time series of orientation matrices based on MAS data. Two methods were employed for this correction, see Model Sensitivity and Parameter Correction in Section 3.3 (the begin-end point method and the regression method). We report the corrections in Tables C.4-C.9 in Appendix C, and in Figure 3.13. This figure contains the histogram of corrections per individual of the begin-end point method. For left and right trials, in part (a) and (b) of this figure, the histogram is presented for ten selected time intervals, as defined in Section 3.3, using a one standard deviation band. The graphes depicted in Figure 3.13, (a) and (b), appear to behave similarly with respect to trend and standard deviation band. In contrast, there does seem to be an offset in the size of correction. This offset is depicted more explicitly for the initial contact phase of Figure 3.13 in parts (c) and (d). Although, there is an offset difference of about 0.1cm, and although this difference might be significant, we emphasize that a sensor width is five times larger than the observed offset difference. Therefore, we

Table 3.1 Population information on the time point at which the CoP paths of the walking sessions of the different heel areas start to deviate. All information is related to left foot trials of specific individuals. Time points are expressed as a percentage of the individuals stance phase. **A** is the average time point were the CoP paths deviate; average with respect to all trials of one individual. **S** is the standard deviation of the time points where the CoP paths deviate and **MM** is the maximum time point minus the minimum time point where the CoP paths deviate. The postfixes -2, -1, $+1$, and $+2$ are related to comparison of CoP paths. For example, -2 means the comparison of the original heel area and this heel area minus two horizontal lines.

Name	A -2	S -2	MM -2	A -1	S -1	MM -1	A +1	S +1	MM +1	A +2	S +2	MM +2
individual 1	11.4%	2.2%	7%	11.4%	2.3%	7.4%	11.4%	2.3%	7.4%	11.3%	1.9%	6%
individual 2	11.6%	1.5%	4.6%	11.7%	1.6%	4.6%	11.7%	1.6%	4.6%	11.6%	1.5%	4.6%
individual 3	13.5%	1.2%	3.6%	13.5%	1.2%	3.6%	13.5%	1.2%	3.6%	13.5%	1.2%	3.6%
individual 4	15.3%	1.1%	3%	15.4%	1.2%	3.3%	15.4%	1.2%	3.3%	15.4%	1.1%	3.3%
individual 5	33.7%	14%	40.9%	34.1%	14.1%	41.8%	34.1%	14.1%	41.8%	33.9%	14.1%	41.8%
individual 6	16.9%	6.1%	18%	17.4%	6.2%	18.4%	16.9%	5.6%	16.8%	14.8%	3.4%	11.2%
individual 7	9.2%	1.9%	6.6%	9.2%	1.9%	6.6%	9.2%	1.9%	6.6%	9.2%	1.9%	6.6%
individual 8	15.6%	9.3%	31.5%	15.9%	9.7%	33%	15.9%	9.7%	33%	15.9%	9.7%	33%
individual 9	13.2%	6.3%	21.4%	13.4%	6.8%	22.7%	11.8%	2.3%	6.9%	11.5%	1.6%	4.9%
individual 10	11.8%	6.1%	16.6%	12.1%	6.3%	16.6%	12.1%	6.3%	16.6%	12.1%	6.3%	16.6%
individual 11	8%	0.6%	1.8%	8.2%	0.7%	2%	8.2%	0.7%	2%	8%	0.5%	1.5%
individual 12	14.8%	1.9%	5.9%	15%	1.9%	5.6%	15%	1.9%	5.6%	14.9%	1.9%	5.6%
individual 13	11.2%	1.1%	4.1%	11.3%	1.1%	4.1%	11.2%	1.2%	4.4%	11.1%	1.2%	4.4%
individual 14	8.9%	0.5%	1.7%	8.9%	0.5%	1.7%	8.9%	0.5%	1.7%	8.9%	0.5%	1.7%
individual 15	9.1%	0.4%	1%	9.2%	0.3%	1%	9.1%	0.3%	1%	8.9%	0.4%	1.2%
individual 16	8.6%	0.9%	2.5%	8.6%	0.9%	2.5%	8.6%	0.9%	2.5%	8.5%	0.9%	2.4%
individual 17	10.5%	2.3%	7%	10.6%	2.4%	7%	10.6%	2.4%	7%	10.6%	2.4%	7%
individual 18	71.4%	37.3%	75.6%	71.6%	37.1%	75.6%	71.2%	37.6%	76.4%	69.9%	39.2%	79.8%
individual 19	10.5%	3.8%	9.5%	10.9%	4.1%	10.5%	9.9%	3.9%	9.2%	6.6%	1.6%	5.6%
individual 20	13.7%	3.9%	11.7%	13.7%	3.9%	11.7%	13.7%	3.9%	11.7%	13.7%	3.9%	11.7%
individual 21	34.2%	23.7%	83.6%	41.5%	31.3%	83.6%	41.5%	31.3%	83.6%	35%	23.6%	83.6%
individual 22	10.1%	0.6%	1.6%	10.2%	0.6%	1.6%	10.2%	0.6%	1.6%	10%	0.5%	1.5%
individual 23	18.1%	3.4%	13%	18.3%	3.4%	13.3%	18.2%	3.4%	13.3%	17.8%	3.4%	13.6%
individual 24	36.3%	12.7%	38%	37.1%	13%	37.7%	35.9%	12.8%	38%	29.5%	11.8%	32.7%
individual 25	40.1%	34.1%	88%	40.2%	34%	88%	40.2%	34%	88%	39.9%	34.2%	88%
individual 26	17.6%	3.1%	8.6%	17.8%	3%	8.6%	17.8%	3%	8.6%	17.6%	2.8%	8.3%
individual 27	15.5%	2.5%	7.2%	15.8%	2.5%	7.2%	15.8%	2.5%	7.2%	15.7%	2.5%	7.2%
individual 28	17.1%	1.6%	4.6%	17.3%	1.7%	5.2%	17.1%	1.7%	4.9%	16.6%	1.8%	5%
individual 29	14.3%	1.8%	6.3%	14.4%	1.9%	6.6%	13.9%	1.5%	5.1%	13%	1.3%	4.6%
individual 30	12.5%	0.9%	3.1%	12.6%	0.9%	2.8%	12.5%	0.9%	3.1%	12.3%	0.6%	1.8%
individual 31	9.2%	0.6%	2.1%	9.3%	0.7%	2.5%	9.3%	0.7%	2.5%	9.2%	0.7%	2.1%
individual 32	15.1%	1.8%	6.5%	15.1%	1.9%	6.8%	15.1%	1.9%	6.8%	15.1%	1.9%	6.8%
individual 33	8.5%	0.7%	1.9%	8.6%	0.7%	1.9%	8.6%	0.7%	1.9%	8.5%	0.7%	1.9%
individual 34	8.5%	0.7%	2.3%	8.5%	0.7%	2.3%	8.5%	0.7%	2.3%	8.5%	0.7%	2.3%
individual 35	9.2%	1%	2.9%	9.2%	1%	2.9%	9.2%	1%	2.9%	9.2%	1%	2.9%
individual 36	10.7%	0.9%	3%	10.8%	1%	3.4%	10.7%	0.9%	3%	10.5%	0.9%	2.7%
individual 37	10.2%	1%	3%	10.2%	1%	3%	10.2%	1%	3%	10.2%	1%	3%
individual 38	12.5%	1.9%	5.7%	12.5%	1.9%	5.7%	12.5%	1.9%	5.7%	12.5%	1.9%	5.7%
individual 39	8.8%	1.1%	3.2%	8.9%	1.1%	3.2%	8.9%	1.1%	3.2%	8.9%	1.1%	3.2%
individual 40	51.1%	38.5%	86.9%	51.2%	38.4%	86.9%	51%	38.5%	86.9%	43.1%	34.1%	86.9%
individual 41	6.7%	0.9%	2.6%	6.7%	0.9%	2.6%	6.7%	0.9%	2.6%	6.7%	0.9%	2.6%
individual 42	15.7%	2.5%	8.4%	16%	2.4%	8.1%	15.8%	2.5%	8.4%	15%	2.5%	8.1%
individual 43	11.9%	1%	3.8%	12%	1%	3.5%	12%	1%	3.5%	12%	0.9%	3.5%
Average	16.6%			16.9%			16.6%			16.0%		

Table 3.2 Population information on the deviations in inversion/eversion curves calculated from CoP paths of the different heel areas. Individual information is related to all trials of that individual. Deviations are expressed in average differences in degrees: **A**, maximum differences in degrees: **M**, and times to maximum difference in percentage of heel contact: **IM**. To clarify further, the average differences in degrees of an individual is the average over all trial average differences. The same holds for maximum difference and the time point of maximum difference. The postfixes -2, -1, $+1$, and $+2$ are related to comparison of CoP paths. For example, -2 means the comparison of the original heel area and this original heel area minus two horizontal lines.

Name	A -2	M -2	IM -2	A -1	M -1	IM -1	A +1	M +1	IM +1	A +2	M +2	IM +2
individual 1	0.5°	1°	91.2%	0.2°	0.5°	87.1%	0.3°	0.7°	87.2%	1.3°	3.4°	93.7%
individual 2	0.6°	1.3°	84.5%	0.2°	0.6°	77.5%	0.3°	0.9°	72.1%	0.9°	2.6°	72.9%
individual 3	2.6°	5.8°	99.8%	1.6°	3.4°	99.9%	2.9°	6.1°	99.7%	7.2°	14°	99.7%
individual 4	1°	1.9°	83.6%	0.6°	1.2°	83.1%	1.1°	2.5°	88.6%	2.9°	6.4°	91.3%
individual 5	0.1°	0.4°	70.8%	0°	0.2°	47.1%	0.1°	0.3°	46.7%	0.4°	1.2°	57.8%
individual 6	0.4°	0.9°	84.2%	0.2°	0.4°	85%	0.4°	1.3°	87.1%	1.6°	5.2°	94.6%
individual 7	1°	1.9°	92%	0.5°	1°	92.9%	0.6°	1.5°	95.3%	1.6°	3.6°	96.5%
individual 8	0.2°	0.4°	70.1%	0.1°	0.1°	51.8%	0°	0°	22.1%	0°	0.1°	28.5%
individual 9	0.8°	1.7°	93.4%	0.5°	1.3°	93.2%	1.3°	3.8°	96.4%	3.9°	9.9°	99.4%
individual 10	0.5°	1.1°	79.8%	0.2°	0.4°	77%	0.1°	0.2°	65%	0.2°	0.5°	65.7%
individual 11	2°	3.5°	92.3%	1°	2°	91.9%	1.8°	3.8°	97.4%	5.2°	10.9°	99.8%
individual 12	0.3°	0.6°	82.1%	0.1°	0.3°	80.1%	0.1°	0.4°	82.1%	0.6°	1.6°	88%
individual 13	4.5°	9.1°	99.7%	2.9°	5.7°	99.6%	5.1°	9.2°	99.8%	12.2°	20.6°	99.8%
individual 14	2.8°	5.7°	99%	1.7°	3.7°	99.1%	2.5°	5.2°	99.7%	5.5°	10.7°	99.9%
individual 15	5.6°	12.8°	99%	3.4°	7.8°	98.6%	5°	9.3°	97.8%	11.2°	18.8°	96.9%
individual 16	1.3°	2.8°	91.1%	0.8°	1.9°	91.5%	1.4°	3.2°	94.2%	3.8°	7.8°	94.6%
individual 17	0.2°	0.3°	86%	0.1°	0.2°	77%	0°	0.1°	69%	0°	0.1°	67.7%
individual 18	0.1°	0.2°	71.6%	0°	0.1°	57.2%	0.1°	0.3°	64.2%	0.6°	2°	83.9%
individual 19	0.7°	1.4°	91.6%	0.4°	0.9°	91.7%	1°	2.5°	95.2%	4.1°	9.2°	99.4%
individual 20	0.1°	0.2°	65%	0°	0.1°	60.9%	0°	0°	16.2%	0°	0°	16.3%
individual 21	0.1°	0.3°	72.3%	0°	0°	38%	0°	0°	11.2%	0°	0°	20.6%
individual 22	1.3°	2.3°	83.3%	0.7°	1.3°	83.3%	1.3°	3.1°	88.4%	4.5°	10.1°	91.1%
individual 23	0.4°	0.9°	85.7%	0.2°	0.5°	85.1%	0.6°	1.7°	92.7%	2.1°	5.4°	96.8%
individual 24	0.6°	1.8°	88.5%	0.4°	1.4°	89.9%	1.4°	4.4°	97.2%	4.5°	12°	98.5%
individual 25	0.5°	1.1°	76.5%	0.2°	0.5°	68%	0.4°	0.9°	57.3%	1.3°	2.9°	65.2%
individual 26	2.9°	5.5°	97.6%	1.8°	3.3°	97.4%	2.7°	4.8°	98.2%	5.9°	10.1°	98.2%
individual 27	0.7°	1.7°	87.6%	0.4°	1°	89%	0.6°	1.8°	93.4%	2.1°	5.8°	94.6%
individual 28	1.1°	2.7°	90.9%	0.8°	2.3°	97.2%	2.5°	7.2°	100%	6.8°	17.1°	100%
individual 29	1.7°	4.9°	94%	1.3°	3.8°	93.6%	3.4°	8.7°	96.1%	9.9°	22.2°	99.9%
individual 30	1.6°	3.7°	99.2%	0.9°	2°	99.2%	1.7°	3.8°	99.8%	5°	10.5°	99.9%
individual 31	1.4°	3.3°	94%	0.9°	2.4°	96%	2.5°	6.7°	99%	7°	16.8°	99.9%
individual 32	0.7°	1.8°	93.8%	0.4°	1.1°	94.6%	0.9°	2.2°	97.3%	2.6°	6°	98.6%
individual 33	1.8°	3.8°	98.7%	1°	2.2°	99.2%	1.5°	3.6°	99.9%	3.8°	8.7°	100%
individual 34	2.2°	4.4°	99.9%	1.4°	2.8°	99.7%	2.5°	4.6°	99.9%	5.9°	10.3°	99.9%
individual 35	1°	1.8°	95.7%	0.5°	1°	94.9%	0.6°	1.3°	95.9%	1.4°	3°	97.6%
individual 36	0.6°	1.1°	86.7%	0.3°	0.7°	87.8%	1°	3.2°	97.8%	3.4°	10.1°	99.6%
individual 37	1.2°	3.4°	98.1%	0.8°	2.1°	98.4%	1.8°	4.5°	99.3%	4.6°	10.9°	100%
individual 38	1.5°	3.7°	99.2%	0.9°	2.2°	99.4%	1.6°	3.7°	99.9%	4.1°	8.6°	99.9%
individual 39	1.2°	2.1°	82.3%	0.6°	1.1°	74.4%	0.7°	1.5°	74.2%	2.2°	4.8°	76.5%
individual 40	0.2°	0.4°	69.8%	0.1°	0.2°	69.8%	0.1°	0.4°	60%	0.4°	1.2°	63.7%
individual 41	2.3°	3.9°	98.8%	1.4°	2.3°	98.7%	2.3°	3.6°	99%	5.7°	8.7°	99.2%
individual 42	3.1°	8.3°	97.3%	2°	5.3°	98.5%	3.5°	8°	98.7%	8.3°	17°	98.5%
individual 43	0.5°	1.2°	85.5%	0.3°	0.6°	85.1%	0.4°	1.2°	88.6%	1.3°	3.5°	91.5%
Average	1.2°	2.7°	88.4%	0.7°	1.7°	85.6%	1.4°	3.1°	84.2%	3.6°	7.8°	86.9%

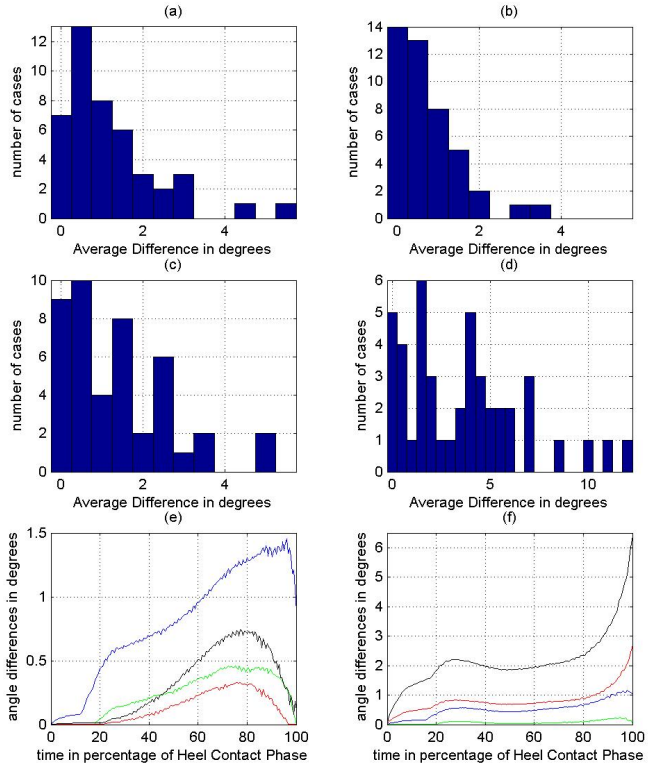

Figure 3.12 The distributions of the average differences in inversion/eversion curves are depicted in graphs (a) to (d). The numerical data for these distributions can be found in columns one, four, seven and ten of Table 3.2, respectively. The other two graphs, (e) and (f) are examples of the angle difference inversion/eversion curves for two trials of the same individual. The blue line is the angle difference for an heel area of two lines less than the original heel area. The green line is the difference for an heel area of one line less than the original heel area. The red line is the difference for an heel area of one line more than the original heel area. The black line is the difference for an heel area of two lines less than the original heel area.

regard this as insignificant from a measurement accuracy point of view. A similar figure is also constructed for the regression method, leading to the same conclusions, and can be found in Appendix C; Figure C.1.

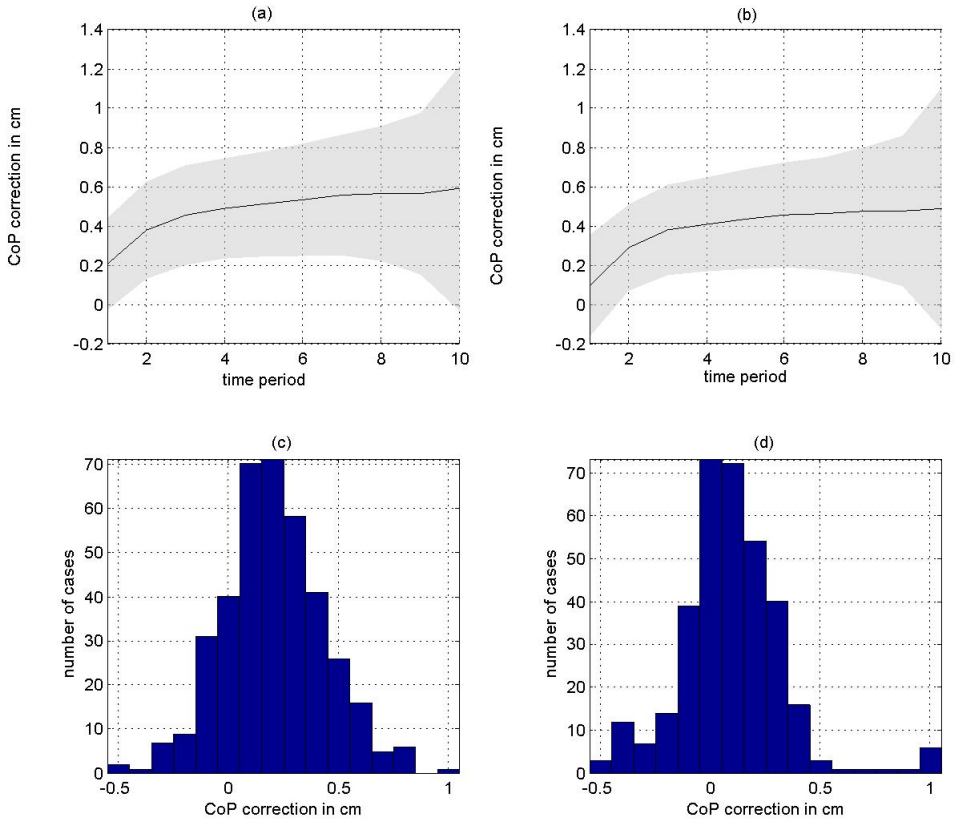

Figure 3.13 In this figure, the CoP path correction based on begin-end point correction is depicted. In graph (a) and (b), the average and standard deviations of the x-direction corrections are depicted for left and right trials of the walking sessions, respectively. In graphs (c) and (d), the left and right distribution of corrections for the initial contact phase are depicted.

The optimal radii were based on MAS data. Since the distributions of corrections

are narrow, we use the average corrections for both the begin-end point and regression method. Thus, we reach our objective to use only plantar pressure data as input to obtain heel motion.

Validation of the model

We validated the model for the inversion/eversion angle for a variety of methods. In Section 3.3, we introduced two approaches for the initial orientation problem. Furthermore, from the above mentioned topics in this section, we were able to distinguish optimal radii and average radii, and optimal corrected CoP paths and average corrected CoP paths. Even in more detail, the corrected CoP paths were calculated using two methods: begin-end point method and regression method. Finally, the model validation was performed for all ten time intervals. Validation results for the individuals that performed walking sessions are presented In Table 3.3.

The results show that the initial orientation based on least square fitting is in all cases preferred over the initial orientation that sets the local heel reference frame equal to the global reference frame at first metatarsal contact. Further, no major changes are observed between the results using begin-end point method and regression method for correcting the CoP paths. Also, no major distinction can be made between left and right trials.

Taking optimal CoP path corrections and optimal radii renders more than 90% predictive power for the initial contact phase. The predictive power of the model using only pressure plate data as input is about 75% for the initial contact phase. The predictive powers for different selected time intervals show a rapid decrease from first foot contact to heel lift. In the worst case, a drop from 74.4% to 7.0% was observed.

Although previous results show favorable predictive powers, one issue remains. Both the calculations of average radii and average CoP path corrections, and the validation of the mechanical model were based on the same population of 43 individuals performing the walking condition. Therefore, parameters may be fitted to accommodate this population. To verify that parameters are not fitted, we took the walking trials from the other two conditions, containing data from 82 individuals, and calculated the predictive powers of the mechanical model for this population taking the average radii and average corrections values of the walking condition. The results confirm that parameters were not fitted, see Table 3.4. Only slight differences from the 43 individuals were observed.

Table 3.3 Model validation results of inversion/eversion angles of individuals that performed the walking session. In the first column, the correction type is given. The postfix '1' or '2' is connected to the initial orientation approach, '1' being the least square approach and '2' being the initial metatarsal contact approach. The prefix 'L.T' or 'R.T' stands for left or right trials; 'A. Correction' stands for corrections based on average radii and average CoP correction using the begin-end point method; 'R. Correction' stands for corrections based on average radii and average CoP corrections using the regression method; 'O. Correction' stands for corrections based on optimal radii and optimal CoP corrections using the begin-end point method; 'OR. Correction' stands for corrections based on optimal radii and optimal CoP corrections using the regression method. Columns two to eleven are related to the different time intervals, ranging from Initial Contact Phase(ICP) to Heel Lift

Correction type	ICP	2	3	4	5	6	7	8	9	Heel Lift
L.T. A.Correction1	78.0%	73.2%	63.4%	51.2%	46.3%	46.3%	39.0%	36.6%	24.4%	17.1%
R.T. A.Correction1	74.4%	62.8%	53.5%	48.8%	44.2%	41.9%	30.2%	25.6%	20.9%	7.0%
L.T. A.Correction2	48.8%	46.3%	36.6%	34.1%	34.1%	29.3%	24.4%	19.5%	14.6%	7.3%
R.T. A.Correction2	51.2%	44.2%	34.9%	32.6%	32.6%	25.6%	18.6%	18.6%	11.6%	2.3%
L.T. R.Correction1	78.0%	73.2%	68.3%	56.1%	43.9%	46.3%	39.0%	36.6%	22.0%	12.2%
R.T. R.Correction1	74.4%	69.8%	62.8%	53.5%	48.8%	34.9%	32.6%	27.9%	18.6%	9.3%
L.T. R.Correction2	51.2%	48.8%	41.5%	39.0%	26.8%	24.4%	24.4%	14.6%	14.6%	7.3%
R.T. R.Correction2	53.5%	46.5%	34.9%	41.9%	27.9%	20.9%	20.9%	16.3%	14.0%	2.3%
L.T. O.Correction1	92.7%	92.5%	87.8%	75.0%	65.9%	58.5%	46.3%	36.6%	31.7%	22.0%
R.T. O.Correction1	90.0%	80.5%	75.0%	67.5%	55.0%	41.5%	36.6%	35.7%	35.7%	33.3 %
L.T. O.Correction2	70.7%	77.5%	63.4%	45.0%	43.9%	43.9%	31.7%	29.3%	22.0%	12.2 %
R.T. O.Correction2	57.5%	63.4%	47.5%	45.0%	37.5%	34.1%	31.7%	23.8%	16.7%	11.9%
L.T. OR.Correction1	90.2%	87.5%	85.4%	82.5%	78.0%	70.7%	58.5%	48.8%	41.5%	29.3%
R.T. OR.Correction1	87.5%	78.0%	75.0%	80.0%	77.5%	70.7%	51.2%	45.2%	40.5%	33.3%
L.T. OR.Correction2	75.6%	80.0%	63.4%	55.0%	51.2%	46.3%	36.6%	31.7%	29.3%	19.5%
R.T. OR.Correction2	60.0%	65.9%	52.5%	52.5%	52.5%	43.9%	41.5%	31.0%	28.6%	21.4%

The conditions under which the mechanical model was tested so far, concerned choices for model parameters and calculation methods. Table 3.6 contains the results of various divisions of the population. We divided the population in four ways: with respect to gender (two groups), with respect to use of a heel marker plate (two groups), with respect to age (three groups), and with respect to weight (three groups).

There is negligible difference between women ($N = 48$) and men ($N = 77$) and both groups have comparable overall predictive powers.

The groups without marker heel plates ($N = 22$) and with marker heel plates

Table 3.4 Model validation results of inversion/eversion angles of individuals that performed walking trials combined with either running or fast walking and running. In the first column, the correction type is given. The postfix '1' or '2' is connected to the initial orientation approach, '1' being the least square approach and '2' being the initial metatarsal contact approach. The prefix 'L.T' or 'R.T' stand for left or right trials; 'A. Correction' stands for corrections based on average radii and average CoP corrections using the begin-end point method; 'R. Correction' stands for corrections based on average radii and average CoP corrections using the regression method. Columns two to eleven are related to the different time intervals, ranging from Initial Contact Phase(ICP) to Heel Lift

Correction type	ICP	2	3	4	5	6	7	8	9	Heel Lift
L.T. A.Correction1	75.8%	68.2%	60.7%	51.7%	42.9%	37.9%	27.8%	22.8%	15.5%	10.3%
R.T. A.Correction1	75.7%	67.6%	48.6%	37.8%	32.4%	24.3%	21.6%	13.5%	13.5%	2.7%
L.T. A.Correction2	53.2%	58.2%	50.7%	39.3%	33.0%	24.1%	16.4%	13.9%	9.0%	7.8%
R.T. A.Correction2	45.9%	51.4%	43.2%	35.1%	29.7%	29.7%	21.6%	13.5%	16.2%	8.1%
L.T. R.Correction1	78.3%	74.6%	61.9%	53.2%	42.8%	35.4%	27.8%	26.5%	14.1%	12.7%
R.T. R.Correction1	75.7%	67.6%	62.2%	45.9%	43.2%	32.4%	21.6%	16.2%	16.2%	2.7%
L.T. R.Correction2	53.2%	55.8%	51.9%	43.0%	29.2%	21.6%	16.5%	13.9%	10.3%	6.4%
R.T. R.Correction2	48.6%	54.1%	43.2%	40.5%	35.1%	27.0%	18.9%	13.5%	16.2%	8.1%

($N = 103$) also show only a slight difference.

The population was split into three age groups: the first group ($N = 38$) contains the individuals younger than 21 years, the second group ($N = 64$) contains individuals with an age between 21 and 30, and the individuals in the third group ($N = 23$) where older than 30 years. The results show predictive powers over 70% for all age groups in case of initial contact phase. There are differences between left and right trials in the first two age groups and there are differences among the age groups ranging from 3.9% to 13.5%.

The population was also split in three weight groups: the first group ($N = 19$) contains individuals lighter than 56kg, the second group ($N = 86$) contains individuals with a weight between 56kg and 85kg, and the third group ($N = 20$) contains individuals heavier than 85kg. There are differences between these groups. The second weight group has the highest predictive powers, 81.2% left and 78.8% right, followed by the third group with 5-8% lower values, and finally by the first group with predictive powers 5-7% lower than in the third group.

The mechanical model does simulate the *complete* orientation of the heel, in Car-

dan angles, obtained from pressure measurements. Till now, we have looked only at the inversion/eversion curve. To conclude this result section, we briefly look at how valid the mechanical model is in determining dorsal/plantar flexion angles and abduction/adduction angles. Table 3.5 contains the predictive powers for these two complementing angles. In the validation criterion defined in Section 3.3, the absolute angle difference is normally set at 1.5°. In case of the dorsal/plantar flexion angles, however, we use 2° degrees because of the much larger range of motion of this angle. The predictive powers are of the same magnitude or higher than the ones of the inversion/eversion angles with the exception of the abduction/adduction angle of right trials, which is about 4-5% smaller.

In Figures 3.14 and 3.15, we depict examples of the comparison of model curves and MAS curves using the trial-to-trial least square initial orientation approach. we distinguish here between 'successful' and 'unsuccessful' comparisons. A comparison is called successful if it satisfies the criterion on page 97.

Table 3.5 Predictive powers of model validation for dorsal/plantar flexion and abduction/adduction angles in the walking session group. All predictive powers are calculated using the average radii and the regression method for CoP path correction. The postfixes 'L1','R1', 'L2', and 'R2' are related to left and right trials for the least square approach and to left and right trials of the first metatarsal contact approach.

Correction type	ICP	2	3	4	5	6	7	8	9	Heel Lift
DP. Flexion L1	78.0%	48.8%	48.8%	46.3%	39.0%	29.3%	14.6%	7.3%	4.9%	2.4%
DP. Flexion R1	74.4%	53.5%	39.5%	34.9%	23.3%	18.6%	14.0%	16.3%	14.0%	9.3%
DP. Flexion L2	61.0%	24.4%	22.0%	17.1%	9.8%	0.0%	0.0%	0.0%	0.0%	0.0%
DP. Flexion R2	51.2%	25.6%	16.3%	9.3%	9.3%	4.7%	2.3%	2.3%	2.3%	0.0%
Abd./Add. L1	87.8%	68.3%	36.6%	26.8%	19.5%	22.0%	19.5%	19.5%	22.0%	26.8%
Abd./Add. R1	69.8%	39.5%	25.6%	25.6%	18.6%	16.3%	16.3%	16.3%	18.6%	23.3%
Abd./Add. L2	43.9%	29.3%	9.8%	7.3%	7.3%	4.9%	2.4%	2.4%	0.0%	7.3%
Abd./Add. R2	25.6%	23.3%	14.0%	9.3%	9.3%	9.3%	9.3%	4.7%	4.7%	2.3%

3.5 Discussion

In this chapter, we focussed on simulating calcaneal motion using pressure plate measurement only. To make this possible, a mechanical modelling approach was required. We believe that the modelling approach introduced in this chapter is new and an in-

Table 3.6 Predictive powers of model validation of the inversion/eversion angles in dividing the population into different groups. Abbreviations are the same as in Table 3.3.

Correction type	ICP	2	3	4	5	6	7	8	9	Heel Lift
Women L1	79.5%	72.7%	63.6%	52.3%	43.2%	38.6%	25.0%	27.3%	13.6%	11.4%
Women R1	76.7%	76.7%	70.0%	53.3%	43.3%	36.7%	30.0%	26.7%	16.7%	6.7%
Women L2	43.2%	50.0%	47.7%	38.6%	25.0%	20.5%	18.2%	9.1%	6.8%	4.5%
Women R2	56.7%	70.0%	60.0%	56.7%	33.3%	20.0%	20.0%	10.0%	10.0%	0.0%
Men L1	77.6%	75.0%	64.5%	55.3%	43.4%	39.5%	35.5%	31.6%	18.4%	13.2%
Men R1	74.0%	64.0%	58.0%	48.0%	48.0%	32.0%	26.0%	20.0%	18.0%	6.0%
Men L2	57.9%	55.3%	48.7%	43.4%	30.3%	23.7%	19.7%	17.1%	14.5%	7.9%
Men R2	48.0%	38.0%	26.0%	32.0%	30.0%	26.0%	20.0%	18.0%	18.0%	8.0%
With Cup L1	78.4%	74.5%	64.7%	54.9%	42.2%	38.2%	31.4%	27.5%	14.7%	9.8%
With Cup R1	74.2%	68.2%	63.6%	53.0%	48.5%	33.3%	25.8%	21.2%	16.7%	7.6%
With Cup L2	50.0%	52.9%	48.0%	44.1%	28.4%	23.5%	19.6%	13.7%	10.8%	6.9%
With Cup R2	47.0%	45.5%	39.4%	40.9%	34.8%	24.2%	18.2%	13.6%	13.6%	6.1%
Without Cup L1	77.8%	72.2%	61.1%	50.0%	50.0%	44.4%	33.3%	44.4%	27.8%	27.8%
Without Cup R1	78.6%	71.4%	57.1%	35.7%	35.7%	35.7%	35.7%	28.6%	21.4%	0.0%
Without Cup L2	66.7%	55.6%	50.0%	27.8%	27.8%	16.7%	16.7%	16.7%	16.7%	5.6%
Without Cup R2	71.4%	71.4%	35.7%	42.9%	14.3%	21.4%	28.6%	21.4%	21.4%	0.0%
Weight Group1 L1	68.8%	62.5%	50.0%	43.8%	37.5%	37.5%	25.0%	25.0%	25.0%	18.8%
Weight Group1 R1	63.6%	63.6%	63.6%	45.5%	36.4%	18.2%	18.2%	9.1%	9.1%	0.0%
Weight Group1 L2	31.3%	37.5%	37.5%	31.3%	25.0%	18.8%	18.8%	18.8%	12.5%	6.3%
Weight Group1 R2	45.5%	72.7%	54.5%	45.5%	18.2%	18.2%	9.1%	9.1%	9.1%	0.0%
Weight Group2 L1	81.2%	76.5%	69.4%	58.8%	48.2%	41.2%	32.9%	31.8%	15.3%	11.8%
Weight Group2 R1	78.8%	71.2%	63.5%	50.0%	46.2%	32.7%	25.0%	23.1%	15.4%	5.8%
Weight Group2 L2	58.8%	56.5%	50.6%	44.7%	31.8%	24.7%	20.0%	12.9%	11.8%	8.2%
Weight Group2 R2	51.9%	51.9%	40.4%	42.3%	32.7%	23.1%	19.2%	13.5%	15.4%	5.8%
Weight Group3 L1	73.7%	73.7%	52.6%	42.1%	26.3%	31.6%	31.6%	26.3%	15.8%	10.5%
Weight Group3 R1	70.6%	64.7%	58.8%	52.9%	52.9%	47.1%	41.2%	29.4%	29.4%	11.8%
Weight Group3 L2	42.1%	52.6%	47.4%	36.8%	15.8%	15.8%	15.8%	15.8%	10.5%	0.0%
Weight Group3 R2	52.9%	29.4%	23.5%	35.3%	35.3%	29.4%	29.4%	23.5%	17.6%	5.9%
Age Group1 L1	70.6%	70.6%	64.7%	50.0%	47.1%	41.2%	29.4%	23.5%	11.8%	11.8%
Age Group1 R1	81.0%	71.4%	66.7%	47.6%	38.1%	28.6%	19.0%	9.5%	9.5%	4.8%
Age Group1 L2	50.0%	52.9%	52.9%	41.2%	29.4%	20.6%	14.7%	14.7%	5.9%	2.9%
Age Group1 R2	52.4%	61.9%	47.6%	47.6%	38.1%	23.8%	14.3%	4.8%	4.8%	0.0%
Age Group2 L1	84.1%	79.4%	69.8%	61.9%	44.4%	38.1%	31.7%	30.2%	14.3%	11.1%
Age Group2 R1	74.4%	71.8%	64.1%	53.8%	48.7%	33.3%	25.6%	23.1%	15.4%	5.1%
Age Group2 L2	54.0%	57.1%	50.8%	42.9%	27.0%	23.8%	20.6%	12.7%	9.5%	6.3%
Age Group2 R2	46.2%	48.7%	35.9%	38.5%	28.2%	20.5%	17.9%	17.9%	17.9%	5.1%
Age Group3 L1	73.9%	65.2%	47.8%	39.1%	34.8%	39.1%	34.8%	39.1%	30.4%	17.4%
Age Group3 R1	70.0%	60.0%	55.0%	45.0%	50.0%	40.0%	40.0%	35.0%	30.0%	10.0%
Age Group3 L2	52.2%	43.5%	34.8%	39.1%	30.4%	21.7%	21.7%	17.4%	26.1%	13.0%
Age Group3 R2	60.0%	40.0%	35.0%	40.0%	30.0%	30.0%	30.0%	20.0%	20.0%	10.0%

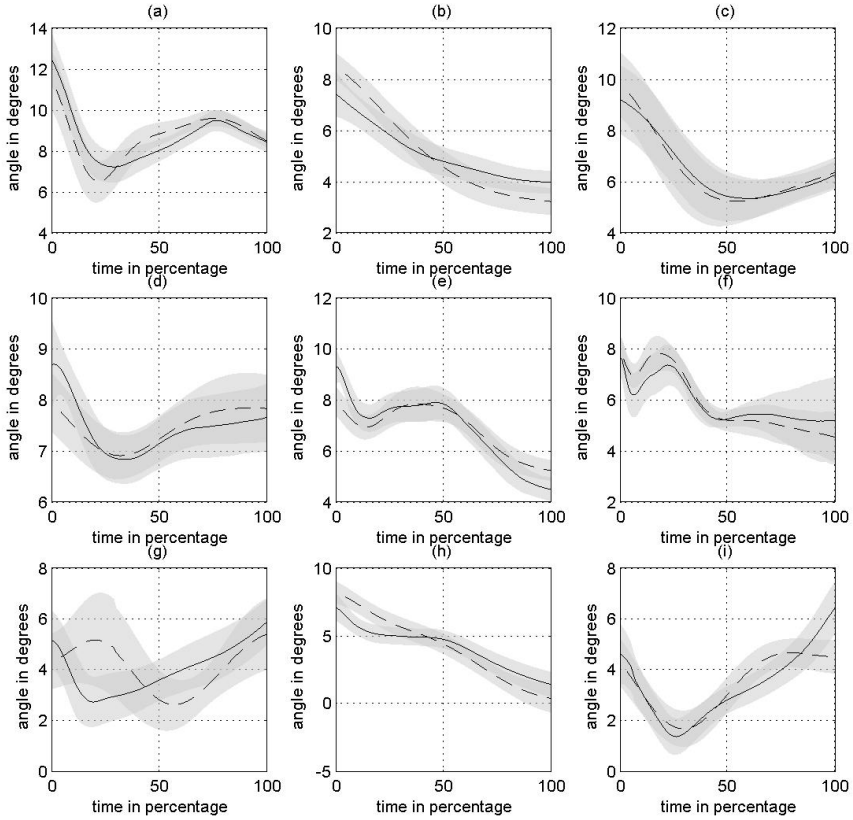

Figure 3.14 Example graphs of the comparison between average inversion/eversion curves and their standard deviation band based on MAS data and based on the mechanical model using PPPS data. The solid lines are related to the mechanical model and the dashed lines are related to the MAS data. In the first row, we depict three successful comparisons for the time interval one. In the second row, we depict the comparisons of one individual for the time intervals one (initial contact phase), three, and six, which were all successful comparisons. In the third row, we depict three unsuccessful comparisons. Comparison criterion is found on page 3.3.

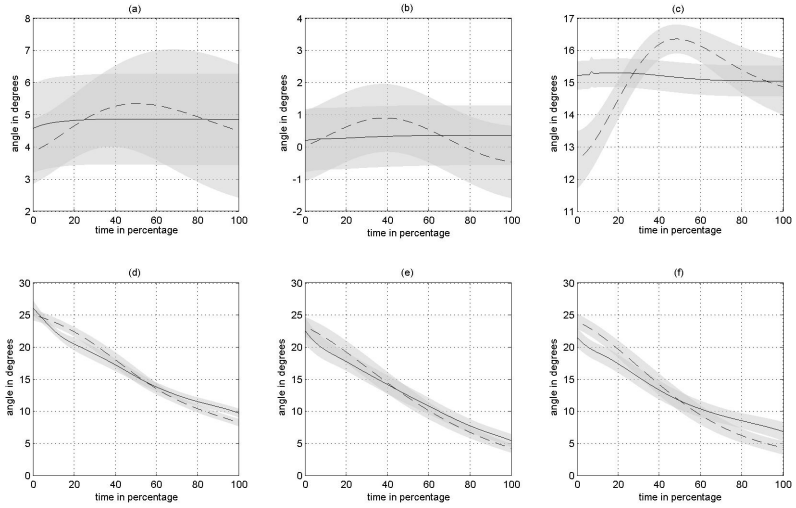

Figure 3.15 Example graphs of the comparison between average dorsal/plantar flexion curves and abduction/adduction curves, and their standard deviation band based on MAS data and based on the mechanical model using PPPS data. The solid lines are related to the mechanical model and the dashed lines are related to the MAS data. In the first row, we depict the abduction/adduction angles of two successful comparisons, (a) and (b), and one unsuccessful comparison, (c). In the second row, we depict the dorsal/plantar flexion angles of two successful comparisons, (d) and (e), and one unsuccessful comparison, (f). The chosen time interval is one, or initial contact phase

novative way of modelling motion.

Apart from giving heel motion, the use of simulation has an additional advantage. Simulation yields insight into the mechanics of the motion under study. The motion of the human heel is simulated by a sphere that is rolling over a plate. Contact path and radius of the sphere are the necessary input parameters of this mechanical model. Before we discuss details about these parameters and the calculation aspects, we focus on the general model. For the choice of average calculated parameters, we notice a high predictive power of about 75% during the initial contact phase in

most situations where the model was tested. Perhaps the general model of a rolling rigid body over a rigid plate is not able to achieve a higher predictive power, even if the parameters are individualised. This means that other mechanical behaviour plays a role in the motion of the heel during this phase. Luckily, the predictive power of individual optimal parameters is above 90%. Therefore, we believe that the rolling model describes the actual motion of the heel quite well. *In other words, we believe that the predictive powers above 90% show that heel motion during the initial contact phase can be thought of as the rolling of a sphere over a rigid plate.* We expect that the remaining percentages can be obtained by expanding the idea of a rolling body over a plate in the following way: all results obtained so far are based on a rigid body with a *spherical* geometry. The advantage of this choice is the simple form of the curvature tensor needed in the simulation of heel motion. Changing the geometry to an ellipsoid will enhance the model's predictive power. The ellipsoidal geometry makes it possible to have different values of curvatures in the frontal plane, related to dorsal/plantar flexion, and in the sagittal plane, related to calcaneal inversion/eversion. The drawback would be that the curvature tensor is no longer determined by one parameter, but by two parameters in case of a revolted ellipse, or even three parameters in case of the general ellipsoid. On the other hand, there is a possibility that the remaining percentages are lost due to measurement inaccuracy such that no change in geometry will help. Another argument for keeping the spherical geometry comes from anatomy. In the assumptions part of Section 3.2, it was pointed out that because of the two tuberculi no convex bone geometry could exist. The absence of a double hump in pressure distribution data suggests that the calcaneus and the soft tissues act together as one functional unit. Since fat pads and calcanei have an individually determined geometry, it is highly unlikely that their measures do not influence the geometry of the rolling rigid body individually. It is even more unlikely that we will be able to obtain these subtle differences in geometry from pressure distribution measurements, because limitations in sensor size are present and pressure data is two-dimensional in nature.

In the above, we had to restrict our statements to the initial contact phase. In all validation tables of the previous section, we saw that the predictive power of the model diminishes in time. For the initial contact phase, the predictive powers are high at about 75%, but when we look at the heel contact phase these values drop to about 7%. The results of the sensitivity of the CoP paths give us a possible answer for this

phenomenon. From Table 3.1, it follows that the CoP paths calculated from different heel areas start to diverge just after the initial contact phase. By combining results in Table 3.2 and Figure 3.12, we conclude that the model inversion/eversion angles start to deviate at this point from the MAS angles to an extent that is unacceptable within our chosen criterion. So, the deviation of CoP paths just after the initial contact phase is directly responsible for the decrease in predictive power of the mechanical model. We believe that in the initial contact phase, the pressure distribution in the heel area is solely induced from part of the heel surface that can be described by a sphere. In subsequent phases, the heel area may incorporate parts of the midfoot, or may contain pressures values from other parts of the heel not directly related to the simulated rolling motion. These values may be related to the compression of soft tissue underneath the more distal part of the calcaneus. Because of its structure, this part of the calcaneus is more elevated from the ground than the proximal part is. We think that this distal part, containing the two tuberculi, is that part of the heel surface that is simulated by our model. This hypothesis might be substantiated by studying the size of the number of active sensors within the constructed heel area over time. We propose to search for relationships between the geometry and the number of active sensors in the initial contact phase. These relationships could provide us with rules to separate the area of interest from the complete heel area at a later stage. Although the predictive power of the model decreases as time increases, some individual's heel motion was simulated satisfactorily up to heel lift. This could be explained by the position of the calcaneus with respect to the rest of the foot. We expect to find a more dorsal flexed position of the calcaneus for these individuals. However, at present, extending the model's predictive power to larger time intervals remains a topic for future study.

The optimal radii of the spheres were calculated such that the dorsal/plantar flexion curves of the model and those of MAS had the same range of motion. This was done on a trial-to-trial basis such that all individuals had a set of optimal radii corresponding to their trials. Although, the range of the radii for the initial contact phase are about [4cm,12cm], the consequence of taking the average radius of 7cm did not change the calculated inversion/eversion angles seriously. It is of course remarkable that all individuals have a functional heel that rolls as a sphere with a 7cm radius. However, we do not think that the above statement goes without nuances. First, it was already mentioned that the predictive power of the mechanical model is about 75% with an

average radius and above 90% with an optimal radius. So, there is a loss in predictive power going from optimal to average. Second, also already noticed, the range of optimal radii for the initial contact phase is about [4cm,12cm]. Therefore a more appropriate statement is that the radius parameter of the model is not critical.

The corrections to the CoP paths to better fit the contact paths were chosen to be linear. Two methods were employed to fit the contact paths calculated from MAS data and the CoP paths calculated from PPPS Data. Although, the begin-end point method only takes into account the begin and end point of both curves, the predictive power of the model using the begin-end point method is only slightly less than the one using the regression method. The corrections show that predominantly the begin points of the CoP paths have to be moved medially to overlay the contact path in an optimal way. Some general indications why the CoP path must be corrected were mentioned in the assumptions part of Section 3.2. These indications considered the violation of the assumption that the heel pad has uniform thickness and consists of isotropic material. It was suggested in Section 3.2 that the CoP paths should be shifted medially if the elasticity diminishes going from the midline of the foot outwards to the medial and lateral side of the heel.

Most of the validation processes were performed on the bases of a comparison of the inversion/ eversion curve. This choice for calcaneal inversion/eversion curves was taken because of the link between these angles and running-related injuries. Clinically, it might be of interest to know the other two angles, also. For instance, one might be interested in the initial dorsal flexion angle or its angle velocity. From the final validation test in Section 3.4, we learned that these angles can be used with the same confidence as the inversion/eversion angles originating from our model. We expected beforehand that all angles should be validated with the same predictive power, since the mechanical model describes the three-dimensional motion of the heel without favoring a certain cardinal plane.

The limitation of our mechanical model at present is the inability to find the initial condition from the pressure plate measurements. This does not mean that the model is useless. Still the model allows to study the trends in curves of heel orientation angles on a trial-to-trial basis. Variables such as range of motion of angle curves, time points when maximum or minimum values are reached, and angle velocity can be obtained from the mechanical model. Therefore, the overall conclusion is that our model is able to simulate the motion of the heel with pressure measurement data, at

least during the period from first foot contact up to first metatarsal contact. This presents an alternative method for determining the orientation of the heel, resulting in a reduction of measurement costs and set-up time by avoiding simultaneous three-dimensional motion measurements.

Chapter 4

Metatarsal Heads

motion characteristics during contact

4.1 Introduction

In a foot model with pressure measurements as input parameter to describe foot motion, it is of no surprise that the anatomical structures that are in contact with the ground during part of the stance phase are incorporated. In the present chapter, the motion of the metatarsal heads during the stance phase of walking at self-chosen velocity is studied. The outcome of this study results in a proposal of a forefoot model, see the discussion section of this chapter.

Studying metatarsal head motion is part of the general research into foot mechanics. Only recently, research into kinematics and kinetics of the foot has been oriented towards an approach in which the foot is modelled by multiple segments ([5], [26],[98], [97], [42], [115], [38], [150], [166], and [79], [48], [109], [189]). We were not able to trace specific literature containing a description of metatarsal head motion during the stance phase by directly measuring their motion. In a recent article by De Cock et al, [48, 2005], temporal characteristics of foot unroll during barefoot jogging are discussed. In their article, among others, they report on the common patterns exhibited by the metatarsal heads for initiating contact and for pushing off. In almost 75% of the cases the metatarsal heads contacted the ground in the sequence $M_{5/4}$, M_3, M_2, and M_1. By $M_{5/4}$, we mean that metatarsal heads four and five could not be distinguished

between. In almost 81% of the cases the metatarsal head pushed off in accordance to the sequence: M_5, M_4, $M_{3/1}$, and M_2. The lateral-medial motion of the metatarsal heads is described by this study as is the time interval in which this motion occurs; about 9% of stance duration during forefoot contact phase and about 20% of stance duration during forefoot push off phase. The reported contact time of the metatarsal heads ranges from 65.8% to 79.3%. Blanc et al. [20, 1999] performed a similar study for walking and found similar results. Besides the above temporal characteristics, we found one paper that describes a spatial characteristic of metatarsal heads. Robbins [174, 1981] suggests that the metatarsal heads are points on a curve.

In a mechanical foot model, the metatarsals as a whole must be described by a geometric structure. Measuments of the motion of these metatarsal heads and their interaction with the ground are necessary ingredients to design and validate a mechanical model. Although, we were not able to find such a model that describes the motion of the metatarsal heads during the stance phase, the mentioned literature does give an indication of their motion. The conclusion of this chapter is a proposal of a forefoot model. Therefore, we have to gain knowledge on metatarsal head motion during their contact with the ground. The acquisition of more knowledge is addressed in the following questions:

1. *Do the metatarsal heads move when in contact with the ground?*
   It is an assumption that the metatarsal heads do not move during contact. For verification, we observed metatarsal head motion by direct measurement with a three-dimensional motion analysis system (a 612 Vicon system). This motion is in the order of the spatial accuracy of the plantar pressure system. So, for plantar pressure systems with comparable sensor dimensions the assumption is validated.

2. *How does the distance between metatarsal head one and five change during the stance phase?*
   This question is related to the first question and its answer describes part of the motion of the metatarsal heads.

3. *How accurate does the plantar pressure distribution underneath the forefoot during the stance phase determine a curve on which the metatarsal heads are situated: the Metatarsal Curve (MC)?*

Since the answer to question one is that no motion can be observed by a plantar pressure system, MCs are time independent. Moreover, a validation process is needed in order to relate curves determined by pressure plate measurements with curves determined from a motion analysis system, hereby giving an answer to question three.

4.2 Methods

4.2.1 Devices and Population

The measurements were conducted using a 612 Vicon system with six M-cameras running at 250Hz. Furthermore, an 1.0m by 0.4m pressure plate system manufactured by RSscan International was used to measure the plantar foot pressures at a frequency of 500Hz (8192 sensors, 8bits, maximum value of 127N/sensor). Also, an 0.9m by 0.6m force plate running at 1250Hz, manufactures by Kistler, was used to dynamically calibrate the pressure plate. Finally, a 3D data box manufactured by RSscan International was used to connect all measurement devices. The connection between the Vicon system and the 3D box provided us with a synchronised integrated measurement system.

Three markers were attached to the Metatarsal heads to track their motion. The markers were placed on the side of metatarsal heads one and five, and between metatarsal heads two and three, see Figure 2.4.

From the registered pressure distributions, the forefoot area was isolated as described in Section 2.2.6. Besides the division in a rearfoot, midfoot, forefoot, and toe area, the aforementioned section contains also a subdivision of the forefoot area into five areas all containing one of the metatarsals. Both the pressure distribution of the forefoot and the pressure distribution of the five metatarsals are used for determining metatarsal head motion.

Three session types were employed: (1) walking (ten trials for both the left and the right foot), (2) walking and running (five trials for both the left and the right foot, and for both walking and running), and (3) walking, fast-walking and running (five trials for the left foot only in all three conditions). For the present analysis of metatarsal head motion, walking trials were selected. The only selection criterion was that at

least three trials were available for analysis. In 83 individuals out of a total of 125 that participated in this study, left and right foot were measured at least 5 times and at most 10 times per foot. For the remaining 42 individuals, 5 trials for the left foot only were measured. The individuals had an average age of 25.7 years with a standard deviation of ± 11.9 years ([10y,72y]) and an average weight of 68.9kg with a standard deviation of ± 14.9kg ([32kg,116.5kg]). The population consisted of 48 women and 77 men.

A detailed description of measurement methodology is found in Chapter 2.

4.2.2 Data Processing

A first requirement to perform the necessary analysis was that the registration of data from the pressure plate system and the motion analysis system were synchronised and aligned. Specific details about the employed methods to facilitate both are found in Section 2.2.1. The accuracy of synchronisation between both systems is of the order of the sampling time of the pressure plate system. In case of aligning local reference frames of both systems, the accuracy was for most measurement days within a sensor size of the pressure plate system. In this chapter, we discard the data from measurement days that contain errors larger than one sensor size.

To answer questions one and three, first contact of all metatarsal heads until a metatarsal head lifts off the ground is chosen as the time period. To answer question two, the complete stance duration is chosen as time period.

When calculating averages of position data from the pressure measurement system and average marker positions from the motion analysis system, the chosen time period was divided into three time intervals. Subsequently, the middle time interval was taken to calculate these averages. The rational behind this choice is the motion performed by the foot at the start and the end of the chosen time period. At the start of this time period, the pressure underneath the forefoot foot is not yet well established which could lead to errors in the determination of position within pressure data. At the end of the time period, a rotation takes place about the metatarsal heads which could imply motion of the metatarsal heads. Therefore, the middle time interval was taken

for average position calculations because in this time interval the eventual movement of the metatarsal heads is thought to be less than in the other two time intervals. Position differences are calculated with respect to this average position expressed as the distance between momentary position and average position.

As in the other chapters, specific details of processing are contained in the appendix accompanying this chapter, Appendix D. In this appendix, the constructed Matlab application that were used in performing the analysis are described.

4.2.3 Performed Analysis

To answer question one "Do metatarsal heads move when in contact with the ground?" , the average position of markers attached to the side of metatarsal one and five, and between the heads of metatarsal heads two and three were calculated in a way as mentioned above. The distances between these average positions and momentary positions were expressed as a ratio of the diagonal of a pressure sensor ($\sqrt{7.62^2 + 5.08^2} \approx$ 9.16mm). The diameters of the circles with as centre points the average positions of metatarsal heads were calculated such that these circles contain the marker positions in 90% of the chosen time period.

To answer question two "How does the distance between metatarsal head one and five change during the stance phase?", the distance was simply calculated from motion data. The trend of this distance curve was expressed in the following variables:

1. the maximum difference in distance between the metatarsal heads one and five during the stance phase,
2. the time point at which the maximum distance occurs expressed as a percentage of the stance phase,
3. the difference between the maximum distance and the distance at initial contact of metatarsal five,
4. the difference between the occurrence of maximum distance and initial contact of metatarsal five expressed as a percentage of the stance phase,
5. the difference between the maximum distance and the distance at initial contact of metatarsal one,

6. the difference between the occurrence of maximum distance and initial contact of metatarsal expressed as a percentage of the stance phase .
7. the difference between the maximum distance and the distance at heel off,
8. the difference between the occurrence of maximum distance and heel off expressed as a percentage of the stance phase .
9. the difference in distance between the start and end of foot-to-ground

Correlation coefficients were calculated between these metatarsal-distance variables and 92 pressure variables. In the result section, the pressure variables that had a significant ($P < 0.05$) correlation coefficient of more than .5 are discussed.

The Kolmogorov-Smirnov goodness of fit test was used to determine which variables were normally distributed. In case normality could not be established, Spearman correlations were calculated.

To answer question three "How accurate does the plantar pressure distribution underneath the forefoot during the stance phase determine a curve on which the metatarsal heads are situated: the Metatarsal Curve (MC)?", a few methods were applied to calculate MCs out of pressure data. Both from the pressure data and the three-dimensional position data points were isolated and used to construct MCs. MCs are defined to be second order polynomials. The isolated points were used to fit these polynomials using the **polyfit** function of Matlab. This functions calculates a best fit in a least squares sense. Five methods were used to calculate MCs from pressure distributions of the forefoot:

1. *Positions of peak values over the complete time period with the original forefoot pressure distribution.*
   This method determines the position of local maxima in the forefoot pressure distribution. Local maxima are those points for which a neighbourhood exists consisting of points at which the pressure is less than in the points of local maxima. Having calculate the maxima for all time points of the forefoot pressure distribution, the ones most present over time are selected as points for calculating MC. To calculate the ones with largest impact, a new pressure distribution in time is constructed. First, for a certain time point the new pressure distribution is the one that only contains the local maxima at that time point. Second, one

pressure distribution is constructed by summing up these new pressure distributions over the time period. Third, the local maxima of this aggregated pressure distribution are calculated and used as input for determining the Metatarsal Curve.

2. *Positions of peak values in the pressure distribution aggregated over the time period.*
   The same procedure is used as in the case of the first method, only the input of the forefoot pressure distribution differs. Instead of taking the pressure distribution for the complete time period, an aggregated pressure distribution is made and used as input.

3. *Positions of peak values over the complete time period with an adjusted forefoot pressure distribution.*
   The same procedure is used as in the case of the first method, only the pressure values in the forefoot pressure distribution are adjusted. All values below a certain threshold are set to zero (here 10N/cm^2). Then the remaining values of a pressure distribution at a certain time point are divided by the average pressure value at that time point and raised to the power four. The calculated pressure distribution enhances the separation of local maxima.

4. *Average positions of maximal pressure sensors in the five areas of the forefoot.*
   In Section 2.2.6, we discuss a division of the forefoot into five subareas such that each contains a metatarsal head. During the chosen time period, the positions of the sensors with the highest value were determined from the five individual pressure distributions. The average positions of these five sensor points were calculated for the middle time interval as explained in Section 4.2.2. Subsequently, these five points were used in constructing the Metatarsal Curve.

5. *The location of the Gaussian mixtures that in combination represent the forefoot pressure distribution in time.*
   When all values of a forefoot pressure distribution at a certain time point are divided by the sum of all pressure values at that time point a normalised pressure distribution arises for that time point. A normalised pressure distribution is thought of as a multi-modal bivariate statistical distribution. It is possible to describe such a multi-modal bivariate distribution by a superposition of probability density functions. In this case, we used Gaussian probability density

functions characterised by (μ_i, Σ_i), where $i = 1, \ldots, k$ and k is the total number Gaussians used. The pressure distribution given at a certain time point has an approximated value that is realised by a mixture of k Gaussian distributions such that

$$p(x) = \sum_{i=1,\ldots,k} \pi_i \, p(x; \mu_i, \Sigma_i), \quad \sum_{i=1,\ldots,k} \pi_i = 1, \tag{4.1}$$

where π_i, $i = 1, \ldots, k$, are the mixing proportions of the different Gaussian distributions. Details of this method and its application on forefoot pressure distributions can be found in Okoulevitch and Bykova [160, 2004] and a graphical example is found in Figure 4.1

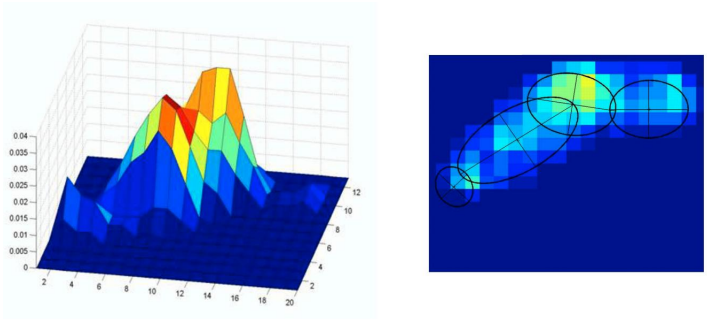

Figure 4.1 Example of a Gaussian mixture. On the left-hand side, a three-dimensional representation of a forefoot pressure distribution and on the right-hand side an example of four Gaussian distributions fitted to the underlying forefoot pressure distribution.

After MCs were calculated using one of the five methods, these MCs were compared to the MC constructed from the three markers that were measured with the motion analysis system. Two types of comparison were made: (1) the difference in distance of the position of the point between metatarsal heads two and three, (2) the average difference in distance of all points over the width of the foot, see Figure 4.2. The first type of comparison is a specific one point measure while the second one is a measure for the complete MC. Normally, we would favour the second type over the first type because it is a more global measure. We used both types of comparison because the

MC based on motion data does not contain all meta heads as points on its curve. Since metatarsal heads one and five were attached at the side of these heads, only the point (marker) between metatarsal head two and three is certainly on this curve.

4.3 Results

In Figure 4.3 (a), (b) and (c), the diameters of the circles that cover 90% of the marker position during the chosen time period are depicted as distributions in histograms. In Figure 4.3 (d), average marker curves of the trials of one individual are depicted. They show the relationship between the size of the diameter of the covering circle and the percentage of position data within these circles for all three markers. Although, we present an example here, the trend of the curves is exemplary for our data set.

If the data is split into left and right trials, there is no drastic change in the behaviour of these curves. To verify, we present the distributions of the left and right trials in Appendix D. The average diameter of the circles that covers 90% of the marker motion is given in Tabel 4.1 Also, the 90% confidence interval of diameter size is presented and the percentage of diameter sizes smaller than the length of one and two times the length of pressure-sensor diagonal. A 90% confidence interval of this diameter size was chosen since the normality test (Lillifors test) showed that diameter's distributions are not normal.

The change in distance between metatarsal heads one and five during the stance phase follows a pattern that is common in the walking trials of all 125 individuals. First, the distance increases to a platform level. Second, the platform level is maintained for a certain period. Third, the distance decreases at the end of foot-to-ground contact. An example of a change of distance curve is depicted in Figure 4.4,.

The behaviour of the distance relationship between heads one and five can be expressed in the variables introduced in Section 4.2.3. The results of these variables for the whole population are found in Table 4.2, presenting both the average and the 90% confidence intervals of these variables. The correlations between significant pressure variables and the significant distance variables are expressed in Table 4.3. Since only the pressure variables that correlate significantly with a coefficient of more than .5 are contained in this table, the number of pressure variables is reduced from 92 to 8.

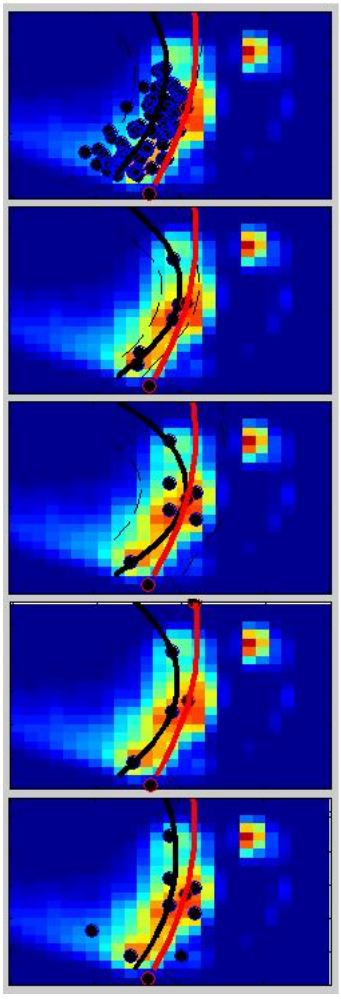

Figure 4.2 Example of comparison between MCs from pressure measurements and MC from motion measurements. An arbitrary trial was used for this example. The order of the rows is: (1) Gaussian Mixtures, (2) Five area forefoot, (3) Peak positions from an adjusted pressure distribution, (4) Peak positions from an aggregated pressure distribution, and (5) Peak positions from an original pressure distribution.

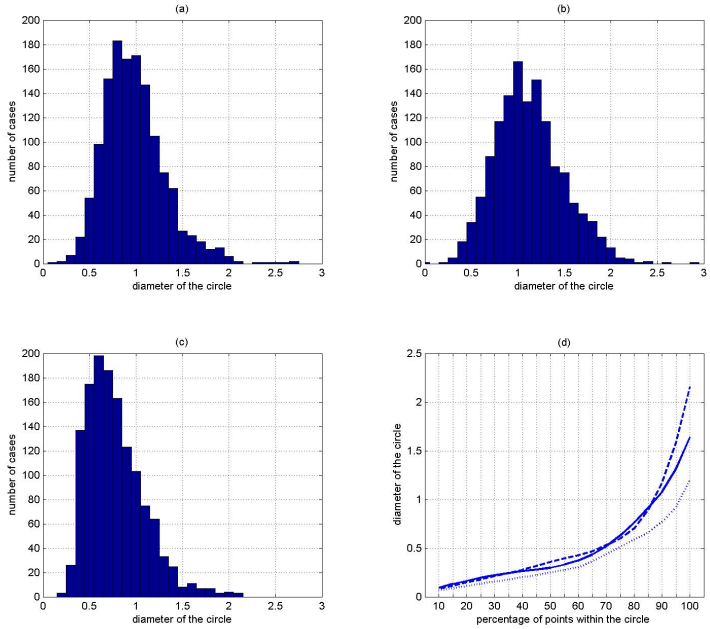

Figure 4.3 The movement of the metatarsal heads during the time period starting at the moment all metatarsal heads are in contact and ending at the moment one of these heads loses contact. In (a), (b), and (c) the distributions of all trials are depicted with respect to the diameter of the circles containing 90% of the motion of the markers attached to metatarsal head one, attached between metatarsal heads two and three, and attached to metatarsal head five, respectively. The diameter size is scaled with respect to the length of the diagonal of a pressure sensor. In (d), the relationship between the size of the diameter of the circle and the percentage of motion covered by this circle is depicted. The relationship is an example of the average curves calculated for an arbitrary individual of the three markers on the forefoot: the solid line is related to the marker attached to the side of metatarsal head one, the dashed-dotted line is related to the marker attached between metatarsal heads two and three, and the dashed line is related to the marker attached to the side of metatarsal head five.

Table 4.1 The motion of the metatarsals. This table contains data of the motion of the three markers attached to the metatarsals: two markers attached at the side of metatarsal heads one (MT1) and five (MT5), and one marker attached between metatarsal heads two and three (MT2/3). The first row contains the averages of the diameters of the circles containing 90% of the motion. The second row contains the data size of 90% confidence intervals (C.I.). The third row contains the percentage of diameters that are smaller than the length of one pressure sensor's diagonal. The fourth row contains the percentage of diameters that are smaller than two times the length of one pressure sensor's diagonal. The values of the diameter sizes in rows one and two are expressed in the length of one pressure sensor's diagonal ($\approx$ 9.2mm).

	MT1			MT3/4			MT5		
	All	Left	Right	All	Left	Right	All	Left	Right
Average	1.08	1.15	1.00	1.24	1.32	1.14	0.90	1.00	0.78
90% C.I	$\pm$0.56	$\pm$0.57	$\pm$0.55	$\pm$0.63	$\pm$0.66	$\pm$0.65	$\pm$0.51	$\pm$0.57	$\pm$0.49
< 1	57.6%	58.7%	56.4%	39.9%	40.7%	39.0%	78.9%	79.3%	78.4%
< 2	99.3%	99.7%	98.7%	98.3%	98.8%	97.7%	99.6%	99.5%	99.8%

The validation of the Metatarsal Curves from each of five methods to determine MCs from pressure distributions was performed by comparing curves of the these methods with the curve from motion data. In the sequence of analysis, this type of validation was the most time consuming. We started our processing by applying all five methods to a given trial. This type of processing could not be maintained because the method employing Gaussian mixtures did not always converge. Therefore, we decided to redesign the validation method and focus on the remaining four other methods. The validation of the selected four methods is presented in Table 4.4. The table contains the average, the 90% confidence interval, and the percentage of trials that were rejected for analysis. Trials were rejected for a given method because the number of points that could be used to calculate the second-order polynomial was less than three. For these trials, MCs could not be constructed.

Analogue to the analysis of the movement of markers attached to metatarsal heads, or the marker attached between metatarsal heads, we looked at movement of the points used in method four. This method used the five forefoot areas that should contain one

Table 4.2 The distance between metatarsal heads one an five. This table contains the following distance variables: (1) maximum distance difference over the complete stance phase (D_Max_dif), (2) time to maximum distance (D_Max_T), (3) difference between maximum distance and distance at M5 contact (D_Max-D(M5), (4) time between maximum distance and distance at M5 contact (D_Max_T-D(M5)_T), (5) distance difference between maximum distance and distance at M1 contact (D_Max-D(M1), (6) time between maximum distance and distance at M1 contact (D_Max_T-D(M1)_T), (7) difference between maximum distance and distance at heel lift (D_Max-D(Heel lift)), (8) time between maximum distance and distance at heel lift (D_Max_T-D(Heel lift)_T), (9) difference between the distance at the start and at the end of the stance phase (D(begin)-D(end)).

	Average	90% C.I.
D_Max_dif	11.2mm	±1.6mm
D_Max_T	46.0%	±4.5%
D_Max-D(M5)	9.1mm	±0.1mm
D_Max_T-D(M5)_T	36.8%	±5.0%
D_Max-D(M1)	5.6mm	±1.14mm
D_Max_T-D(M1)_T	32.4%	±6.9%
D_Max-D(Heel lift)	0.5mm	±0.3mm
D_Max_T-D(Heel lift)_T	-9.2%	±1.9%
D(begin)-D(end)	-1.3mm	±2.9mm

Table 4.3 The significant ($P < 0.05$) correlation coefficients between pressure variables and M1-M5 distance variables. The significant distance variables are: (1) time to maximum distance (D_Max_T), (2) time between maximum distance and distance at M5 contact (D_Max_T-D(M5)_T), (3) time between maximum distance and distance at M1 contact (D_Max_T-D(M1)_T), (4) difference between maximum distance and distance at heel lift (D_Max-D(Heel lift)). The significant pressure variables are: (1) Forefoot Contact Phase (FFCP), (2) Foot Flat Phase (FFP), (3) Time to maximum pressure underneath M5 (Max_T(M5)), (4) Force-Time Integral of the medial heel area (Int(Heel_Med)), (5) Force-Time Integral of the lateral heel area (Int(Heel_Lat)), (6) Contact duration of medial heel (Dur(Heel_Med)), (7) Contact duration of lateral heel (Dur(Heel_Lat)), and (8) Contact duration of the lesser toes (Dur(Toes)). Pairs of variables with significant correlations are divided into two groups. One group has correlation values in the range from .5 to .7 and the other group has values larger than .7. The pairs are indicated by "x" and "o", respectively.

	D_Max_T	D_Max_T-D(M5)_T	D_Max_T-D(M1)_T	D_Max-D(Heel lift)
FFCP	x	x	o	
FFP	o	x	o	
Max_T(M5)			x	
Int(Heel_Med)	x	o	o	o
Int(Heel_Lat)	x	o	o	o
Dur(Heel_Med)	o	o	o	
Dur(Heel_Lat)	o	o	o	
Dur(Toes)	x	x		

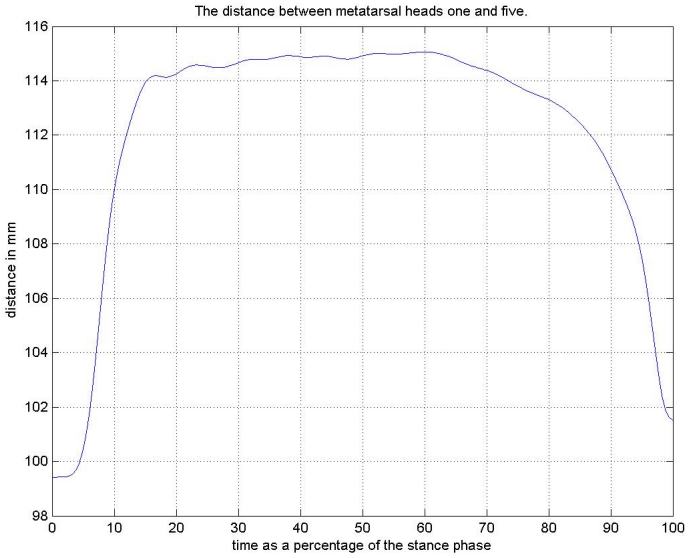

Figure 4.4 The change in distance between metatarsal heads one and five during the stance phase of walking. This graph depicts the aforementioned relationship for one trial of an arbitrarily selected individual. The trend of this curve is seen in the walking trials of all 125 participants of our study.

metatarsal each. At each time instance, five points are determined in the five areas at which pressure is maximum for that area. The result of this analysis is found in Table 4.5.

4.4 Discussion

4.4.1 Posed Questions

Whether the metatarsal heads move when in contact with the ground was question one in the introduction section. The answer to this question is not so straightforward. We obtained an answer by using a motion analysis system, but the inherent inaccuracy of the system prohibits drawing conclusions if distance variations of markers are below a certain threshold. The threshold of the presently used set-up is hard to determine since

Table 4.4 Validation of Metatarsal Curves. In this table, methods one to four (Meth.1 to Meth.4) are validated with MCs from motion data. Both the local criterion, distance between the point between metatarsal heads 2 and 3 (MT2/3) as given by MCs from pressure and motion data, and the global criterion, average distance between MCs from pressure and motion data, are presented. Incorporating all trials, the average, 90% confidence interval, and the percentage of trials that could not be analysed are given.

	Meth.1		Meth.2		Meth.3		Meth.4	
	MT2/3	Curve	MT2/3	Curve	MT2/3	Curve	MT2/3	Curve
Average	1.15	1.82	0.96	2.07	0.93	1.86	0.90	1.53
90% C.I	1.14	1.25	0.96	1.57	0.92	1.31	0.88	0.85
% trials	0.3%	0.3%	29.4%	30.2%	6.2%	6.2%	0.1%	0.1%

not all technical details of the system were known. However, the variation of marker positions during the static trials of individuals may provide some indications. The average variation of the three markers attached to, or close to, the metatarsal heads is 0.1mm with a 90% confidence interval in the order of 0.01 millimeters. Another indication is provided by the variation in fixed distances during dynamic trials as described in Chapter 2 and graphically depicted in Figure 2.14. The latter figure shows a decrease in variation when distances become smaller, in the order of 0.1mm. With these two considerations in mind, metatarsal heads do move if measurements of these heads are directly related to the movement of the attached markers. In our set-up, the direct measurement of movement of metatarsal heads is impossible. They are replaced by markers attached to the skin. Therefore, by measuring marker motion, we measure also the superimposed motion of the skin and all soft tissue structures between skin and bone. In Figure 4.5, we depict a few examples of marker paths during the contact phase of all metatarsal heads. These examples are representative of the measurement population and show a strong posterior-anterior motion in the finale stage of metatarsal contact. In this stage, the heel has lifted from the ground and the foot is rotating about the metatarsal heads. We expect a slight forward motion of the metatarsal heads during this stage, cf. Stokes et al. [194, 1979]. On one hand, with our present measurement set-up, we are not able to conclude that this forward motion is "real" motion. On the other hand, forward motion is present if rotation takes place about the metatarsal heads, a less speculative statement. From Section

Table 4.5 The movement of the five maximum points in the metatarsal areas. This table contains data of the movement of the point of maximum pressure in the five metatarsal areas. Here, metatarsal areas one, two, three, four and five are related to MT1, MT2, MT3, MT4 and MT5. For all trials, we calculated the diameter of the circle containing 90% of the motion. The diameter sizes were expressed as lengths of a pressure sensor's diagonal. Average and 90% confidence interval values are expressed for the size of these diameters. In the rows with the heading < 1 and < 2 the percentage of trials that are within one and two times the length of the diagonal of a pressure sensor are given. The division into three blocks is such that the first is related to the movement during the complete metatarsal contact period, the second is related to the last two thirds of this period, and the third block of rows is related to movement during the middle third of this period.

	MT1	MT2	MT3	MT4	MT5
Average	2.3	1.7	1.8	2.6	2.3
90% C.I	2.7	1.6	1.7	2.1	1.7
< 1	20.4%	20.7%	21.5%	16.0%	13.1%
< 2	50.0%	60.2%	59.9%	39.2%	42.4%
Average	1.8	1.3	1.2	2.1	2.5
90% C.I	2.5	1.5	1.5	2.6	2.0
< 1	35.6%	38.5%	41.9%	30.7%	11.4%
< 2	64.1%	74.6%	76.0%	53.1%	35.5%
Average	0.8	0.7	0.6	1.0	0.6
90% C.I	1.8	1.2	1.1	2.0	1.0
< 1	69.5%	69.3%	72.2%	63.8%	74.2%
< 2	85.8%	92.0%	92.6%	79.6%	94.8%

4.3, Table 4.1, we see that circles with a diameter size of 18.3mm (= 2 times the length of a pressure-sensor diagonal) contain 90% of the motion of the three markers related to the metatarsal heads for 97.7% of all trials. Therefore, rotation about the metatarsal heads can take place from heel lift until metatarsal lift and might be restricted to the 90% covering circles.

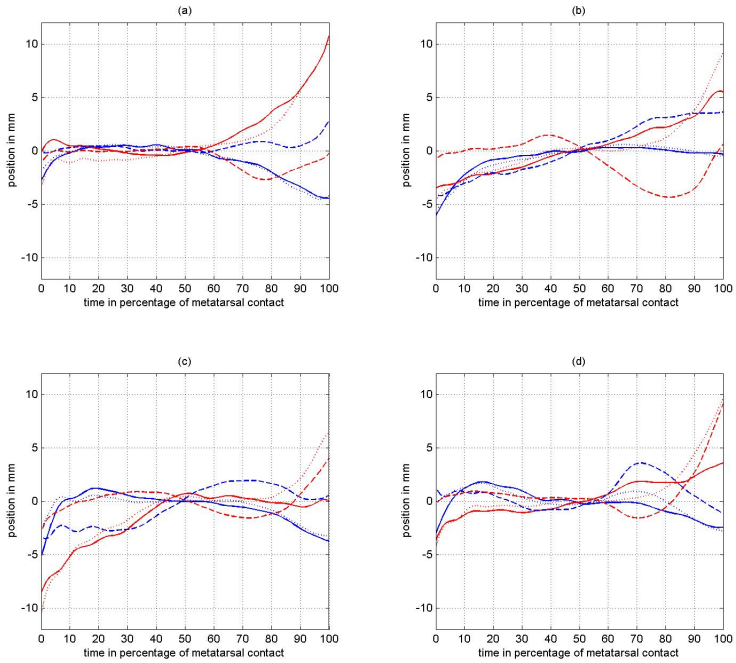

Figure 4.5 Examples of metatarsal head motion. In the four graphs (a), (b), (c), and (d), examples of the motion of the markers attached to the metatarsal heads one (solid lines) and five (dashed lines), and attached between metatarsal heads two and three (dotted lines) are depicted. In each graph, a trial of a different individual is shown. The red lines depict the y-coordinate of these markers, and the blue lines depict the x-coordinate of these markers. The time is expressed as percentage of metatarsal contact, the period starting at the moment that all metatarsal heads are in contact with the ground until the moment one head is lifted from the ground.

The previous consideration, tells us that a pressure plate with sensors not smaller than 7.62mm by 5.08mm can not determine the position of metatarsal heads. For measuring the position of metatarsal heads, we have to take an area of about 14mm by 10mm to cover these heads completely. Only a few studies employing plantar pressure plate systems use such small metatarsal areas ([48], [77]). Most studies employ divisions of the forefoot area in much larger areas. Although manual placement of such small areas in a plantar pressure distribution is far from evident, De Cock et al. [48] showed that it can be done in a repeatable manner. Besides knowing the position of the metatarsal heads with such an approach, the local loading characteristics of the metatarsal heads are determined more precisely when using such small areas.

The way the distance changes between metatarsal head one and five during the stance phase was question two as mentioned in the introduction. From Figure 4.4 and Table 4.2, it follows that the distance between metatarsal heads one and five does change during the stance phase. The spreading of the forefoot, in the order of 1cm, could be a mechanism to enhance medio-lateral stability of the forefoot in the crucial forefoot push-off phase. From Table 4.2, it follows that at the start of propulsion this distance already reached its maximum, about 10% of stance duration before heel lift, but that the amount of spreading is the same as this maximum (differences are less than a millimeter). In some texts on functional anatomy (for example [104]), the presence of a medio-lateral foot arch in the frontal plane is discussed. Together with the anterior-posterior arches of the foot, these texts describe the contact between foot and ground by a tripod structure. Since pressure plate systems have been introduced, the medial-lateral arch has been disputed. Loading underneath the inner metatarsal heads, two, three and four, is substantial ([48], [11], [14]). With recent research in temporal foot roll-over patterns ([48], [20], [209]), a lateral to medial forefoot unroll is observed. Such a pattern can theoretically not be the consequence of medial-lateral foot arch. The explanation does not support the the fact that this foot arch is collapsing during impact, because the end points (metatarsal heads one and five) would still remain the lowest points on the arch. Moreover, if the metatarsal heads are all in one transverse plane, then unroll should theoretically be about metatarsal head five consequently followed by the other metatarsal heads at the same instance of time. With the change in distance between metatarsal head one and five, and with the forefoot unroll and push off sequences found in the paper by DeCock et al. [48], we come to a model of the

motion of the metatarsal heads in any frontal plane. This motion is described as the motion of an inverse arch that flattens during metatarsal ground contact, see Figure 4.6. An explanation for the existence of an inverse arch might be the activity of the flexor muscles of the hallux and the lesser toes from first foot contact until foot flat.

At the end of contact, push off sequence behaviour of the metatarsal heads can not be explained by a curve in the frontal plane alone. Therefore, we need a curve through the metatarsal heads in the transverse plane; the metatarsal curve.

Figure 4.6 An example of forefoot unroll (from right to left). The metatarsal arch described from an inverse arch at first metatarsal contact to a flat arch during the foot flat phase.

Before, we start the discussion about the metatarsal curve, we shortly outline the results presented in Table 4.3. This table shows that timing events in the distance relation between the exterior heads have a strong linear correlation to total loading of the medial and lateral heel area and the duration of contact of both these areas. For the design of a model of the forefoot, these strong linear correlations are of no interest. However, in a future study, design of a mechanical structure that describes this coupling could be the main goal. The fact that we found these correlations at least suggests coupling and might lead us to the direction in which this coupling could be described.

Whether the plantar pressure distribution underneath the forefoot during the stance phase could be used to establish a curve on which the metatarsal heads are situated, was question three in the introduction. Since, motion of metatarsal heads during contact is present, see the answer to the question one, but since this motion is in total of the same order as the length of a pressure sensor's diagonal, we needed to find stationary metatarsal curves. Five methods were used to construct these metatarsal

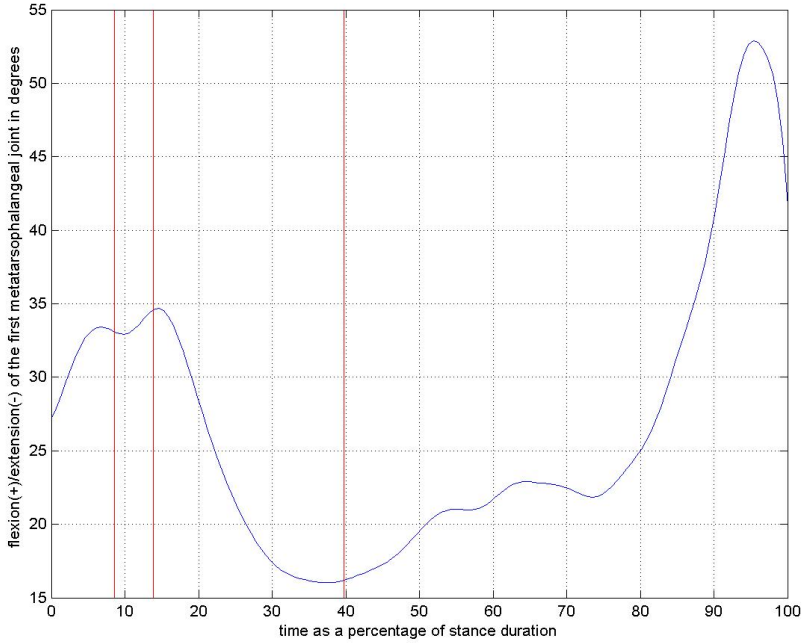

Figure 4.7 An example of the flexion(+)/extension(-) motion of the first metatarsophalangeal joint; third individual of the walking session type, trial one. The vertical lines represent the moment at which metatarsal head five contacts the ground, the moment at which metatarsal head one contacts the ground, and the moment of heel lift.

curves, see Figure 4.2 for examples. From Table 4.4, it follows that method four performs overall better than the other methods. We recall that this method uses the points at which pressure reaches its maximum in five areas. The MC determined by method four and the MC determined by the motion analysis measurements are compared at the point between metatarsal heads two and three. The average distance between these corresponding points at both MCs was 0.9 times the length of a pressure sensor diagonal. The value of the 90% confidence interval for this distinct method ranges from 0 to 1.78. The results of comparison of the complete MC curves in Table

4.4 indicate method four also as the overall best performing method. We need to be cautious in our interpretation of the values of Table 4.4 if we compare complete MCs. Placement of the markers on the side of the metatarsal heads one and five implies that MCs based on motion data are less accurate at the most exterior metatarsal heads. Nevertheless, method four gives us the most relevant metatarsal curve from pressure plate measurements.

Intermezzo

The motion of the maximum pressure within a metatarsal area is given in Table 4.5. Since the accuracy of a pressure plate is restricted by its sensor size in the determination of positions, the sizes of diameter of the circles containing 90% of the movement of the points are larger than points obtained with MAS, see the discussion of question one. An advantage of method four is that there is a relationship between points of highest pressure and underlying anatomical structures. Indeed, previously performed research ([70], [31], [83]) showed a good agreement of anatomical structures and high-pressure areas within a plantar pressure distribution. Figure 4.2 indicates that for the chosen example there are only three areas in the forefoot with a high pressure. Visual inspection of this example revealed that the middle high-pressure area is a combination of pressure exhibited by metatarsal heads two and three. Since the heads are connected through various soft tissues, it is conceivable that local pressures of the two metatarsal heads through the soft tissue layers result in a distribution with only one peak, see Figure 4.8. Therefore, we deduce that the peak pressure values are on the metatarsal curve and could be between heads as well as at the head.

From a clinical standpoint, the local loading around the metatarsal heads is of interest for the determination of tissue stress injuries and other local phenomena. Pressure variables calculated from large forefoot areas might not yield identical values if more local areas were selected. Results of a preliminary study to the research in this thesis indicate that only 9 variables have the same results for a large forefoot area and a one-sensor forefoot area. The matching variables are alle time related: the four foot phases, time of maximum pressure of metatarsal area one, time of maximum loading rate of metatarsal areas three and four, and the contact duration of metatarsal areas one and five. In total 81 pressure variables using both large forefoot areas, see Section 2.2.6, and one-sensor forefoot were compared: (1) the four foot phases, (2) maximum pressures (for eleven areas), (3) times of maximum pressures, (4) average pressures,

(5) maximum loading rates, (6) times of maximum loading rates, (7) pressure-time integrals, (8) contact durations. We came to above findings using student t-tests in case of normal distributed variables and Wilcoxon Matched-Pairs Signed-Ranks Tests in case of non-normal distributed variables. Apart from these 9 variables, determination of pressure variables from local pressure areas underneath metatarsal heads gave generally different results than the normally used larger areas. In clinical pre- and post test situations the difference in absolute values might be of less importance than the absolute values. Whether, besides differences in maximum values there are also differences in the trend of the loading curves is still an open question. For completeness, we present Table 4.6 containing maximum pressures, average pressures, maximum loading rates, and pressure-time integrals in case of both types of forefoot areas.

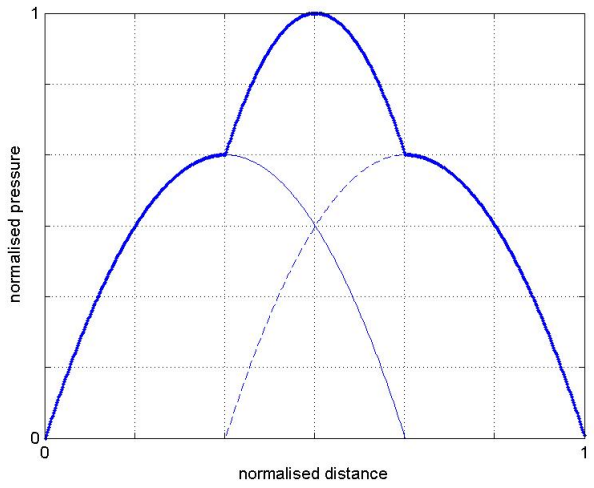

Figure 4.8 An example of how the pressure of two metatarsal heads through soft tissue layers can result in a distribution with one peak.

4.4.2 Forefoot Model Proposition

In this section, we propose a model to describe the motion of the forefoot; for a sketch of the model see Figure 4.9. The forefoot motion starts at the event First Metatarsal Contact (FMC) and lasts till the event Last Foot Contact (LFC), or, in other terms,

Table 4.6 Average and standard deviation of pressure variables calculated from global and local forefoot areas The abbreviations have the following meaning: M.P is Maximum Pressure, A.P. is Average Pressure, M.L.R is Maximum Loading Rate, P-T Int. is Pressure-Time Integral, MT1 till MT5 are the metatarsal areas related to metatarsals one to five. The postfix (G) is related to the global metatarsal areas, while the postfix (L) is related to the one-sensor metatarsal areas.

	M.P. in N/cm2	A.P. in N/cm^2	M.L.R. in N/cm^2 s	P-T Int. in Ns/cm^2
MT1(G)	13.2 ± 2.9	6.8 ± 1.4	241.5 ± 101.2	3.5 ± 0.8
MT1(L)	28.7 ± 6.3	15.0 ± 3.3	463.0 ± 191.8	7.7 ± 1.9
MT2(G)	20.3 ± 5.3	10.3 ± 2.5	339.5 ± 141.7	5.4 ± 1.5
MT2(L)	32.9 ± 8.2	17.3 ± 4.5	646.5 ± 304.6	9.2 ± 2.7
MT3(G)	18.5 ± 4.5	9.6 ± 2.3	435.3 ± 197.2	5.1 ± 1.4
MT3(L)	31.8 ± 7.8	17.1 ± 4.6	883.2 ± 422.4	9.2 ± 2.7
MT4(G)	13.2 ± 8.0	1.9 ± 1.4	612.4 ± 268.4	4.3 ± 1.1
MT4(L)	25.6 ± 14.5	3.7 ± 3.6	1090.6 ± 447.2	7.9 ± 2.2
MT5(G)	8.8 ± 5.4	1.4 ± 0.7	484.6 ± 200.4	2.9 ± 0.8
MT5(L)	21.3 ± 12.5	3.6 ± 2.4	992.5 ± 427.9	6.6 ± 2.1

during the phases Fore Foot Contact Phase (FFCP), Foot Flat Phase (FFP), and Fore Foot Push Off Phase (FFPOP). For the introduction of these events and phases, see Section 2.2.4.

The contact of the forefoot with the ground plane is represented by a (virtual) bent cylinder; the cylinder is deformable and bents in two directions: with respect to the frontal plane and with respect to the transverse plane (= ground plane). At FMC, this curved cylinder is with one point in contact with the transverse plane. During FFCP, the cylinder flattens (making more contact) and unrolls itself over the transverse plane (lateral to medial). In FFP, the cylinder is in full contact with the ground plane, and the contact curve of the cylinder with the plate then coincides with the positions of the metatarsal heads in the transverse plane (as observed using a pressure plate). In other words, the curve of contact is the *metatarsal curve*.

The flattening of the medial-lateral arch during FFCP is controlled by the neuromuscular system. We try to model this system in the following way: At a point between the metatarsal heads two and three a rigid straight beam is fixed to the cylin-

der, as depicted in Figure 4.9. This beam ends in a control unit, at which two rigid hollow tubes are mounted; see again Figure 4.9. The two hollow beams each encapsulate a rope connecting the end points of the bent cylinder to the control unit. By shortening or lengthening the two ropes, the control unit is able to change the bending of the cylinder in the frontal plane (thus making the cylinder more flat or less flat).

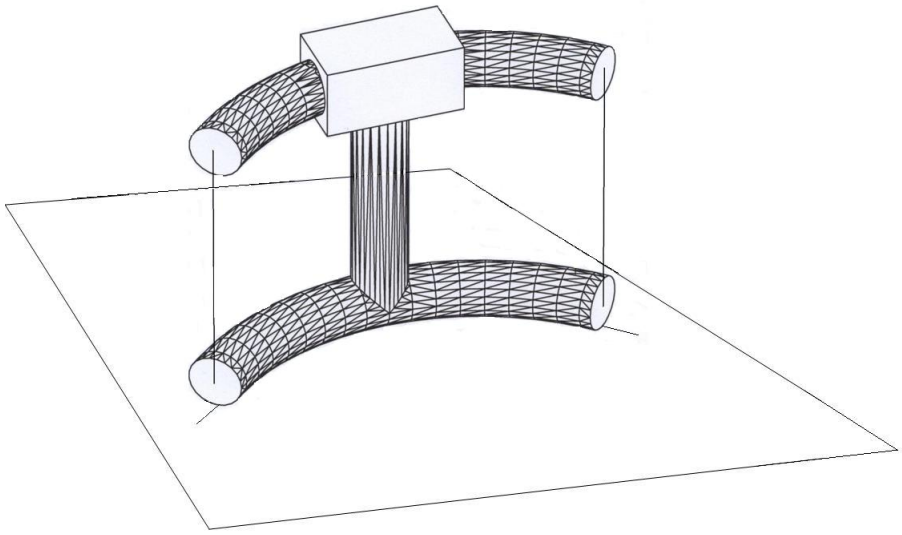

Figure 4.9 A sketch of the proposed forefoot model.

To be able to use this forefoot model to describe forefoot motion from plantar pressure plate measurements, its parameters should be known. Although, further research to know the exact working of the control unit, to know the radius of the cylinder, and to know the external mechanism that controls the rotation about the cylinder is needed, we speculate on the possibilities to find this necessary information.

The control unit is active at the start and active at the end of metatarsal contact. Using direct motion data of metatarsal heads employing a motion analysis system, would be useful to characterize the frontal motion of the metatarsals. The frontal motion might be described by a (linear) function. The working of the control unit would be determined by this function of time. If such a function is not stable within

an individual motion pattern or between individuals, we are able to use information of the pressure plate system. Since the metatarsal curve can be determined quite accurately within the pressure data, we do have a curve on which the metatarsal heads are positioned. The geometrical pattern of the loading on and around this metatarsal curve could also be used to determine the working of the control unit. After all, the length of the metatarsal curve remains constant and therefore the part not in contact with the ground can be determined from the part that is in contact with the ground. The latter reasoning only applies for the forefoot push-off phase (FFPOP). In this phase, metatarsal head two is the last head that remains in contact with the ground.

Some research ([194], [56]) was done on the determination of the radius of curvature of metatarsal heads. Since these papers describe values for the heads themselves, they might not be precisely what is needed here. For the model, a functional radius of the cylinder is needed such that the rotation about the bent cylinder is restricted in such a way that the resulting displacement of the contact point is less than two diagonal lengths of a pressure sensor ($\approx$ 18.2mm). Still, we belief that functional radius of curvature is a parameter that should be based on biometric data based on pressure measurements of the foot, which might follow from pressure measurements.

The external mechanism is strongly linked to the radius of curvature of the cylinder. At this moment, we might be able to use the velocity of surface size change within the pressure distribution in the rearfoot and midfoot pressure areas just prior to heel lift and after heel lift. This is only possible if this velocity can characterise the rotation of rearfoot and midfoot about the metatarsals. A higher spacial resolution will visualise the motion of the metatarsal heads. Thereby, the mechanism that controls the rotational motion can be obtained directly from pressure measurements and the curvature of the cylinder.

Chapter 5

First Metatarsophalangeal Joint Motion

the relationship between motion and pressure

5.1 Introduction

The rotation of the foot about the metatarsal heads from the moment of heel lift till metatarsal push off causes a flexion in the first metatarsophalangeal joint. Since the hallux remains in contact with the ground during this period, the metatarsals, and connected to them the midfoot and the rearfoot, move with respect to the ground.

In Chapter 4, a mechanical model was proposed that accommodates the motion of the metatarsals during the stance phase of walking. In this mechanical model, an external mechanism controls the rotation about the bend cylinder. Also in Chapter 4, we suggested using the gradient of the function of the size of the supporting surface of the pressure distribution in the rearfoot and midfoot to describe this rotation. In this chapter, we suggest another approach, namely considering the connection between hallux and the metatarsals. At least part of the rotation about the metatarsals, and therefore the bent cylinder, takes place at the first metatarsophalangeal joint (MTPH-I).

Acquiring the pressure variables that are characteristic for the motion of MTPH-I is therefore the focus of this chapter.

5.2 Methods

5.2.1 Devices and Population

The measurements were conducted using a 612 Vicon system with six M-cameras running at 250Hz. Furthermore, a 1.0m by 0.4m pressure plate system manufactured by RSscan International was used to measure the plantar foot pressures at a frequency of 500Hz (8192 sensors, 8bits, maximum value of 127N/sensor). Also, a 0.9m by 0.6m force plate running at 1250Hz, manufactured by Kistler, was used to dynamically calibrate the pressure plate. Finally, a 3D data box manufactured by RSscan International was used to connect all measurement devices. The Vicon system in connection with the 3D box provided us with a synchronised integrated measurement system.

Motion was traced by attaching markers to the foot and by recording their three-dimensional positions. Three markers were attached to the medial forefoot to track their motion. Two markers were placed medially; on the side of the base and head of metatarsal. The third marker on the medial forefoot was attached between metatarsal heads two and three. A marker plate was attached to the hallux containing three markers. In Figure 2.4, the marker set-up is depicted. The angular representation of the metatarsophalangeal joint was obtained by calculating the joint coordinate system (Grood and Suntay [74], Cole et al. [39]).

From the registered pressure distributions, the foot was divided into areas as described in Section 2.2.6. In total, the foot surface was divided into eleven areas: a medial and lateral rearfoot area, a medial and lateral midfoot area, five metatarsal areas all containing one metatarsal, a hallux area, and an area containing the lesser toes.

Three session types were employed: (1) walking (ten trials for both the left and the right foot), (2) walking and running (five trials for both the left and the right foot, and for both walking and running), and (3) walking, fast-walking and running (five trials for the left foot only in all three conditions). For the present analysis of MTPH-I motion, the individual's walking trials within all session types were selected. The only selection criterion was that at least three trials were available for analysis. In 83 individuals out of a total of 125 that participated in this study, left and right foot were measured at least 5 times and at most 10 times per foot. For the remaining 42 individuals, 5 trials for the left foot only were measured. The individuals had a

mean age of 25.7 years with a standard deviation of ± 11.9 years ([10y,72y]) and a mean weight of 68.9kg with a standard deviation of ± 14.9kg ([32kg,116.5kg]). The population consisted of 48 women and 77 men.

The detailed description of measurement methodology is found in Chapter 2.

5.2.2 Data Processing

For describing the metatarsophalangeal joint, we use the following angles: flexion/extension, abduction/adduction, and inversion/eversion. These angles were calculated for the walking trials and static trial performed by each individual. From these angles, the following characteristics of motion are deduced:

1. angles of the static trial,
2. angles at initial contact,
3. minimum values of the angles,
4. time at which the minimum value of the angle occurs (in % stance duration),
5. maximum values of the angles,
6. time at which the maximum value of the angle occurs (in % stance duration),
7. range of motion of the angles during the stance phase,
8. the angles at the end of the stance phase.

For flexion/extension, we also introduced velocity variables:

1. minimum velocity in the first half of contact (from 0% to 50% of stance duration),
2. time at which minimum velocity in the first half of contact occurs,
3. maximum velocity of the complete stance duration,
4. time at which maximum velocity occurs of the complete stance duration,
5. minimum velocity of the complete stance duration,

6. time at which minimum velocity of the complete stance phase occurs.

The timing variables related to time events are all expressed as a percentage of stance duration. In Figure 5.1, we depicted the three angles for averaged left and right trials. Also, the meaning of the extra variables introduced for flexion/extension is interpreted graphically in this figure. The flexion/extension curve shows two time points at which velocity is minimum, one in the first half and one in the second half of stance duration.

From the eleven pressure areas and their corresponding pressure distributions, we calculated the values of 92 force related variables. These variables describe maximum force, time of maximum force, average force, maximum loading rate, time of maximum loading rate, force-time integrals, total duration, foot phases, and ratios and differences of previous variables. We study the interrelationship between the motion variables of MTPH-I and the 92 force variables.

To establish the pressure-motion relationships, we used Spearman and Pearson correlations. Furthermore, linear regression equations were calculated for the motion variables on the basis of the force variables. Only those force variables were taken into account in the regression equation for which their correlation with a motion variable was significant ($p < 0.05$) and higher than 0.3. Regression equations were calculated using all these relevant force variables and using a backward stepwise approach.

The statical calculations were performed in Matlab and SPSS v10.

5.3 Results

From the correlation study, we found no force variables that correlated significantly with inversion/eversion and abduction/adduction motion. The only exception was the static inversion/eversion position, but for studying MTPH-I motion, this variable is not relevant. For the flexion/extension curve, a number of significant correlations were found. The ones with strongest correlation are *Max_Force(H/MT1)* and *End_Contact(H-MT1)* with coefficients of 0.62 and 0.69, respectively. The range of motion of both average inversion/eversion and abduction/adduction curves are also a lot smaller, about 5°, than the range of motion of the flexion/extension curve, about 60°. This tells us that the rotation about the metatarsals seen in MTPH-I is predominately a posterior-anterior motion.

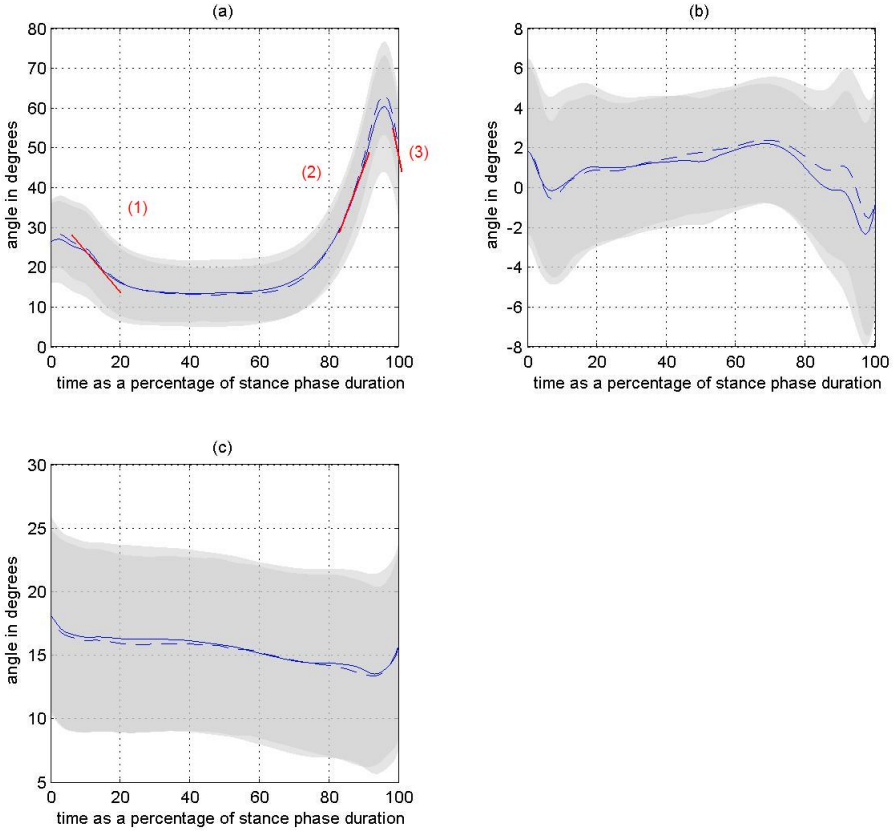

Figure 5.1 The average flexion/extension (a), inversion/eversion (b) and abduction/adduction (c) curves of the metatarsophalangeal joint. The averages are calculated for trials of left feet (sold line) and for trials of right feet (dashed line). The red lines in (a) depict the velocity at the moment of minimum velocity in the first half of contact (1), at the moment of maximum angular velocity (2), and at the moment of overall minimum angular velocity (3).

The significant ($p < 0.05$) correlation coefficients together with complete and backward stepwise regression equations are given in the following ten tables. Also, the value

of the explained variance R^2 of these regression equations is given. In the ten tables, we couple each of ten specific motion variables of MTPH-I to force variables with significant correlation coefficients higher than 0.3. In these tables, we use the following abbreviations:

1. Corr.coeff., Correlation coefficient,
2. Eqn.coeff.L., coefficients of the regression equation of the left trials,
3. Eqn.coeff.R., coefficients of the regression equation of the right trials,
4. LoadingR_Max, maximum loading rate,
5. LoadingR_Max_Time, the moment at which the loading rate is maximal,
6. Begin_Contact, start of contact as a percentage of stance duration,
7. End_Contact, end of contact as a percentage of stance duration,
8. Max_Force, maximum force, and Max_Force_Time is the moment at which maximum force occurs,
9. Average, average force.

Almost every force variable has a postfix that indicates the area or areas to which it applies. We use the following abbreviations:

1. MT1,...,MT5, metatarsal areas one to five,
2. Heel_Med and Heel_Late, medial and lateral heel area,
3. MF_M and MF_L, medial and lateral midfoot area,
4. H, hallux area,
5. T, lesser toe area.

In case two areas are referred to in the postfix, there is also an operation indicated. Operations are division, addition and substraction. To explain our notation, we mean by Duration(H/MT1) the duration of contact in H divided by the duration of contact in MT1, both expressed as a percentage of stance duration.

In all tables, the first column contains the name of the force variables. The second column contains the linear correlation coefficients with reference to the motion variable indicated in the heading of the table. The third column contains the coefficients of the regression equations for left trials. The fourth column contains the coefficients of the regression equations for right trials. The bullets denote the force variables used in the backward stepwise regression equations.

Table 5.1 Time point of maximum flexion in MTPH-I.

	Corr.coeff.	Eqn.coeff.L.		Eqn.coeff.R	
Foot Flat Phase	+0.42	0.30		5.57	•
Forefoot Push Off Phase	-0.36	-4.06	•	0.11	
LoadingR_Max_Time(MT1)	+0.32	0.04		-0.06	
LoadingR_Max_Time(MT3)	+0.31	0.00		0.00	
Duration(Heel_Med)	+0.45	-2.92		0.06	
Duration(Heel_Lat)	+0.42	-3.51	•	-1.87	•
Duration(Hallux)	-0.43	0.24		-3.63	•
Begin_Contact(H-MT1)	+0.46	0.52	•	0.22	
Duration(H-MT1)	-0.39	-0.21		-1.77	•
Duration(H/MT1)	-0.39	-16.18		258.79	
Regression Equation R^2		0.41	0.38	0.47	0.46

Table 5.2 Maximum extension of MTPH-I

	Corr.coeff.	Eqn.coeff.L.		Eqn.coeff.R	
Max_Force_Time(H)	0.33	8.23	•	4.64	
Max_Force(MT1/MT2)	-0.34	-1.12	•	-1.05	•
Regression Equation R^2		0.19	0.19	0.19	0.15

Table 5.3 Time point of maximum extension in MTPH-I.

	Corr.coeff.	Eqn.coeff.L.		Eqn.coeff.R	
Foot Flat Phase	+0.57	-0.65	•	-0.59	•
Forefoot Push Off Phase	-0.51	-1.19	•	-1.11	•
Max_Force(T)	-0.36	-0.00	•	0.00	
Max_Force_Time(MF_M)	+0.41	0.00		0.02	
Max_Force_Time(MT4)	+0.59	-0.00		0.00	
Max_Force_Time(MT5)	+0.51	0.01		-0.01	
LoadingR_Max_Time(T)	-0.36	0.00		0.00	
LoadingR_Max_Time(MF_M)	+0.31	0.00		-0.06	•
Force-Time Integral(MF_M)	+0.33	0.09		-0.04	
Force-Time Integral(T)	-0.43	0.01		-0.01	
Duration(Heel_Med)	+0.59	-0.30	•	-0.19	•
Duration(Heel_Lat)	+0.60	-0.21	•	-0.30	•
Duration(MF_M)	+0.37	0.00		0.02	•
Duration(MF_L)	+0.54	-0.00		-0.02	
Duration(MT1)	+0.35	0.63	•	0.64	•
Duration(MT2)	+0.45	-0.07		0.02	
Duration(MT3)	+0.48	-0.08		-0.04	
Duration(MT4)	+0.40	-0.06		-0.01	
Duration(MT5)	+0.30	-0.03		-0.08	•
End_Contact(H-MT1)	-0.59	0.06		0.19	
Regression Equation R^2		0.81	0.78	0.74	0.69

Table 5.4 Range of motion in MTPH-I.

	Corr.coeff.	Eqn.coeff.L.		Eqn.coeff.R	
Max_Force(H/MT1)	-0.31	-3.45		-3.02	
Max_Force(M1/MT2)	0.33	2.92		5.57	•
Max_Force(T)	-0.31	-0.08		-0.07	
Max_Force_Time(H)	-0.55	-0.80	•	-1.28	•
LoadingR_Max_Time(MF_L)	0.36	0.00		0.00	•
Max_Force_Time(H-MT1)	-0.53	-0.65	•	-0.00	
Regression Equation R^2		0.41	0.36	0.47	0.44

Table 5.5 Flexion/extension value of MTPH-I at the end of contact

	Corr.coeff.	Eqn.coeff.L.		Eqn.coeff.R	
Average(H)	-0.31	-0.16	•	-0.17	•
Force-Time Integral(T)	-0.31	-0.33	•	-0.11	
Regression Equation R^2		0.13	0.13	0.15	0.15

Table 5.6 The overal minimum of the angular velocity of the MTPH-I flexion/extension curve

	Corr.coeff.	Eqn.coeff.L.		Eqn.coeff.R	
Max_Force_Time(MF_L)	0.46	6.58	•	6.22	•
Max_Force_Contact(MT5)	0.37	3.70	•	0.48	
Regression Equation R^2		0.23	0.23	0.10	0.10

Table 5.7 Time point of the minimum angular velocity of the MTPH-I flexion/extension curve in the first half of contact.

	Corr.coeff.	Eqn.coeff.L.		Eqn.coeff.R	
Max_Force($\frac{MT1+MT2}{MT4+MT5}$)	0.37	5.28	•	3.28	•
Begin_Contact(H-MT1)	0.44	0.32	•	0.15	•
Regression Equation R^2		0.39	0.39	0.16	0.16

Table 5.8 Minimum of the angular velocity of the MTPH-I curve in the first half of contact.

	Corr. coeff.	Eqn. coeff. L.		Eqn. coeff. R	
Initial Contact Phase	+0.42	-16.1	•	18.6	•
Max_Pres_Time(Heel_Lat)	+0.41	11.1	•	7.83	•
LoadingR_Max_Time(MT1)	0.31	-0.00		0.71	
LoadingR_Max_Time(MT2)	0.40	0.10		0.98	
LoadingR_Max_Time(MT3)	0.42	-0.18		0.29	
LoadingR_Max_Time(MT4)	0.41	7.95		1.24	
LoadingR_Max_Time(MT5)	0.31	3.73	•	-1.71	
Duration(MT1)	-0.39	-17.01	•	-5.43	
Duration(MT2)	-0.36	-9.40		-6.31	
Max_Force_Time(H-MT1)	0.41	3.76		7.17	•
Regression Equation R^2		0.44	0.41	0.29	0.27

Table 5.9 Maximum of the angular velocity of the MTPH-I flexion/extension curve.

	Corr.coeff.	Eqn.coeff.L.		Eqn.coeff.R	
Initial Contact Phase	-0.37	-116.98	•	-60.68	
Max_Force(H/MT1)	0.62	13.5	•	-2.55	
Max_Force_Time(MT1)	0.40	0.01		0.01	•
LoadingR_Max(MF_L)	0.40	0.01		0.01	
LoadingR_Max(MT5)	-0.32	-5.70	•	-5.31	
Max_Force_Time(H-MT1)	-0.39	-8.89	•	-13.79	•
Force-Time Integral(H/MT1)	-0.30	-31.68		-97.22	
Regression Equation R^2		0.49	0.48	0.18	0.15

Table 5.10 Time point of the maximum of the angular velocity of the MTPH-I flexion/extension curve.

	Corr.coeff.	Eqn.coeff.L.		Eqn.coeff.R	
Foot Flat Phase	+0.53	-0.91	•	-0.75	•
Forefoot Push Off Phase	-0.51	-1.20	•	-1.14	•
Max_Force(H/MT2)	-0.31	0.21		-0.17	
Max_Force(MF_M)	0.32	0.03		0.03	
Max_Force(H)	-0.33	-0.01	•	-0.00	
Max_Force_Time(MF_M)	+0.38	-0.00		0.01	
Max_Force_Time(MT4)	+0.54	-0.00		0.01	
Max_Force_Time(MT5)	+0.49	0.01		0.00	
Average(H)	-0.30	-0.01		-0.01	
Average(T)	-0.32	0.00		-0.01	
LoadingR_Max(T)	-0.34	-0.00		-0.00	
Force-Time Integral(MF_M)	+0.34	0.12		0.39	
Force-Time Integral(H)	-0.33	0.02		-0.01	
Force-Time Integral(T)	-0.38	0.01		-0.01	
Duration(Heel_Med)	+0.54	-0.23		-0.36	•
Duration(Heel_Lat)	+0.55	-0.26	•	0.11	
Duration(MF_M)	+0.32	-0.00		0.01	
Duration(MF_L)	+0.49	0.00		0.03	
Duration(MT1)	+0.35	0.89	•	0.81	•
Duration(MT2)	+0.47	0.02		0.10	
Duration(MT3)	+0.50	0.00		0.02	
Duration(MT4)	+0.43	-0.01		0.04	
Duration(MT5)	+0.32	0.02		0.00	•
End_Contact(H-MT1)	-0.69	0.02		-0.18	
Regression Equation R^2		0.84	0.81	0.61	0.55

5.4 Discussion

The correlations coefficients between force variables and motion variables of the first metatarsophalangeal joint are not sufficiently high that we can conclude that pressure plate measurements can predict the motion of this joint. The highest correlation value is .69 describing the linear dependence of the time point of maximum angular velocity of flexion/extenstion in MTPH-I on the difference in end time points of ground contact between hallux and metatarsal I. A direct linear relationship between motion variables describing flexion/extension motion in MTPH-I and force variables obtained from a pressure plate measurement is not established.

Using the technique of linear regression, we found equations that could explain the variance of a motion variable up to 0.84, but on average 0.5. The highest R^2-values were found for two motion variables describing time events: (1) time point of maximum angular velocity in the flexion/extension curve, and (2) time point of maximum extension in the flexion/extension curve. We observe that R^2-values for left trials are generally larger than the ones for right trials, but left and right R^2-values do show the same behaviour. At present, we are not able to explain this difference in values.

The initial goal mentioned at the start of this thesis is a construction of a mechanical foot model that explains the motion of the foot on the basis of plantar pressure measurements. We described already a mechanical model for the heel and for the forefoot. The findings of this chapter should lead to a description of a mechanical model of the forefoot that improves the model mentioned in the previous chapter. This improvement should be found in adding an external mechanism to the existing forefoot model. The statistical analysis described in this chapter does not give sufficient convincing characteristics that describe the motion of MTPH-I from pressure data. Thus from this analysis, we can not design the suggested external mechanism completing the forefoot model.

Chapter 6

Conclusions and Recommendations

The research on foot mechanics discussed in this thesis was initiated as a joint project of the universities: Technisch Universiteit Eindhoven, Vrije Universiteit Brussel, and Universiteit Gent. Measurements were performed in the laboratories of biomechanics of the latter two universities in the period from May 2001 till August 2005.

The overall goal of the research, we describe in this thesis, is to discover the relationships between pressure data and foot motion. The connection between the plantar pressure exerted by the foot on the ground and the kinematics of the foot has been studied. Our study results in a mechanical model of the heel, analysis and introduction of the metatarsal curve, an inverse arch, and a statistical analysis of motion in the first metatarsophalangeal joint.

Experiments
Measurement data of plantar pressure distributions and foot kinematics are the critical ingredients of this study. The data obtained from the three measurement devices have been registered in an integrated set-up. All devices are synchronised in time and aligned in space.

A set-up has been created that simultaneously and integratedly measured force, pressure, and motion. To asses the level of accuracy of synchronisation and alignment for this unique set-up, tests were designed. The accuracy level of synchronisation has been tested with the force signal registered by both the pressure system and the motion system. A commonly used threshold scheme and a signal correlation measure have been employed. For the latter test, sensitivity in detecting errors with respect

to delay and frequency effects has been verified. The overall conclusion is that we are able to sychronise the plantar pressure system and the motion analysis system within the measurement accuracy. To obtain a high accuracy level of spacial alignment, we have used a wooden block of known dimensions. The centre of the surface impressed by the wooden block on the pressure plate was calculated from both pressure and motion data. At the start of each measurement day, a multiple of measurements has been performed such that the alignment is determined and from there its accuracy. For the study of motion of the metatarsal heads, only data of those individuals is used that guaranties an accuracy of alignment within pressure sensor dimensions.

Besides accuracy of synchronisation and alignment of the measurement devices, we have also looked at the accuracy of each of them. Our conclusion is that all measurement devices operate with an accuracy that is well within the requirements of our study.

Having installed the measuring set-up, we measured the 126 individuals that participated in our study. On the basis of a kinematic foot model, markers have been placed such that the motion analysis system tracked the motion of four segments of the foot: the heel, the hallux, and the medial and lateral metatarsals. Correspondingly, measurement data of pressure distributions was divided into elven areas of interest. The motion of the four segments could be explained by the evolution of pressure data in our chosen areas of interest.

Measurement data and calculations based on these data are stored in a 4.9GB database, as well as over 200 applications that can be used to process and analyse this data. Accessing the database is possible only after having read the details of the variables used in the database and the corresponding applications.

Rearfoot
From measurement data of plantar pressure, the motion of the rearfoot can be determined during the initial contact phase. The rearfoot motion is modelled as the rolling of a rigid sphere over a rigid plate. The contact path of the sphere is the path determined by the centre of pressure of the impressed heal area.

The radius of the sphere is an essential parameter in the rearfoot model. The optimal radii have a range of 4cm to 12cm. The radius is not a sensitive parameter; the average radius of 7cm does not change the orientation of the rolling sphere in a

serious way. A fixed sphere with radius 7cm used in our simulations describes rearfoot motion of all individuals of our population.

Using the corresponding heel reference frames from the motion analysis system, CoP paths from motion data can be calculated. CoP paths are not in complete agrement with CoP paths from pressure data. With a linear shift, largest at the start of contact and smallest at the end of the described time interval, both CoP paths coincide. Correction of CoP paths is necessary because the fat pad underneath the calcaneus has a non-isotropic and non-uniform thickness..

Predictive power of the model is 75% using an average CoP correction and an average radius of 7cm. If optimal values for both corrections and radii are used, predictive power of the model is 90% and higher. The rearfoot model as developed in this study describes the motion of the heel from a pressure measurement system and as observed from a motion analysis system.

Forefoot

From the analysis of the measurement data, we conclude that the metatarsal heads form an inverse medial-lateral arch, which changes its height during the stance phase from a more pronounced inverse arch to a flat arch when all metatarsal heads are in contact back again to an inverse arch during propulsion. Furthermore, the metatarsal heads describe a curve in the transversal plane, the metatarsal curve. From these observations, we propose a mechanical model for the forefoot consisting of a bent cylinder. Rolling of the cylinder describes posterior-anterior motion and upward bending of the cylinder describes the medial-lateral motion.

The sensor size of the used plantar pressure plate does not allow to determine the radius of the cylinder. The motion performed by the metatarsal heads remains within the length of two sensor diagonals. Thus, we are not able to track the motion of the metatarsal heads by using the pressure plate.

The motion analysis system reveals that there is a substantial change in length between the metatarsal heads during the stance phase. Even after all metatarsal heads contacted the ground the length between the heads increased significantly, about half of the maximum length difference during the stance phase. Only well after heel lift the distance between heads decreased again significantly. Increase of inter metatarsal distance contributes to the stabilisation function of the forefoot during propulsion.

The chapter on the first metatarsophalangeal joint is a starting point for further

study. By standard regression methods, we conclude that pressure variables can partly predict motion.

With this thesis, we meet to great extent three out of four objectives as mentioned in Section 1.3. Thus one objective remains; to describe the coupling between rearfoot and forefoot in one model. Starting point for such a model are the found relationships between pressure variables of the heel and metatarsal motion.

We would like to conclude this thesis with some recommendations for further study:

1. *use of a circular plate for aligning a pressure measurement system with a motion analysis system instead of a rectangular block.*
   Since the sensors in a pressure plate are arranged in a rectangular manner, we expect that the reconstruction of a circular plate from pressure data is more accurate in aligning the two systems than the rectangular shape as used in this research project.

2. *implementation of an application to calculate the accuracy of alignment directly after alignment measurements have taken place.*
   With such an application, no longer data should be disregarded because of alignment inaccuracies.

3. *discover the reasons why some inversion/eversion curves can be simulated with the rearfoot model up to heel lift and some are not.*
   With these reasons at hand, we might be able to enhance the predictive power of the rearfoot model after the initial contact phase.

4. *to analyse the relationship between pressure and motion of the first metatarsophalangeal joint.*
   In particular, this analysis should focus on the motion in the first metatarsophalangeal joint matched to the rotation about all metatarsal heads.

5. *to analyse the coupling between rearfoot and forefoot by studying the rigidity of the foot during the stance phase.*
   The windlass mechanism described in anatomy may be responsible for a rigid foot during propulsion. Therefore, the separate forefoot model describes the

complete foot motion during this phase, and the model in which rearfoot and forefoot are coupled comes down to the separate forefoot model.

Appendix A

Pressure Literature in more Detail

In this Appendix, we discuss plantar pressure literature indirectly related to our research. Literature of the same topic is discussed in one section.

In all sections, the articles were sorted with respect to publication dates. For all studies, we tried to summarise the topic, the methodology used, and the main results.

A.1 Methodology

This section on methodology is subdivided in a few topics. This will enhance the readability of this section.

Methodology of Devices

In the review of Hughes et al. [95, 1987], three different commercially available methods of measurement are compared: a device using the direct imprint method, a 128 load cell measurement device (size 15mm^2, 25cm by 12.5cm), and the pedobarograph. Normal subjects were invited to participate in this study. Besides pressure measurements, also radiographs of both feet were registered. The radiographs were used to define areas of interest. Eleven areas were defined: the heel, the metatarsal heads, and the toes. The two mentioned dynamic methods are compared using relative pressures. Consequent differences in peak pressures are found between these systems. Higher spatial and higher sampling frequencies are mentioned as the causes of these differences.

Hughes et al. [94, 1993] compared two different pressure measurement systems:

the pedobarograph and the Emed F system. Different to a previous study of Hughes et al. [95, 1987], this study focussed secondarily on pressure measurements themselves. Especially, the loading across the metatarsal heads was looked at by measuring a 100 adult individuals during three walking trials on both systems. For the pedobarograph, the sampling rate was 25Hz, the resolution was 1mm, and the collection area was 360mm by 360mm. For the Emed F system, the sampling rate was 20Hz, the resolution was 2 sensors/cm^2, and the collection area was 226mm by 196mm. A manual masking procedure was used to determine twelve areas from which peak pressures and contact times were calculated. The twelve areas were the heel, the five metatarsal heads, the five toes, and the base of the fifth metatarsal. A few differences were found between the measurement systems. The Emed F system showed higher pressures underneath the heel, metatarsal heads I-IV, and the hallux. Lower pressures and shorter contact times were found for the four most lateral toes. With respect to the loading across the metatarsal heads, four peak pressure profiles were found using cluster analysis. Both measurement systems gave about the same four pressure profiles: a medial pattern, a medial central pattern, a central pattern, and a central lateral pattern.

In another study by Mueller and Stube [145, 1995], the topic was generalisability of peak pressures measured with the F-scan insole system. They used two methods of calibration and measured over multiple steps, sensors, and days. The overall conclusion is that absolute peak pressure values are comparable between conditions when a stable external calibration method is used.

Davis et al. [47, 1996] studied the frequency content of plantar pressure profiles of diabetics and non-diabetics, and discussed its implementation on the selection of transducer size. Discrete Fourier Transform techniques were used to determine the spatial frequency content in diabetics and non-diabetics. Further, the sensor sizes were quadrupled from 5mm by 5mm to 10mm by 10mm. From an analysis based on 25mm^2 transducers, the authors concluded that transducer sized greater than 6.36mm by 6.18mm (medio-lateral and antero-posterior directions) results in sub-optimal samplings of plantar pressure distributions. They used an emed-SF 50Hz, 190mm by 360mm plate.

In a study from Lord [120, 1997], the influence of spatial resolution on peak pressures was looked at using a pedobarograph. She used direct measurements as well as a mathematical abstraction to study the effect of sensor size. She concluded that the average pressure from a transducer of area 100mm^2 may register only 60%-70% of the

true peak pressure in barefoot standing.

Nicolopoulos et al. [151, 2000] tested the F-scan insole system using an axial loader system for local loading and an Instron device for global loading. They concluded that large errors due to mechanical effects raises serious questions about the reliability of the F-Scan system.

Urry and Wearing [199, 2001] compared footprint indexes from ink with footprint indexes from electronic devices. For the latter, a Musgrave, system, 38.5cm by 16cm running at 50Hz, was used. Contact area, arch index, and long plantar angle were compared between the systems. Both contact area and arch index were significantly different between methods. Taking the ink footprints as the golden standard, the musgrave system underestimated both contact area and arch index.

Barnett et al. [12, 2001] compared force and temporal parameters between an in-shoe pressure measurement system, Pedar (50Hz), with a force platform, Kistler running at the same frequency. Barefoot and within three different shoes were the measurement conditions. Five individuals were found to participate in this study. In barefoot, the timing variables correlated well. However, some absolute values such as first peak and average peak were significantly higher in case of the force platform.

Fregly and Sawyer [60, 2003] studied the effect of discretisation errors in contact pressure measurements for total knee replacement. They used a simulation approach to estimate the order of these errors in relationship to contact pressures measurement. Simulated discretisation errors were in the order of 1-4% for contact force, and 3-9% for average pressure and contact area.

Reliability, Repeatability and Variability of Pressure Measurements

Kernozek et al. [109, 1996] studied reliability of an in-shoe pressure measurement system during treadmill walking. They used an emed insole system with 99 sensors running at 50Hz. Multimask software was used to determine seven anatomical regions. This study showed that the velocity of gait significantly influences loading and timing variables of the whole foot. Variables used were peak force, force-time integral, peak pressure, pressure-time integral. Reliability was high (>0.9) from eight steps on.

McPoil and Cornwall [134, 1998] studied variability of the centre of pressure pattern integral during walking. Both an Emed pressure plate and an insole system were used to study the variance of this variable. For the calculation of CoP-pattern integral, an axis in the pressure distribution of the foot was needed. Novell software was used to

create this axis. The authors did check the position of the axis by comparing it to manually determined axes. Results indicated that the CoPI is a variable with a high standard deviation and therefore is not usable in the assessment of foot orthoses.

Mathieson et al. [130, 1999] compared Arch Index, Chippaux-Smirak Index, and Footprint Angle between static and dynamic footprints using a Musgrave system. They concluded that the ability to relate these variables from the static condition to the dynamic condition are limited.

VanZant et al. [206, 2001] studied the symmetry of plantar pressures between left and right feet and vertical force in healthy individuals during walking. Twelve steps were analysed from 30 volunteers using an Emed pedar insole system running at 50Hz. The variables being maximum vertical force, peak pressure, and pressure-time integrals were calculated for hallux/toes, forefoot, midfoot, and rearfoot. No significant gender differences, and left and right differences were found. Only, the forefoot and rearfoot showed minimal significant differences.

Taylor et al. [196, 2004] studied the influence of walking speed on plantar pressure measurements using the so-called two-step gait initiation protocol. They studied the effects of three walking speeds on contact time, maximum force, peak pressures, force-time integrals, and pressure-time integrals in the medial and lateral heel, the lateral midfoot, the first, second, and third to fifth metatarsal head, the hallux, the second toe, and the third to fifth toes. Overall, they concluded that controlling small variations in walking speed is not critical for contact time percentages, maximum force and peak pressures, but is critical for force-time and pressure-time integrals.

Methodology of measurement protocol

Most of the previous studies use a midgait protocol, or don't mention the protocol used. In the study of Meyers-Rice et al. [139, 1994], the midgaite protocol was compared to the one and two step protocol. Ten individuals walked over a 23 by 44cm Emed SF platform measuring at a frequency of 70Hz in the middle of a 9m walkway. For all three conditions, three trials were measured. The plantar surface of the foot was divided into three regions: rearfoot, midfoot, and forefoot. From all regions, peak pressures, peak vertical force, and impulses were calculated. The one step protocol was previously used in individuals unable to perform the midgait protocol. The concern of the authors was the difference in measurement values between the midgait and one

step protocol. From the present study, it followed that the values from the two step method (115cm before the plate) were in most cases more representative of the values of the midgait protocol than the values of the first step method.

Harrison et al. [82, 1997] studied the influence of gait protocols on dynamic pedobarography using five different modes of walking from full control to a first-step method. Their findings suggested little difference between the five protocols on peak pressures and pressure-time integrals within seven areas (heel, five metatarsal heads, and the hallux). The used measurement device was the not well-known Biokinetics Dynamic Pedobarograph running at 25Hz. Results with respect to the first step protocol were different to those in literature. The authors contributed this difference to the specific first-step protocol adopted for their study. The first-step protocol used in their study lead to overreaching with the first step.

Wearing et al. [209, 1999] studied three types of gait protocols, namely midgait, two step initiation and two step termination. The latter two were compared to the standard, midgait. The variables looked at were contact duration, percentage of contact duration, peak pressure, peak force, pressure-time integral, and force-time integral at seven sites of the foot. They used an Emed-sf 23cm by 44cm plate running at 50Hz to register pressure distributions of 25 individuals. The authors defined midgait as three steps before the platform and 4m continued walking after the platform. They used the Novel Win Mask software to automatically determine the seven sites: heel, midfoot, first metatarsal head, 2-4th metatarsal head, fifth metatarsal head, hallux, and lesser toes. No real differences were found in the number of trials necessary to obtain a good reliable level in the three different methods. However, the pressure variables determined in case of the termination and initiation protocol were only partly related to pressure variables determined in case of the midgait protocol. the initiation method resulted in similar forefoot pressures as compared to midgait, while the termination method resulted in similar timing parameters as compared to midgait, expect for the hallux area.

McPoil et al. [135, 1999] studied variability of plantar pressure data between two-step and midgait protocols. From previous research, they came to the conclusion that the two-step protocol is a useful alternative to the midgait protocol. In this specific study, the authors used an Emed sf 23 by 44cm pressure plate running at 70Hz to study pressure parameters: peak pressure and pressure-time integral in five foot areas determined by the Novel Multimasks software (heel, lateral, central and medial fore-

foot, and hallux). The results of this study indicated similar values for the pressure variables using the two protocols, and three to five trials to obtain between-trial reliability for the two-step protocol and for the midgait protocol.

Introduction of New Pressure Related Variables
Han et al. [80, 1999] quantified the CoP using F-scan in-shoe transducers. The authors determined a number of variables from the CoP path: average displacement AP and ML, CoP velocity, slope of CoP, average CoP, and initial CoP. The variables showed to be reliable after conducting a test-retest analysis. How this variables could be applied was not mentioned.

Cornwall et al. [41, 2000] described the velocity of the Centre of Pressure during walking. They introduced the variables: maximum velocity, time of maximum velocity, average velocity, percentage of time spent in a foot region. The foot regions were the rearfoot, midfoot, forefoot, and toes. Most variables were proven to be between-trial reliable through interclass correlations. They indicated that the velocity of CoP may be a useful measurement in future gait research.

Leung et al. [117, 2001] introduced a foot index, which they called the contact area ratio. This new ratio was remarkably similar to the arch index of Cavanagh and Rodgers. The only difference we were able to observe was taking the instant of time just before heel off as the time point at which this measure was calculated.

A.2 High Heels

In our present day society, a large number of women occasionally or frequently wear shoes with high heels. In general, researchers warn against wearing shoes with high heels for a prolonged period of time.

In a study by Gastwirth et al. [64, 1991], high-heel shoes are the topic of research using local transducers. The placement of the transducers is the same as in the case of Rzonca et al. [181, 1984] except for an addition of one transducer beneath the head of metatarsal three. Gastwirth et al. suggest that the duration of forefoot loading is increased rather than the loading of the forefoot. They conclude that "high heels have a detrimental effect on gait".

In another study on heel height by Eisenhardt et al. [53, 1996], the focus was on

temporal characteristics of the pressure distribution. Barefoot walking was compared with walking on high heels (4 conditions). Plantar pressure data was obtained using electrodynography with the sensors placed at the lateral and medial heel, heads of metatarsal one, two, three, and five, and the distal phalanx of the hallux. Overall walking on high heels prolonged stance phase and the duration of weight-bearing on the medial forefoot. Also, for the third and fifth metatarsal head, peak pressure occurred later in the case of bare feet than in the case of high heels.

Mandato and Nester [129, 1999] studied the effect of heel height on forefoot peak pressure. They used the F-scan insole system and three types of footwear: sneakers, 2-inch heels, and 3-inch heels to study effect of the choice of footwear in 35 women. Overall, the pressure increased from sneakers to 2-inch heels with 63%, and from 2-inch heels to 3-inch heels with 30%. A shift of peak pressure was noticed to the first metatarsal head and the hallux.

Speksnijder et al. [189, 2005] studied the effect of heel height on forefoot-pressures. They used the Pedar system to measure inside two shoes: low heeled (1.95cm +/- 1.06cm) and high heeled (5.91cm +/- 1.03cm), for ten healthy women. The pressure distribution was divided into seven areas: heel, midfoot, hallux, lesser toes, and lateral, central, and medial forefoot. The authors gave a mathematical description of this division. Pressure variables used were contact area, contact time, peak force (in BW), peak pressure, force-time integral (in BW), and pressure-time integral. Overall, the pressures in the forefoot increased up to 40% when wearing high heeled shoes.

A.3 Insoles

The use of insoles and their effects on force and plantar pressure redistribution have peaked the interest of many researchers. In this section, we summarise some of the articles found in literature.

Insole material and orthotics effect on force and plantar pressure was studied by McPoil and Cornwall [133, 1992], Sanfilippo et al. [184, 1992], and Novick et al. [156, 1993]. The first two researchers used the EMED-SF pressure platform of 23cm by 44cm, 2 sensors per cm^2 measuring at a frequency of 70Hz. The third researcher used two measurement techniques: the Hercules system with four capacitive pressure transducers and the F-Scan insole systeem running at 50Hz. The number of individ-

uals participated in these studies was twelve, ten and ten, respectively. The first two compared insole materials of almost the same materials. More specific, McPoil and Cornwall used three materials of which two were also used by Sanfilippo et al., which used a total of five materials. Studied variables were slightly different. The conclusions of the study by Sanfilippo et al. suggested a reduction in peak plantar pressure and pressure-time integral underneath the whole foot due to use of insole material. McPoil and Cornwall were able to give a more detailed conclusion because they divided the foot area into a rearfoot, a midfoot and a forefoot area. Comparing to barefoot walking, the use of all insole materials led to a significant decrease of peak plantar pressure. In the rearfoot, two out of the three insole materials led to a decrease in peak pressure. In the study of Novick et al., the four transducers were placed underneath the heel, the midfoot, and the third and first metatarsal head. In the F-Scan analysis, masks were placed manually at the same sides as the transducers. Significant differences were found in the values of recorded pressure values between the two systems. In studying the three different orthoses, both measurement devices produced similar results. In general, they concluded that the relieve of pressure underneath the first metatarsal head was combined with an increase of pressure underneath the midfoot for all orthoses.

Bennet et al. [15, 1996b] looked into the effects of custom-molded orthoses using a standard Root-type orthoses. A combination of measurements were employed: underneath the shoe with a Musgrave system, and inside the shoe with a Electrodynogram. Overall, maximum peak pressures were reached 5% to 7% earlier in the stance phase with the orthoses, and the medial plantar surface of the forefoot reaches its maximum pressure at a later stage.

Lavery et al. [114, 1997] looked at a way to obtain biomechanical characteristics of insole material using techniques feasible for a physician. They related Young's modules of insoles made by PPT and Pelite to insole pressure variables, peak-pressures, and pressure-time integrals. They employed the Emed Pedar system running at 50Hz with 85 sensors to register pressure distribution underneath the foot. The relationship found can also be inverted such that a test of the viscoelastic insoles gave an indirect measure of the pressure underneath a patient's feet. Overall, the authors concluded that the stiffness decreases initially and is followed by an increase of stiffness over time. The latter, however, was not studied in the present article.

The focuss on shock attenuation characteristics of four different insoles when in

military boots during running and marching was the topic of an article by Windele et al. [212, 1999]. Four insoles were used to investigate attenuation of pressure underneath the heel and the forefoot. A Parotec system of measuring pressure was used with 24 sensors. The overal conclusion was that Sorbothane insoles reduced pressure with 27% in running and 23% in marching under the conditions of wearing extra weight and being on a stone floor. In the future, these authors would like to study the difference in lower extremity injuries with and without the use of insoles in military boots.

In a literature review of Landorf and Keenan [113, 2000]. the efficiency of foot orthoses was looked at in six outcome areas. One of these areas was plantar pressure. They described a number of studies also described above, but with a total of about fourteen studies, they described the topic of plantar pressure in orthoses quit extensively.

Reed et al. [168, 2001] looked at the difference between Root and Blake orthoses using the EDG system. They concluded that the orthoses behaved similar.

Offloading properties of a rocker insole were studied by Frykberg et al. [62, 2002]. The rocker insole has the same principle as a rocker shoe. In the present study, this insole was tested in customary footwear and surgical boots. Both these shoes were tested with and without the rocker insoles. Overall, the rocker insoles reduced forefoot pressure significantly in both shoes. The F-scan insole system was used to study the pressure distribution.

In a study by House et al. [93, 2002], the influence of simulated wear upon the ability of insoles to reduce peak pressures during running when wearing military boots was researched. Instrumented insoles from Parotec were used to measure nine individuals in eight conditions: three insoles before and after simulated wear was applied, no insoles, and a Saran insole. Overall, the insoles ability to reduce peak pressure was not reduced by a simulated wear of 100-130km. The most effective insole reduced peak pressures at the heel by 37% and at the forefoot by 24%.

A.4 Running

In this section, the reader is able to find some of the literature on running research using measured a plantar pressure system. Although, a lot of articles exist with running as topic, the ones using plantar pressure measurements are not yet of the same order as the number of articles using other measurement methodology.

In a study by Wilson and Kernozek [211, 1999], the topic of fatique was looked at using the Pedar insole pressure system with 99 sensors running at 150Hz (normally 70Hz, but running at 150Hz due to the reduction in the number of measured sensors to 67 sensors, not containing the heel). Running relaxed and during fatique were assessed in different areas for the well-know variables peak force, force-time integral, peak pressure, pressure-time integral. Overall, the reaction to fatique was a decrease in heel plantar pressure, an increase in cadence and an increase in medial forefoot loading.

Kwak et al. [112, 1994] published a study about midsole hardness and thickness of marathon shoes. Five different midsole hardness levels and three thicknesses were used to study its influence on rearfoot motion (two dimensional), force generation, and plantar pressure. The eleven male individuals that performed the study were measured separately on the force plate (AMTI) and the pressure plate (EMED, 44.5cm by 22.5 cm) both measured with a frequency of 100Hz. Plates were contacted with shoes on. The foot contact area was divided in six areas: a medial and lateral rearfoot, a medial and lateral midfoot, and a medial and lateral forefoot. The absorption characteristics were studied using the time of first vertical force peak, the duration of this peak, and the average force loading in this period. Hardness and thickness did not change most of the measured variables. Only peak pressures did change and showed higher values in stiffer and thinner midsoles.

In a study by Van Gheluwe et al. [203, 1994], plantar pressure measurements were studied during both treadmill and overgrond locomotion. An electrodynogram was used to study 30 individuals where the pressure transducers were located at the medial and lateral heel, the first, second, third and fifth metatarsal head, and the hallux. A number of walking and running velocities were used with a sampling frequency of 100Hz and 200Hz respectively. Timing information and maximum pressure were used as variables together with loading rate, which was the first time we encountered loading rate as a variable. The overall conclusion of this study is that use of a treadmill significantly influences foot function with the distinction that walking is changed much more than running.

Busseuil et al. [25, 1998] studied rearfoot-forefoot orientation and traumatic risk for runners in a population of 216 healthy controls and 66 individuals suffering an overuse injury. Static and dynamic foot prints were measured on photosensitive sheet. Based on a method by Freychat et al. [61, 1996], an angle between rearfoot and

forefoot was constructed. These angles from static and dynamic measurements were related by the authors to pronation and supination motions. Subsequently, the authors concluded that pronation seems to be a risk factor in the occurrence of stress injuries in running.

In an extensive study performed by De Wit et al. [49, 2000], plantar pressure measurements were only part of a complete data-set studying both barefoot and shod running. Pressure measurements were performed using a Footscan system running at 200Hz with 4 sensors/cm^2. Specific for the pressure measurements, they found a correlation ($r = -.7, p < 0.05$) between flatter foot placement and lower peak pressures. The authors, therefore, assume that runners adopt a flatter foot placements in barefoot running in an effort to limit local pressures underneath the heel.

A.5 Diabetic Feet

The effects of foot problems in the diabetic foot has led to a lot of research in this area, some of which is described below. Elevated peak pressures are found in this patient group, but the cause of foot problems in generally is thought to be multi-factorial.

The dynamic pressure of the diabetic charcot foot was studied by Wolfe et al. [215, 1991] using the commercial pressure plate of the Novel company. There EMED SF pressure plate consisted out of 2016 sensors based on the capacitive principle with two sensors every square centimeter and a sampling frequency of 143Hz. A mask (certain sensors of the complete array) was constructed based on the maximum pressure image to isolate the lesser tarsus (including the talonavicular joint, the calcaneoucuboid joint, the naviculocuneiform joint, and the tarsometatarsal joints). The lesser tarsus and the total foot were analysed using total contact time, total force, peak pressure, time to peak pressure and time to maximum force, pressure-time and force-time integral, and contact area. The analysis of the lesser tarsus show that the pressure exerted by the lesser tarsus of a Charcot foot is about eight times higher than in their control group. More conclusions with respect to weight-bearing of the lesser tarsus, led these authors to conclude that the lesser tarsus is the primary weight-bearing area of the Charcot foot.

Rodgers et al. [176, 1988] performed a study with 110 feet of diabetics. They

used a 1000 element, sensor size 6.5mm by 7.5mm, pressure plate to register pressure distributions. The first step approach was used to limit patient risk. In contrast to previous findings, they found a medial shift of maximum local load in the forefoot accompanied by an increasing neuropathic involvement.

Fleischli et al. [58, 1997] looked at strategies to reduce pressure at sites of neuropathic ulcers. They used five strategies from total contact casts to accommodative dressings to study the effect on peak pressures in 26 individuals with the Pedar in-shoe pressure measurement system (50Hz with 99 sensors).

Armstrong et al. [10, 1999] performed a study about total contact casts and removable cast walkers and their ability to remove pressure in the plantar heel area during locomotion. In total four types were studied among them the aircast pneumatic walker, and a Reebok shoe as control. The 25 individuals with diabetic mellitus were measured with the Pedar in-shoe system. Pressure variables for the heel area were used: peak pressures and pressure-time integrals. The total cast reduced pressure most successfully with an average of 33% in comparison to the Reebok shoes.

In a study by Zhu et al. [220, 1993], plantar pressures underneath feet of sensate and diabetic insensate individuals were studied. They augmented that isolated trials of barefoot plantar pressure measurements do not give insight into possible step-to-step variations. To overcome this problem, the authors used seven pressure sensors per foot embedded in the insoles and located at the posterior heel, the metatarsal heads, and the hallux. The insole measurement device was able to measure all channels for 4 minutes at 35Hz. The sensors had a 11mm diameter and a thickness of 0.5mm. Ten sensate and five insensate individuals were involved in this study. Pressure variables used in this study were the pressure-time integral, the contact time, and the peak pressures. Significant differences between sensate and insensate were found in all pressure variables for the heel and first metatarsal head. A larger step-to-step variation in plantar pressures was found in the insensate group and the authors worn against the interpretation of plate measurement for insensate individuals.

A study of Bennet et al. [16, 1996a], the analysis of risk factors for neuropathic foot ulceration in diabetes mellitus was studied with the musgrave footprint system. The metatarsal heads, hallux, and heel were selected for pressure analysis. Overall pressure was significantly elevated in the the case of diabetes mellitus together with lower vibratory perception, higher HbA1c blood levels (indicator of the rate of nonenzymatic glycosylation), and reduced ankle joint flexibility.

McPoil et al. [136, 2001] discussed peak pressure and pressure-time integral underneath the feet of American Indians with diabetes mellitus. The 45 individuals with diabetes participating in this study were compared to individuals with no diabetics using a three group design: no diabetes, diabetes without neuropathy, and diabetes with neuropathy. An Emed pressure plate was used running at 70% that automatically divided the pressure distribution into eight areas with their Multimask software. The authors concluded that American Indians with diabetes have a similar pattern with respect to peak pressure to non Indians with diabetes.

In a study on foot ulceration in type 2 diabetes, Kastenbauer et al. [105, 2001] performed a prospective study about risk factors for foot ulceration. It was found that following variables were risk factors: vibration perception threshold, plantar pressure, and daily alcohol intake. The study incorporated 186 volunteers of whom 10 developed 18 forefoot ulcerations. Plantar pressure was measured employing a two step protocol using an Emed pressure platform. Average plantar pressure were calculated in different areas: hallux, lesser toes, first metatarsal head, second to fifth metatarsal head.

A.6 Infants and Young Children

Most articles summarised in this section discuss the very interesting topic of acquiring the ability to walk independently. Since both structure and function of the infant feet are undergoing rapid changes, this research suffers from additional methodological problems, but offers a diversity of mechanical behaviour.

A comparison of the pressure distribution patterns between infants (age between 14 and 32 months) and adults was made by Henning and Rosenbaum [87, 1991]. They used an pressure plate (EMED- Novel company) of 1344 sensors covering an area of 20cm by 34cm, and measuring at 20Hz. The pressure distribution of walking at self-selected slow walking pace was analysed in seven selected areas: medial heel, lateral heel, midfoot region, first metatarsal head, second metatarsal head, third metatarsal head, and hallux. The parameters of interest were maximum pressure values, pressure quantities with respect to body weight and contact area, regional force-time integrals, and regional relative impulses (relative means the ratio between the local impulses and the sum of the impulses under all regions). From the results followed that there

does not exist a functional medial-lateral arch in the forefoot. With respect to the comparison between adults and infants, the authors concluded that infants have substantial lower peak pressures with the exception of the midfoot. The authors believe this phenomenon to be caused by the softer structures of the infant foot and a 1.5 times higher body-weight to foot-contact area ratio in adults.

In a study by Kellis [106, 2001], plantar pressure data from preschool boys was looked at for the conditions standing, walking, and landing. The author used a Musgrave system, 390mm by 195mm; 60Hz, and calculated the peak pressures in eight areas: hallux, second to fourth metatarsal heads, first metatarsal head, fifth metatarsal head, medial and lateral midfoot, and the heel. Not surprisingly, the landing condition have higher peak pressures than all other conditions.

Hallemans et al. [77, 2003] studied pressure distribution patterns under the feet of new walkers. In their study, seven able-bodied subjects were measured in the first two month of independent walking. As many researchers, they used local pressures underneath the plantar side of the foot. The areas chosen for this analysis were the heel, the midfoot, the hallux, and lateral, medial, and central metatarsals. They used peak pressures and relative impulses to characterize foot unroll. Furthermore, they introduced a new variable for quantifying CoP deviations from the line of progression. In this study, a Footscan system was used measuring pressure at a frequency of 250Hz with a plate size of 2m by 0.5m and a sensor size of 7.6mm by 5mm. Hallemans continued their research of this longitudinal project and reported on the five month results [78, in press].

Bertsch et al. [17, 2004] studied plantar pressure distributions of 42 children in the first year of independent walking. Plantar pressure of five right steps and five left steps were registered using an Emed system. Pressure distributions were divided into five areas: heel, midfoot, forefoot, hallux, and lesser toes. Pressure variables used for analysis were: contact area size, peak force, peak pressure, contact time, and impulse with all variables normalised to foot size and body weight. Overall, the development of the longitudinal arch correlated with significantly reduced pressure underneath the midfoot, but with a wide variation between individuals.

A.7 Therapeutic Shoes

Therapeutic shoes have been in practice for healing certain injuries and deceases. Research using plantar pressure has been used to asses the working of these devices.

In a publication by Nawoczenski et al. [148, 1988], the effect of rocker sole design on plantar forefoot pressures was studied. The transducers were placed on the hallux, and the first, third, and fifth metatarsal heads. Five different rocker designs and a shoe with no sole modification were compared. Different types of pressure reduction were found between rocker designs. They concluded that rocker placement should be given more attention and that a curved rocker design may be more acceptable and more effective in the management of plantar foot lesions.

Hodge et al. [90, 1999] looked at the topic of orthotic management of plantar pressure and pain in rheumatoid arthritis of patients with second metatarsal head pain. Four styles of orthosis were compared to a shoe only control. The custom molded orthosis with metatarsal dome was most effective in reducing plantar pressure underneath the second metatarsal head and in reducing the perceived pain. The study was performed with an Emed insole system running at 50H and its accompanying Multimask program to evaluate: average pressure, peak pressure, pressure-time integrals and contact duration of the lateral and medial midfoot, the first, second and 3th-5th metatarsal heads. Pain could not be related to peak pressures on the plantar surface.

Remond et al [167, 2000] studied plantar pressure during normal gait in individuals with excessive pronation. Three condition were used for this study: Dunlop Volley (DV) shoes, DV shoes with a noncast insole containing a 6° varus rearfoot wedge, and DV shoes with a modified Root orthosis. Overall, the Root device was superior in reducing pressure and force variables: peak pressure, pressure-time integral, maximum averagfe pressure, peak force, and force-time integral. The contact area increased for all orthosis. In rearfoot and midfoot the Root device reduced pressure and increased contact area. Forefoot loading was also reduced both laterally and medially. Measurements were performed using the Pedar system running at 50Hz with the Novel Multimask software, masking the maximum pressure image into six areas.

Fuller et al. [63, 2001] compared rigid rocker shoes of two designs, one new postoperative shoe and one existing, to normal shoes. The variables taken were peak pressure, peak force, and force-time integral. Sixteen women were selected to participate in this study and were measured using the Pedar insole system running at 50Hz.

The new postoperative shoe reduced forefoot pressure by 20% while only having a rocker bottom of 11°.

A.8 Databases

Reference data are very important in analysing individual plantar pressure data in clinical settings. Some efforts in this area are described below. We explicitly mention the study by the De Cock et al., [48, 2005], since it the largest database of normative data known to us.

Bennet et al. [14, 1993] used a Musgrave Footprint plate system to determine 95 percentile limits for the average pressure underneath the foot. The specific areas of interest were the hallux, the first metatarsal head, the second to fourth metatarsal heads, the fifth metatarsal head, the lateral calcaneus, and the medial calcaneus. Besides the average pressure values per gender, the authors also described the order of average peak pressures, from high to low: the second to fourth metatarsal heads, the hallux, the first metatarsal head, and the fifth metatarsal head.

Blanc et al, [20, 1999], described normative data for temporal parameters and foot unroll patterns for walking based on a data set of 105 healthy individuals using foot switches. Some asymmetry coefficients were found in metatarsal head, great toe latency, and support.

Kelly et al., [107, 2000] studied the timing of peak plantar pressure underneath the forefoot during the stance phase of walking. Patients with diabetes mellitus, patients with transmetatarsal amputation, and normals were studied. In all groups peak pressures occurred at 80% $\pm$ 5%. No significant differences were found between the groups for the variables peak plantar pressure, peak force, contact area at peak plantar pressure, and percentage of stance of peak plantar pressure.

De Cock et al. [48, 2005] performed similar research as Blanc et al., but on a population with more than 200 participants performing a running condition. They used a Footscan pressure plate of size 2m by 0.4cm containing over 16000 sensors, about 3 sensors per square centimetre. They used a local masking procedure as illustrated in the first row of Figure 1.9 to obtain temporal information from the pressure distribution data. The results of their study were the introduction of terminology of foot contact phases and a database with temporal information of these foot contact phases.

A.9 Structure and Function

A research topic of importance is the one relating structure of an organism to its function. In this section, we sum up some of the relationships between structure and function of the foot using plantar pressure data.

Walker et al. [208, 1998], studied the relationship between foot pressure patterns and foot types. The foot types were pronated, supinated, and normal feet based on the position of certain bones in the foot. Also, callus sites were taken into account when looked at the pressure pattern. They used a BTE Dynamic Pedobarograph running at 30Hz for this study. The pressure patterns were divided into three patterns on the basis of peak pressures underneath the metatarsal heads: a medial, central, and lateral pressure pattern were identified. Overall, they concluded that other factors beside foot type influence the area of peak pressure underneath the metatarsal heads.

Cavanagh et al. [31, 1997], and Morag and Cavanagh. [142, 1999] described the relationship between structural and functional predictors of regional peak pressures during walking. The regions of pressure are the rearfoot, the midfoot, MTPH1, and the hallux with a Emed SF2 system. Structural and functional characteristics were obtained from a large amount of different types of measurements (physical characteristics, anthropometric data, passive range of motion, radiographs, mechanical properties, stride parameters, foot motion in 3D and EMG). Regression equations were obtained from these measurements related to peak pressures based on structural parameters, functional parameters, or both. Structural and functional parameters are not additive in their contributions to explained variance. Overall the explained variance is between 48.5% and 56.6%. The authors do note that their regression equations can not be used for cause-effect relationships, but might be useful in gait training.

In a study by Mueller et al. [146, 2003], forefoot structural predictors of dynamic plantar pressures during walking in people with diabetes and peripheral neuropathy were looked for. An Fscan plate system was used to register pressure data from 20 healthy individuals and 20 patients with diabetes and peripheral neuropathy. Hierarchial multiple regression was employed to predict peak pressures at the hallux and the five metatarsal heads. It was found that the metatarsal phalangeal joint angle accounted for 19-45% of peak pressure variance at five of the six locations in the diabetes group. Overall, 46-71% of the variance could be accounted for in the diabetes group and 52-83% in the control group.

A.10 Hemiparetic patients

A group of patients that visits the gait laboratory on a regular basis are the hemiparetic patients. In this section, three papers are discussed in connection to this patient group.

In a study by Gaviria et al. [65, 1996], the methodological aspects of measuring plantar dynamics of hemiplegic gait are discussed. The overall conclusion of the authors was that from a methodological point of view, plantar pressure measurements make it possible to relate physical quantities to degree of involvement. They used a insole system with 127 sensors per insole measuring at 40Hz, from Dynalyser. The pressure image was masked into four areas, but the basis of this division was not described.

Meyring et al. [140, 1997] studied dynamic plantar pressure distributions in hemiparetic patients which resulted in finding considerably lower peak pressures in all anatomical structures underneath the foot with respect peak pressures found in literature on "normals" (seven areas: medial and lateral heel, the midfoot, first, third and fifth metatarsal heads, and the hallux). They used an EMED platform of 200mm by 340mm and reported problems in targeting this small area, at least for the patients. Finally, also, a medial load shift in the forefoot was observed. They authors accounted for this by stating that the first ray had been identified as the most prominent structure during push off.

Femery et al. [55, 2002] studied plantar pressure distribution in hemiplegic children. They studied two groups of patients with different deficiencies, and a normal group. They used a Parotec insole system with 16 sensors measuring at 150Hz. Relative impulses were used as primary variables. They concluded that the neuromuscular disorders and foot deformities accompanying cerebral lesions led to specific plantar pressure distribution profiles.

A.11 The Foot as a Sensory Organ

The relationship between the sensory mechanism in the plantar aspect of the foot and the plantar pressure distribution during locomotion is the topic of this section. One might expect little change in gait pattern due to loss of sensory information because the foot is small and does not weigh much in relationship to the rest of the body. The

studies in this section dispute this hypothesis.

In a study by Chen et al. [33, 1995], the influence of sensory input on plantar pressure distribution was studied using three pairs of socks filled with different amounts of sand, and one pair of normal socks. Data from the left feet of ten individuals was measured using a Pedar system running at 100Hz. Using the Emed software, the pressure distribution was divided in eight areas: lateral and medial heel, lateral and medial midfoot, lateral and medial forefoot, hallux, and lesser toes. Pressure variables used were peak force, peak pressure, pressure-time integral, force-time integral, and maximum active area. Measurement conditions were walking and running. Results of this study indicated an increase in midfoot area and a decrease in toe area with increasing sensory input. Furthermore, pressure-time integrals were more sensitive to the different sensory input than peak pressure.

The foot as a sensory organ is studied by Nurse and Nigg [157, 1999], in their paper on the relationship between tactile and vibration sensitivity of the human foot with plantar pressure distributions during walking (1.5 m/s) and running (3.5 m/s). Monofilaments were used to evaluate the pressure threshold at five locations: heel, lateral arch, medial arch, first metatarsal head and hallux. Vibration thresholds were determined by a vibration exciter. Plantar pressure was assessed with a Pedar insole system during walking the system measured at a frequency of 99Hz while during running at 189Hz, both assessing five trials. Overall, vibrations were significantly correlated to pressure. An example is the relationship between higher frequency vibrations in the hallux which are coupled to a higher peak pressure during walking. In running, an increase in average sensitivity to higher frequency vibrations corresponds with an increase in peak forces underneath the foot.

A follow up study by the same authors [158, 2001] looked into the effect of changes in foot sensation on plantar pressure and muscle activity. The plantar side of the foot was treated with an ice exposure to change its sensation. Three exposure conditions were inflicted upon the volunteers: whole foot, rearfoot, and forefoot. The ten subjects were measured with a pedar insole measurement device. The overall conclusion is that sensory feedback can be used to alter gait kinetics and muscular activation patterns. Moreover, cutaneous feedback is important in the regulation and modification of gait parameters.

Chesnin et al. [34, 2000] compared CoP measurements between in-shoe measure-

ments from Parotec (100Hz) and an AMTI force plate (200Hz). The insoles were taped to the sole of the feet of the 35 volunteers. A dampened sock was put over the insoles. During the five trials the dampened sock resulted in an outline of the foot on the force plate. The authors introduced a method the use this outline to relate the two different local reference systems. Correlations were calculated for both medial-lateral and anterior-posterior differences in CoP coordinates. Since the force plate was taken to be the golden standard in measuring CoP paths, the conclusion of these researchers was that the CoP paths of the Parotec system were valid.

Eils et al. [52, 2002] studied the effect of reduction of plantar sensation on pressure distribution in walking. Forty healthy individuals were measured barefoot using a EMED SF4 system (360 by 190mm, 50Hz) and a first step protocol. The footprint was divided using the PRC-mask, which is not further explained in this article (or referred to in other articles. The reduction of plantar sensation was obtained by an ice immersion approach and tested with Semmes-Weinstein monofilaments. A load shift from heel and toes toward central and lateral forefoot, and lateral midfoot was observed going from normal to reduced plantar sensation. Also, modified plantar pressure distribution patterns and changes in peak pressures were observed.

In a similar study to the one of Elis et al. [52], Taylor et al. [197, in press] also studied the effect of plantar sensation reduction in walking using an ice immersion method. They used the same pressure measurement system, but used the two step protocol instead of the first step. The plantar pressure distribution was divided into ten areas: lateral and medial heel, lateral and medial midfoot, lateral, central and medial forefoot, hallux, second toe, and toes two to five. Peak force, peak pressure, contact time, force-time integrals, and pressure-time integrals were used to analyse the changes in sensation. This study revealed an increase in contact time for all areas and an increase in pressure-time integrals for certain areas. Overall, they suggested that changes in plantar sensation may be partly responsible for the redistribution of pressure under the neuropathic foot.

A.12 Miscellany

This section contains all papers, we were not able to classify under one of the other topics. It contains a lot of different research from shear pressure via postural research to research into different types of injuries.

In a publication by Rzonca et al. [181, 1984], Haglund's deformity was studied. The transducers were placed beneath the medial and lateral plantar calcaneal tubercles, beneath the metatarsal heads one, two, and five, beneath the hallux interphalangeal joint and beneath the location at the calcaneus where Haglund's deformity is formed (posterolateral superior of the calcaneus). Generally, they found that the deformity bears weight up to seven times higher with respect to a control group. In a study by D'Amico et al. [45, 1985], the effect of limb length discrepancy was looked at. The transducers sides were the same as in the study of Rzonca et al.[181] without the transducer placed at Haglund's deformity. They found a repetitive compensatory mechanism for the longer leg. This leg contacted the ground for an extended period of time. In a study that looked at bunion deformity and stress production in classical ballet by Kravitz et al. [111, 1985], the development of hallux abducto valgus formation in classical ballet point stance was researched using local transducers. The transducers were placed differently than in the previous two studies: beneath the two tuberculi of the calcaneus, beneath the hallux interphalangeal joint, beneath the medial and plantar aspect of the first metatarsal head, distal tip of the hallux, above (dorsal aspect) the hallux interphalangeal joint, beneath the distal aspect of the second digit, and above the distal interphalangeal joint of the second digit. The dorsal placement of the transducers was done to detect plantar flexion of the interphalangeal joints. The analysis showed high pressure values on the medial aspect of the foot. More specifically, high values were found at the medial aspect of the first metatarsal and the medial hallux.

The study of Rose et al. [178, 1992] discussed the insole pressure measurement system of F-Scan and applied it to different heel wedges. They introduced a masking scheme consisting out of six areas to study the effect of pressure underneath the foot: the medial heel, the lateral heel, the medial metatarsal heads (the first and second metatarsal heads), the lateral metatarsal heads (the third, fourth and fifth metatarsal heads), the hallux, and the second toe. With respect to the pressure system, the researchers found a 20.5% decrease in pressure values after an individual performed their twelfth trial and noticed discrepancies between different insoles. The latter led to the recommendation to use one pair of insoles per individual. With respect to the different heel wedges, the researchers found that medial heel wedges decreased the plantar pressure underneath the first and second metatarsal, and the first toe, while

lateral heel wedges decreased the plantar pressure underneath the other metatarsal heads. The center of force was shifted medially with a lateral wedge and laterally with a medial wedge.

Thompson et al. [198, 1993] studied the difference between walking and four aerobic movements. The aerobic movements were divided in two high impact and two low impact movements. A 23cm by 44cm Emed-SF system located flush in a 10m walkway positioned directly over an AMTI force plate (51cm by 56cm) was used to measure pressure distributions. The systems ran at 70Hz and 200Hz, respectively. Three trials were measured for all five conditions. Peak pressures were comparable between the aerobic movements and walking at the shoe-floor interface while vertical forces were higher for all four aerobic conditions, especially in case of the high impact movements. These findings result in the conclusion that clinicians should advise their clients of the importance of good shoes.

Mueller published a paper about two clinical cases [145, 1995], one with neuropathic ulcers and one with metatarsalgia. In the paper, the author clarified the important role of a insole measurement system as an aid in the design of a treatment plan. Also, the use of the measurements as a visual feedback to the patients was mentioned as a positive use of an insole system.

Jordan and Barlett were one of the first to focus on the concept of comfort in casual footwear, [103, 1995]. In their publication, they measured both pressure distribution on the plantar and the dorsal side of the foot. They used insole pressure systems for Emed where the dorsal pad had a measurement frequency of 30Hz and only gave the overall pressure. The plantar insole system was used to divide the foot area into six sub-areas: medial and lateral rearfoot, midfoot, and forefoot. The pressure variables used in this study were: contact area, pressure-time and force-time integrals, and peak values. They were combined with a questionaire that was used to investigate perceived comfort. Overall, total plantar force and force-time integral were related to perceived plantar comfort and dorsal forces and pressures were related to upper comfort.

Yamamoto et al [218, 1996] studied forefoot pressures during walking in feet afflicted with hallux valgus and in feet after hallux valgus surgery. They used a Harris-type mat, 27cm by 39cm, and divided the population into groups on the basis of forefoot pressure types; using the maximal pressure image. Peak pressures were higher than in normals with respect to hallux and first metatarsal head.

Wu and Chiang [217, 1996] studied the effect of surface compliance on foot pres-

sure in stance. This postural balance study used the pressure variables peak pressure, contact area and range of anterior posterior CoP movement to characterise the difference between standing on a hard surface and standing on a hard surface covered with layers of foam. Generally, peak pressure decreased and maximum contact area increased while changing from a hard surface to a surface covered with foam (Pedar system).

Kernozek and LaMott [109, 1996] compared the plantar pressure distributions between elderly and young adult individuals. They used an Emed plate system running at 70Hz and divided the plantar pressure surface into a heel area, a midfoot area, a hallux area, a lesser toe area, and medial, central, and lateral forefoot areas. Barefoot walking at self-selected pace was employed. They found similar loading characteristics for the heel, central forefoot, and lateral toes. Different loading characteristics were found for the midfoot and the medial forefoot. Variables used, were: contact area in the maximum pressure picture, total force in the maximum pressure picture (in BW), peak pressure in the maximum pressure picture, duration of contact phases, pressure-time integral, force-time integrals, instance of peak pressure, and instance of peak force.

Chiang et al. [35, 1997] studied postural control during a toes-up movement of the supporting base using a rotational platform with two foam types and a hard surface. The pressure was measured using insole system of Emed with 99 sensors running at 50Hz. They analysed peak pressure in the forefoot, midfoot, and rearfoot while standing on the three different surfaces (the two foams and the hard surface). The surface had no impact on pressures underneath the midfoot. However, the forefoot and the rearfoot pressures became lower with more compliant surface material.

In a study of Luger et al. [123, 1999], 66 healthy individuals and 294 patients were measured with a Emed SF2 445 by 225mm plate running at 71Hz to look into metatarsal weight distribution during walking. The forefoot containing the metatarsal was divided into three areas. Overall, they concluded that a medio-laterale arch does not exist during walking since only 3% of the population was found to have such an arch. Early anatomical knowledge had to be updated, containing the difference in metatarsal heads geometry for non weight-baring and for weight-baring.

In a paper by Potter and Potter [165, 2000], the effect of callus removal on peak plantar pressures was studied. They used a Musgrave system running at 55Hz and measured a population with 15 individuals having a callus and with 5 individuals with-

out a callus. No significant changes between peak pressures before and after callus removal were obtained. However between individuals with callus and without, the authors obtained a 25% lower peak pressure for individuals that had no callus. The authors concluded that the removal of callus itself does not decrease pressure and therefore, does not justify removal and should be accompanied by functional orthoses or pressure relieving strategies.

Hosein and Lord [92, 2000] reported on the use of in-shoe plantar shear in normals. Three biaxial transducers were mounted flush into an inlay such that the heel and two metatarsal heads were measured. Two inlays were constructed, each with a transducer placed at heel side, but one inlay covered metatarsal one and three while the other covered metatarsal heads two and four. The insole shear pressures were not equal to resultant force measurements on the plantar aspect of shoes. The authors believe that this difference could be attributed to the shoe and more specifically to the upper of the shoe. In a follow-up study by Lord and Hosein [121, 2000], a diabetic neuropathy population was measured with the same technology. A medial shift was noticed in the shear forces underneath the metatarsal heads. However, the step-to-step variability was found to be reliable.

Hillmann et al. [88, 2000] described the plantar and dorsal loading in patients after rotationplasty with a Pedar system. Fourteen individuals participated in this study. The researchers concluded that plantar and dorsal pressure measurements inside the shaft are feasible and reproducible. Moreover, peak pressure patterns related to callosities in the foot. Measurements were able to distinguish between prosthetic design. The authors formulated their ultimate goal to be able to avoid pressure peaks in areas not well cushioned.

An ambulatory foot pressure device with feed-back alarm for patients with sensory impairment was introduced by Pataky et al. [161, 2000]. This new device has two channels and a sampling rate of 96Hz. It is able to measure pressure for maximally eight days. The feedback was implemented in the form of an acoustic signal when plantar pressure exited a predetermined threshold.

Oeffinger et al. [159, 2000] studied the relationship between foot pressure and radiographic outcome measures of lateral lengthening for pes planovalgus deformity. An Emed pressure plate was used and the accompanying software was used to divide the foot outline into six parts: lateral and medial parts of the forefoot, the midfoot, and

the rearfoot. Pressure variables were normalised contact area in all masks and centre of pressure index (=area lateral/area medial). The latter was calculated without mentioning the definition of the foot axis necessary to perform this calculation. Overall, they concluded that there were relationships between the changes seen in radiographic and foot pressure parameters.

Bryant et al. [22, 2000] studied the plantar pressure distribution in normal, hallux valgus, and hallux limitus feet using an Emed SF-4 system, size 360 by 190mm running at a frequency of 50Hz. In all three groups, 30 individuals were presented and measured. The one-way ANOVA's showed hallux feet to have a medial forefoot loading pattern and hallux limitus to have a lateral forefoot loading pattern when both were compared to the normal group.

Also in ergonomics, plantar pressure measurement is used. In a study by Messing and Kilbom [138, 2001] a pressure algometer was used to asses an individuals plantar pain-pressure threshold (PPPT). The outcome of this study was that foot PPPT was a promising quantitative indicator of the effects of standing work.

Gefen et al. [66, 2001] studied in-vivo behaviour of the human heel pad during the stance phase of gait with a pressure plate measurement device and with a digital fluoroscopy device. Combing these two devices, the authors were able to calculate compression of the heel fat pad and the stress-strain relationship of the heel fat pad during barefoot walking in two subjects.

Kimmeskamp and Hennig [110, 2001] studied plantar pressure distributions in Parkinson patients during free walking. They employed a Pedar insole system with 99 sensors running at 50Hz. Twenty-four Parkinson patients and twenty-four matched normal individuals participated in this study. Parkinson patients experienced reduced impact at heel strike, which could be related to the severity of the disease determined with a Webster score. Also, Parkinson patients showed higher relative loads under the forefoot and a medial load shift. The latter could be identified though masking the foot into 10 distinct areas: lateral and medial heel, lateral and medial midfoot, first metatarsal head , second metatarsal head, third to fifth metatarsal head, hallux, second toe, lateral toes. A lateral index was introduced to quantify the medial-lateral position of the gait-line.

Gefen et al. [68, 2002] were one of the first to combine EMG and plantar pressure distribution measurement. In their study they analysed muscular fatique and foot stability during high-heeled gait.

In a study by Perry et al. [164, 2002], simultaneous measurement of plantar pressure and shear forces in diabetic individuals were studied. In comparison to the work done by Lord et al. [121, 2000], the amount of pressure sensors was raised to sixteen (4 by 4 sensors; sensor size 2.5 cm by 2.5cm). Also, these sensors were part of a plate and not incorporated in an insole. The measurement frequency was 37Hz. One of the conclusions was that peak shear and peak pressure did not occur at the same time point.

Ledoux et al. [116, 2002] studied plantar pressure distribution in case of neutrally aligned and pes planus feet. The nineteen individuals who participated in this study were measured with a musgrave system running at 28Hz. The pressure distribution was divided into six areas: hallux, heel, and the five metatarsal heads. The pressure variables used were peak force, time to peak force and two self-defined variables called the centre of pressure excursion index and the malleolar valgus index.

Internal pressures were measured by Richter et al. [173, 2002], in a study of midfoot fractures. Novel custom made pressure sheets were place inside the ankle, talonavicular, and calcaneocuboid joints, measuring at a frequency of 500Hz (sensor size 1cm by 1cm, sheet sizes 3cm by 3cm for the ankle and 2cm by 2cm for the other two joints). the researchers were able to induce midfoot fractures in eleven cadaver feet (out of sixteen) by hitting the foot on the plantar side of Lisfranc's joint with a bar impactor on a pendulum. Maximum pressure occurred for 50% in the ankle, for 44% in the talonavicular and for 6% in the calcaneocuboid joint.

In a paper by Hills et al. [89, 2002], the biomechanics of structural and functional limitations of obesity and its implications on movement was reviewed. In the section on plantar pressures, the authors mention four papers that reported on obesity and plantar pressure. In these studies, no relationship was found between body weight and plantar pressures. In a study were obese and non obese children were matched for gender, age, and height, significantly higher pressures were found underneath the forefoot of obese children.

In a study by Arndt et al. [11, 2003], a comparison between two different military boots on external plantar loading and in-vivo local metatarsal deformation was researched. After the introduction of a new less stiff boot, an increase in second metatarsal stress fractures was found. Plantar pressures were measured with an insole Pedar system running at 50Hz. Overall, the researchers concluded that the increase of metatarsal two stress fractures are due to pressure distribution loading decreased un-

derneath the majority of the foot with the exception of the second to fifth metatarsal head, and an increase of dorsal tension in metatarsal two.

Birtane and Tuna [19, 2004] evaluated the plantar pressure distribution in obese (N=25) and non-obese (N=25) adults in both standing and walking. A mini emed system was used to register pressure with a measurement frequency of 16Hz. Individuals were considered obese when they had a BMI between 30 and 34.9 kg/m^2. In standing, forefoot peak pressure, total plantar force, and total contact area were significantly higher in obese individuals. In walking, only peak midfoot pressure was significantly higher.

In a study by Burnfield et al. [23, 2004], the influence of both walking speed and footwear on plantar pressures was studied in older adults. Three walking speeds and two footwear condition (barefoot and shot) were measured using a Pedar insole measurement system. Novel groupmask evaluation software was used to mask the pressure area into a heel area, a medial and lateral midfoot area, a medial, central and lateral metatarsal area, a hallux area, and a little toes area. Pressure variables were peak pressure, peak force, pressure time integral, and contact area.

In a study by Hof et al. [91, 2005], a pressure plate system was used to observe the relationship between CoP and foot surface in a study that investigated the condition of dynamic stability.

Taranto et al. [195, 2005] studied the angle of gait and performed a comparative reliability study using footprints and an EMED-SF system. The overall conclusion is that the angle of gait from footprints is a reliable, repeatable, and similar to the angle of gait obtained from the EMED system.

Schmid et al. [186, in press] studied the difference in CoP displacements in trans-femoral amputees during gait using an FScan insole system. They found significant asymmetries between CoP displacements in prosthetic limbs in comparison to the patients "normal" limbs. Also, the comparison between trans-femoral amputees and individuals without amputations showed a redistribution of time duration in the different areas underneath the foot.

Appendix B

Details about Methodology

B.1 Data Registration Steps

This section is an annex to Section 2.1.4. Therefore, content of the present section is better understood after having read Section 2.1.4.

The data registration of a measurement session consisted of a preparatory part and a dynamic part in which the registration of trials took place. In the preparatory part, the following taks were performed:

1. *Completing a personal information sheet for each individual that took part in the experiment*, see Figure B.1. They should contain among others the individuals name, weight (measured at the biomechanics laboratory), age, shoe size (European), and the date of measurement.

2. *Measuring two anthropological characteristics of the individual*: maximum flexion in the first metatarsophalangeal joint and width of the calcaneus. An example of these measurements is illustrated in Figure B.2. The result of these two measurements were also put in the personal information sheet.

3. *Extending the measurement database in MAS.* In the Vicon system, a database was constructed that contained five branches. Three of these were named after the three session types: walking, walking/running, and walking/fast walking/running. The other two contained tests of the measurement set-up. One branch contained the tests that were performed to achieve the best camera po-

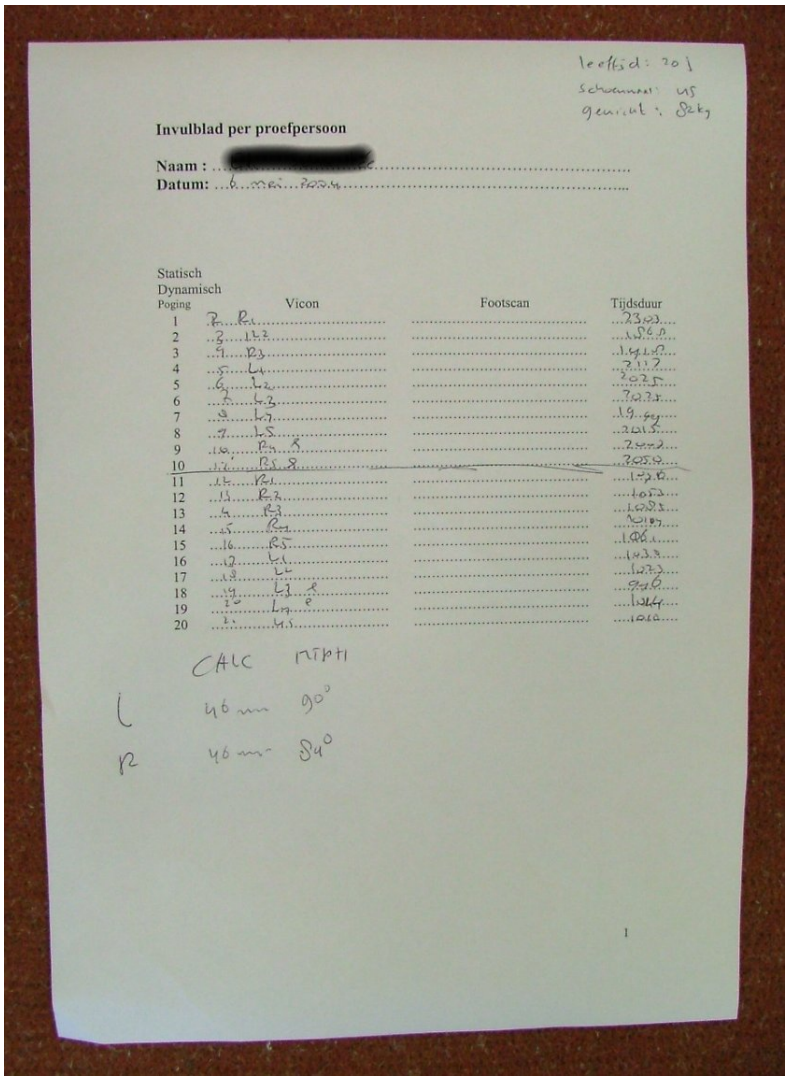

leeftijd: 20 j
schaamwet: US
geslacht: Stky

Invulblad per proefpersoon

Naam : [redacted]
Datum: 6 mei 2004

Statisch
Dynamisch

Poging	Vicon	Footscan	Tijdsduur
1	R1		2303
2	L2		1960
3	R3		1914
4	L4		2112
5	L5		2025
6	L6		2023
7	L7		1965
8	L8		2015
9	R9 R		2002
10	R8 8		2059
11	R1		1926
12	R2		1653
13	R3		1982
14	R4		2019
15	R5		1961
16	L1		1933
17	L2		1923
18	L3 8		2026
19	L4 8		1964
20	L1		1960

CALC MTPH

L 46 mm 90°

R 46 mm 84°

1

Figure B.1 An example of a personal information sheet.

Figure B.2 An illustration of the two anthropological measurements: on the left hand side the measurement of maximum flexion in the first metatarsophalangeal joint, and on the right hand side the measurement of calcaneal width.

sition set-up and to couple PPPS and MAS. These tests were performed before the start of the experiment. The other of the two contained the tests that were performed at the start of every measurement day: the alignment measurements and the data accuracy measurements.

Data obtained from a measurement session were stored in one of the session types branches according to session type. An individuals measurement session data was stored in a sub-branche of the session type branche. These sub-branches, containing measurement data, were named after the individual, first name followed by last name. Thus the names of all saved data starts with the full name of the individual followed by a blank, followed by the trial number, followed by a dot, and finally followed by an extension. For example, the motion data was saved in the well-known *'c3d'* format. So, the c3d data set of individual Joe Black trial 10 was saved as *'Joe Black 10.c3d'*. The database structure was stored at a workstation through the use of directories. The root of the database is a directory named after the study. In this root, the five branches are found also as sub-directories. Within the three session types directories, an individuals session data was stored within a directory named after the individual.

4. *Extending the measurement database in PPPS.* In the software application (version 6.3.42) of the RSscan system, a database as compared to the one in MAS was not present. Therefore, we constructed a database based on directories similar to the Vicon database. Extending the measurement database in PPPS came down to constructing a subdirectory in the right session type directory named after the individual (as in the case of MAS).

The following dynamic registration taks were performed:

1. *Reset the force plate before a new trial was measured, see Figure B.3*;
2. *Prepare the pressure plate system to accept a signal from MAS as the starting time point of measurement (press the F1 button in the Measurement screen, see Figure B.3)*;
3. *Prepare the MAS to start measuring (push the new trial button and push return, see Figure B.4)*;
4. *Reset the electronic timing device before a new trial was measured, see Figure B.4*;

Figure B.3 Steps one and two of the dynamic registration tasks: above the resetting of the force plate and below the preparation the PPPS for measurement.

Figure B.4 Steps three and four of the dynamic registration tasks: above the preparation of MAS and below the resetting of the electronic timing device.

Figure B.5 Steps eight and nine of the dynamic registration tasks: above the saving of PPPS data and below the writing down of the time spend between the infra red gates.

5. *Instruct the individual that he or she could commence the next trial*;

6. *Start measuring when the individual had final foot contact with the ground prior to foot contact on the combined plate system*;

7. *Stop measuring when the foot of the individual was no longer in contact with the plate systems*;

8. *Save the data registered by PPPS in the folder named after the individual as described in the preliminary registration tasks, see Figure B.5.* The file name was given by the individuals name (combination of first and last name) followed by an underscore, the trial number, and ends by ' .mst'. For example, Joe Black had performed the walking condition and trial number 10 was just measured. The PPPS data is saved as '...\wandelen\Joe Black\Joe Black_10.mst'. After this directory was set, the automated save button in the main measurement screen was used to perform the save operation;

9. *Write down trial information on the in individual's information sheet, see Figure B.5.* This information contained the foot (left or right) that contacted the combined plate system and the time spent between the two pairs of photo cells. This information was used to guide the individual during the dynamic trials. For example, if all left trials were registered within a condition the researcher would help and direct the individual towards contacting the plate systems with the other foot. We did not impose a specific sequence with respect to left and right foot trials within one measurement session. Only at the end of a condition, it was sometimes necessary to single out one foot such that the pre-determined number of trials for this foot could be obtained.

Besides all the dynamic trials, also the static trial was registered in the above manner. In the different directories within MAS and PPPS workstations, the static trial was the first trial. Keeping up with the previous example, the exported static trial from MAS was 'Joe Black 1.csv' then the first dynamic trial from PPPS was 'Joe Black 2.mst'.

After the experiments were carried out, the data had to be exported to an ASCII file format such that it could be further analysed in the Matlab environment. In the next section, we describe the different file formats.

B.2 File Structure Exported Data

In Section 2.1.4, we gave an example of a trial and its export files. Here, we recall this example:

Vicon system	**Footscan system**
'Joe Black 10.csv'	'Joe Black L10.dyn'
	'Joe Black L10.max'
	'Joe Black L10.Fs'
	'Joe Black L10.Fv'

The MAS exported file, 'Joe Black 10.csv', contains marker paths and force plate data. The PPPS exported files contain the total pressure distribution (extension '.dyn'), the aggregated (or maximum) pressure image (extension '.max'), the force platform data during the stance phase (extension '.Fs'), and the force platform data during the complete measurement (extension '.Fv'). The pressure distribution data and the force platform data with the extension '.Fs' are both limited to the stance phase. This stance phase was determined by an algorithm in the PPPS software.

An example of an export file of MAS data is presented in Figure B.6. As visualisation tool, we used Excel. This does, however, mask the fact that all entries are separated by commas. The illustrated example shows header information added to interpret the measurement data. The frequencies of both marker and force data are mentioned as well as the column headings such that we know where different force components and where the position components of a marker are stored. Each row represents the measured data of a specific time point. The time points are expressed as frame numbers given in the first column.

In case of the exported data from PPPS, a similar strategy was used for the two exported files describing force platform data. Some header information was added to relate the columns to the different force components, and again, the frame numbers are related to the rows and the force components are the columns. The full force signal export files, '.Fv', have a straight forward relationship between force components and columns, in contrast to the export files expressing force signals restricted to the stance phase, '.Fs'. The restricted force signals export file has no force components as header information but instead eight channels. These eight channels are related to the force components by the attachment of the force cables that connect the force platform to the 3D-box. The cables are connected to the 3D-box such that the first channel is

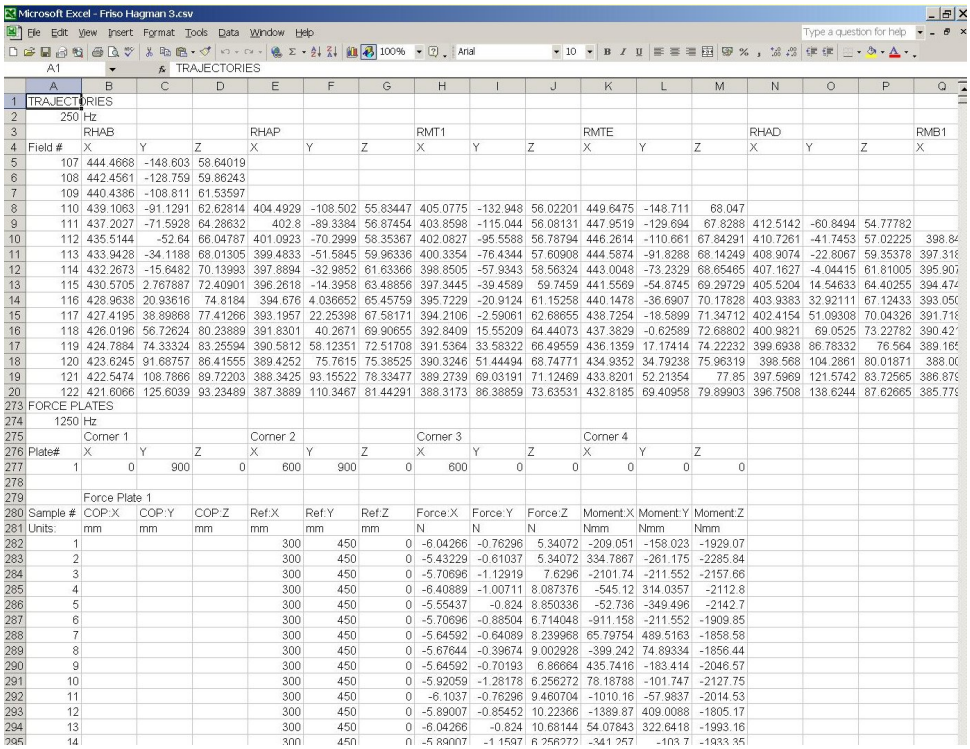

Microsoft Excel - Friso Hagman 3.csv

File Edit View Insert Format Tools Data Window Help

A1 TRAJECTORIES

	A	B	C	D	E	F	G	H	I	J	K	L	M	N	O	P	Q
1	TRAJECTORIES																
2	250	Hz															
3		RHAB			RHAP			RMT1			RMTE			RHAD			RMB1
4	Field #	X	Y	Z	X	Y	Z	X	Y	Z	X	Y	Z	X	Y	Z	X
5	107	444.4668	-148.603	58.64019													
6	108	442.4561	-128.759	59.86243													
7	109	440.4386	-108.811	61.53597													
8	110	439.1063	-91.1291	62.62814	404.4929	-108.502	55.83447	405.0775	-132.948	56.02201	449.6475	-148.711	68.047				
9	111	437.2027	-71.5928	64.28632	402.8	-89.3384	56.87454	403.8598	-115.044	56.08131	447.9519	-129.694	67.8288	412.5142	-60.8494	54.77782	
10	112	435.5144	-52.64	66.04787	401.0923	-70.2999	58.35367	402.0827	-95.5588	56.78794	446.2614	-110.661	67.84291	410.7261	-41.7453	57.02225	398.84
11	113	433.9428	-34.1188	68.01305	399.4833	-51.5845	59.96336	400.3354	-76.4344	57.60908	444.5874	-91.8288	68.14249	408.9074	-22.8067	59.35378	397.318
12	114	432.2673	-15.6482	70.13993	397.8894	-32.9852	61.63366	398.8505	-57.9343	58.56324	443.0048	-73.2329	68.65465	407.1627	-4.04415	61.81005	395.907
13	115	430.5705	2.767887	72.40901	396.2618	-14.3958	63.48856	397.3445	-39.4589	59.7459	441.5569	-54.8745	69.29729	405.5204	14.54633	64.40255	394.474
14	116	428.9638	20.93616	74.8184	394.676	4.036652	65.45759	395.7229	-20.9124	61.15258	440.1478	-36.6907	70.17828	403.9383	32.92111	67.12433	393.050
15	117	427.4195	38.89868	77.41266	393.1957	22.25398	67.58171	394.2106	-2.59061	62.68655	438.7254	-18.5899	71.34712	402.4154	51.09308	70.04326	391.718
16	118	426.0196	56.72624	80.23889	391.8301	40.2671	69.90655	392.8409	15.55209	64.44073	437.3829	-0.62589	72.68802	400.9821	69.0525	73.22782	390.421
17	119	424.7884	74.33324	83.25594	390.5812	58.12351	72.51708	391.5364	33.58322	66.49559	436.1359	17.17414	74.22232	399.6938	86.78332	76.564	389.165
18	120	423.6245	91.68757	86.41555	389.4252	75.7615	75.38525	390.3246	51.44494	68.74771	434.9352	34.79238	75.96319	398.568	104.2861	80.01871	388.00
19	121	422.5474	108.7866	89.72203	388.3425	93.15522	78.33477	389.2739	69.03191	71.12469	433.8201	52.21354	77.85	397.5969	121.5742	83.72565	386.879
20	122	421.6066	125.6039	93.23489	387.3889	110.3467	81.44291	388.3173	86.38859	73.63531	432.8185	69.40958	79.89903	396.7508	138.6244	87.62665	385.779
273	FORCE PLATES																
274	1250	Hz															
275		Corner 1			Corner 2			Corner 3			Corner 4						
276	Plate#	X	Y	Z	X	Y	Z	X	Y	Z	X	Y	Z				
277	1	0	900	0	600	900	0	600	0	0	0	0	0				
278																	
279		Force Plate 1															
280	Sample #	COP:X	COP:Y	COP:Z	Ref:X	Ref:Y	Ref:Z	Force:X	Force:Y	Force:Z	Moment:X	Moment:Y	Moment:Z				
281	Units:	mm	mm	mm	mm	mm	mm	N	N	N	Nmm	Nmm	Nmm				
282	1				300	450	0	-6.04266	-0.76296	5.34072	-209.051	-158.023	-1929.07				
283	2				300	450	0	-5.43229	-0.61037	5.34072	334.7867	-261.175	-2285.84				
284	3				300	450	0	-5.70696	-1.12919	7.6296	-2101.74	-211.552	-2157.66				
285	4				300	450	0	-6.40889	-1.00711	8.087376	-545.12	314.0357	-2112.8				
286	5				300	450	0	-5.55437	-0.824	8.850336	-52.736	-349.496	-2142.7				
287	6				300	450	0	-5.70696	-0.88504	6.714048	-911.158	-211.552	-1909.85				
288	7				300	450	0	-5.64592	-0.64089	8.239968	65.79754	489.5163	-1858.58				
289	8				300	450	0	-5.67644	-0.39674	9.002928	-399.242	74.89334	-1856.44				
290	9				300	450	0	-5.64592	-0.70193	6.86664	435.7416	-183.414	-2046.57				
291	10				300	450	0	-5.92059	-1.28178	6.256272	78.18788	-101.747	-2127.75				
292	11				300	450	0	-6.1037	-0.76296	9.460704	-1010.16	-57.9837	-2014.53				
293	12				300	450	0	-5.89007	-0.85452	10.22366	-1389.87	409.0088	-1805.17				
294	13				300	450	0	-6.04266	-0.824	10.68144	54.07843	322.6418	-1993.16				
295	14				300	450	0	-5.89007	-1.1597	6.256272	-341.257	-103.7	-1933.35				

Figure B.6 An example of an export file of MAS data.

Microsoft Excel - Friso Hagman L10.Fs

	A	B	C	D	E	F	G	H	I
1	Force plate data								
2	Left foot								
3	Time(ms)	Channel 1	Channel 2	Channel 3	Channel 4	Channel 5	Channel 6	Channel 7	Chan
4	0	-8.189	NaN	0	#NAME?	-4.961	Inf	#NAME?	NaN
5	4	-0.744	NaN	0	Inf	-1.145	Inf	#NAME?	NaN
6	8	14.145	NaN	3.688	#NAME?	-4.961	Inf	#NAME?	NaN
7	12	43.924	NaN	14.753	#NAME?	-4.961	#NAME?	Inf	NaN
8	16	96.037	NaN	25.818	Inf	-8.778	Inf	#NAME?	NaN
9	20	215.153	NaN	47.948	#NAME?	-16.411	#NAME?	#NAME?	NaN
10	24	498.052	NaN	92.207	#NAME?	-35.493	#NAME?	#NAME?	NaN
11	28	870.289	NaN	140.155	Inf	-66.025	#NAME?	#NAME?	NaN
12	32	1041.518	NaN	129.09	#NAME?	-77.475	#NAME?	#NAME?	NaN
13	36	1011.739	NaN	129.09	Inf	-81.292	Inf	#NAME?	NaN
14	40	870.289	NaN	147.532	#NAME?	-81.292	#NAME?	#NAME?	NaN
15	44	773.507	NaN	147.532	Inf	-81.292	Inf	Inf	NaN
16	48	691.615	NaN	162.285	Inf	-77.475	Inf	Inf	NaN
17	52	669.281	NaN	177.038	Inf	-81.292	#NAME?	#NAME?	NaN
18	56	669.281	NaN	191.791	#NAME?	-81.292	#NAME?	#NAME?	NaN
19	60	713.95	NaN	224.986	Inf	-69.842	Inf	#NAME?	NaN
20	64	751.173	NaN	243.427	Inf	-54.576	Inf	#NAME?	NaN
21	68	788.397	NaN	265.557	#NAME?	-35.493	#NAME?	#NAME?	NaN
22	72	803.286	NaN	295.064	#NAME?	-35.493	#NAME?	#NAME?	NaN
23	76	818.176	NaN	295.064	#NAME?	-27.86	Inf	#NAME?	NaN
24	80	840.51	NaN	295.064	Inf	-20.227	Inf	#NAME?	NaN
25	84	840.51	NaN	272.934	#NAME?	-31.677	Inf	#NAME?	NaN
26	88	825.621	NaN	254.492	Inf	-35.493	Inf	#NAME?	NaN
27	92	825.621	NaN	236.051	Inf	-35.493	#NAME?	#NAME?	NaN
28	96	825.621	NaN	210.233	#NAME?	-35.493	#NAME?	#NAME?	NaN
29	100	833.065	NaN	191.791	#NAME?	-31.677	#NAME?	#NAME?	NaN
30	104	840.51	NaN	177.038	#NAME?	-16.411	#NAME?	#NAME?	NaN
31	108	847.955	NaN	177.038	#NAME?	-8.778	#NAME?	#NAME?	NaN
32	112	847.955	NaN	177.038	#NAME?	-4.961	Inf	#NAME?	NaN
33	116	855.4	NaN	177.038	Inf	-4.961	#NAME?	#NAME?	NaN
34	120	855.4	NaN	177.038	Inf	-4.961	#NAME?	#NAME?	NaN
35	124	855.4	NaN	184.415	Inf	2.672	Inf	#NAME?	NaN
36	128	855.4	NaN	195.48	Inf	10.305	Inf	#NAME?	NaN
37	132	855.4	NaN	206.545	#NAME?	10.305	#NAME?	#NAME?	NaN

Microsoft Excel - Friso Hagman L10.Fv

	A	B	C	D	E
1	3d Data				
2	Frame	Time (ms)	X	Y	Z
3	0	0	6.49	0	-8.19
4	1	2	2.67	0	-8.19
5	2	4	-4.96	0	-8.19
6	3	6	-1.14	0	-8.19
7	4	8	10.3	0	6.7
8	5	10	10.3	0	14.14
9	6	12	10.3	0	21.59
10	7	14	-4.96	0	-8.19
11	8	16	-4.96	0	-8.19
12	9	18	-1.14	0	-8.19
13	10	20	2.67	0	-8.19
14	11	22	6.49	0	14.14
15	12	24	-4.96	0	-0.74
16	13	26	-1.14	0	-8.19
17	14	28	-4.96	0	-8.19
18	15	30	-1.14	0	-8.19
19	16	32	-1.14	0	-8.19
20	17	34	2.67	0	-8.19
21	18	36	-1.14	0	-8.19
22	19	38	6.49	0	-8.19
23	20	40	10.3	0	14.14
24	21	42	6.49	0	-0.74
25	22	44	-4.96	0	-8.19
26	23	46	-1.14	0	-8.19
27	24	48	-1.14	0	-8.19
28	25	50	-1.14	0	-8.19
29	26	52	-4.96	0	-8.19
30	27	54	-1.14	0	-8.19
31	28	56	-1.14	0	-8.19
32	29	58	-1.14	0	-8.19
33	30	60	-4.96	0	-8.19
34	31	62	6.49	0	-0.74
35	32	64	-1.14	0	-8.19
36	33	66	-4.96	0	-8.19
37	34	68	10.3	0	14.14

Figure B.7 An example of the exported data from PPPS. On the left-hand side, the force data from the stance phase and on the right-hand side the data from the full measurement period

the z-component of the force, the second channel is the y-component, and the third channel is the x-component. Again, we used Excel to illustrate both types of exported data, cf. Figure B.7. In this case *'tab'* is the masked column delimiter.

The other two types of exported data from PPPS have a form different from the previous two. Both describe pressure distribution and therefore PPPS software expresses them in matrix form. To know the sensors of the pressure plate described, the header information was used to acquire the left bottom coordinate in the local reference frame of PPPS combined with the number of sensors in the width and length direction of the scanned area. Header information also reveals if the data came from a left or right foot. In case of aggregated export data (or maximum pressure), no

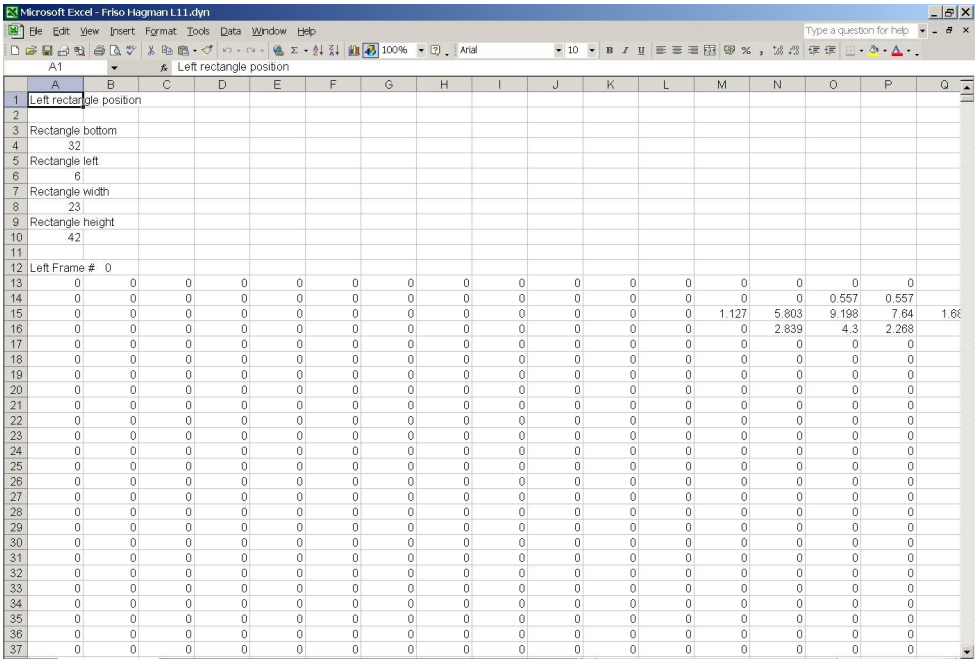

Figure B.8 An example of the export format of a dynamic pressure distribution measurement; extension '.dyn'.

more information is required to interpret its contents. In case of the dynamic pressure distribution, the export file contains a series of matrices presided each time by a frame number. So, rows are no longer associated with frames. Since both export types are the same besides the use of frame numbers in the dynamic pressure distribution, we illustrate these export types with one example of a dynamic pressure distribution, see Figure B.8.

Knowledge of the precise format of the export files enabled us to write applications in the Matlab environment that read and subsequently stored all data within a Matlab M-file. The read applications and fail saves are described in this Appendix in the section Matlab Applications. Before the applications will be discussed, we present a section that deals with errors in data registration and data processing into the Matlab environment. One of the errors is related to the way PPPS software was exporting its

data to ASCII format.

B.3 Description of the Errors during Registration and Processing

The trials with errors that were made during registration and processing fall into two categories. The first category were trials with errors that could be fixed and the second category were trials with errors that could not be fixed. Using a different criterion the trials with errors were separated into the same two groups. The other criterion was errors during registration and errors during processing. Registration errors were made during trial registrations and subsequent saving of raw data and could not be fixed. Processing errors were made in the time period from exporting data to ASCII formats until the data (of one session) was saved as a Matlab M-file and could be fixed.

Two non fixable errors occurred. The most frequent one, 95% of all excluded trials, was forgetting to press the F1 button in the main measurement screen of the PPPS software before the start of a new trial (step 2 in the dynamic registration tasks described in the first section of this appendix). After measurement, this error type was found by a combination of an automatic checking algorithm in our Matlab applications, and a manual comparison of the suspected trial with the trials preceding it. The automatic checking algorithm detected significantly different start time points of the stance phase between force signals of PPPS and MAS. These difference errors were reported in an individuals report file. In case of an error message, the trial numbers of the exported trial files were manually verified and in case they did not correspond, we corrected the problem.

The second non fixable error was a distorted force signal from MAS. After measurement in MAS, the force signal could not be viewed directly after measurement. In PPPS, the force signal was presented *directly*. We did check the force signal in PPPS for all trials and were, therefore, puzzled with the distorted force signal from MAS. Using the marker path data, we found the source of this error. The pressure plate hang 10cm over at the end of the force plate. In case of the distorted force signals from MAS, the foot was placed partly on these last 10cm of the pressure plate such that plate and runway were in contact. During the measurement of trials, the most obvious cases of foot placement in the last 10cm of the plate were spotted and the

specific measurement was repeated.

Three types of errors occurred that we were able to fix. the first was mentioned already in the previous paragraph and was the exporting of PPPS data with a wrong trial number. The second error was the exporting in PPPS of a data-set with a wrong file extension. In this case, an individuals report file mentioned a trial not having the desired file format. We returned to PPPS to fix this error by exporting all data-sets of a specific trial again. However, the new report file still gave the same error message. We manually looked at the files in Excel and noticed that the new exported data was appended to the existing files. Therefore, the initial header information remained and errors were still found. Thereafter, as a rule, we deleted all exported files of PPPS data of a given trial and subsequently exported the desired trial. The third fixable error was reported by a message about marker names. Specifically, it reported on inconsistencies between left and right trials as they were determined by PPPS and MAS, respectively. The error occurred when a left foot was given right marker names, or the other way around .

B.4 Matlab Applications

Applications used to perform the research in Chapter 2 and applications used to read in all exported data into the Matlab environment are the topic of this section.

B.4.1 Exported Data Read in Applications

Eight applications were written to perform the task of converting all exported data of an individuals session into one Matlab M-file. The are called: **GroupDataRetrieveFriso, PersonDataRetrieveFriso, DataFromPressurePlateFriso, DataFromViconMasFriso, Comp_DataDetermination, MarkerSortVicon_Friso, Sinc_Pressure_Force_Analysis**, and **ExtractForceData**.

GroupDataRetrieveFriso processes data of individual measurement sessions that were stored as subdirectories, named after the individual, within a directories named after the different session types. The name of the session type directory was the only input of this application. As output, a report file was created in this directory containing the names of the subdirectories that were analysed. Within this application,

PersonDataRetrieveFriso was called with as only input the name of a subdirectory.

PersonDataRetrieveFriso processes the exported data of one individuals session and stored the information in two Matlab m-files named *'RawData.m'* and *'CompData.m'*. The *'RawData.m'* file contained all exported data from an individuals session while the *'CompData.m'* file contained data of those trials for which a complete set of export data existed and were free of errors. A trial had a complete set of export data when the MAS data was present (one exported file; extension: csv) and the PPPS data was present (four exported files; extensions: dyn, mas, Fs, and Fv). A trial had no errors when all the exported files had the correct file structure, when the appropriate marker lists were used, and when no synchronisation problems had occurred . The report file created by this application described the names of the trials with errors and without errors such that we knew the trials that were used in creating an individuals *'CompData.m'* file. This report file was used to correct the errors described in previous section and to be able to count the trials that could no be used for further analysis. In this application, five sub-applications were called subsequently. The first two processed the exported data from PPPS and MAS, respectively, followed by the construction of the *'RawData.m'* file. After all applications were called, the 'CompData.m' file was constructed. Details of the variables contained in this Matlab M-files are discussed in the next section.

DataFromPressurePlateFriso processes the exported data of PPPS of an individuals session. It was called as the first application in **PersonDataRetrieveFriso** and inherited the name of the sub-directory as input. As output, it created cell arrays containing the different data-sets from PPPS in the Matlab environment.

DataFromViconMasFriso processes the exported data of MAS of an individuals session. It was called as the second application in **PersonDataRetrieveFriso** and inherited the name of the sub-directory as input. As output, it created cell arrays containing the two different data-sets, marker positions and force plate data, from MAS in the Matlab environment.

Comp_DataDetermination processes the data of an individual in search for trials with complete data-sets (all six exported files). First, two list were created with

trial numbers, one list contained the trial numbers that did have all the complete data set and the other list contained the trial numbers that did not. Secondly, the cell arrays in Matlab that contained all data of an individual were adapted such that they contained the data of trials with a complete data set only. Thirdly, the number of left and right trials were calculated and stored in variables. Also, the cell arrays were sorted such that the left trials were followed by the right trials. Within the left and right parts of the originated cell array, the data was sorted further with respect to trial number in increasing order. Fourthly, the static trial was found within the data-set. Two possibilities indicated the use of a specific trial as static trial: (1) in the individuals data directory, a file containing the necessary information was present, named: 'static_info_file.txt', or (2) no information was given, in which case the first trial was taken to be the static trial. For this research project, the second option was always used.

MarkerSortVicon_Friso uses the data from the previous application to check if left and right trials determined in PPPS had been correctly labelled in MAS. In Table B.1, the relationship between marker labels, as presented in de marker list, and the anatomical location are given. A second task performed by the application was sorting the marker data. The export files from MAS vary from trial to trial with respect to the column order in which marker labels occurred. We choose the order as given in Table B.1 and therefore, for example, the second, third and fourth column of a matrix containing marker path information always contains the x-, y-, and z-component of the lateral calcaneus marker.

Sinc_Pressure_Force_Analysis compares force signals from MAS and PPPS. In particular, force data from PPPS that contained force signal information from the start time point of measurement was taken. **PersonalDataRetrieveFriso** used this application to determine the existence of synchronisation errors. To determine the start time point of the stance phase, the application **ExtractForceData** was used. This application is discussed in the next paragraph. The criteria in **PersonalDataRetrieveFriso** is that the mean absolute difference of 200 threshold levels, from 1N to 200N, between begin time point of the stance phase for the force signals from MAS and PPPS is within 3ms.

Table B.1 The relationship between the marker labels as used in MAS and Matlab, and their anatomical location. The calcaneus markers and the hallux markers were attached to marker plates, see Figure 2.4. In this table, MH is the abbreviation of Metatarsal Head.

Left Marker Labels	Anatomical Location	Right Marker Labels
LCAL	Lateral Calcaneus	RCAL
LCAM	Medial Calcanues	RCAM
LCAA	Proximal Calcaneus	RCAA
LCAE	Distal Calcaneus	RCAE
LMT1	Medial Side Metatarsal Head I	RMT1
LMT5	Lateral Side Metatarsal Head V	RMT5
LMTE	Between MH II and MH III	RMTE
LMB1	Medial Side Metatarsal Base I	RMB1
LMB5	Lateral Side Metatarsal Head V	RMB5
LHAP	Proximal Hallux	RHAP
LHAD	Distal Medial Hallux	RHAD
LHAB	Distal Lateral Hallux	RHAB

ExtractForceData calculates the frame numbers that signify the start time point and the end time point of the stance phase. Both force signals from PPPS and MAS were used as input to ExtractForceData with threshold levels from 1N up to 200N with increments of 1N. Since both force signals contained data from the start time point of measurement, their start and end time points should have been the same.

Most applications are supplied with further explanations regarding input, output and crucial calculation steps. Input and output is given after the definition of the function in the first line. The information regarding crucial calculation steps are given within the code itself at the specific place were the applications performs these crucial steps. Acces to this information can be obtained by opening the applications in any text editor capable of reading ASCII format.

B.4.2 Research Applications

In Section 2.2.1, a signal correlation measure was introduced. This measure is integrated in the application **force_times_dif_checker** which is called from **GroupSynchTest**. The latter application has only one input, a directory name. The directory connected to this name contains subdirectories of individual session data, in particular their *'CompData.m'-file*. The *'CompData.m'*-files had been loaded and the signal measure was calculated for all trials within a session. Besides the signal measure, **GroupSychTest** also used **Sinc_Pressure_Force_Analysis** to compare begin and end time points of the stance phase to study synchronisation between MAS and PPPS. With respect to the latter, thresholds from 30N up to 200N were used.

In Section 2.2.1, also the spacial alignment was studied using a five step approach. First, a manual determination of the centre of the wooden block from PPPS data. Secondly, the coordinates were stored in a Matlab m-file. Thirdly, the MAS data was processed by the Matlab application, **DataToAllign**. In this application, all alignement trials of all measurement days were read in and the average of the centre of the wooden block was calculated. Fourthly, average centre coordinates were also stored in the same Matlab M-file. Fifthly, optimal rotation and translation were calculated by the application **PressurePlate_Rotation** using the coordinates of the centre of the block from both systems.

In Section 2.2.2, the accuracy of the three-dimensional data was assessed. The first tests were based on a hand-shaped object performing simulated foot motion. The data was read in with the **DataFromViconMASFriso** application as described in the previous subsection. We choose three markers on the hand-shaped object. These three markers made up a triangle. The position data of these markers were used in the application **Cam_Accuracy_Angle** that calculates the variation of these three angles. The variation of each angle in time was expressed using a 90% confidence band. Calculation of this band was performed in the application **Determine_Percent_Range**. This application used an interval division method to calculate the limit that sets the confidence interval. To find a limit value containing exactly 90% of the data is not realistic. For example with only 21 values in a time series, the closest number representing 90% is 19, which means 90.5% and adding one is already 95.2%. Therefore, **Determine_Percent_Range** uses a part from the absolute value a criteria to de-

cide this limit value, see the application code for further information. Consequently, the analysis of the hand-shaped object by the application **Cam_Accuracy_Distance** used all pairs of markers to analyse the variation in distances on the hand-like object. Again, 90% confidence intervals were calculated for all distances such that a relationship between variation and mean distance established, see Figure 2.14 .

For assessing three-dimensional data accuracy, a second test was performed. In this test, the marker position data of the three markers attached to the hallux marker plates were used to assess the data accuracy. The application **GroupCamAccTest** calculates the variation in the angle between the two vectors that are largest in length, analogously to the calculation of angle variation for the hand-shaped object. **GroupCamAccTest** has a directory name as input, the name of a session type. **GroupCamAccTest** uses **ToeAngle** to calculate the angle and the **Determine_Percent_Range** application to calculate the limit of the 90% confidence interval.

In Section 2.2.6, ideas and algorithms are discussed about the division of the pressure distribution into different foot areas. In application **Foot_Area_Division_v4** this division was implemented. It used the aggregated pressure data as input and created output that describes the borders of the division into the different pressure areas. The application **Foot_Area_Division_Write_Database** was used to process the division of pressure distributions for the complete database.

Also, in Section 2.2.6, we mention the calculation of local pressure data from the different foot areas. In **GroupLocalPressuresCalculations**, these local pressure data are calculated for a given directory. The directory name is the only input to this application. Within **GroupLocalPressuresCalculations**, **Determination_of_Sensor_Areas_from_Foot_Division** is called to calculate the local pressure data for an individuals' data set. As input, this application uses the borders of the division obtained with **Foot_Area_Division_v4**.

In Section B.6, the sensitivity of the signal correlation measure is discussed. The application used to study this phenomenon is **GroupSynchTestAdjust**. This application is an adaption of the previously discussed **GroupSycnTest**. **GroupSynchTestAdjust** contains three distinct part: pure delay effects, pure frequency effects, and

combined delay and frequency effects.

In Section B.7, three methods for determining a foot axis on the basis of pressure measurements is discussed. The application **FootSimulatie_projectie_Max** is used to calculate the position and orientation of the foot axes. The application **FootAxis-Determination** is used to compare the pressure determined foot axes to the foot axis based on motion data.

The time events and foot phases as introduced in Section 2.2.4 are calculated on the basis of the local pressure variables obtained with **GroupLocalPressuresCalculations**. The calculations of the time events and foot phases were performed for the complete population with **GroupBulkCalculationsTwo_v2**. This application has as input the directory name, which should contain a session type, and the session type as a number; 1 for walking, 2 for walking running, and 3 for walking fast-walking and running. The *'CompData.m'*-file is adapted by this application such that the variables **Events** and **Timing** are added.

B.5 Description of the Database

In the previous section, we discussed the applications related to Chapter 2. Describing **PersonDataRetrieveFriso**, we referred to the contents of *'CompData.m'*. This file contains the exported data from an individual's session. More specifically, it contains only the data of trials with a complete data-set from both MAS and PPPS. This file is the building block of our Database.

The Database consists of a rout directory with four entries. One of this is the Matlab file *'doc_database.m'*. It contains two variables: 'doc_database' and 'align', which are structured arrays. At the end of Section 2.1.4, we discuss the fields of 'doc_database'. The fields of the variabele 'align' together with an example contents from March 18, 2004 read:

MeasurementDate:	[18 3 2004]	
x:	151	in mm
y1:	36.8	in mm
y2:	524.5	in mm
angle:	-0.4°	in degrees

The information in the 'align' variable was used for the spacial alignment of PPPS and MAS Data.

The three other entries in the directory are subdirectories named, after the three session types: 'wandelen' (walking), 'wandelen lopen' (walking and running), and 'wandelen snelwandelen lopen' (walking, fast walking and running). In turn, these sub-directories contain the individuals session data in sub-directories named after the individual: a combination of the first and last name. In these individuals sub-directories two files are present, namely 'CompData.mat' and *'Log_DataRetrieve.PDR'*. The latter is the individuals report file discussed in the previous section.

With the variables from *'doc_database.m'*, a researcher is able to acces the measurement information stored in the respective subdirectories by extracting the necessary information from the variable 'doc_database'. Using the example of Joe Black, Section 2.1.4, we combined entries of the fields Session, FirstName, and LastName into *'...\wandelen lopen\Joe Black\CompData.mat'*, which is the complete path to the *'CompData.mat'* of Joe Black.

The combined information from *'doc_database.m'* and an individuals *'CompData.mat'* is the complete data-set of an individual that can be used for further analysis.

As building block of our database, *'CompData.mat'* contains 42 variables that are discussed in the following paragraphs. The first 38 variables are calculated within the context of the processing performed in connection to Chapter 2, while the last four variables are calculated within the context of the processing performed in connection to Chapter 3.

1. **NameList** is a character array variable that contains a list of trial numbers combined with the basic file type (first name combined with last name) and a character 'L' or 'R' to denote a left or right trial. It is a list of file names analogue to the file names used for the PPPS export data without the extensions. The order of the list represents the general order for all variables, first sorted with respect to left and right, and second sorted with respect to trial number.

2. **LeftMarkerlist** and **RightMarkerlist** are cell array variables with twelve entries containing the marker labels discussed in Section B.4.1, Table B.1. The

order of the marker labels is the same order as in Table B.1 and are related to the variable **MarkerD**.

3. **MarkerD** is a cell array variable that has as many entries as there are trials described by the variable **NamesList**. The entries of **MarkerD** are matrices with 37 columns describing the marker position data. The first column contains the frame numbers and therefore the rows of the matrices are related to frame numbers. The next 12*3 columns contain triples of the twelve marker positions. The chosen marker order is expressed in the variables **LeftMarkerlist** and **RightMarkerlist** and the underlying triple order is x, y, and z. The first column of frame numbers does not always start with one, meaning that the marker data is not always given from the on-set of measurement. The export function in MAS decides the first frame number based on the presence of marker position data.

4. **SMarkerD** is a cell array variable that has an identical structure and meaning as **MarkerD**. The only difference is that the motion data in **SMarkerD** is filtered and interpolated using the least squares spline technique described in Section 2.2.3. The specific spline parameters used by this technique are contained in the variable **Spline**, which is a cell array with as many entries as there are trials. The entries themselves are given in the Matlab spline information format.

5. **Static** and **StaticName** are variables related to a static file and to the variables described previously. The **StaticName** contains the name of the static file as in **Namelist**. **Static** is a cell array containing two entries. The first entry contains the marker position matrix as in the matrices of **MarkerD**. The second entry is a cell array containing in the first row the left marker list and in the second row the right marker list, a combination of **LeftMarkerlist** and **RightMarkerlist**.

6. **Lcounter** and **Rcounter** are double arrays containing the number of left and right trials.

7. **DynM** and **MaxM** are two cell arrays with entries trial information as in **MarkerD**. Each entry of **MaxM** is a matrix that contains the maximum pressure distribution. Each entry of **DynM** is a stack of matrices containing the dynamic pressure distribution where the third dimension is related to the frame number. To establish the position of the active sensor grid related to the matrices of **DynM** and **MaxM**, the variable **DynInf** was introduced.

8. **DynInf** is a matrix of the double array type. The rows represent the different trials in the order previously discussed. The columns are related to position and time information of the trial. The last two columns contain information about stance duration where the last column is related to number of frames of a right trial and the other column to number of frames of a left trial. A zero frame number in the left column means that it is a right trial and visa versa. The first four columns are related to the position of the active sensor grid with respect to the local origin of the LRF of PPPS expressed in number of sensors. Each entry in the first column is the y-component of the bottom left corner of the active sensor grid, and each entry in the second column is the x-component of the bottom left corner. The third and fourth column contain entries that represent the number of sensors in the active sensor grid in the x- and y-direction respectively.

9. **ForcePData**, **PPLFData**, and **PPSFData** are cell arrays containing force plate data. All cells contain matrices with three columns. Again, cells are related to the previously described trial order. The variables are the force plate data obtained by MAS from the on-set of measurement, the force plate data obtained by PPPS from the on-set of measurement, and the force plate date obtained by PPPS restricted to the stance phase as defined by the PPPS software. All matrices have three columns that represent the x-, y-, and z-component of the resultant force. The rows of these matrices represent the frame numbers. In case of the first two variables, this means that the first row of the matrix coincides with the first measurement frame (In contrast to the data in **MarkerD**). In case of the third variable, the first row coincides with the first frame of the stance phase as determined by PPPS.

10. **FrameNumFP** and **FrameNumPPLF** are cell arrays containing 200 cells. Each cell is a matrix with two columns and as much rows as there are trials. The entries of these matrices are the frame numbers of the start and the end of the stance phase, which we determined using 200 threshold scheme. The first variable is related to the force plate data obtained by MAS and the second variable is related to the force plate data obtained by PPPS from the on-set of measurement. The rows represent the trials where the first column is the start frame numbers and the second column is the end frame numbers. The 200 cells are related to the thresholds, cell i means a threshold of iN. The way the stance

phase was determined using a threshold scheme is explained in Section 2.2.1.

11. **ZeroLevFP** and **ZeroLevPPLF** are matrices of the double array form. These matrices contain information about the noise and the zero level of the x-, y-, and z-component of the resultant force obtained by MAS and PPPS. Their nine columns represent the zero level, the noise level expressed as standard deviation, and the noise level expressed as the maximum value minus the minimum value (worst case) for the x-, y-, and z-component respectively. Again, the rows represent the trials. **FrameNumFP** and **FrameNumPPLF** do take into account the zero level and correct the z-component of the force with this zero level before the threshold schemes are applied.

12. **VbeginShortFull** and **VeindShortFull** are two vectors that relate the force signal data from **PPLFData** to **PPSFData**. Since **PPSFData** is force data restricted to the stance phase as defined by the Footscan software and **PPLFData** is also force data from PPPS but for the complete duration of measurement, we know that the three curves described by **PPSFData** are a part from the curves described by **PPLFData**. the components of **VbeginShortFull** and **VeindShortFull** contain the the frame number in **PPLFData** where **PPSFData** data begins and ends, respectively.

13. **Vbegintijden**, **Veindtijden**, and **Vduurtijden** are matrices of the double array format. Every row width length 200 corresponds to one trial where the first entry is related to a threshold of 1N and the last entry is related to a threshold of 200N. The entries of the rows are the differences in milliseconds between the start, the end, and the duration of the stance phase determined using the force plate data from MAS and PPPS. **Vbegintijden** expresses the differences in the beginning of stance phase, **Veindtijden** expresses the differences in the end of stance phase, and **Vduurtijden** expresses the differences in the duration of the stance phase.

14. **begintijdenForcePlate** is a matrix of the double array format. As for **Vbegintijden**, the rows are, as always, related to the trials and the columns to the thresholds. The entries in the matrix are the begin time point of the stance phase in milliseconds. The information in this matrix is almost the same as the first column of the matrices in **FrameNumFP** with the difference that the latter is

expressed in frame numbers.

15. **FootAngle_PPPS** is a cell array variable with as many entries as there are trials. The entries themselves are also cell arrays containing three subentries. These three subentries contain a 2 by 2 matrix with the first column of the matrix being the direction of the foot axis and the second column being a point of the foot axis in the pressure distribution area, expressed in sensor numbers. The subentries are ordered such that the first entry is the global geometric inertial method, the second entry is the local geometric inertial method, and the third entry is the CoP method.

16. **heel_area** and **Forefoot_area** are vectors of the double array format. Their entries are y-direction sensor values that determine the division of the foot three foot areas: rearfoot (or heel), midfoot, and forefoot. There are as many entries as there are trials. An example of how these two variables determine the three foot areas: from the variable **DynInf**, we obtain that the size of a certain pressure distribution is 39 sensors in the y-direction and 19 sensors in the x-direction. For the same trial, we obtain from **heel_area** and **Forefoot_area** the values 12 and 20. Therefore, the heel are is between y-direction sensors 1 and 12, while the forefoot area is defined to be between y-direction sensors 12 and 39.

17. **Rearfoor_areas** and **MidFoot_ares** are cell array variables containing as many entries as there are trials. The entries themselves are 2 by 2 matrices that define the line in the heel area and midfoot area such that these areas are divided in a medial and lateral part. The first column is the point (y-coordinate followed by x-coordinate) at at the low end of an area and the second column is the point at the high end of an area.

18. **Toe_line** is a cell array variable that contains as many entries as there are trials. The entries themselves contain a vector with as many entries as the number of x-direction sensors of the accompanied pressure distribution. For all x-direction sensors, this vector contains the sensor number in the y-direction that marks the end of the metatarsal area and the beginning of the toe area.

19. **Metas_areas** is a cell array variable containing as many entries as there are trials. Just as for the variables **Rearfoor_areas** and **MidFoot_ares**, the entries

of **Metas_areas** divide the metatarsal area (are between **Forefoot_area** and **Toe_line**) with lines. In this case into five areas containing the five metatarsals. Therefore, an entry of **Metas_areas** is a 3 by 4 matrix with the first row containing the x-coordinate on the forefoot line, with the second row containing the x-coordinate on the toe line, and with the third row containing the y-coordinates on the toe line.

20. **Hallux_vert_area** is a double array that contains as many entries as there are trials. The entries are the x-direction sensor number at which the toe area is divided into a medial area, or hallux area, and a lateral area, or lesser toe area.

21. **LRchecker** is double array that contains as many entries as there are trials. The entries are zero or one. A zero means that the division algorithm has determined that the pressure distribution originates from a right foot, while a one means a left foot.

22. **Events** and **Timing** are variables that describe the temporal foot events and the foot phases as discussed in Section 2.2.4. **Events** is a cell array variable with as many entries as there are trials. An entry contains a 3 by 5 matrix were the columns contain the frame numbers of first foot contact, first metatarsal contact, fore foot flat, heel off, and last foot contact, respectively. The first row is related to the motion data, the second to the pressure data, and the third to the force plate data. **Timing** is a matrix with as many row as there are trials and with five columns with the same meaning as for the rows of a **Events** entry. The difference is that instead of frame numbers the entries of this matrix contain percentages of stance duration.

23. **LocalPressures** is a cell array with as many entries as there are trials. An entry itself contains again a cell array with four entries. These subentries are matrices that contain local pressure data of the rearfoot, midfoot, metatarsals, and toes, respectively. The rows of these matrices are the frame numbers of the pressure data while the columns are multiples of six. Every six columns contain the force in an area, the number of active sensors of an area, the total pressure of an area, the value of the pressure sensor with maximum value in an area, the x-direction sensor position of this pressure sensor, and the y-direction sensor position of this pressure sensor. In case of the rearfoot and midfoot, the first six columns are

related to the medial area and the second six columns are related to the lateral area. In case of the metatarsal area, the six times six columns are related to the first, second, third, fourth, and fifth metatarsal, respectively. In case of the toes, the first six columns are related to the hallux area and the second six columns are related to the lesser toe area.

24. **Hiel_CoPS** is a cell array with as many entries as there are trials. An entry contains 2 rows and as many columns as there are frames in the pressure distribution data of that specific trail. With this matrix the CoP path of the heel area is described. The first row contains the x-coordinates of the path and the second row contains the y-coordinates.

25. **AngleInf** is a double array variable. It is a vector if the individual performed the walking condition or the walking fast-walking running condition. It is 2 by 2 matrix if the individual performed the walking running condition. The values in the vectors and the matrices are related to the number of performed trials of a locomotion type. In case of the walking condition, it is a vector of length two with the first entry the number of left trials used for calculation LAngles and the second entry the number of right trials for calculation RAngles. In case of the walking fast-walking and running condition, it is a vector of length three with the entries related to number of performed trials in the walking type, in the fast-walking, and the running type, respectively. In case of the walking running condition, it is a two by two vector with the first column related to the number of left trials in the walking and running type, and the second column related to the number of right trials in the walking and running type.

26. **LAngels** and **RAngles** contain the angular data of the rearfoot segment, the medial and lateral metatarsal segments, and the hallux segment. Both the variables are cell arrays containing six entries. The entries are: (1) rearfoot orientation with respect to the laboratory reference frame with the static position of the rearfoot taken to coincide with the laboratory reference frame, (2) rearfoot orientation with respect to the laboratory reference frame, (3) medial metatarsal orientation with respect to the rearfoot, (4) lateral metatarsal orientation with respect to the rearfoot, (5) hallux orientation with respect to the medial metatarsal, and (6) hallux orientation with respect to the laboratory reference frame. These entries themselves are cell arrays containing *more* entries

as there are trials. The first entries are related to the trials, followed by the angular orientation of the segment in the static trail, followed by the average and standard deviation of angular orientation of the performed locomotion types. Until the static trial, all entries are matrices with 3 columns related the flexion/extension, abduction/adduction, and inversion/eversion, respectively. The entries containing average and standard deviation data have 6 columns related to the same motions and are given per pair of columns; first average and second standard deviation. The rows in all these entries are related to the frame numbers.

We hope that with this lengthy description of variables in the *'CompData.mat'*-files and the set-up of the directories, every researcher is able to access this database and use it to its full potential.

B.6 Sensitivity of the Signal Correlation Measure

In Section 2.2.1, we conclude that no delays and no inaccuracies in the internal clocks of both systems were found. Also, in Section 2.2.1, we mention the results of a sensitivity analysis of the signal correlation measure. In the present section, we describe the background of the sensitivity analysis in detail and, thus assume here that the definition of the measure is known.

To investigate the sensitivity of the signal correlation measure, we performed three checks using all 126 sessions.

In the first check, we considered the pure delay effect. To be preciese, we removed one up to five frames from the beginning of the PPPS force signals. Signal correlation measure was calculated for all the five delay conditions and it was checked in which cases the zero shift, or no shift condition, gave no longer the highest correlation. With the removal of two frames, the zero shift no longer gave the highest correlation in 124 sessions out of 126 sessions (the other two sessions needed three and four frames). Obviously, a smaller value than two frames can not be obtained because the force signals were down sampled to 250Hz. However, we calculated the minimum delay condition (meaning the condition where the smallest number of frames were removed) where not all trials had a zero shift, and all 126 sessions showed at least one trial with a non zero shift when only one frame was removed. In Figure B.9, the percentages of

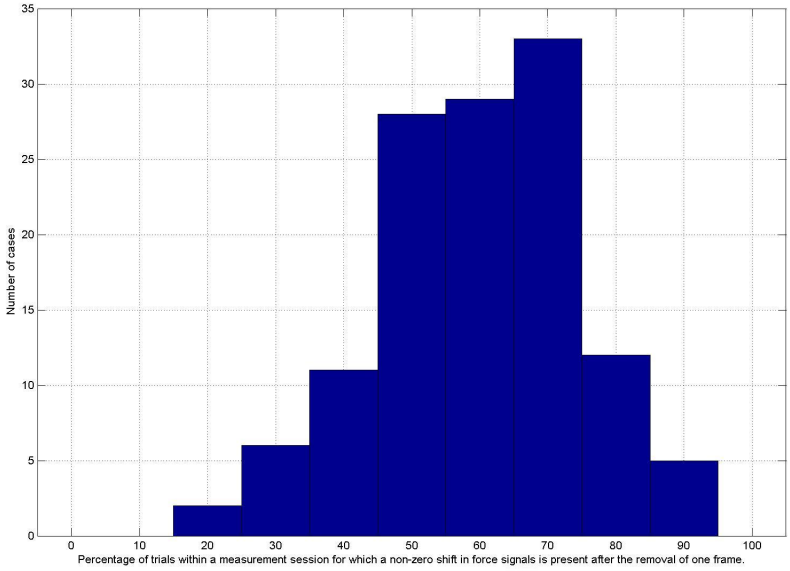

Figure B.9 The distribution of sessions with respect to their percentage of trials with a non zero shift after the removal of one frame.

trials within a session that had a non zero shift with the removal of only one frame are depicted, the minimum percentage is 22.2%.

In the second check, we considered a pure frequency effect. It used the cubic spline routine from Matlab to lengthen and shorten the force signals from PPPS such that they ranged from 490Hz to 499Hz and from 501Hz to 510Hz with 1Hz increments. Similar to the delay check, we looked for the first frequency for which all trials within a session had a non zero shift, both in [501Hz,510Hz] and [490Hz,499Hz]. The results were less evident than the results for the delay effects, a distribution emerged in both the lengthening and shortening cases, where 496Hz and 503Hz were related to the largest number of sessions, about 33% and 47% of total respectively, see Figure B.6 together with the minimum frequency condition. This condition is defined as the first frequency where not all trials in the same session had a zero shift. From Figure B.6, it follows that 498Hz and 502Hz were the two distinguishable frequencies. In the same

figure, we also depicted the percentage of non zero shift trials within a session. It is seen that the percentage of trials in case of 498Hz are almost distributed uniformly and that the percentage of trials in case of 502Hz are minimally 93%. Frequency effects can be detect on the bases of the same arguments as the delay effects. Although the 498Hz frequency border might be less easy to detect as the 502Hz frequency border.

In the third check, we considered a combination of both delay and frequency effects. The same range of frequencies was selected as in the second check combined with the same delay conditions from the first check. The order was first to lengthen or shorten the signal and secondly to remove frames. The results in detecting a combined effect were generally beter than for a single effect.

We conclude that the measure of signal correlation used to detect delay and frequency errors, due to inaccuracy and instability of the internal clocks, is sensitive at the 2ms delay level and at the 2Hz frequency level.

B.7 Determination of a Foot Axis

Three foot axes were determined from plantar pressure distributions by three methods: the global geometric inertial axis method, the local geometric inertial axis method, and the centre of pressure method. First, the complete pressure distribution was used in the global geometric inertial axis method. To determine this foot axis, all non-zero pressure values were set to one. The longest inertial axis of this pressure distribution was chosen to be the foot axis. Second, Centre of Pressures (CoPs) were used in the local geometric inertial axis method. CoPs were calculated for the heel and forefoot area, still with all non-zero pressure values set to one. The line from the CoP of the heel area to the CoP of the forefoot area was defined to be the foot axis. Third, CoPs were used in the CoP method. CoPs were calculated for the heel and forefoot area using the normal pressure distribution and its pressure values. The line from the heel area CoP to the forefoot area CoP was taken to be the foot axis.

An example of foot axes determined by these methods and the foot axis determined from motion analysis data is depicted in Figure B.11. Together with Table B.2, we conclude that the local geometric inertial method is slightly better than the other two. Correlation coefficients are all significant and show high values for the three methods.

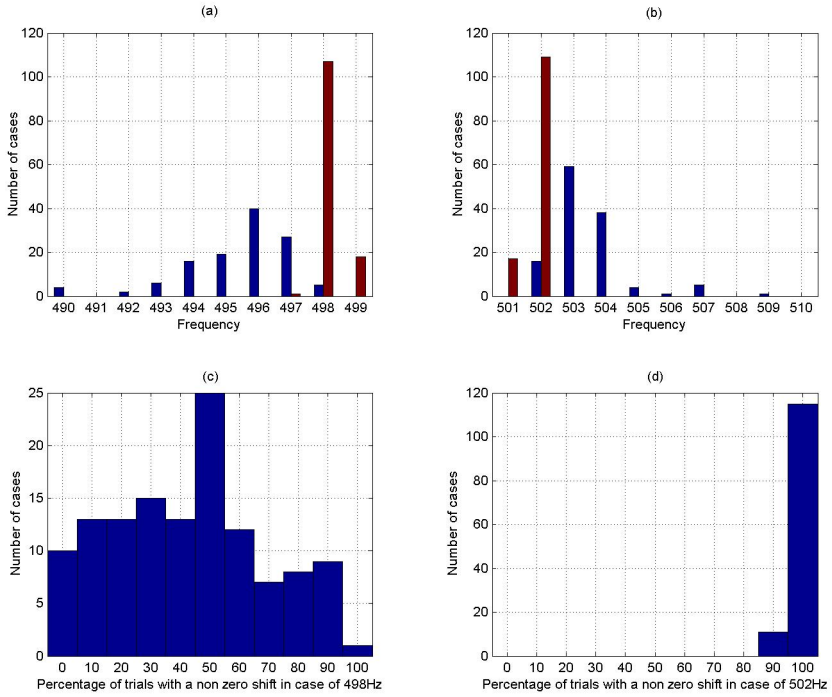

Figure B.10 In (a) and (b), the number of cases of the frequencies where all trials within a session have a non zero shift and the number of cases of the frequencies where the minimum frequency condition holds. In (a) the lower frequency band is depicted, [490Hz,499Hz], and in (b) the higher frequency band is depicted, [501Hz,510Hz]. Below (a) and (b), in (c) and (d), the distributions of the sessions with respect to their percentage of trials that have a non zero shift in case of 498Hz and 502Hz are depicted, respectively.

Average distance difference between foot axes calculated by this method and the one calculated by motion data is within pressure plate dimensions.

Table B.2 Accuracy of foot axis determination. The first column denotes the characteristics used to describe the three methods of foot axis determination. The abbreviations A. and SD. refer to Average and Standard Deviation. The distance difference is defined to be the Root Mean Square calculated between the two foot axes over the complete foot length. The second, third, and fourth column denote these characteristics for the global geometric inertial (g.i.) method, the local geometric inertial method, and the CoP method, respectively.

	global g.i.		local g.i.		local CoP	
	L	R	L	R	L	R
A. angle difference	4.6°	-5.8°	2.5°	-3.8°	2.7°	-4.1°
SD. of angle difference	1.7°	1.7°	1.6°	1.7°	1.9°	2.1°
A. Distance Difference	11.2mm	9.6mm	7.7mm	7.9mm	7.0mm	8.9mm
SD. of distance difference	8.5mm	8.0mm	8.6mm	8.1mm	8.5mm	8.2mm
correlation coefficient	.93	.94	.94	.94	.91	.91

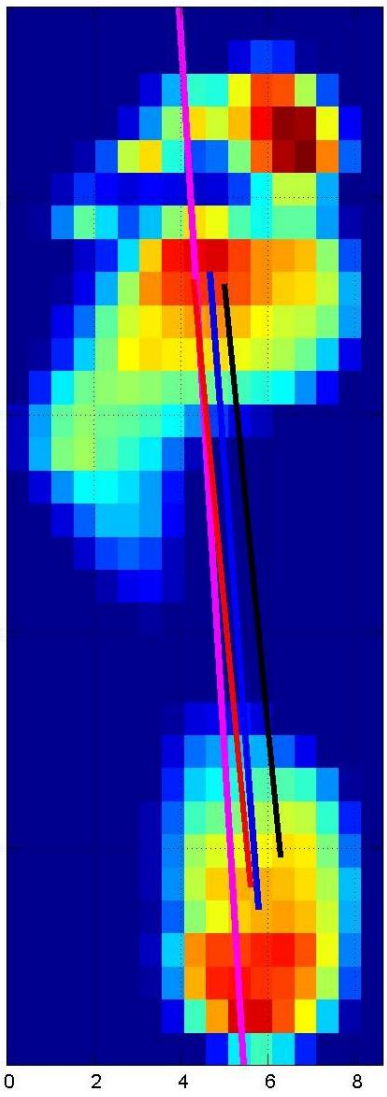

Figure B.11 Examples of foot axes. The black solid line is the foot axis determined from motion data. The blue solid line is the foot axis determined with the CoP method. The red solid line is the foot axis determined with the local geometric inertial axis method. The magenta solid line is the foot axis determined with the global geometric inertial axis method.

Appendix C

Studying the Rearfoot: Details

In this Appendix, information accompanying Chapter 3 is presented. Most information is not understandable without having read, Chapter 3.

This Appendix contains two sections. The first section is on CoP sensitivity as expressed in one figure and nine tables on this subject. The second section describes the Matlab applications used to calculate the results of Chapter 3.

The variables that were calculated for Chapter 3 and were stored in *'Compfile.mat'*-files are described in the previous appendix. As mentioned in the previous appendix, we choose to describe all variables of the *'Compfile.mat'*-files at one location such that this information is accessible for a researcher using the database. To be complete, the variables in *'Compfile.mat'* that are calculated with applications from research into rearfoot simulation are **AngleInf**, **LAngles**, **RAngles**, and **Hiel_CoPS**. The first three variables contain all angular information of the performed trials: the angles of dynamic trials, the angular position of the segments during the static trial, and the average and standard deviation curves of these angles. Average and standard deviation curves were calculated for all locomotion types: walking, fast-walking, running, within a measurement session and this for both the left and right trials. Finally, the CoP paths of all trials are found in **Hiel_CoPS**.

C.1 CoP sensitivity information

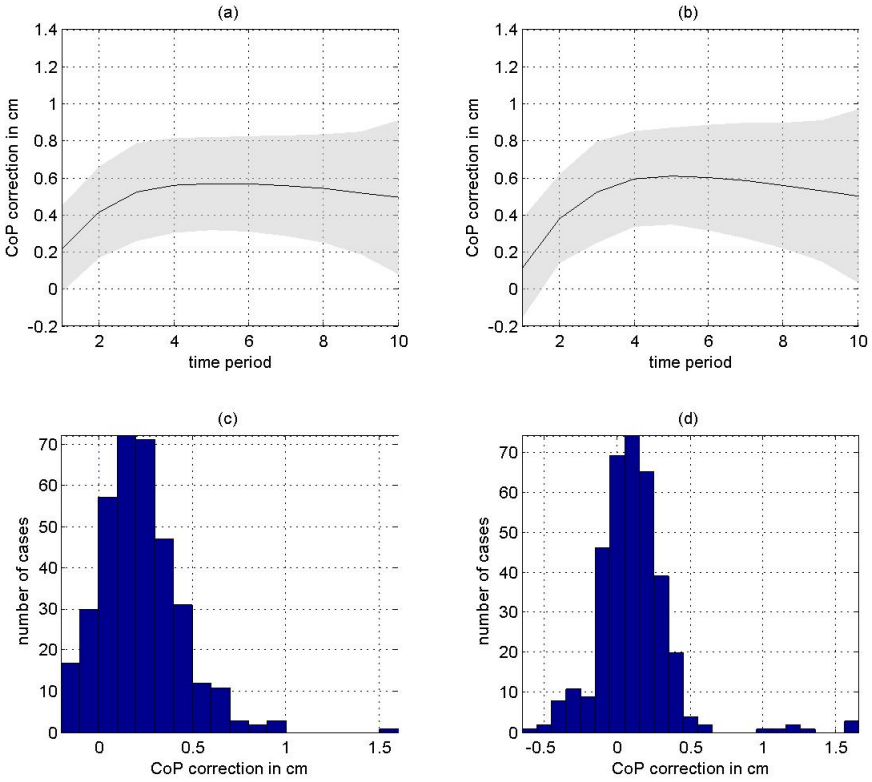

Figure C.1 In this figure, the CoP path correction based on regression correction is depicted. In graph (a) and (b), the average and standard deviations of the x-direction corrections are depicted for left and right trials of the walking sessions, respectively. In graphs (c) and (d), the left and right distribution of corrections for the initial contact phase is depicted.

Table C.1 Population information on the time point at which the CoP paths of the walking sessions the different heel areas start to deviate. All information is related to right foot trails of the specific individuals. Time point are expressed as a percentage of stance phase. **A** is the average time point were the CoP paths deviates; average with respect to all trials of one individual. **S** is the standard deviation of the time points where the CoP paths deviates and **MM** is the maximum time point minus the minimum time point where the CoP paths deviates. The postfixes -2, -1, $+1$, and $+2$ are related to comparison of CoP paths. For example, -2 means the comparison of the original heel area and this heel area minus two horizontal lines.

Name	A -2	S -2	MM -2	A -1	S -1	MM -1	A +1	S +1	MM +1	A +2	S +2	MM +2
individual 1	11%	1.2%	3.7%	11.1%	1.3%	4%	11.1%	1.3%	4%	10.9%	1.2%	3.7%
individual 2	18%	11.5%	36.1%	18.2%	11.5%	36.1%	18.2%	11.5%	36.1%	18.2%	11.5%	36.1%
individual 3	11.9%	0.5%	1.6%	11.9%	0.5%	1.6%	11.9%	0.5%	1.6%	11.9%	0.5%	1.6%
individual 4	11.9%	1.3%	3.8%	12%	1.3%	3.8%	12%	1.3%	3.8%	11.9%	1.3%	3.8%
individual 5	86.2%	24.8%	55.2%	86.2%	24.7%	55.2%	86%	25.1%	55.8%	84.7%	27.5%	60.3%
individual 6	10.1%	1.3%	3.9%	10.3%	1.3%	3.6%	10.3%	1.2%	3.4%	9.8%	0.9%	2.6%
individual 7	8%	0.4%	1.2%	8%	0.4%	1.2%	8%	0.4%	1.2%	8%	0.4%	1.2%
individual 8	9.8%	1.2%	3.3%	9.8%	1.2%	3.3%	9.8%	1.2%	3.3%	9.8%	1.2%	3.3%
individual 9	10.8%	1.1%	3.2%	10.9%	1%	3.1%	10.8%	1.1%	3.2%	10.6%	1%	2.9%
individual 10	9.1%	1.8%	5.4%	9.3%	1.8%	5.6%	9.3%	1.8%	5.6%	9.3%	1.8%	5.6%
individual 11	7.4%	0.6%	1.8%	7.5%	0.7%	2%	7.5%	0.7%	2%	7.4%	0.7%	1.8%
individual 12	11.6%	2%	6.1%	11.7%	2.1%	6.4%	11.7%	2.1%	6.4%	11.6%	2%	6.1%
individual 13	12.8%	1.2%	3.4%	12.9%	1.2%	3.4%	12.9%	1.2%	3.4%	12.9%	1.2%	3.4%
individual 14	7.7%	0.3%	0.9%	7.8%	0.3%	1%	7.8%	0.3%	1%	7.8%	0.4%	1%
individual 15	7%	0.5%	1.7%	7%	0.5%	1.7%	7%	0.5%	1.7%	6.8%	0.6%	1.7%
individual 16	11.1%	1%	2.9%	11.2%	1%	2.9%	11.1%	1%	2.9%	10.9%	0.8%	2.6%
individual 17	8.9%	0.8%	2.7%	8.9%	0.8%	2.7%	8.9%	0.8%	2.7%	8.9%	0.8%	2.7%
individual 18	30.5%	25.2%	85.4%	30.7%	25.2%	85.4%	30.7%	25.2%	85.4%	24.7%	8.8%	30.7%
individual 19	12.1%	2.7%	8%	12.2%	2.8%	8.3%	11.5%	2.7%	8%	9%	1.9%	6.9%
individual 20	14.2%	3.4%	10.2%	14.3%	3.4%	10.2%	14.3%	3.4%	10.2%	14.3%	3.4%	10.2%
individual 21	31.4%	24.5%	84.1%	31.9%	24.3%	83.7%	31.9%	24.3%	83.7%	31.9%	24.3%	83.7%
individual 22	9.1%	0.4%	1.4%	9.2%	0.4%	1.4%	9.2%	0.4%	1.4%	9.1%	0.4%	1.7%
individual 23	15.5%	0.9%	2.9%	15.6%	0.9%	2.9%	15.6%	0.9%	2.9%	15.3%	0.9%	2.7%
individual 24	25.8%	26.3%	86.1%	26.5%	26.2%	85.8%	25.3%	26.5%	86.4%	16.8%	8.7%	29.1%
individual 25	14.2%	0.7%	2.4%	14.4%	0.7%	2.4%	14.3%	0.7%	2.4%	14.2%	0.6%	2.1%
individual 26	11.5%	0.6%	1.9%	11.6%	0.7%	2.2%	11.6%	0.7%	2.2%	11.6%	0.7%	2.2%
individual 27	14.6%	2.8%	8.5%	15%	3%	8.7%	15.1%	3.1%	9.2%	14.8%	3%	9.2%
individual 28	13.6%	1.1%	3.6%	13.6%	1.1%	3.8%	13.3%	1.1%	3.7%	12.3%	0.9%	3.4%
individual 29	12.8%	2.2%	6.6%	13%	2.3%	6.9%	12.8%	2.2%	6.6%	11.6%	1.7%	5%
individual 30	10.1%	1.2%	3.3%	10.1%	1.2%	3.3%	10.1%	1.2%	3.3%	10%	1.2%	3.3%
individual 31	10.6%	0.9%	3.3%	10.7%	0.9%	3.2%	10.4%	1%	3.3%	9.8%	0.8%	2.4%
individual 32	7.6%	0.7%	2.6%	7.6%	0.7%	2.6%	7.6%	0.7%	2.6%	7.5%	0.7%	2.6%
individual 33	8.1%	1%	3.7%	8.1%	1%	3.7%	8.1%	1%	3.7%	8.1%	1%	3.7%
individual 34	9.7%	1.3%	4.6%	9.7%	1.3%	4.6%	9.7%	1.3%	4.6%	9.7%	1.3%	4.6%
individual 35	10.5%	0.8%	3.1%	10.6%	0.7%	2.8%	10.6%	0.7%	2.8%	10.6%	0.7%	2.8%
individual 36	7.9%	0.7%	2.1%	8%	0.7%	2.5%	7.9%	0.8%	2.7%	7.5%	0.6%	2.1%
individual 37	10.7%	1.2%	3.7%	10.8%	1.2%	4.1%	10.8%	1.3%	4.1%	10.7%	1.2%	3.7%
individual 38	17.5%	2.6%	9.1%	17.6%	2.6%	9.1%	17.6%	2.6%	9.1%	17.6%	2.6%	9.1%
individual 39	9.3%	1%	3.7%	9.4%	1%	3.7%	9.4%	1%	3.7%	9.3%	1%	3.7%
individual 40	11.9%	2.5%	7.8%	12%	2.5%	7.8%	11.9%	2.5%	7.8%	11.6%	2.5%	7.8%
individual 41	9.8%	1.2%	3.5%	9.8%	1.2%	3.5%	9.8%	1.2%	3.5%	9.8%	1.2%	3.5%
individual 42	8.1%	2%	5.4%	8.2%	2%	5.8%	8.2%	2%	5.8%	7.6%	1.7%	5.4%
individual 43	12.4%	1.3%	3.7%	12.6%	1.3%	3.9%	12.6%	1.3%	3.9%	12.4%	1.2%	3.4%
AVERAGE	14.0%			14.1%			14.1%			13.5%		

Table C.2 Population information on the time point at which the CoP paths of the different heel areas deviate in case of walking sessions. All information is related to left foot trails of the specific individuals. Time points are expressed as a percentage of midstance (from first metatarsal contact til heel lift). **A** is the average time point were the CoP paths deviates; average with respect to all trials of one individual. **S** is the standard deviation of the time points where the CoP paths deviates and **MM** is the maximum time point minus the minimum time point where the CoP paths deviates. The postfixes -2, -1, $+1$, and $+2$ are related to comparison of CoP paths. For example, -2 means the comparison of the original heel area and this heel area minus two horizontal lines.

Name	A -2	S -2	MM -2	A -1	S -1	MM -1	A +1	S +1	MM +1	A +2	S +2	MM +2
individual 1	6.5%	5.7%	18.9%	6.7%	6%	20%	6.7%	6%	20%	6.2%	5%	15.8%
individual 2	5.2%	2.7%	7.4%	5.4%	2.9%	8.7%	5.4%	2.9%	8.7%	5.2%	2.6%	7.4%
individual 3	-0.3%	1.4%	3.5%	-0.3%	1.4%	3.5%	-0.3%	1.4%	3.5%	-0.3%	1.4%	3.5%
individual 4	14%	6.2%	17.5%	14.4%	6.4%	18.1%	14.4%	6.4%	18.1%	14.2%	6.3%	16.9%
individual 5	50.7%	27.5%	79.5%	51.4%	27.8%	81.3%	51.4%	27.8%	81.3%	51.2%	27.8%	81.3%
individual 6	19.3%	14.8%	44.9%	20.5%	15.2%	44.9%	19.4%	13.7%	42.8%	14.1%	8.1%	26.9%
individual 7	5.2%	4.3%	14.2%	5.2%	4.4%	14.2%	5.2%	4.4%	14.2%	5.2%	4.4%	14.2%
individual 8	13.6%	15.8%	53.2%	14.1%	16.6%	56%	14.1%	16.6%	56%	14.1%	16.6%	56%
individual 9	10.4%	11.5%	38.5%	10.9%	12.4%	41.4%	7.8%	3.7%	10.9%	7.1%	2.8%	8.9%
individual 10	12.7%	15.2%	44.2%	13.1%	15.6%	44.2%	13.1%	15.6%	44.2%	13.1%	15.6%	44.2%
individual 11	4.1%	1%	3.2%	4.3%	1.1%	3.2%	4.3%	1.1%	3.2%	4%	0.9%	3.2%
individual 12	15.2%	4.1%	10.7%	15.6%	4.1%	11.1%	15.6%	4.2%	11.9%	15.3%	3.9%	10.7%
individual 13	2.6%	0.6%	2.1%	2.7%	0.7%	2.1%	2.6%	0.7%	2.2%	2.4%	0.7%	2.2%
individual 14	-1.1%	0.5%	1.1%	-1.1%	0.5%	1.1%	-1%	0.4%	1.1%	-1.1%	0.5%	1.1%
individual 15	1.3%	0.8%	2.5%	1.5%	0.7%	2.5%	1.2%	0.7%	2.5%	0.9%	0.5%	1.7%
individual 16	1.8%	1.7%	4.4%	1.8%	1.7%	4.4%	1.9%	1.7%	4.4%	1.7%	1.6%	4.4%
individual 17	6.6%	6.5%	20.2%	6.6%	6.6%	20.2%	6.6%	6.6%	20.2%	6.6%	6.6%	20.2%
individual 18	78.1%	27.8%	64.5%	78.7%	27.2%	64.5%	77.5%	28.6%	66.8%	73.8%	33.3%	75.7%
individual 19	10.7%	8.9%	21.7%	11.5%	9.6%	23.6%	9.2%	9.1%	21.4%	1.2%	3.3%	11.2%
individual 20	12.7%	8.4%	28.4%	12.7%	8.4%	28.4%	12.7%	8.4%	28.4%	12.7%	8.4%	28.4%
individual 21	47.2%	21%	77.7%	52.4%	26.4%	77.9%	52.4%	26.4%	77.9%	49%	21.4%	77.7%
individual 22	5.2%	1.1%	3.2%	5.5%	1.2%	4.2%	5.3%	1.1%	3.4%	5%	0.9%	3.1%
individual 23	22%	6.6%	23.7%	22.8%	6.8%	24.5%	22.5%	6.8%	24.5%	21.2%	7.1%	25.7%
individual 24	45.4%	21%	60.8%	46.5%	21.4%	60.2%	44.6%	21.2%	60.8%	33.6%	19.6%	54.8%
individual 25	38.8%	38.1%	95.9%	39.2%	38%	95.9%	39%	38%	95.9%	38.6%	38.2%	95.9%
individual 26	19.1%	6.2%	19.4%	19.5%	6.1%	19.5%	19.5%	6.1%	18.9%	19.2%	5.7%	18.2%
individual 27	23.9%	6.7%	19.8%	24.8%	6.7%	19.6%	24.7%	6.6%	19.6%	24.5%	6.7%	20.8%
individual 28	9%	2%	5.9%	9.5%	2.2%	6.4%	9.1%	2.2%	6.4%	8.2%	2.3%	7.3%
individual 29	5.8%	2%	5.8%	6.2%	2.6%	7.8%	4.9%	1.8%	5%	2.4%	0.9%	2.5%
individual 30	6.2%	1.9%	5.8%	6.4%	1.9%	5.8%	6.2%	1.9%	5.8%	5.9%	1.4%	4%
individual 31	2.7%	0.6%	2.1%	3%	0.8%	2.8%	2.9%	0.8%	2.8%	2.8%	0.7%	2.1%
individual 32	17.7%	4%	13%	17.7%	4.2%	13.2%	17.7%	4.2%	13.2%	17.7%	4.2%	13.2%
individual 33	2.8%	1.4%	4.4%	2.9%	1.4%	4.4%	2.9%	1.4%	4.4%	2.7%	1.2%	4.4%
individual 34	0.5%	0.4%	1.1%	0.5%	0.5%	1.7%	0.5%	0.5%	1.7%	0.5%	0.4%	1.1%
individual 35	2.9%	1%	3.2%	3%	1.1%	3.2%	3%	1.1%	3.2%	3%	1.1%	3.2%
individual 36	8.2%	2.8%	8.7%	8.4%	3.2%	9.8%	8.2%	2.8%	8.7%	7.7%	2.7%	7.6%
individual 37	2.8%	1.7%	6.3%	2.9%	1.6%	6.3%	2.9%	1.6%	6.3%	2.7%	1.4%	5.2%
individual 38	3.4%	3%	9.6%	3.4%	3%	9.6%	3.4%	3%	9.6%	3.4%	3%	9.6%
individual 39	1.7%	0.8%	2.9%	1.8%	0.8%	2.9%	1.9%	0.9%	2.9%	1.8%	0.8%	2.9%
individual 40	55%	37.3%	87.8%	55.2%	37.1%	87.8%	54.9%	37.3%	87.8%	48.2%	33.9%	87.8%
individual 41	-2.8%	0.9%	3%	-2.8%	0.9%	3%	-2.8%	0.9%	3%	-2.8%	0.9%	3%
individual 42	31.5%	7.1%	23.8%	32.3%	6.8%	22.8%	31.7%	7%	23.8%	29.3%	6.7%	22.7%
individual 43	2.6%	1.9%	5.7%	3.2%	2%	6.9%	3.2%	2%	6.9%	3%	1.7%	5.7%
AVERAGE	14.4%			14.9%			14.6%			13.4%		

Table C.3 Population information on the time point at which the CoP paths of the different heel areas deviate in case of walking sessions. All information is related to right foot trails of the specific individuals. Time points are expressed as a percentage of midstance (from first metatarsal contact til heel lift). **A** is the average time point were the CoP paths deviate; average with respect to all trials of one individual. **S** is the standard deviation of the time points where the CoP paths deviate and **MM** is the maximum time point minus the minimum time point where the CoP paths deviate. The postfixes -2, -1, $+1$, and $+2$ are related to comparison of CoP paths. For example, -2 means the comparison of the original heel area and this heel area minus two horizontal lines.

Name	A -2	S -2	MM -2	A -1	S -1	MM -1	A +1	S +1	MM +1	A +2	S +2	MM +2
individual 1	4.9%	1.9%	5.8%	5.1%	2.1%	6.2%	5.1%	2.1%	20%	4.7%	1.7%	5.4%
individual 2	15.5%	23.3%	74.8%	15.9%	23.3%	74.2%	15.9%	23.3%	8.7%	15.9%	23.3%	74.2%
individual 3	1.6%	0.9%	3.3%	1.7%	1%	3.3%	1.7%	1%	3.5%	1.7%	1%	3.3%
individual 4	7.5%	2.7%	9%	7.7%	2.7%	9%	7.6%	2.6%	18.1%	7.4%	2.6%	9%
individual 5	93.2%	11.5%	26.3%	93.3%	11.4%	26.3%	92.9%	12%	81.3%	90.4%	16.7%	36.3%
individual 6	8%	2.8%	8.1%	8.6%	2.6%	6.9%	8.5%	2.4%	42.8%	7.2%	1.8%	5.6%
individual 7	-0.8%	0.6%	1.6%	-0.8%	0.6%	1.6%	-0.8%	0.6%	14.2%	-0.8%	0.6%	1.6%
individual 8	3.1%	1.7%	5.8%	3.1%	1.7%	5.8%	3.1%	1.7%	56%	3.1%	1.7%	5.8%
individual 9	6.5%	1.7%	5%	6.6%	1.5%	5%	6.6%	1.6%	10.9%	6.2%	1.4%	4.8%
individual 10	7.7%	3.8%	12.8%	8.1%	4%	13.6%	8.2%	4%	44.2%	8.1%	4%	13.6%
individual 11	1.3%	0.7%	1.9%	1.4%	0.9%	2.8%	1.4%	0.9%	3.2%	1.4%	0.8%	2.3%
individual 12	9.1%	4.5%	14%	9.4%	4.8%	14.8%	9.4%	4.8%	11.9%	9.2%	4.6%	14%
individual 13	2.2%	1%	3.4%	2.4%	1.2%	4%	2.4%	1.2%	2.2%	2.3%	1%	3.4%
individual 14	0.3%	0.3%	0.5%	0.4%	0.3%	1%	0.4%	0.3%	1.1%	0.4%	0.3%	1%
individual 15	1.3%	0.7%	2.3%	1.3%	0.7%	2.3%	1.3%	0.7%	2.5%	0.7%	0.6%	1.7%
individual 16	4.8%	1.7%	5.6%	5.1%	1.8%	5.6%	4.9%	1.7%	4.4%	4.4%	1.4%	4.8%
individual 17	1.7%	1.3%	4.6%	1.8%	1.3%	4.6%	1.8%	1.3%	20.2%	1.8%	1.3%	4.6%
individual 18	37.7%	24.7%	84.5%	38.2%	24.6%	84.5%	38.2%	24.6%	66.8%	35.4%	20.6%	70.3%
individual 19	8.2%	5%	13.8%	8.4%	5.2%	14.5%	7.1%	5%	21.4%	2.4%	2.9%	10%
individual 20	14.4%	9.1%	30.6%	14.5%	9.2%	30.6%	14.5%	9.2%	28.4%	14.5%	9.2%	30.6%
individual 21	42.5%	23.1%	82.3%	43.8%	22.9%	81.4%	43.8%	22.9%	77.9%	43.8%	22.9%	81.4%
individual 22	1.3%	0.6%	1.8%	1.5%	0.7%	1.8%	1.5%	0.7%	3.4%	1.4%	0.6%	1.8%
individual 23	13.6%	2.1%	6.7%	13.9%	2%	6.7%	13.8%	2%	24.5%	12.7%	1.7%	5.7%
individual 24	24%	26.9%	90%	25.3%	26.8%	89.4%	23.3%	27.2%	60.8%	14.7%	16.5%	55.1%
individual 25	3.2%	0.9%	2.6%	3.6%	1.1%	2.9%	3.4%	1%	95.9%	3%	0.7%	2.2%
individual 26	11.5%	2.2%	8.1%	11.8%	2.2%	8.2%	11.9%	2.3%	18.9%	11.8%	2.2%	8.2%
individual 27	9.7%	4.3%	14.3%	10.6%	4.6%	14.4%	10.7%	5%	19.6%	10.1%	5%	15.6%
individual 28	8%	1.7%	5.7%	8%	1.8%	5.7%	7.4%	1.9%	6.4%	5.1%	1.3%	4%
individual 29	5.6%	3.1%	8.7%	6.1%	3.5%	10.4%	5.7%	3.3%	5%	2.6%	1.4%	4.2%
individual 30	2.9%	1.3%	4.1%	2.9%	1.3%	4.1%	2.9%	1.3%	5.8%	2.7%	1.2%	3.7%
individual 31	2.7%	1.3%	3.7%	2.9%	1.5%	4.4%	2.4%	1.4%	2.8%	1.2%	1%	3%
individual 32	2.8%	0.7%	2.2%	2.8%	0.7%	2.2%	2.8%	0.7%	13.2%	2.6%	0.4%	1.4%
individual 33	2.9%	1.5%	5.1%	2.9%	1.5%	5.1%	2.9%	1.5%	4.4%	2.8%	1.5%	5.1%
individual 34	1.2%	1.3%	4.5%	1.2%	1.3%	4.5%	1.2%	1.3%	1.7%	1.2%	1.3%	4.5%
individual 35	5%	1.8%	5.3%	5.3%	1.7%	4.6%	5.3%	1.6%	3.2%	5.3%	1.6%	4.4%
individual 36	4.3%	1.3%	3.8%	4.5%	1.3%	4%	4.3%	1.6%	8.7%	3%	1.2%	3.7%
individual 37	3.5%	2.3%	7.5%	3.7%	2.4%	7.8%	3.6%	2.4%	6.3%	3.5%	2.2%	7.1%
individual 38	5.5%	2.6%	8.1%	5.7%	2.8%	8.1%	5.8%	2.8%	9.6%	5.8%	2.8%	8.1%
individual 39	1.1%	0.7%	2.4%	1.3%	1%	3.3%	1.3%	1%	2.9%	1.2%	0.9%	3.3%
individual 40	9.3%	3.5%	10.6%	9.3%	3.5%	10.6%	9.2%	3.6%	87.8%	8.6%	3.6%	10.6%
individual 41	-2.4%	0.9%	3.3%	-2.4%	0.9%	3.3%	-2.4%	0.9%	3%	-2.4%	0.9%	3.3%
individual 42	12.1%	6%	16.1%	12.5%	6%	17.1%	12.3%	6.1%	23.8%	10.5%	4.8%	15.1%
individual 43	5.1%	3.7%	10.9%	5.5%	3.8%	10.6%	5.5%	3.8%	6.9%	5%	3.3%	9.8%
AVERAGE	9.4%			9.6%			9.5%			8.6%		

Table C.4 Correction values based on the begin-end point method. Moreover, this table contains the average correction for the *left* trials of all individuals that performed the walking condition. Corrections are given for all selected time intervals ranging from Initial Contact Phase (ICP) to Heel Lift

Name	ICP	2	3	4	5	6	7	8	9	Heel Lift
individual 1	0.223	0.409	0.533	0.575	0.613	0.647	0.67	0.689	0.693	0.687
individual 2	0.569	0.701	0.711	0.7	0.738	0.763	0.775	0.778	0.786	0.789
individual 3	0.277	0.392	0.436	0.475	0.501	0.526	0.533	0.532	0.527	0.675
individual 4	0.197	0.362	0.447	0.493	0.538	0.59	0.6	0.565	0.483	0.292
individual 5	0.179	-0.028	-0.087	0.003	-0.066	-0.089	0.007	-0.084	-0.11	-0.204
individual 6	0.715	0.614	0.627	0.483	0.394	0.404	0.424	0.434	0.426	0.331
individual 7	0.36	0.514	0.583	0.615	0.63	0.663	0.713	0.765	0.882	1.045
individual 8	0.21	0.416	0.49	0.506	0.504	0.487	0.457	0.416	0.348	0.141
individual 9	0.061	0.37	0.452	0.477	0.504	0.497	0.486	0.48	0.48	0.413
individual 10	0.16	0.077	0.131	0.17	0.193	0.183	0.185	0.225	0.198	0.142
individual 11	0.053	0.503	0.613	0.639	0.713	0.772	0.8	0.787	0.772	0.742
individual 12	0.12	0.261	0.348	0.385	0.392	0.387	0.372	0.336	0.251	0.078
individual 13	0.463	0.829	0.879	0.849	0.855	0.921	0.975	0.974	1.132	1.61
individual 14	0.357	NaN	0.618	0.696	0.716	0.774	0.854	0.925	1.047	1.389
individual 15	0.029	0.405	0.55	0.6	0.632	0.674	0.729	0.83	1.101	1.889
individual 16	0.426	0.657	0.802	0.912	0.966	1.024	1.07	1.102	1.111	1.089
individual 17	0.079	0.212	0.288	0.298	0.32	0.348	0.342	0.322	0.193	0.155
individual 18	0.001	0.087	0.116	0.136	0.153	0.146	0.085	-0.01	-0.151	-0.408
individual 19	0.24	0.503	0.548	0.617	0.641	0.714	0.791	0.868	0.894	0.898
individual 20	NaN	NaN	NaN	NaN	NaN	NaN	NaN	NaN	NaN	NaN
individual 21	0.197	0.308	0.369	0.379	0.391	0.411	0.383	0.301	0.207	0.099
individual 22	0.008	0.298	0.412	0.458	0.464	0.471	0.468	0.42	0.316	0.146
individual 23	0.195	0.303	0.377	0.422	0.451	0.465	0.46	0.464	0.449	0.359
individual 24	0.31	0.558	0.643	0.662	0.698	0.682	0.664	0.648	0.69	0.682
individual 25	0.511	0.602	0.625	0.627	0.636	0.636	0.648	0.691	0.66	0.499
individual 26	0.017	0.126	0.221	0.342	0.441	0.54	0.669	0.82	0.97	1.22
individual 27	0.13	0.29	0.428	0.541	0.498	0.537	0.581	0.653	0.647	0.473
individual 28	-0.069	0.132	0.165	0.186	0.233	0.263	0.294	0.349	0.311	0.026
individual 29	0.14	0.333	0.406	0.428	0.451	0.474	0.529	0.574	0.63	0.881
individual 30	-0.115	0.269	0.325	0.353	0.376	0.398	0.428	0.427	0.392	0.453
individual 31	0.513	0.465	0.455	0.452	0.421	0.399	0.361	0.26	0.207	0.063
individual 32	0.372	0.55	0.681	0.745	0.79	0.808	0.816	0.861	0.796	0.579
individual 33	0.267	0.391	0.412	0.395	0.48	0.536	0.562	0.638	0.796	1.035
individual 34	0.213	0.542	0.578	0.572	0.564	0.553	0.611	0.546	0.486	0.725
individual 35	0.164	0.397	0.484	0.62	0.716	0.776	0.822	0.834	0.863	0.93
individual 36	-0.086	-0.023	0.027	0.06	0.073	0.06	0.045	0.024	-0.034	-0.14
individual 37	0.262	0.403	0.36	0.47	0.532	0.572	0.635	0.673	0.682	0.822
individual 38	0.427	0.585	0.616	0.664	0.722	0.751	0.743	0.766	0.743	0.912
individual 39	NaN	NaN	NaN	NaN	NaN	NaN	NaN	NaN	NaN	NaN
individual 40	-0.255	-0.039	0.051	0.051	0.038	-0.006	-0.04	-0.085	-0.215	-0.381
individual 41	0.537	0.866	0.911	0.938	0.93	0.892	0.853	0.901	1.027	1.612
individual 42	0.254	0.425	0.66	0.734	0.875	0.975	1.064	1.14	1.197	1.294
individual 43	0.09	0.171	0.24	0.299	0.331	0.343	0.363	0.364	0.301	0.109
AVERAGE	0.215	0.381	0.452	0.489	0.513	0.536	0.557	0.566	0.565	0.565

Table C.5 Correction values based on the begin-end point method. Moreover, this table contains the average correction for the *right* trials of all individuals that performed the walking condition. Corrections are given for all selected time intervals ranging from Initial Contact Phase (ICP) to Heel Lift

Name	ICP	2	3	4	5	6	7	8	9	Heel Lift
individual 1	0.277	0.549	0.681	0.693	0.701	0.746	0.751	0.689	0.696	0.431
individual 2	0.022	0.132	0.131	0.093	0.074	0.035	-0.025	-0.102	-0.081	-0.142
individual 3	0.413	0.604	0.671	0.698	0.729	0.774	0.821	0.89	1.027	1.544
individual 4	-0.388	-0.173	-0.023	0.062	0.145	0.261	0.329	0.396	0.395	0.181
individual 5	0.174	0.074	0.041	0.134	0.086	0.045	0.026	0.017	0.004	-0.154
individual 6	0.386	0.367	0.339	0.271	0.222	0.204	0.213	0.206	0.218	0.124
individual 7	1.14	0.274	0.486	NaN	0.966	0.514	0.509	0.411	0.32	0.234
individual 8	0.193	0.376	0.473	0.49	0.479	0.45	0.401	0.361	0.283	0.144
individual 9	0.028	0.388	0.5	0.537	0.574	0.569	0.512	0.585	0.639	0.697
individual 10	0.268	0.324	0.398	0.398	0.373	0.403	0.425	0.426	0.403	0.357
individual 11	-0.016	0.405	0.552	0.598	0.67	0.689	0.696	0.767	0.801	1.175
individual 12	0.136	0.269	0.374	0.419	0.434	0.426	0.41	0.389	0.341	0.268
individual 13	-0.005	0.219	0.269	0.29	0.325	0.354	0.364	0.427	0.537	1.101
individual 14	0.078	0.625	0.687	0.702	0.751	0.864	0.968	1.057	1.09	1.217
individual 15	-0.02	0.393	0.58	0.674	0.713	0.769	0.802	0.845	0.891	1.268
individual 16	0.199	0.53	0.652	0.702	0.752	0.779	0.772	0.704	0.545	0.382
individual 17	0.055	0.204	0.29	0.32	0.336	0.355	0.351	0.325	0.155	0.071
individual 18	-0.14	-0.045	0.001	0.01	0.01	-0.008	-0.051	-0.186	-0.325	-0.587
individual 19	0.003	-0.04	NaN	0.182	0.21	0.217	0.264	0.317	0.412	0.489
individual 20	0.298	0.303	0.159	0.084	0.036	0.001	-0.023	-0.065	-0.129	-0.276
individual 21	0.206	0.43	0.479	0.477	0.462	0.47	0.449	0.362	0.236	0.061
individual 22	-0.263	0.052	0.146	0.166	0.196	0.234	0.245	0.251	0.241	0.178
individual 23	-0.033	0.101	0.188	0.192	0.181	0.137	0.137	0.11	0.101	-0.058
individual 24	0.005	0.295	0.397	0.459	0.532	0.551	0.53	0.5	0.473	0.217
individual 25	0.091	0.301	0.376	0.423	0.452	0.482	0.484	0.493	0.638	0.635
individual 26	0.002	0.167	0.312	0.466	0.575	0.711	0.826	0.903	0.999	1.148
individual 27	0.221	0.627	0.741	0.819	0.909	0.925	0.954	0.991	1.029	0.741
individual 28	-0.454	-0.107	0.072	0.122	0.149	0.203	0.23	0.131	0.017	-0.271
individual 29	0.111	0.296	0.4	0.436	0.467	0.5	0.549	0.565	0.577	0.692
individual 30	-0.056	0.378	0.48	0.523	0.536	0.556	0.566	0.571	0.538	0.767
individual 31	0.296	0.528	0.587	0.526	0.536	0.603	0.574	0.548	0.595	0.795
individual 32	-0.01	0.223	0.323	0.368	0.372	0.385	0.412	0.471	0.532	0.619
individual 33	0.045	0.186	0.285	0.298	0.383	0.43	0.485	0.581	0.649	0.697
individual 34	0.255	0.585	0.645	0.634	0.644	0.718	0.726	0.929	0.955	1.277
individual 35	0.083	0.29	0.381	0.449	0.483	0.508	0.562	0.645	0.687	0.789
individual 36	-0.005	0.18	0.297	0.313	0.338	0.36	0.385	0.401	0.338	0.007
individual 37	0.183	0.401	0.747	0.616	NaN	NaN	0.797	0.568	0.578	0.583
individual 38	0.175	0.272	0.316	0.319	0.301	0.261	0.162	0.151	0.125	0.183
individual 39	-0.061	0.239	0.313	0.337	0.377	0.332	0.347	0.411	0.49	0.388
individual 40	0.27	0.624	0.793	0.842	0.832	0.775	0.672	0.498	0.349	0.07
individual 41	0.222	0.382	0.415	0.417	0.432	0.43	0.437	0.531	0.718	1.155
individual 42	0.019	0.151	0.465	0.518	0.627	0.707	0.783	0.907	1.1	1.713
individual 43	0.108	0.212	0.291	0.342	0.37	0.391	0.418	0.432	0.393	0.203
AVERAGE	0.105	0.293	0.398	0.415	0.446	0.455	0.471	0.475	0.479	0.479

Table C.6 The *constant* correction values based on the regression point method. Moreover, it contains the average correction for the *left* trials of all individuals that performed the walking condition. Corrections are given for all selected time intervals ranging from Initial Contact Phase (ICP) to Heel Lift

Name	ICP	2	3	4	5	6	7	8	9	Heel Lift
individual 1	-0.048	-0.013	0.03	0.085	0.119	0.147	0.177	0.202	0.2	0.216
individual 2	0.07	0.06	0.12	0.124	0.105	0.11	0.132	0.141	0.149	0.178
individual 3	-0.093	-0.031	0.042	0.077	0.104	0.125	0.153	0.18	0.197	0.112
individual 4	-0.007	-0.029	0.003	0.039	0.057	0.066	0.099	0.139	0.196	0.315
individual 5	0.084	0.115	0.01	-0.069	0.001	-0.001	-0.106	0.001	0	0.061
individual 6	0.235	0.142	0.071	0.138	0.138	0.082	0.049	0.037	0.055	0.135
individual 7	0.023	0.06	0.08	0.103	0.114	0.114	0.103	0.101	0.041	-0.02
individual 8	-0.003	-0.002	0.052	0.091	0.118	0.14	0.159	0.167	0.191	0.313
individual 9	-0.027	-0.055	0.032	0.082	0.102	0.138	0.155	0.162	0.15	0.193
individual 10	0.01	0.03	0.004	-0.025	-0.01	0.031	0.051	0.044	0.088	0.131
individual 11	-0.06	-0.033	0.095	0.143	0.156	0.16	0.169	0.166	0.168	0.191
individual 12	-0.044	-0.014	0.013	0.048	0.086	0.114	0.138	0.163	0.203	0.307
individual 13	-0.023	0.068	0.165	0.216	0.227	0.212	0.092	0.198	0.138	-0.078
individual 14	-0.218	NaN	0.104	0.142	0.168	0.151	0.139	0.123	0.076	-0.118
individual 15	-0.085	-0.081	0.011	0.102	0.143	0.153	0.151	0.112	-0.045	-0.536
individual 16	-0.021	0.016	0.042	0.073	0.122	0.159	0.198	0.241	0.29	0.348
individual 17	-0.107	-0.017	0.037	0.077	0.086	0.083	0.102	0.124	0.222	0.202
individual 18	-0.065	-0.046	-0.005	0.018	0.031	0.056	0.113	0.173	0.243	0.389
individual 19	-0.022	-0.049	0.096	0.099	0.125	0.114	0.113	0.123	0.154	0.222
individual 20	NaN	NaN	NaN	NaN	NaN	NaN	NaN	NaN	NaN	NaN
individual 21	-0.025	0.03	0.056	0.084	0.091	0.093	0.122	0.175	0.215	0.244
individual 22	-0.079	-0.055	0.028	0.091	0.141	0.166	0.186	0.222	0.275	0.379
individual 23	-0.038	-0.045	-0.025	0.007	0.036	0.063	0.097	0.11	0.151	0.243
individual 24	-0.037	0.007	0.088	0.143	0.159	0.202	0.206	0.218	0.189	0.203
individual 25	0.012	0.061	0.096	0.119	0.126	0.121	0.142	0.093	0.137	0.309
individual 26	-0.053	-0.034	-0.019	-0.019	-0.002	0.011	0.004	-0.014	-0.028	-0.1
individual 27	-0.043	-0.055	-0.044	0.059	0.047	0.061	0.069	0.043	0.093	0.257
individual 28	-0.132	-0.094	-0.039	0.017	0.026	0.02	0.07	0.048	0.115	0.373
individual 29	-0.011	-0.026	0.041	0.095	0.121	0.13	0.116	0.118	0.105	-0.069
individual 30	-0.039	-0.107	0.029	0.095	0.122	0.132	0.165	0.163	0.207	0.173
individual 31	-0.068	0.176	0.179	0.159	0.147	0.131	0.123	0.165	0.16	0.261
individual 32	0.026	0.027	0.045	0.099	0.134	0.171	0.197	0.186	0.227	0.306
individual 33	-0.009	0.017	0.063	0.09	0.039	0.04	0.043	0.026	-0.049	-0.151
individual 34	-0.088	0.016	0.159	0.183	0.187	0.196	0.142	0.198	0.223	0.045
individual 35	-0.008	-0.025	0.016	0	0.021	0.068	0.112	0.172	0.21	0.238
individual 36	-0.027	-0.028	-0.045	-0.032	-0.01	0.023	0.045	0.063	0.099	0.148
individual 37	-0.032	0.024	0.056	0.092	0.095	0.115	0.119	0.155	0.195	0.137
individual 38	0.046	0.02	0.066	0.072	0.072	0.099	0.13	0.131	0.165	0.047
individual 39	NaN	NaN	NaN	NaN	NaN	NaN	NaN	NaN	NaN	NaN
individual 40	-0.095	-0.094	-0.016	0.061	0.096	0.124	0.122	0.128	0.189	0.298
individual 41	-0.031	0.082	0.193	0.23	0.277	0.327	0.322	0.224	0.14	-0.166
individual 42	0.08	-0.011	-0.014	0.044	0.049	0.084	0.11	0.136	0.169	0.155
individual 43	-0.078	-0.037	-0.024	-0.005	0.026	0.052	0.07	0.092	0.156	0.311
AVERAGE	-0.028	-0.001	0.046	0.079	0.097	0.112	0.119	0.133	0.148	0.148

Table C.7 The *linear* correction values based on the regression point method. Moreover, this table contains the average correction for the *left* trials of all individuals that performed the walking condition. Corrections are given for all selected time intervals ranging from Initial Contact Phase (ICP) to Heel Lift

Name	ICP	2	3	4	5	6	7	8	9	Heel Lift
individual 1	0.261	0.502	0.671	0.741	0.774	0.791	0.793	0.787	0.736	0.7
individual 2	0.593	0.661	0.679	0.625	0.606	0.6	0.588	0.563	0.537	0.51
individual 3	0.316	0.515	0.624	0.673	0.694	0.71	0.709	0.697	0.668	0.685
individual 4	0.126	0.286	0.403	0.466	0.504	0.534	0.546	0.522	0.466	0.356
individual 5	0.162	-0.073	-0.23	-0.18	-0.157	-0.181	-0.185	-0.15	-0.184	-0.225
individual 6	0.79	0.485	0.433	0.347	0.233	0.168	0.138	0.118	0.097	0.038
individual 7	0.388	0.531	0.576	0.586	0.566	0.548	0.54	0.543	0.557	0.615
individual 8	0.198	0.411	0.521	0.541	0.523	0.481	0.423	0.345	0.263	0.133
individual 9	0.011	0.345	0.516	0.56	0.566	0.549	0.504	0.452	0.4	0.336
individual 10	0.211	0.127	0.169	0.185	0.234	0.26	0.268	0.283	0.28	0.229
individual 11	0.025	0.596	0.786	0.793	0.799	0.791	0.772	0.728	0.694	0.653
individual 12	0.097	0.296	0.409	0.467	0.485	0.475	0.444	0.394	0.308	0.192
individual 13	0.452	0.881	0.941	0.869	0.804	0.769	0.656	0.699	0.72	0.87
individual 14	0.199	NaN	0.776	0.818	0.798	0.779	0.83	0.847	0.902	1.084
individual 15	0.066	0.526	0.771	0.88	0.904	0.905	0.911	0.931	1.022	1.342
individual 16	0.347	0.604	0.757	0.869	0.932	0.974	1	1.006	0.991	0.936
individual 17	0.054	0.312	0.441	0.457	0.453	0.444	0.424	0.391	0.312	0.185
individual 18	0.03	0.167	0.247	0.286	0.305	0.306	0.276	0.203	0.094	-0.069
individual 19	0.286	0.464	0.663	0.684	0.681	0.7	0.736	0.786	0.803	0.81
individual 20	NaN	NaN	NaN	NaN	NaN	NaN	NaN	NaN	NaN	NaN
individual 21	0.213	0.378	0.442	0.443	0.425	0.416	0.384	0.316	0.217	0.094
individual 22	0.113	0.476	0.677	0.754	0.764	0.743	0.711	0.648	0.546	0.412
individual 23	0.089	0.216	0.321	0.398	0.445	0.471	0.476	0.465	0.464	0.419
individual 24	0.303	0.611	0.744	0.756	0.744	0.702	0.627	0.565	0.519	0.479
individual 25	0.465	0.568	0.589	0.57	0.538	0.507	0.487	0.466	0.443	0.386
individual 26	0.002	0.171	0.295	0.43	0.552	0.663	0.785	0.921	1.061	1.251
individual 27	0.119	0.277	0.456	0.663	0.595	0.631	0.658	0.697	0.727	0.688
individual 28	-0.174	0.146	0.278	0.359	0.403	0.422	0.472	0.49	0.493	0.424
individual 29	0.343	0.556	0.692	0.74	0.758	0.756	0.775	0.803	0.831	0.91
individual 30	-0.006	0.356	0.595	0.621	0.624	0.603	0.591	0.536	0.475	0.387
individual 31	0.591	0.683	0.577	0.484	0.378	0.292	0.204	0.108	0.014	-0.055
individual 32	0.341	0.507	0.635	0.715	0.747	0.751	0.727	0.704	0.641	0.483
individual 33	0.222	0.374	0.439	0.419	0.43	0.479	0.501	0.543	0.617	0.762
individual 34	0.243	0.706	0.806	0.732	0.663	0.585	0.526	0.468	0.37	0.327
individual 35	0.174	0.374	0.503	0.612	0.718	0.807	0.863	0.891	0.898	0.921
individual 36	-0.111	-0.026	0.021	0.083	0.123	0.139	0.133	0.115	0.073	0.004
individual 37	0.234	0.421	0.5	0.519	0.556	0.571	0.585	0.596	0.568	0.564
individual 38	0.349	0.463	0.529	0.552	0.576	0.592	0.576	0.558	0.517	0.504
individual 39	NaN	NaN	NaN	NaN	NaN	NaN	NaN	NaN	NaN	NaN
individual 40	-0.229	0.111	0.33	0.393	0.373	0.323	0.252	0.182	0.083	-0.034
individual 41	0.604	1.019	1.069	1.02	0.944	0.838	0.679	0.554	0.522	0.673
individual 42	0.256	0.307	0.533	0.655	0.768	0.864	0.93	0.97	1	0.995
individual 43	0.099	0.248	0.342	0.423	0.485	0.512	0.54	0.547	0.525	0.451
AVERAGE	0.216	0.414	0.525	0.561	0.569	0.567	0.557	0.544	0.519	0.519

Table C.8 The *constant* correction values based on the regression method. Moreover, it contains the average correction for the *right* trials of all individuals that performed the walking condition. Corrections are given for all selected time intervals ranging from Initial Contact Phase (ICP) to Heel Lift

Name	ICP	2	3	4	5	6	7	8	9	Heel Lift
individual 1	-0.045	-0.04	0.044	0.137	0.173	0.165	0.199	0.232	0.199	0.371
individual 2	-0.011	-0.03	0.024	0.05	0.062	0.079	0.111	0.138	0.073	0.105
individual 3	-0.119	0.011	0.11	0.158	0.17	0.168	0.162	0.138	0.065	-0.279
individual 4	-0.1	-0.181	-0.118	-0.06	-0.025	-0.036	0.001	0.022	0.096	0.317
individual 5	0.083	0.035	0.009	-0.04	0.026	0.048	0.053	0.04	0.039	0.157
individual 6	0.037	0.077	0.055	0.055	0.053	0.046	0.041	0.057	0.049	0.123
individual 7	0.279	0.536	-0.002	NaN	-0.296	0.166	0.11	0.142	0.146	0.141
individual 8	0.009	-0.012	0.027	0.073	0.113	0.143	0.171	0.168	0.185	0.229
individual 9	-0.047	-0.061	0.034	0.093	0.12	0.159	0.213	0.13	0.101	0.093
individual 10	0.035	0.027	0.017	0.05	0.082	0.063	0.069	0.091	0.117	0.142
individual 11	-0.06	-0.018	0.067	0.139	0.165	0.193	0.207	0.141	0.129	-0.103
individual 12	-0.015	-0.013	0	0.036	0.075	0.111	0.14	0.161	0.195	0.22
individual 13	-0.073	-0.063	0.024	0.067	0.073	0.086	0.095	0.058	-0.022	-0.46
individual 14	-0.193	0.008	0.171	0.221	0.21	0.16	0.156	0.124	0.147	0.127
individual 15	-0.058	-0.09	0.011	0.09	0.147	0.167	0.198	0.198	0.196	-0.024
individual 16	-0.095	-0.044	0.052	0.123	0.161	0.201	0.244	0.321	0.393	0.436
individual 17	-0.108	-0.014	0.025	0.056	0.092	0.108	0.134	0.157	0.296	0.294
individual 18	-0.145	-0.075	-0.015	0.032	0.068	0.09	0.128	0.218	0.268	0.414
individual 19	-0.087	-0.071	NaN	0.037	0.063	0.075	0.064	0.04	0.026	0.014
individual 20	0.025	0.072	0.122	0.097	0.077	0.062	0.045	0.047	0.064	0.144
individual 21	-0.073	0	0.085	0.141	0.168	0.167	0.189	0.23	0.284	0.345
individual 22	-0.167	-0.105	0.006	0.073	0.097	0.104	0.126	0.136	0.155	0.22
individual 23	-0.057	-0.086	-0.062	0.003	0.052	0.103	0.098	0.116	0.108	0.242
individual 24	-0.063	-0.053	0.041	0.083	0.106	0.148	0.178	0.195	0.205	0.389
individual 25	-0.06	-0.051	0.019	0.068	0.106	0.123	0.162	0.17	0.066	0.117
individual 26	-0.062	-0.044	-0.019	-0.017	0.023	0.033	0.054	0.097	0.125	0.115
individual 27	-0.117	-0.07	0.077	0.142	0.16	0.226	0.243	0.228	0.216	0.457
individual 28	-0.156	-0.229	-0.132	-0.011	0.055	0.07	0.102	0.214	0.289	0.494
individual 29	-0.128	-0.05	0.008	0.081	0.111	0.13	0.126	0.146	0.165	0.109
individual 30	-0.098	-0.094	0.028	0.094	0.142	0.166	0.188	0.206	0.253	0.131
individual 31	-0.084	0.021	0.116	0.209	0.172	0.122	0.166	0.172	0.103	-0.061
individual 32	0.013	-0.079	-0.02	0.038	0.09	0.111	0.113	0.093	0.077	0.074
individual 33	-0.066	-0.033	0.01	0.054	0.03	0.045	0.062	0.046	0.062	0.089
individual 34	-0.055	0.026	0.12	0.177	0.189	0.15	0.23	0.11	0.146	-0.019
individual 35	-0.034	-0.04	0.004	0.04	0.077	0.104	0.108	0.092	0.114	0.107
individual 36	-0.044	-0.04	-0.019	0.039	0.062	0.074	0.079	0.089	0.146	0.382
individual 37	-0.083	0.021	0.147	0.166	NaN	NaN	0.175	0.236	0.247	0.257
individual 38	-0.019	-0.02	0.007	0.047	0.082	0.122	0.188	0.146	0.136	0.057
individual 39	-0.155	-0.086	0.042	0.117	0.124	0.169	0.145	0.097	0.055	0.194
individual 40	-0.072	0.023	0.087	0.166	0.219	0.266	0.306	0.34	0.348	0.448
individual 41	-0.093	-0.003	0.079	0.123	0.14	0.168	0.16	0.075	-0.055	-0.348
individual 42	-0.028	-0.062	-0.121	0.024	0.044	0.082	0.103	0.096	0.04	-0.276
individual 43	-0.068	-0.04	-0.019	0.009	0.045	0.067	0.077	0.09	0.134	0.281
AVERAGE	-0.057	-0.024	0.027	0.078	0.093	0.119	0.138	0.141	0.144	0.144

Table C.9 The *linear* correction values based on the regression method. Moreover, it contains the average correction for the *right* trials of all individuals that performed the walking condition. Corrections are given for all selected time intervals ranging from Initial Contact Phase (ICP) to Heel Lift

Name	ICP	2	3	4	5	6	7	8	9	Heel Lift
individual 1	0.26	0.563	0.781	0.837	0.824	0.804	0.79	0.705	0.635	0.512
individual 2	0.062	0.188	0.255	0.229	0.208	0.167	0.11	0.027	-0.04	-0.083
individual 3	0.4	0.746	0.877	0.889	0.869	0.859	0.851	0.854	0.881	1.021
individual 4	-0.334	-0.085	0.217	0.4	0.535	0.65	0.766	0.852	0.916	0.88
individual 5	0.25	0.042	-0.005	0.074	0.105	0.077	0.051	0.01	-0.014	-0.072
individual 6	0.404	0.389	0.319	0.253	0.2	0.169	0.157	0.144	0.124	0.093
individual 7	1.337	0.213	-0.214	NaN	0.175	0.001	-0.156	-0.285	-0.439	-0.617
individual 8	0.199	0.346	0.479	0.521	0.512	0.466	0.396	0.313	0.218	0.103
individual 9	-0.014	0.41	0.621	0.678	0.696	0.677	0.607	0.544	0.536	0.544
individual 10	0.272	0.308	0.376	0.403	0.39	0.377	0.386	0.381	0.353	0.302
individual 11	0.017	0.545	0.773	0.823	0.831	0.81	0.764	0.726	0.71	0.778
individual 12	0.14	0.286	0.415	0.486	0.518	0.516	0.495	0.457	0.403	0.314
individual 13	0.016	0.297	0.44	0.477	0.481	0.482	0.463	0.461	0.46	0.555
individual 14	-0.011	0.923	1.074	1.032	0.98	0.978	1.039	1.058	1.084	1.159
individual 15	-0.016	0.461	0.777	0.922	0.967	0.988	0.997	0.985	0.977	1.067
individual 16	0.187	0.615	0.825	0.902	0.928	0.929	0.893	0.819	0.658	0.466
individual 17	0.003	0.292	0.428	0.464	0.485	0.477	0.454	0.407	0.312	0.152
individual 18	-0.031	0.201	0.327	0.377	0.397	0.37	0.352	0.27	0.133	-0.042
individual 19	0.043	0.152	NaN	0.423	0.452	0.452	0.469	0.49	0.554	0.621
individual 20	0.355	0.383	0.242	0.108	0.016	-0.053	-0.106	-0.149	-0.202	-0.286
individual 21	0.274	0.609	0.714	0.714	0.666	0.62	0.571	0.478	0.354	0.185
individual 22	-0.228	0.293	0.53	0.591	0.61	0.619	0.618	0.601	0.576	0.537
individual 23	0.018	0.16	0.3	0.373	0.398	0.382	0.352	0.319	0.278	0.227
individual 24	0.028	0.401	0.598	0.665	0.717	0.725	0.679	0.619	0.558	0.444
individual 25	0.239	0.494	0.644	0.723	0.758	0.773	0.778	0.765	0.768	0.798
individual 26	-0.001	0.232	0.423	0.583	0.729	0.86	0.975	1.074	1.173	1.235
individual 27	0.209	0.764	1.009	1.098	1.147	1.169	1.149	1.111	1.092	0.995
individual 28	-0.406	0.023	0.39	0.587	0.665	0.713	0.748	0.72	0.627	0.466
individual 29	0.174	0.478	0.654	0.742	0.762	0.777	0.799	0.824	0.82	0.83
individual 30	-0.071	0.428	0.669	0.749	0.759	0.74	0.713	0.633	0.559	0.489
individual 31	0.345	0.731	0.842	0.798	0.693	0.664	0.639	0.568	0.514	0.539
individual 32	-0.014	0.17	0.359	0.457	0.486	0.485	0.478	0.485	0.508	0.552
individual 33	0.028	0.261	0.43	0.465	0.513	0.561	0.619	0.686	0.757	0.813
individual 34	0.333	0.742	0.831	0.8	0.749	0.723	0.691	0.718	0.737	0.82
individual 35	0.126	0.342	0.482	0.575	0.622	0.641	0.664	0.698	0.733	0.778
individual 36	-0.028	0.208	0.357	0.424	0.448	0.459	0.465	0.468	0.438	0.304
individual 37	0.207	0.564	0.846	0.719	NaN	NaN	0.614	0.508	0.51	0.434
individual 38	0.153	0.256	0.334	0.369	0.361	0.323	0.24	0.147	0.07	0.009
individual 39	-0.089	0.434	0.633	0.689	0.708	0.635	0.589	0.58	0.616	0.644
individual 40	0.23	0.719	0.913	0.972	0.928	0.83	0.688	0.457	0.242	-0.014
individual 41	0.235	0.516	0.608	0.606	0.579	0.545	0.485	0.455	0.495	0.652
individual 42	0.009	0.177	0.513	0.705	0.815	0.909	0.977	1.068	1.185	1.464
individual 43	0.148	0.302	0.411	0.488	0.544	0.572	0.592	0.601	0.584	0.501
AVERAGE	0.127	0.386	0.536	0.6	0.601	0.593	0.579	0.55	0.522	0.522

C.2 Research Applications

For the determination of Cardan angles from pressure distribution measurements, we should restrict the pressure distributions to contain only the heel areas. In Section 2.2.6, the general principles are discussed for a division of the pressure distribution. One of the variables added to an individual's *'CompData.m'*-file was **heel_area**. This variable was used to determine CoP path of the heel area of a pressure distribution together with the application **FootCalculationEx**.

In **Validation_Heel_Model**, the orientation of the heel was calculated from CoP paths using the applications **Heel3Dtracker_sphere_fitted** and **Heel3Dtracker**. Furthermore, **Validation_Heel_Model** validated the angles describing heel orientation obtained from pressure measurements with respect to the ones based on motion data. Within the process of validation, a few more applications were used, but the three mentioned above are most important.

In analysing the consequences of the different choices made during the modelling process, we developed a few applications. In **Error_CoP_HeelArea**, we analysed the influence of the choice of the heel area on the CoP paths that followed from this choice. Application **Error_Hiel_Scheme** is similar to **Error_CoP_HeelArea**; it also analyses the influence of the heel area. In this case not the direct influence on the CoP paths, but the indirect influence on the angles calculated from the CoP paths. Consequences of the size of the radius of the sphere were analysed with **Group_Shere_Radius_Analysis** and **Person_Radius_Analysis**.

Finally, we mention the application **LRF_to_CoP** that calculated the CoP path for a sphere given the radius of this sphere and a time series of reference frames.

Appendix D

Studying Metatarsal Head Motion: Details

D.1 Left and Right Covering Circles

This appendix accompanies Chapter 4. We show the diameters of the circles that cover 90% of the marker positions during a chosen time period, see Figure D.1. The markers are attached on the side of metatarsal head one, on the side of metatarsal head five, and attached between metatarsal heads two and three. The chosen time period is metatarsal contact period starting from forefoot flat till one metatarsal is lifted from the ground. The difference between Figure 4.3 and Figure D.1 is that in the latter figure the histograms of the distributions are split in left and right trials. The left-hand side of Figure D.1 contains data from the left trials and the right-hand side contains data from the right trials.

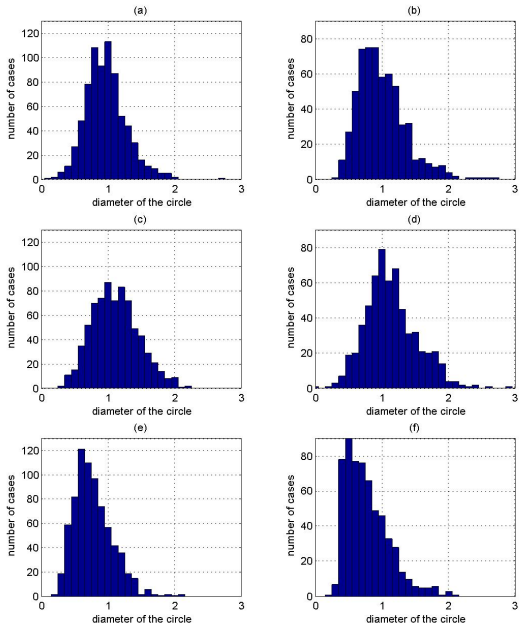

Figure D.1 The movement of the metatarsal heads during the time period starting from the moment that all metatarsal heads are in contact and ending at the moment that one of these heads loses contact. In (a), (c), and (d) the distributions of the left trials are depicted and in (b), (d), and (e) the distributions of the right trials are depicted. Both columns contain the distributions of the diameters of the circles containing 90% of the motion of the markers attached to metatarsal head one ((a) and (b)), attached between metatarsal heads two and three ((c) and (d)), and attached to metatarsal head five ((e) and (f)). The diameter sizes are scaled with respect to the length of the diagonal of a pressure sensor.

D.2 Research Applications

For the study of metatarsal head motion, the applications:
Group_Max_Pressure_Sensor_Movement and **MetaHead_Movement** were developed. The first application is the shell application that reads in the *CompData.m*-files of all individuals; it calls the second application. As output a Matlab m-file is constructed and saved in the root directory with a name specified in the code of **Group_Max_Pressure_Sensor_Movement**. This file contains one cell array with as many entries as there are individuals. An entry itself is a cell array with two entries. The first one related to the left trials of the individual and the second one to its right trials. These subentries are vectors, they contain the size, expressed in millimeters, of the diameters of 90% covering circles for the left and right trials.

In studying the metatarsal head motion from pressure data, the application **Max_Pressure_Sensor_Movement** was developed. The remarks made above for applications used in studying marker positions do also apply here.

The pressure and motion variables used in studying the distance between metatarsal head one and five are calculated by **PersonPressureDataAnalysis** for an individuals data set. **GroupStatsData** is used as shell for **PersonPressureDataAnalysis** in order to calculate the variables for a session type and produces a file that can be read in Excel and SPSS.

Finally, the comparison of metatarsal curves from pressure data and motion data is performed in **GroupCompare_Meta_Curves**. It saves the comparison data to a file in the root directory with a name specified in the code itself. This Matlab file contains one cell array variable with as many entries as there are individuals. Each entry contains two subentries related to left and right trials, the subentries have a matrix format. The rows of the matrices relate trials and the columns in pairs are related to the comparison methods. These pairs of columns contain give the comparison values in cm of the point comparison and the global comparison, respectively. The comparison data of an individual were computed with **Compare_MetaCurves**, called from within **GroupCompare_Meta_Curves**. These computations in **Compare_MetaCurves** were performed on data contained in *CompData.m* for the five area method, with **MG** and **MGadjusted** to compute Gaussian mixtures, and with **PeaksStudy** to compute local maxima.

Bibliography

[1] M. Acrcan and M. Brull. A fundamental characteristic of the human body and foot, the foot-ground pressure pattern. *Journal of Biomechanics*, 9:453–457, 1976.

[2] P. Aerts, R. Kerr, D. De Clercq, D. Ilsley, and R. Alexander. The mechanical properties of the human heel pad: a paradox resolved. *Journal of Biomechanics*, 28:1299–1308, 1995.

[3] I. Alexander, E. Chao, and K. Johnson. The assessment of dynamic foot-to-ground contact forces and plantar pressure distribution: a review of the evolution of current techniques and clinical applications. *Foot and Ankle*, 11(3):152–167, December 1990.

[4] F. Anderson and M. Pandy. Dynamic optimization of human walking. *Journal of Biomechanical Engineering*, 123:381–390, 2001.

[5] A. Arampatzis, G.-P. Bruggemann, and G. Klapsing. A three-dimensional shank-foot model to determine the foot motion during landings. *Medicine & Science in Sports & Exercise*, pages 130–138, 2002.

[6] G. Arangio, D. Phillippy, D. Xiao, W.-K. Gu, and E. Salathe. Subtalar pronation - relationship to the medial longitudinal arch loading. *Foot and Ankle International*, 21(3):216–220, 2000.

[7] G. Arangio and E. Salathe. Medial displacement calcaneal osteotomt reduces the excess forces in the medial longitudinal arch of the flat foot. *Clinical Biomechanics*, pages 535–539, 2001.

[8] M. Areblad, B. Nigg, J. Ekstrand, K. Olsson, and H. Ekstrom. Three-dimensional measurement of rearfoot motion during running. *Journal of Biomechanics*, 23(9):933–940, 1990.

[9] H. Aritomi, M. Morita, and K. Yonemoto. A simple method of measuring the footsole pressure of normal subjects using prescale pressure-detecting sheets. *Journal of Biomechanics*, 16(2):157–165, 1983.

[10] D. Armstrong and S. Stacpoole-Shea. Total contact casts and removable cast walkers: migration of plantar heel pressure. *Journal of American Podiatric Medical Association*, 89(1):50–53, January 1999.

[11] A. Arndt, P. Westblad, and A. L. I. Ekenman. A comparison of external plantar loading and in vivo local metatarsal deformation wearing two different military boots. *Gait and Posture*, 18:20–26, 2003.

[12] S. Barnett, J. Cunningham, and S. West. A comparison of vertical force and temporal parameters produced by an in-shoe pressure measuring system and a force plate. *Clincal Biomechanics*, 16:353–357, 2001.

[13] M. Benedetti, F. Catani, A. Leardini, E. Pignotti, and S. Giannini. Data management in gait analysis for clinical applications. *Clinical Biomechanics*, 13(3):204–215, 1998.

[14] P. Bennet and L. Duplock. Pressure distribution beneath the human foot. *Journal of American Podiatric Medical Association*, 83(12):674–678, December 1993.

[15] P. Bennett, V. Miskewitch, and L. Duplock. Quantitative analysis of the effects of custom-molded orthoses. *Journal of American Podiatric Medical Association*, 86(7):307–310, July 1996.

[16] P. Bennett, A. Stocks, and D. Whittam. Analysis of risk factors for neuropathic foot ulceration in diabetes mellitus. *Journal of American Podiatric Medical Association*, 86(3):112–116, March 1996.

[17] C. Bertsch, H. Unger, W. Winkelmann, and D. Rosenbaum. Evaluation of early walking patterns from plantar pressure distribution measurements. first year results of 42 children. *Gait and Posture*, 19:235–242, 2004.

[18] R. Betts, c.I. Franks, and T. Duckworth. Analysis of pressures and loads under the foot. part i: Quantitation of the static distribution using the pet computer. *Clin. Phys. Physiol Meas.*, 1(2):101–112, 1980.

[19] M. Birtane and H. Tuna. The evalution of plantar pressure distibution in obese and non-obse adults. *Clincal Biomechanics*, 19:1055–1059, 2004.

[20] Y. Blanc, C. Balmer, T. Landis, and F. Vingerhoets. Temporal parameters and patterns of the foot roll over during walking: normative data for healty adults. *Gait and Posture*, (10):97–108, 1999.

[21] A. Bryant, P. Tinley, and K. Singer. Plantar pressure distribution in normal, hallux valgus and hallux limitus feet. *The Foot*, 9:115–119, 1999.

[22] A. Bryant, P. Tinly, and K. Singer. Normal values of plantar pressure measurements determined using the emed-sf system. *Journal of American Podiatric Medical Association*, 90(6):295–299, June 2000.

[23] J. Burnfield, C. Few, O. Mohamed, and J. Perry. The influence of walking speed and footwear on plantar pressures in older adults. *Clincal Biomechanics*, 19:78–84, 2004.

[24] J. Burns. The assessment and management of a patient with idiopathic pes cavus. *Australian Journal of Podiatric Medicine*, 38(2):49–53, 2004.

[25] C. Busseuil, P. Freychat, E. Brunet Guedj, and J. Lacour. Rearfoot-forefoot orientation and traumatic risk for runners. *Foot and Ankle International*, 19(1):32–36, January 1998.

[26] M. Carson, M. Harrington, N. Thompson, J. O'Connor, and T. Theologis. Kinematic analysis of a multi-segment foot model for research and clinical applications: a repeatability analysis. *Journal of Biomechanics*, 34:1299–1307, 2001.

[27] P. Cavanagh. The biomechanics of lower extremetiy action in distance running. *Foot and Ankle*, 7(4):197–217, February 1987.

[28] P. Cavanagh. *Biomechanics of distance running.* Human Kinetics Books, 1990.

[29] P. Cavanagh and M. Ae. A technique for the display of foot pressure distribution beneath the foot. *Journal of Biomechanics*, 13:69–75, 1980.

[30] P. Cavanagh, E. Hennig, R. Bunch, and N. Macmillan. *A new device for the measurement of pressure distribution inside the shoe,*, volume 8B of *International series on biomechanics*, pages 1089–1095. Human Kinetics Publishers, Champaign, Illinois, 1983.

[31] P. Cavanagh, E. Morag, A. Boulton, K. Deffner, and S. Pammert. The relationship of static foot structure to dynamic foot function. *Journal of Biomechanics*, 30(3):243–250, 1997.

[32] W.-N. Chang, A. Tsirikos, F. Miller, J. Schuyler, and J. Glutting. Impact of changing foot progression angle on foot pressure measurement in children with neuromuscular diseases. *Gait and Posture*, 20:14–19, 2004.

[33] H. Chen, B. Nigg, M. Hulliger, and J. de Koning. Influence of sensory input on plantar pressure distribution. *Clincal Biomechanics*, 10(5):271–274, 1995.

[34] K. Chesnin, L. Selby-Silverstein, and M. Besser. Comparison of an in-shoe pressure measurement device to a force plate: concurrent validity of center of pressure measurements. *Gait and Posture*, 12:128–133, 2000.

[35] J. Chiang and G. Wu. The influence of foam surfaces on biomechanical variables contributing to postural control. *Gait and Posture*, (5):239–245, 1997.

[36] D. D. Clercq, P. Aerts, and M. Kunnen. The mechanical charateristics of the human heel pad during foot strike in running: an in vivo cineradiographic study. *Journal of Biomechanics*, 27(10):1213–1222, 1994.

[37] J. Cobb and D. Claremont. Transducers for foot pressure measurement: survey of recent developments. *Medical & Biological Engineering & Computing*, 33:525–532, 1995.

[38] G. Cole, B. Nigg, G. Fick, and M. Morlock. Internal loading of the foot and ankle during impact in running. *Journal of Applied Biomechanics*, 11:25–46, 1995.

[39] G. Cole, B. Nigg, J. Ronsky, and M. Yeadon. Application of the joint coordinate system to three-dimensional joint attitude and movement representation: a standardization proposal. *Journal of Biomechanical Engineering*, 115(4A):344–349, 1993.

[40] M. Cornwall and T. McPoil. The relationship between maximum plantar pressures and anterior-posterior shear during walking. *The lower extremity*, 2(2):141–146, June 1995.

[41] M. Cornwall and T. McPoil. Velocity of the center of pressure during walking. *Journal of American Podiatric Medical Association*, 90(7):334–338, July/August 2000.

[42] M. Cornwall and T. McPoil. Motion of the calcaneus, navicular, and first metatarsal during the stance phase of walking. *Journal of American Podiatric Medical Association*, 92(2):67–76, 2002.

[43] M. Cornwall and T. McPoil. Reliability and validity of center of pressure quantification. *Journal of the American Podiatric Medical Association*, 93(2):142–149, March/April 2003.

[44] J. D'Amico. The f-scan system with edg module for gait analysis in the pediatric patient. *Journal of American Podiatric Medical Association*, 88(4):166–175, April 1998.

[45] J. D'Amico, H. Dinowitz, and M. Polchaninoff. Limb length discrepancy: an electrodynographic analysis. *Journal of American Podiatric Medical Association*, 75(12):639–643, December 1985.

[46] M. D'Amico and G. Ferrigno. Technique for the evaluation of derivatives from noisy biomechanical displacement data using a model-based-bandwith-selection procedure. *Medical Biology and Engineering Computing*, 28:407–415, 1990.

[47] B. Davis, R. Cothren, P. Quesada, S. Hansen, and J. Perry. Frequency content of normal and diabetic plantar pressure profiles: implications for the selection of transducer sizes. *Journal of Biomechanics*, 29(7):979–983, 1996.

[48] A. De Cock, D. De Clercq, T. Willems, and E. Witvrouw. Temporal characteristics of foot roll-over during barefoot jogging: reference data for young adults. *Gait and Posture*, pages 1–8, 2005.

[49] B. De Wit, D. De Clercq, and P. Aerts. Biomechanical analysis of the stance phase during barefoot and shod running. *Journal of Biomechanics*, 33:269–278, 2000.

[50] L. Draganich, T. Andriacchi, A. Strongwater, and J. Galante. Electronic measurement of instantaneous foot-floor contact patterns during gait. *Journal of Biomechanics*, 13:875–880, 1980.

[51] E. Eils, S. Behrens, O. Mers, L. Thorwesten, K. Volker, and D. Rosenbaum. Reduced plantar sensation causes a cautious walking patten. *Gait and Posture*, in press.

[52] E. Eils, S. Nolte, M. Tewes, L. Thorwesten, K. Volker, and D. Rosenbaum. Modified pressure distribution patterns in walking following reduction of plantar sensation. *Journal of Biomechanics*, 35:1307–1313, 2002.

[53] J. Eisenhardt, D. Cook, I. Pregler, and H. Foehl. Changes in temporal gait characteristics and pressure distribution fore bare feet versus various heights. *Gait and Posture*, 4:280–286, 1996.

[54] J. Eng and D. Winter. Kinetic analysis of the lower limbs during walking: what information can be gained from a three-dimensional model? *Journal of Biomechanics*, 28(6):753–758, 1995.

[55] V. Femery, P. Moretto, H. Renaut, A. Thevenon, and G. Lensel. Measurement of plantar pressure distribution in hemiplegic children: changes to adaptative gait patterns in accordance with deficiency. *Clincal Biomechanics*, 17:406–413, 2002.

[56] J. Ferrari and J. Malone-Lee. The shape of the metatarsal head as a cause of hallux abductovalgus. *Foot and Ankle International*, 23(3):236–242, 2002.

[57] P. Finch. Technology in biomedicine: the emed pedar pressure measurement system. *The Foot*, 9:1–5, 1999.

[58] J. Fleischli, L. Lavery, S. Vela, H. Ashry, and D. Lavery. Comparison of strategies for reducing pressure at the site of neuropathic ulcers. *Journal of American Podiatric Medical Association*, 87(10):466–472, October 1997.

[59] A. Forner Cordero, H. Koopman, and F. van der Helm. Use of pressure insoles to calculate the complete ground reaction forces. *Journal of Biomechanics*, in press.

[60] B. Fregly and W. Sawyer. Estimation of discretization errors in contact pressure measurement. *Journal of Biomechanics*, 36:609–613, 2003.

[61] P. Freychat, A. Belli, J.-P. Carret, and J.-R. Lacour. Relationship between rearfoot and forefoot. *Medicine & Science in Sports & Exercise*, pages 225–232, 1996.

[62] R. Frykberg, L. Bailey, A. Matz, L. Panthel, and G. Ruesch. Offloading properties of a rocker insole: a preliminary study. *Journal of American Podiatric Medical Association*, 92(1):48–53, January 2002.

[63] E. Fuller, S. Schroeder, and J. Edwards. Reduction of peak pressure on the forefoot with a rigid rocker-bottom postoperative shoe. *Journal of American Podiatric Medical Association*, 91(10):501–507, November/December 2001.

[64] B. Gastwirth, T. O'Brien, R. Nelson, D. Manger, and S. Kindig. An electrodynographic study of foot function in shoes of varying heel heights. *Journal of American Podiatric Medical Association*, 81(9):463–472, September 1991.

[65] M. Gaviria, M. D'Angeli, P. Chavet, J. Pelissier, E. Peruchon, and P. Rabischong. Plantar dynamics of hemiplegic gait: a methodological approach. *Gait and Posture*, 4:297–305, 1996.

[66] A. Gefen, M. Megido-Ravid, and Y. Itchak. In vivo biomechanical behavior of the human heel pad during stance phase of gait. *Journal of Biomehanics*, 34:1661–1665, 2001.

[67] A. Gefen, M. Megido-Ravid, Y. Itzchak, and M. Arcan. Biomechanical analysis of the three-dimensional foot structure during gait: a basic tool for clinical applications. *Journal of Biomechanical Engineering*, 122:630–639, December 2000.

[68] A. Gefen, M. Megido-Ravid, Y. Itzchak, and M. Arcan. Analysis of muscular fatique and foot stability during high-heeled gait. *Gait and Posture*, 15:56–63, 2002.

[69] M. Gerber. A system for measuring dynamic pressure distribution under the human foot. *Journal of Biomechanics*, 15(3):225–227, 1982.

[70] C. Giacomozzi, V. Macellari, A. Leardini, and M. Benedetti. Integrated pressure-force-kinematics measuring system for the characteristics of plantar foot loading during locomotion. *Medical & Biological Engineering & Computing*, 38:156–163, 2000.

[71] G. Giakas and V. Baltzopoulos. A comparison of automatic filtering techniques applied to biomechanical walking data. *Journal of Biomechanics*, 30(8):847–850, 1997.

[72] L. Gilchrist and D. Winter. A two-part, viscoelastic foot model for use in gait simulations. *Journal of Biomechanics*, 29(6):795–800, 1996.

[73] D. Grieve and T. Rashdi. Pressures under the normal feet in standing and walking as measured by a foil pedobarography. *Annuals of the Rheumatic Diseases*, 43:816–818, 1984.

[74] E. Grood and W. Suntay. A joint coordinate system for the clinical description of three-dimensional motions: application to the knee. *Journal of Biomechanical Engineering*, 105(2):136–144, 1983.

[75] H. Guler, N. Berme, and S. Simon. A viscoelastic sphere model of the representation of plantar soft tissue during simulations. *Journal of Biomechanics*, 31:847–853, 1998.

[76] F. Hagman. *Foot kinematics described from presuure plate measurements*. Eindhoven university press, 2001.

[77] A. Hallemans, K. D'Aout, D. De Clercq, and P. Aerts. Pressure distribution patterns under the feet of new walkers: the first two month of independent walking. *Foot and Ankle International*, 24(5):444–453, May 2003.

[78] A. Hallemans, D. De Clercq, S. Van Dongen, and P. Aerts. Changes in foot-function parameters during the first 5 months after the onset of independent walking: a longitudinal follow-up study. *Gait and Posture*, pages 1–7, in press.

[79] A. Hamel, N. Sharkey, F. Buczek, and J. Michelson. Relative motions of the tibia, talus, and calcaneus during the stance phase of gait: a cadavar study. *Gait and Posture*, 20(2):147–153, 2004.

[80] T. Han, N. Paik, and M. Im. Quantification of the path of center of pressure (cop) using an f-scan in-shoe transducer. *Gait and Posture*, (10):248–254, 1999.

[81] A. Hansen and D. C. amd E.H. Knox. Roll-over shapes of human locomoter systems: effects of walking speed. *Clinical Biomechanics*, 19:407–414, 2004.

[82] A. Harrison and J. Folland. Investigation of gait protocols for plantar pressure measurement of non-pathological subjects using a dynamic pedobarograph. *Gait and Posture*, (6):50–55, 1997.

[83] M. Hastings, P. Commean, K. Smith, and T. Pilgram. Aligning anatomical structure from spiral x-ray computed tomography with plantar pressure data. *Clinical Biomechanics*, 18:877–882, 2003.

[84] N. Hayafune, Y. Hayafune, and H. Jacob. Pressure and force distribution characteristics under the normal foot during the push-off phase in gait. *The Foot*, 9:88–92, 1999.

[85] R. A. Hennacy and R. Gunther. A piezoelectric crystal method for measuring static and dynamic pressure distributions in the feet. *Journal of American Podiatry Association*, 65(5):444–449, May 1975.

[86] E. Hennig, P. Cavanagh, and N. Macmillan. *Pressure distribution measurement by high precision piezoelectric ceramic force transducers,*, volume 8B of *International series on biomechanics*, pages 1081–1088. Human Kinetics Publishers, Champaign, Illinois, 1983.

[87] E. Hennig and D. Rosenbaum. Pressure distribution patterns under the feet of children in comparison with adults. *Foot and Ankle*, 11(5):306–311, April 1991.

[88] A. Hillmann, D. Rosenbaum, and W. Winkelmann. Plantar and dorsal foot loading measurements in patients after rotationplasty. *Clincal Biomechanics*, 15:359–364, 2000.

[89] A. Hills, E. Hennig, N. Byrne, and J. Steele. The biomechanics of adiposity - structural and funcitonal limitations of obesity and implications for movement. *Obesity Reviews*, 3:35–43, 2002.

[90] M. Hodge, T. Bach, and G. Carter. Orthotic management of plantar pressure and pain in rheumatoid arthritis. *Clincal Biomechanics*, (14):567–575, 1999.

[91] A. Hof, M. Gazendam, and W. Sinke. The condition for dynamic stability. *Journal of Biomechanics*, 38:1–8, 2005.

[92] R. Hosein and M. Lord. A study of in-shoe plantar shear in normals. *Clincal Biomechanics*, 15:46–53, 2000.

[93] C. House, C. Waterworth, A. Allsopp, and S. Dixon. The influence of simulated wear upon the ability of insoles to reduce peak pressures during running when wearing military boots. *Gait and Posture*, 16:297–303, 2002.

[94] J. Hughes, P. Clark, K. Linge, and L. Klenerman. A comparison of two studies of the pressure distribution under the feet of normal subjects using different equipment. *Foot and Ankle*, 14(9):514–519, December 1993.

[95] J. Hughes, S. Kriss, and L. Klenerman. A clincian's view of foot pressure: A comparison of three different methods of measurement. *Foot and Ankle*, 7(5):277–284, April 1987.

[96] R. Hughes, H. Rowlands, and S. McMeekin. A laser plantar pressure sensor for the diabetic foot. *Medical Engineering & Physics*, 22:149–154, 2000.

[97] A. Hunt and R. Smith. Mechanics and control of the flat versus normal foot during the stance phase of walking. *Clinical Biomechanics*, 19:391–397, 2004.

[98] A. Hunt, R. Smith, M. Torode, and A.-M. Keenan. Inter-segment foot motion and grond reaction forces over the stance phase of walking. *Clinical Biomechanics*, 16:592–600, 2001.

[99] W. Hutton and G. Drabble. An apparatus to give the distribution of vertical load under the foot. *Rheum. phys. Med.*, 11:313–317, 1972.

[100] C. Imhauser, S. Siegler, N. Abidi, and D. Frankel. The effect of posterior tibilias tendon dysfunction on the plantar pressure characteristics and the kinematics of the arch and the hindfoot. *Clinical Biomechanics*, 19:161–169, 2004.

[101] H. Jacobs. Forces acting in the forefoot during normal gait - an estimate. *Clincial Biomechanics*, 16:783–792, 2001.

[102] W. James, J. Orr, and T. Huddleston. A load cell system in foot pressure analysis. *Engineering in Medicine*, 11(3):121–122, 1982.

[103] C. Jordan and R. Bartlett. Pressure distribution and perceived comfort in casual footwear. *Gait and Posture*, 3(4):215–220, 1995.

[104] I. Kapandji. *Bewegingsleer deel II. De onderste extremiteit.* Bohn, Scheltema & Holkema, Utrecht, 3 edition, 1986.

[105] T. Kastenbauer, S. Sauseng, G. Sokol, M. Auinger, and K. Irsigler. A prospective study of predictors for foot ulceration in type 2 diabetes. *Journal of American Podiatric Medical Association*, 91(7):343–350, July/August 2001.

[106] E. Kellis. Plantar pressure distribution during barefoot standing, walking, and landing in preschool boys. *Gait and Posture*, 14:92–97, 2001.

[107] V. Kelly, M. Mueller, and D. Sinacore. Timing of peak plantar pressure during the stance phase of walking: a study of patients with diabetes mellitus and transmetatarsal amputation. *Journal of American Podiatric Medical Association*, 90(1):18–23, January 2000.

[108] R. Ker. The time-dependent mechanical properties of the human heel pad in the context of locomotion. *Journal of Experimental Biology*, 199(7):1501–1508, 1996.

[109] T. Kernozek, E. LaMott, and M. Dancisak. Reliability of an in-shoe pressure measurement system during treadmill walking. *Foot and Ankle International*, 17(4):204–209, April 1996.

[110] S. Kimmeskamp and E. Hennig. Heel to toe motion characteristics in parkinson patients during free walking. *Clincal Biomechanics*, 16:806–812, 2001.

[111] S. Kravitz, S. Huber, C. Murgia, K. Fink, M. Shaffer, and L. Varela. Biomechanical study of bunion deformity and stress produced in classical ballet. *Journal of American Podiatric Medical Association*, 75(7):338–345, July 1985.

[112] C. Kwak, J. Lee, S. Jin, and M. Chung. A biomechanical analysis of optimal midsole hardness and thickness of the marathon shoes. *Korean Journal of Sport Science*, (6):121–143, 1991.

[113] K. Landorf and A.-M. Keenan. Efficacy of foot orthoses: what does the literature tell us. *Journal of American Podiatric Medical Association*, 90(3):149–158, March 2000.

[114] L. Lavery. Novel methodology to obtain salient biomechanical characteristics of insole materials. *Journal of American Podiatric Medical Association*, 87(6):266–271, June 1997.

[115] A. Leardini, M. Benedetti, F. Catani, L. Simoncini, and S. Giannini. An anatomically based protocol for the description of foot segment kinematics during gait. *Clinical Biomechanics*, 14:528–536, 1999.

[116] W. Ledoux and H. Hillstrom. The distributed plantar vertical force of neutrally aligned and pes planus feet. *Gait and Posture*, 15:1–9, 2002.

[117] A. Leung, J. Cheng, and A. Mak. Calculation of contact area ratio using dynamic foorprint. *Orthopadie-Technik Quartely*, (1):7–10, 2001.

[118] P. Li and Z. Ladin. Mathematical modelling of the effect of sole elasticity distribution on pronation. *Journal of Biomechanics*, 25(5):501–510, 1992.

[119] M. Lord. Foot pressure measurement: a review of methodology. *Journal of Biomedical Engineering*, 3:91–99, April 1981.

[120] M. Lord. Spatial resolution in plantar pressure measurement. *Med. Eng. Phys.*, 19(2):140–144, 1997.

[121] M. Lord and R. Hosein. A study of in-shoe plantar shear in patients with diabetic neuropathy. *Clincal Biomechanics*, 15:278–283, 2000.

[122] M. Lord, D. Reynolds, and J. Hughes. Foot pressure measurement: a review of clinical findings. *Journal of Biomedical Engineering*, 8:283–294, 1986.

[123] E. Luger, M. Nissan, A. Karf, E. Steinberg, and S. Dekel. Patterns of weight distribution under the metatarsal heads. *The Journal of Bone and Joint Surgery*, 81-B(2):199–201, March 1999.

[124] A. Lundberg. *Patterns of motion of the ankle/foot complex.* PhD thesis, Departement of Orthopaedics, Karolinska Hospital, 1988.

[125] A. Lundberg. Kinematics of the ankle and foot. *Acta Orthop Scand Suppl*, 60(1), 1989.

[126] A. Lundberg, O. Svensson, C. Bylund, I. Goldie, and G. Selvik. Kinematics of the ankle/foot complex - part 2: Pronation and supination. *Foot and Ankle International*, 9(5), 1989.

[127] A. Lundberg, O. Svensson, G. Nemeth, and G. Selvik. The axis of rotation of the ankle joint. *Journal of Bone and Joint Surgery*, 71-B:94–99, 1989.

[128] B. MacWilliams, M. Cowely, and D. Nicholson. Foot kinematics and kinetics during adolescent gait. *Gait and Posture*, 17:214–224, 2003.

[129] M. Mandato and E. Nester. The effect of increasing heel height on forefoot peak pressure. *Journal of American Podiatric Medical Association*, 89(2):75–80, February 1999.

[130] I. Mathieson, D. Upton, and A. Birchenough. Comparison of footprint parameters calculated from static and dynamic footprints. *The Foot*, 9:145–149, 1999.

[131] I. McClay. The evolution of the study of the mechanics of running; relationship to injury. *Journal of the American Podiatric Medical Association*, 90(3):133–148, March 2000.

[132] I. McClay and K. Manal. Three-dimensional kinetic analysis of running: significance of secondary planes of motion. *Medicine & Science in Sports & Exercise*, 31(11):1629–1639, 1999.

[133] T. McPoil and M. Cornwall. Effect of insole material on force and plantar pressure during walking. *Journal of American Podiatric Medical Association*, 82(8):412–416, August 1992.

[134] T. McPoil and M. Cornwall. Variability of the center of pressure pattern integral during walking. *Journal of American Podiatric Medical Association*, 88(6):259–267, June 1998.

[135] T. McPoil, M. Cornwall, L. Dupuis, and M. Cornwell. Variability of plantar pressure data: a comparison of the two-step and midgait methods. *Journal of American Podiatric Medical Association*, 89(10):495–500, October 1999.

[136] T. McPoil, W. Yamada, W. Smith, and M. Cornwall. The distribution of plantar pressures in american indians with diabetes mellitus. *Journal of American Podiatric Medical Association*, 91(6):280–287, June 2001.

[137] D. Meglan. *Enhanced analysis of human locomotion.* PhD thesis, Ohio State Univeristy, 1991.

[138] K. Messing and A. Kilbom. Standing and very slow walking: foot pain-pressure threshold, subjective pain experience and work activity. *Applied Ergonomics*, 32:81–90, 2001.

[139] B. Meyers-Rice, L. Sugars, T. McPoil, and M. Cornwall. Comparison of three methods for obtaining plantar pressures in nonpathologic subjects. *Journal of American Podiatric Medical Association*, 84(10):499–504, October 1994.

[140] S. Meyring, R. Diehl, T. Milani, E. Hennig, and P. Berlit. Dynamic plantar pressure distribution measurement in hemiparetic patients. *Clincal Biomechanics*, 12(1):60–65, 1997. 1997.

[141] J. Miller-Young, N. Duncan, and G. Baroud. Material properties of the human calcaneal fat pad in compression: experiment and theory. *Journal of Biomechanics*, 35(12):1523–1531, 2002.

[142] E. Morag and P. Cavanagh. Stuctural and functional predictors of regional peak pressures under the foot during walking. *Journal of Biomechanics*, (32):359–370, 1999.

[143] M. Morlock. *A generalized three-dimensional six-segment model of the ankle and foot.* PhD thesis, Department of Medical Science, University of Calgary, 1989.

[144] M. Morlock and B. Nigg. Theoretical considerations and practical results of the influence of the representation of the foot for the estimation of internal forces with models. *Clinical Biomechanics*, 6:3–13, 1991.

[145] M. Mueller. Use of an in-shoe pressure measurement system in the mangement of patients with neuropathic ulcers of metatarsalgia. *JOSPT*, 21(6):328–336, June 1995.

[146] M. Mueller, M. Hastings, P. Commean, K. Smith, T. Pilgram, D. Robertson, and J. Johnson. Forefoot structural predictors of plantar pressures during walking in people with diabetes and peripheral neuropathy. *Journal of Biomechanics*, 36:1009–1017, 2003.

[147] M. Mueller and M. Strube. Generalizability of in-shoe peak pressure measures using the f-scan system. *Clincal Biomechanics*, 11(3):159–164, 1996.

[148] D. Nawoczenski, J. Birke, and W. Coleman. Effect of rocker sole design on plantar forefoot pressures. *Journal of American Podiatric Medical Association*, 78(9):455–460, September 1988.

[149] C. Nester. Contemporary issues in foot and ankle kinematics. In P. Scherer, editor, *The sixth international conference on foot biomechanics and orhotic therapy*, 2003.

[150] C. Nester, P. Bowker, and P. Bowden. Kinematics of the midtarsal joint during standing leg rotation. *Journal of American Podiatric Medical Association*, 92(2):77–81, 2002.

[151] C. Nicolopoulos, E. Anderson, S. Solomonidis, and P. Giannoudis. Evaluation of the gait analysis f-scan pressure system: clinical tool or toy. *The Foot*, 10:124–130, 2000.

[152] B. Nigg. *Biomechanics of running shoes*, chapter Experimental techniques used in running shoe research, pages 27–61. Human Kinetics, Champaign, IL., 1986.

[153] B. Nigg, G. Cole, and W. Nachbauer. Effects of arch height of the foot on angular motion of the lower extremities in running. *Journal of Biomechanics*, 26(8):909–916, 1993.

[154] B. Nigg and W. Herzog. *Biomechanics of the musculo-skeletal system.* John Wiley and Sons, 1994.

[155] T. Novacheck. The biomechanics of running. *Gait and Posture*, (7):77–95, 1998.

[156] A. Novick, J. Stone, J. Birke, D. Brasseaux, J. Broussard, A. Hoard, and E. Hawkins. Reduction of plantar pressure with rigid relief orthosis. *Journal of American Podiatric Medical Association*, 83(3):115–122, March 1993.

[157] M. Nurse and B. Nigg. Quatifying a relationship between tactile and vibration sensitivity of the human foot with plantar pressure distributions during gait. *Clincal Biomechanics*, (14):667–672, 1999.

[158] M. Nurse and B. Nigg. The effect of changes in foot sensation on plantar pressure and muscle activity. *Clincal Biomechanics*, 16:719–727, 2001.

[159] D. Oeffinger, R. Pectol, and C. Tylkowski. Foot pressure and radiographic outcome measures of lateral column lengthening for pes planovalgus deformity. *Gait and Posture*, 12:189–195, 2000.

[160] A. Okoulevitch and T. Bykova. Forefoot segmentation. Technical Report 03.22, Technische Universiteit Eindhoven, 2004.

[161] Z. Pataky, L. Faravel, J. Da Silva, and J.-P. Assal. A new ambulatory foot pressure device for patients with sensory impairment. a system for continuous measurement of plantar pressure and a feed-back alarm. *Journal of Biomechanics*, 33:1135–1138, 2000.

[162] A. Pedotti, R. Assente, and G. Fusi. Multisensor piezoelectric polymer insole for pedobarography. *Ferroelectrics*, 60:163–174, 1984.

[163] J. Perry. *Gait Analysis: Normal and Pathological Function.* McGraw-Hill, New York, 1992.

[164] J. Perry, J. Hall, and B. Davis. Simultaneous measurement of plantar pressure and shear forces in diabetic individuals. *Gait and Posture*, 15:101–107, 2002.

[165] J. Potter and M. Potter. Effect of callus removal on peak plantar pressures. *The Foot*, 10:23–26, 2000.

[166] U. Rattanapraser, R. Smith, M. Sullivian, and W. Gilleard. Three-dimentional kinematics of the forefoot, rearfoot, and leg without the function of tibilias posterior in comparison with normals during stance phase of walking. *Clinical Biomechanics*, 14:14–23, 1999.

[167] A. Redmond, P. Lumb, and K. Landorf. Effect of cast and noncast foot orthoses on plantar pressure and force during normal gait. *Journal of American Podiatric Medical Association*, 90(9):441–449, October 2000.

[168] L. Reed and P. Bennett. Changes in foot function with the use of root and blake orthoses. *Journal of American Podiatric Medical Association*, 91(4):184–193, April 2001.

[169] C. Reinschmidt and B. Nigg. Influence of heel height on ankle joint moments in running. *Medicine & Science in Sports & Exercise*, 27(3):410–416, 1995.

[170] C. Reinschmidt, A. van den Bogert, A. Lundberg, B. Nigg, N. Murphy, A. Stacoff, and A. Stano. Tibiofemoral and tibiocalcaneal motion during walking: external vs. skeletal markers. *Gait and Posture*, (6):98–109, 1997.

[171] C. Reinschmidt, A. van den Bogert, N. Murphy, A. Lundberg, and B. Nigg. Tibiocalcaneal motion during running, measured with external and bone markers. *Clinical Biomechanics*, 12, 1997.

[172] A. Rhodes, H. Sherk, J. Black, and C. Margulies. High resolution analysis of ground foot reaction forces. *Foot and Ankle*, 9(3):135–138, December 1988.

[173] M. Richter, B. Wippermann, H. Thermann, G. Schoeder, D. Otte, H. Troeger, and C. Krettek. Plantar impact causing midfoot fractures result in higher forces in chopart's joint than in the ankle joint. *Journal of Orthopaedic Research*, 20:222–232, 2002.

[174] H. Robbins. The unified forefoot: a mathematical model in the transverse plane. *Journal of American Podiatric Medicine Association*, 71:465–471, 1981.

[175] M. Rodgers. Dynamic biomechanics of the normal foot and ankle during walking and running. *Physical Therapy*, 68(12):1822–1830, December 1988.

[176] M. Rodgers, P. Cavanagh, and L. Sanders. *Plantar pressue distribution of diabetic feet*, volume 6A of *International series on biomechanics*, pages 343–348. Human Kinetics Publishers, Champaign, Illinois, 1978.

[177] M. Root, W. Orien, J. Weed, and R. Hughes. *Biomechanical eximination of the foot*. Clinical Biomechanics Corporation, Los Angeles, California, 1 edition, 1979.

[178] N. Rose, L. Feiwell, and A. Cracchiolo. A method for measuring foot pressures using a high resolution, computerized insole sensor: the effect of heel wedges on plantar pressure distribution and center of force. *Foot and Ankle*, 13(5):263–270, June 1992.

[179] D. Rosenbaum, S. Hautmann, M. Gold, and L. Claes. Effects of walking speed on hindfoot angular motion. *Gait and Posture*, 2(3):191–197, 1994.

[180] K. Roy. Force, pressure, and motion measurement in the foot: Current concepts. *Clinincs in Podiatric Medicine and Surgery*, 5(3):491–508, July 1988.

[181] E. Rzonca, P. Shapiro, and J. D'Amico. Haglund's deformity. *Journal of American Podiatry Association*, 74(10):482–485, October 1984.

[182] E. Salathe and G. Arangio. A biomechanical model of the foot: the role of muscles, tendons and ligaments. *Journal of Biomechanical Engineering*, 124:281–287, 2002.

[183] E. Salathe JR, G. Arangio, and E. Salathe. A biomechanical model of the foot. *Journal of Biomechanics*, 19(12):989–1001, 1986.

[184] P. Sanfilippo, R. Stess, and K. Moss. Dynamic plantar pressure analysis: comparing common insole materials. *Journal of American Podiatric Medical Association*, 82(10):507–513, October 1992.

[185] P. Schaff. An overview of foot pressure measurement systems. *Clinics in Podiatric Medicine and Surgery*, 10(3):403–415, July 1993.

[186] M. Schmid, G. Beltrami, D. Zambarbieri, and G. Verni. Centre of pressure displacements in trans-femoral amputees during gait. *Gait and Posture*, in press.

[187] W. Simons and K. Yang. Differentiation of human motion data using combined spline and least squares concepts. *Journal of Biomechanical Engineering*, 113:348–351, 1991.

[188] R. Soutas-Little, G. Beavis, M. Verstraete, and T. Markus. Analysis of foot motion during running using a joint co-ordinate system. *Medicine & Science in Sports & Exercise*, 19(3):285–293, 1987.

[189] C. Speksnijder, R. vd Munckhof, S. Moonen, and G. Walenkamp. The higher the heel the higher the forefoot-pressure in the healthy women. *The Foot*, 15:17–21, 2005.

[190] A. Stacoff, X. Kalin, and E. S. B. Segesser. The torsion of the foot in running. *Journal of Sport Biomechanics*, 5:375–389, 1989.

[191] A. Stacoff, X. Kalin, and E. Stussi. The effects of shoes on the torsion and rearfoot motion in running. *Medicine & Science in Sports & Exercise*, 23(4):482–490, 1991.

[192] A. Stacoff, B. Nigg, C. Reinschmidt, A. van den Bogert, and A. Lundberg. Tibiocalcaneal kinematics of barefoot versus shod running. *Journal of Biomechanics*, 33:1387–1395, 2000.

[193] J. Stebbins, M. Harrington, C. Giacomozzi, N. Thompson, A. Zavatsky, and T. Theologis. Assessment of sub-division of plantar pressure measurement in children. *Gait and Posture*, pages 1–5, in press.

[194] I. Stokes, W. Hutton, and J. Stott. Forces acting on the metatarsal heads during normal walking. *Journal of Anatomy*, (129):579–90, 1979.

[195] J. Taranto, M. Taranto, A. Bryant, and K. Singer. Angle of gait: a comparative reliability study using footprints and the emed-sf. *The Foot*, 15:7–13, 2005.

[196] A. Taylor, H. Menz, and A.-M. Keenan. The influence of walking speed on plantar pressure measurements using the two-step gait initiation protocol. *The Foot*, 14:49–55, 2004.

[197] A. Taylor, H. Menz, and A.-M. Keenan. Effects of experimentally induced plantar insensitivity on forces and pressures under the foot during normal walking. *Gait and Posture*, in press.

[198] D. Thompson, M. Hatley, T. McPoil, and M. Cornwall. Vertical forces and plantar pressures in selected aerobic movements versus walking. *Journal of American Podiatric Medical Association*, 83(9):504–508, September 1993.

[199] S. Urry and S. Wearing. A comparison of footprint indexes calculated from ink and electronic footprints. *Journal of American Podiatric Medical Association*, 91(4):203–209, April 2001.

[200] G. Valiant. *A determination of the mechanical characteristics of the human heel pad in vivo.* PhD thesis, Pennsylvania State University, 1984.

[201] B. Van Gheluwe, K. Kirby, P. Roosen, and R. Philips. Reliability and accuracy of biomechanical measurements of the lower extremities. *Journal of the American Podiatric Medical Association*, 92(6):317–326, June 2002.

[202] B. Van Gheluwe and C. Madsen. Frontal rearfoot kinematics in running prior to volitional exhaustion. *Journal of Applied Biomechanics*, (13):66–75, 1997.

[203] B. Van Gheluwe, J. Smekens, and P. Roosen. Electrodynographic evaluation of the foot during treadmill versus overground locomotion. *Journal of American Podiatric Medical Association*, 84(12):598–606, December 1994.

[204] B. Van Gheluwe, R. Tielemans, and P. Roosen. The influence of heel counter rigidity on rearfoot motion during running. *Journal of Applied Biomechanics*, 11(1):47–67, 1995.

[205] E. van Wegen, R. van Emmerik, and G. Riccio. Postural orientation: age-related changes in variability and time-to-boundary. *Human movement science*, 21:61–84, 2002.

[206] R. VanZant, T. McPoil, and M. Cornwall. Symmetry of plantar pressures and vertical forces in healty subjects during walking. *Journal of American Podiatric Medical Association*, 91(7):337–342, July/August 2001.

[207] J. Volf, S. Holy, and J. Vlcek. Using of tactile transducer for pressure-distribution measurement on the sole-of the foot. *Sensors and Actuators*, (62):556–561, 1997.

[208] M. Walker and H. Fan. Relationship between foot pressure pattern and foot type. *Foot and Ankle International*, 19(6):379–383, 1998.

[209] S. Wearing, S. Urry, J. Smeathers, and D. Battistutta. A comparison of gait initiation and termination methods for obtaining plantar foot pressures. *Gait and Posture*, (10):255–263, 1999.

[210] M. Whittle. *Gait analysis: an introduction*. Oxford: Butterworth-Heinemann, 3 edition, 2002.

[211] J. Wilson and T. Kernozek. Plantar loading and cadence alterations with fatique. *Medicine & Science in Sports & Exercise*, 31(12):1828–1833, 1999.

[212] C. Windle, S. Gregory, and S. Dixon. The shock attenuation characteritics of four different insoles when worn in military boot during running and marching. *Gait and Posture*, (9):31–37, 1999.

[213] D. Winter. *Biomechanics and Motor Control of Human Gait: Normal, Elderly and Pathological*. Wiley-Interscience, 2 edition, 1991.

[214] J. Wittenburg. *Dynamics of Systems of Rigid Bodies*. Teubner, Stuttgart, 1977.

[215] L. Wolfe, R. Stess, and P. Graf. Dynamic pressure analysis of the diabetic charcot foot. *Journal of American Podiatric Medical Association*, 81(6):281–286, 1991.

[216] H. Woltering. A fortran package for generalised cross-validatory spline smoothing and differentiation. *Advanced Engineering Software*, 8:104–107, 1986.

[217] G. Wu and J.-H. Chiang. The effects of surface compliance on foot pressure in stance. *Gait and Posture*, 4:122–129, 1996.

[218] H. Yamamoto, T. Muneta, S. Asahina, and K. Furuya. Forefoot pressures during walking in feet afflicted with hallux valgus. *Clinical orthopaedics and related research*, (323):247–253, February 1996.

[219] C. Young. The f-scan system of foot pressure analysis. *Clinics in podiatric medicine and surgery*, 10(3):455–461, July 1993.

[220] H. Zhu, J. Wertsch, G. Harris, and H. Alba. Sensate and insensate in-shoe plantar pressures. *Arch Phys Med Rehabil*, 74:1362–1368, December 1993.

Samenvatting

In zijn voortbewegen onderscheidt de mens zich van andere zoogdieren door het gebruik van slechts twee benen. De meest voorkomende vormen van voortbewegen van de mens zijn wandelen, lopen, en sprinten. Het menselijk voortbewegingssyteem is onderhevig aan blessures en afwijkingen die het patroon verstoren van zijn natuurlijke vorm naar een onnatuurlijk, pijnlijk of inefficient patroon. Hierdoor belemmeren ze de mens in zijn voortbewegen en functioneren.

Een verstoring van het voortbewegingssysteem heeft een grote invloed op het individu, in het bijzonder het beperken van zijn mobiliteit, als mede op de maatschappij, in de vorm van ziektekosten en vermindering van arbeidsproductiviteit. Het moge duidelijk zijn dat er een uitgebreide medische en wetenschappelijke gemeenschap actief is op het gebied van de ganganalyse. Eerst genoemde is het aanspreekpunt voor individuen met letsels of afwijkingen en poogt met een behandelingsplan de verstoringen van het systeem op te lossen. Laatst genoemde gemeenschap poogt een beter zicht te krijgen op de gang van de mens door het uitvoeren van onderzoek en experimenten. De opgedane kennis wordt op zijn beurt terug gekoppeld naar de medische gemeenschap.

Bij het menselijk voortbewegen is de voet de verbinding tussen de omgeving en de zich voortbewegende mens. De voet bestaat uit tenminste 26 botjes en uit een veelvoud aan ligamenten, pezen en spieren. Samen vormen ze één functionele structuur die een aantal functies vervult tijdens de voortbeweging. Bij één voetafwikkeling onderscheiden we vier fases: hielcontact, voorvoet vorming, stand, en propulsie. Tijdens de eerste fase maakt de voet het eerste contact met de grond en absorbeert het zachte weefsel rond de hiel een deel van de schokgolf die door het contact ontstaat. Deze absorptie is vereist omdat hoger gelegen organen, zoals bijvoorbeeld de hersenen, slecht bestand zijn tegen schokgolven. Tijdens de voetafwikkeling is de kinematica van

de voet gericht op een efficient gebruik van de beweging van de rest van het lichaam. De voet gedraagt zich als een stabiele basis tijdens het middelste gedeelte van voet-grond contact, stand. In de propulsie fase verandert de taak van de voet van een stabiliserend systeem naar een voortstuwingssyteem.

Het onderzoek naar het mechanisch gedrag van de voet is een belangrijk onderdeel van de ganganalyse, dat echter pas de laatste decennia de voet als een drie-dimensional segment is gaan beschouwen. Daarvóór bestond de meetapparatuur die kwantitatieve metingen mogelijk maakte niet. In het onderzoek dat geleid heeft tot dit proefschrift is gebruik gemaakt van een meetopstelling waarin drie typen metingen zijn uitgevoerd: plantaire drukverdelingen, krachten en drie-dimensionale bewegingen van de voet. De doelstelling van het onderzoek is het ontwerpen van een mechanische voetmodel dat de voetbeweging simuleert. Input van het model is data van plantaire drukmetingen uitgevoerd met een drukplaat. Het ontwerp richt zich vooral op de structuren van de voet die het meest bijdragen aan de beweging tijdens voet-grond contact, zoals het hielcomplex, de metatarsale hoofden, en de grote teen.

Het onderzoek is gebaseerd op een breed opgezet experiment waaraan 126 individuen hun medewerking hebben verleend. In dit experiment uitgevoerd in het biomechanisch laboratorium van de Vrije Universiteit Brussel is gebruik gemaakt van een bewegingsanalysesysteem, een krachten platform en een drukplaat. Deze meetapparaten zijn op elkaar afgestemd zowel in tijd als ruimte. Voor zover bekent, is er in het verleden slechts één experiment uitgevoerd en gerapporteerd waarin deze meetapparaten op elkaar werden afgestemd. Validatie van tijd- en ruimteafstemming komen in ons onderzoek ruim aan bod. Er werd aangetoond dat de afstemming binnen de meetnauwkeurigheid valt van het minst nauwkeurige apparaat.

Het bewegingsanalysesysteem heeft 3D-posities bepaald van markers die bevestigd werden op de voet. In totaal is gebruik gemaakt van 12 markers per voet: 4 op de hiel, 3 op de grote teen, en 5 op de metatarsalen. Door deze marker set-up ontstaat een vier segmenten voetmodel. Het krachten platform en de drukplaat leggen grootte en plaats van de drukverdeling tijdens voetafrol vast.

Onze populatie van 126 individuen bestond uit 78 mannen en 48 vrouwen met een leeftijdsvariatie van 10jaar tot 72jaar en een gewichtsvariatie van 32kg tot 116.5kg. De leeftijdsgroep tussen 15 en 25 jaar domineerde de populatie. Een belangrijk resultaat van het onderzoek is de database waarin de resultaten van de metingen op een gestructureerde wijze zijn weergegeven. Deze database wordt samen met het

proefschrift beschikbaar gesteld. Achtereenvolgens is deze database geanalyseerd met betrekking tot de hielbeweging tijdens hielcontact, de bewegingen van de metatarsale hoofden, en de bewegingen in het eerste metatarsofalangaal gewricht.

De hiel voert aan het begin van contact tussen voet en grond een rolbeweging uit die stopt ergens tijdens volledig voet contact. Het hielcomplex werd gemodelleerd als een star lichaam met een convexe vorm. De gemeten plantaire drukverdeling onder de hiel beschrijft in het model het contact tussen het rollende stare lichaam en de grond. De rollende beweging van het starre lichaam wordt eenduidig vastgelegd door de hoeksnelheid van het starre lichaam en het contactpad.

Voor validatie werd als star lichaam een bol gebruikt. Een bol met een vaste straal van 7cm leidde tot acceptabele resultaten, waarbij het model 75% van de gemeten hielbewegingen verklaart tijdens de initiële contact fase.

Voor de metatarsale hoofden blijkt beweging in zijwaartse en voor-achterwaartse richting te bestaan. Deze bewegingen zijn klein met betrekking tot de totale voetbewegingen. De gebruikte drukplaat kan deze bewegingen van de metatarsale hoofden niet waarnemen omdat de grote van de bewegingen binnen de sensor grootte liggen. In het model is dus aangenomen dat de grootte van de beweging van de metatarsale hoofden verwaarloosbaar is tijdens het grootste deel van contact. Met behulp van de plantaire drukverdeling kan een kromme bepaald worden, de metatarsale boog, waarop de hoofden zich blijvend bevinden. Validatie van de bepaling van de metatarsale boog op basis van drukverdelingen vond plaats met behulp van dezelfde boog maar bepaald op grond van het bewegingsanalysesysteem. Het voorvoetmodel maakt dus gebruik van het concept metatarsale boog. De bewegingsbepalende component van dit model is een gekromde cilinder waarbij de contactkromme met de grond gelijk is aan de metatarsale boog. Rollen rond deze cilinder beschrijft de propulsie fase van voetcontact. Deze beweging kan echter niet rechtstreeks uit de drukverdeling onder de metatarsale hoofden worden afgeleid. Het proefschrift beschrijft enige suggesties hoe deze rolbeweging indirect uit deze drukverdeling zou kunnen worden afgeleid.

Één suggestie is deze beweging te bepalen vanuit de beweging van het eerste metatarsofalangaal gewricht. In het onderzoek is de relatie tussen 92 druk gerelateerde variabelen en 30 variabelen van de beweging van het eerste metatarsofalangaal gewricht nagegaan. Met correlaties en regressievergelijkingen is aangetoond dat de flexie/extensie beweging in het gewricht druk gerelateerd is.

Het onderzoek dat we met dit proefschrift afsluiten concentreert zich op de vraag of

met plantaire drukverdeling het bewegingsverloop van de voet kan worden voorspeld. We menen een bevestigend antwoord te hebben gevonden op de vraag die als titel van dit proefschrift fungeert.

About the Author

Friso Hagman was born on March 14, 1974 in Heino, the Nederlands. In June 1992, he finished secondary school at Rythoviuscollege in Eersel. From September 1992 until December 1998, he studied Mathematics at Technische Universiteit Eindhoven. His final M.Sc. project was in the field of cryptology performed for Koninklijke Nederlandse Bibliotheek. Until 1995, he was an active track and field athlete specialised in shot put. In his athletic career, he was fortunate to represent his country in a number of international competitions and championships such as the European Youth Olympic Days and the European Junior Championships. After completing his university studies, he wanted to change focus. He enrolled in the postgraduate program Mathematics for Industry at Stan Ackermans Instituut of Technische Universiteit Eindhoven (from January 1999 till April 2001). Within the frame of this program, his specialism became biomechanics. Part of his training in biomechanics was at Vrije Universiteit Brussel during a three month stay. He performed an eight month industrial project at RSscan International. The project was aimed at the design of a mechanical model that describes foot motion solely based on plantar pressure distribution input.

The financial support of Vrije Universiteit Brussel, Technische Universiteit Eindhoven, and Universiteit Gent enabled him to continue his research in the form of a Ph.D. project. He performed his Ph.D. project from May 2001 until August 2005. For his research, he made use of the laboratories of biomechanics of Vrije Universiteit Brussel and Universiteit Gent.

Having completed his Ph.D., Friso remains working at the Vrije Universiteit Brussel. The research from his Ph.D. project will be continued, together with the start of

a new research direction studying biomechanical aspects of track and field.